Chair of Subsurface Engineering

Master's Thesis

Numerical simulation of an underground hydrogen storage

Matthias Böck, BSc

September 2024

MONTANUNIVERSITÄT LEOBEN
www.unileoben.ac.at

EIDESSTATTLICHE ERKLÄRUNG

Ich erkläre an Eides statt, dass ich diese Arbeit selbstständig verfasst, andere als die angegebenen Quellen und Hilfsmittel nicht benutzt, den Einsatz von generativen Methoden und Modellen der künstlichen Intelligenz vollständig und wahrheitsgetreu ausgewiesen habe, und mich auch sonst keiner unerlaubten Hilfsmittel bedient habe.

Ich erkläre, dass ich den Satzungsteil „Gute wissenschaftliche Praxis" der Montanuniversität Leoben gelesen, verstanden und befolgt habe.

Weiters erkläre ich, dass die elektronische und gedruckte Version der eingereichten wissenschaftlichen Abschlussarbeit formal und inhaltlich identisch sind.

Datum 24.09.2024

Unterschrift Verfasser/in
Matthias Böck

Danksagung

Ich möchte mich hiermit bei allen Mitwirkenden bei der Erstellung dieser Masterarbeit für deren Unterstützung bedanken. Das gewissenhafte Ausarbeiten und ordnungsgemäße Verfassen einer Masterarbeit verlangt viel Engagement seitens des Studenten aber auch von dessen Betreuungsteam an der Universität. Vor allem aber braucht es Rückhalt und Verständnis aus dem privaten Umfeld, um die notwendigen Arbeiten erledigen zu können.

Mein Dank gebührt in erster Linie meiner Betreuerin assoz. Prof. Phd Marlene Villeneuve. Ihre Expertise in der Numerischen Simulation im Gebiet der Geotechnik, sowie bei der Betreuung einer Masterarbeit waren eine große Unterstützung bei der Ausarbeitung dieser Arbeit. Durch ihre Lehrveranstaltungen im Zuge des Masterstudiums entwickelte sich meine Begeisterung für das Gebiet der numerischen Simulation und Gebirgsmechanik. Auch bei Arsham Moayedi Far möchte ich mich für dessen Unterstützung und Ratschläge bedanken.

Weiters möchte ich mich auch bei Herrn Univ.-Prof. Dipl.-Ing. Dr. mont. Robert Galler für die Möglichkeit der Ausarbeitung dieser Masterarbeit und der lehrreichen Zeit im Masterstudiengang bedanken. Ich bin froh den Schritt an die Montanuniversität Leoben gewagt zu haben, denn ich könnte mir keinen besseren Masterstudiengang zum Erlernen der Philosophie des Tunnelbaus vorstellen. Hiermit bedanke ich mich bei allen Vortragenden des Masterstudiengangs Geotechnik und Tunnelbau für ihr Engagement im Unterricht und die schöne Zeit auf und abseits der Universität.

Ich möchte mich auch bei meiner Familie für die Unterstützung im Laufe des Studiums bedanken. Der größte Dank gebührt meiner Lebensgefährtin Alisa Weintögl, welche mir den notwendigen Rückhalt und Ausgleich gab und maßgebenden Anteil an meinem erfolgreichen Studium hatte.

Abstract

At the beginning of this thesis, the underground high-pressure storage facilities for the media air and hydrogen are explained. This includes an explanation of common underground storage types and methods as well as a list of current projects in operation for civil use or for research purposes.

As part of a research project dealing with the storage of excessive energy in the supply network of the future, an underground hydrogen storage facility is to be built at the Zentrum am Berg (ZaB) research facility of the Montanuniversität Leoben on the Styrian Erzberg. The numerical simulation of this hydrogen storage facility is part of a series of master's and bachelor's theses dealing with the storage of energy under high pressure in underground storage facilities.

The construction of the hydrogen storage is based on the 'lined rock cavern - LRC' principle, which is described in the theoretical part of this thesis. The components of the cavern lining, possible failure mechanisms and a test facility in Sweden are described in more detail. Based on many years of experience in the construction of pressure tunnels for hydropower plants, a large number of lining options for pressure tunnels and their analytical calculation have been developed. A pre-stressed concrete lining or steel lining are used at locations of the pressure tunnel where higher operating pressures occur and are being considered as possible lining variants for the hydrogen storage facility. Experience and execution methods from pressure tunnel construction for steel linings and the pre-stressing process of a concrete inner lining complete the theoretical part of this thesis.

The analytical method from Seeber is used to dimension the lining of pressurised tunnels. A previous master's thesis as part of the research series on underground hydrogen storage dealt with the calculation of the lining of the high-pressure storage facility according to Seeber. Based on the results of the Seeber calculation method, a numerical simulation of the pre-stressed concrete lining and the steel lining is carried out in this thesis.
For the pre-stressed concrete lining, a method for the generation of a numerical model is developed that uses an input parameter that has been previously calibrated to Seeber's results. In combination with numerical models to simulate the gap injection process and to investigate the influence of the in-situ stress state in the rock mass, Seeber's analytical method and the numerical simulation can now be used in combination for the design of a pre-stressed concrete lining.

The minimum steel thickness resulting from Seeber's calculation to withstand the storage internal pressure is analysed by a numerical simulation with regard to the maximum steel elongation and the utilisation of the steel strength. Various influences such as the in-situ stress state and a possible failure of the surrounding rock mass are taken into account.

Kurzfassung

Zu Beginn dieser Arbeit werden die unterirdischen Hochdruckspeicher für die Medien Luft und Wasserstoff erläutert. Dazu gehören die Erläuterung der gängigen unterirdischen Speicherformen und Speichermethoden sowie die Auflistung aktueller in Betrieb befindlicher Projekte zur zivilen Nutzung oder zu Forschungszwecken.

Im Rahmen eines Forschungsprojektes, das sich mit der Speicherung von überschüssiger Energie im Versorgungsnetz der Zukunft beschäftigt, soll ein unterirdischer Wasserstoffspeicher in der Forschungseinrichtung Zentrum am Berg (ZaB) der Montanuniversität Leoben am steirischen Erzberg errichtet werden. Die numerische Simulation dieses Wasserstoffspeichers ist Teil einer Reihe von Master- und Bachelorarbeiten, die sich mit der Speicherung von Energie unter hohem Druck in unterirdischen Speichern beschäftigen.

Der Bau des Wasserstoffspeichers erfolgt nach dem Prinzip der „lined rock cavern - LRC“, das im theoretischen Teil dieser Arbeit beschrieben wird. Dabei werden die Komponenten der Kavernenauskleidung, mögliche Versagensmechanismen und eine Versuchsanlage in Schweden näher beschrieben. Basierend auf den langjährigen Erfahrungen beim Bau von Druckstollen für Wasserkraftwerke wurde eine Vielzahl von Auskleidungsmöglichkeiten für Druckstollen und deren analytische Berechnung entwickelt. Eine vorgespannte Betoninnenschale oder eine Innenauskleidung mittels Stahlpanzerung sind für höhere Betriebsdrücke ausgelegt und werden als mögliche Auskleidungsvarianten für den Wasserstoffspeicher in Betracht gezogen. Erfahrungen und Ausführungsmethoden aus dem Druckstollenbau zu den Themen Stahlauskleidung und Vorspannung einer Ortbetoninnenschale runden den Theorieteil ab.

Das analytische Verfahren nach Seeber dient zur Dimensionierung der Auskleidung von Druckstollen. Eine vorangegangene Masterarbeit im Rahmen der Forschungsreihe zur unterirdischen Wasserstoffspeicherung befasste sich mit der Berechnung der Auskleidung des Hochdruckspeichers nach Seeber. Aufbauend auf den Ergebnissen des Berechnungsverfahrens nach Seeber wird in dieser Arbeit eine numerische Simulation der Spannbetoninnenschale und der Stahlauskleidung durchgeführt.
Für die vorgespannte Betoninnenschale wird ein Verfahren zur Erstellung eines numerischen Modells entwickelt, das einen zuvor an den Ergebnissen von Seeber kalibrierten Eingabeparameter verwendet. In Kombination mit numerischen Modellen zur Simulation des Spaltinjektionsvorganges und zur Untersuchung des Einflusses des in-situ Spannungszustandes im Gebirge können die analytische Methode von Seeber und die numerische Simulation nun ergänzend bei der Bemessung einer vorgespannten Betoninnenschale eingesetzt werden.

Die sich nach den Formeln von Seeber ergebende minimale Stahldicke zur Aufnahme des Speicherdrucks wird durch eine numerische Simulation hinsichtlich der Einhaltung der maximalen Stahldehnung und des Ausnutzungsgrades der Stahlfestigkeit untersucht. Dabei werden verschiedene Einflüsse wie der in-situ Spannungszustand und ein mögliches Versagen des umgebenden Gebirges berücksichtigt.

Table of contents

List of abbreviations

ESS	Energy storage systems
PHS	Pumped hydroelectric storage
CAES	Compressed air energy storage
ZaB	Zentrum am Berg
TES	Thermal energy storage
UHS	Underground hydrogen storage
A-CAES	Adiabatic compressed air energy storage
D-CAES	Diabatic compressed air energy storage
I-CAES	isothermal compressed air energy storage
LRC	Lined rock cavern
HCF	High cycle fatigue
LCF	Low cycle fatigue
PDE	Partial differential equations
PDF	Probability density function
FOS	Factor of safety
FEM	Finite element method
FDM	Finite difference mathod
V_F	Deformation modulus of the rock mass
ν	Poisson's ratio
m	Transverse strain number
E_{rm}	Rock mass modulus
E_i	Young's modulus of the intact rock
E_{gap}	Stiffness of the liquid gap injection material
$E_{gap,hardened}$	Stiffness of the hardened gap injection material
E_{cm}	Young's modulus of the concrete
p_i	Internal pressure of the storage
$p_{v,0}$	Maximum gap injection pressure
p_v	Residual pre-stressing pressure
ε_{zul}	Maximum allowable strain of the steel lining
ε_{steel}	Strain of the steel lining
t	Thickness of the steel lining
Δt	Additional thickness of the steel lining
σ_v	Vertical in-situ stress in the rock mass
σ_1	Major principal stress in the rock mass
σ_3	Minor principal stress in the rock mass
K_0	Side pressure coefficient
σ_t	Tangential stress at the boundary of the storage
GSI	Geological strength index
$f_{y,k}$	Characteristic yield strength of steel
$f_{y,d}$	Design yield strength of steel
$f_{c,k}$	Characteristic concrete cylinder compressive strength
$f_{c,d}$	design concrete cylinder compressive strength
f_{cm}	Mean value of concrete cylinder compressive strength
γ_c	Safety factor for concrete
γ_s	Safety factor for steel

1 Introduction

The storage of excess electrical energy will be important in the future due to the rise of intermittent power feed-in by renewable sources like wind power and photovoltaics. Compressed air can store excess energy and release it when production is insufficient. [1, p. 251] Energy storage systems (ESS) on a large scale are going to play a major role to balance the fluctuations in energy production and consumption in the future. Pumped hydroelectric storage (PHS) and compressed air energy storage (CAES) represent the most viable large-scale technologies. PHS has the disadvantage of high initial costs during construction, as well as the requirement for specific geological and topographical conditions. In contrast, CAES is characterised by lower costs in construction and maintenance during operation. [2, p. 2671]

The Montanuniversität Leoben aims to build an underground hydrogen storage according to the principle of a lined rock cavern (LRC) in a depth of around 200 m at the research facility Zentrum am Berg (ZaB) in Eisenerz, Austria. Hydrogen or compressed air will be stored with a maximum pressure of 10 MPa in a cavern with an outer diameter of 3 m and a length of 15 m. A static design of the storage lining was done by Gabriel Loucky in his master's thesis about the "*Investigation of lining solutions for a lined rock cavern at the site of Zentrum am Berg*". He carried out a design of two lining solution with a steel and pre-stressed concrete lining, which is based on the analytical calculation from Seeber. [3]
Taking up the achieved results from Gabriel Loucky, this master's thesis is built on generated results for the dimensioning of the lining using the numerical analysis software RS2. A calibration of the numerical simulation on the results for the pre-stressed concrete lining from the analytical solution from Seeber was carried out and the obtained accuracies as well as a potential application under realistic conditions analysed. The required steel lining thickness according to Seeber was used in a numerical simulation and the achieved utilization of the steel capacity in the numerical model was determined and analysed. To investigate the application limits from the design method from Seeber, the criterion for the magnitude of the maximum gap injection pressure for pre-stressing of the concrete lining was analysed numerically. At the end, different numerical simulations were carried out to investigate the influence of the in-situ stress on the design of the storage lining.

The aim of this work is to combine the advantages of the quick analytical solution from Seeber for the design of an underground storage with the possibility of representing complex rock mass behaviours from the numerical analysis.

2 Hydrogen storage

Hydrogen plays an important role as a future low-carbon energy carrier in multiple fields like the transportation, power and heating sector. Renewable energy from solar, wind or hydro electrical energy with daily and seasonal fluctuation can be supported by hydrogen as a storage medium. [4, p. 1] Hydrogen has a high energy potential, enabling it to replace up to 60% of natural gas used in nonindustrial activities. [5]
It can chemically react with steel and leads under certain circumstances to the degradation phenomenon called hydrogen embrittlement resulting in concentrated plastic processes, enhanced crack propagation and a reduction of the life length. The presence of hydrogen in the material can reduce strength and ductility and increase the crack growth rate in a static loading scenario. The crystalline structure of austenitic stainless steel is less susceptible to hydrogen embrittlement and therefore a possible candidate for future applications. [6, pp. 17-18]

2.1 Properties of hydrogen

The gravimetric energy density of hydrogen is the highest of any substance known today with 120 kJ/g. On the other hand, hydrogen has the lowest atomic mass and therefore a low volumetric density. [4, p. 1] Burning one cubic meter of hydrogen generates 12.7 MJ of energy, which is relatively high but lower than methane with 40 MJ. [5]
The low density of hydrogen has the effect that the amount of stored hydrogen gas in a rock cavern with the same temperature and pressure is less than the amount of natural gas in terms of Nm^3. [6, p. 16] Liquefying hydrogen can increase its volumetric energy density but is not economical on the scale needed to store seasonal energy in the future. Hydrogen gas can be described as highly diffusive due to its small size, low viscosity, low molecular weight, low density and positive buoyancy over -251°C. [4, p. 1]

Human senses cannot detect hydrogen because it is colourless, tasteless, and odourless as odorant compounds like sulphur cannot be added. Hydrogen has a wide range between 4 and 75% of the flammable concentration, which has the consequence that the storage facility must be free of heat flames and sparks. [6, p. 14] The behaviour of hydrogen differs from most other gases and the classical gas theory cannot be applied. Many other gases cool down because of expansion during decompression to atmospheric pressure, but hydrogen instead heats up as a result of the Joule-Thomson effect. [6, p. 15]

2.2 Storage types

Limited storage capacities of surface-based hydrogen storage facilities like tanks and pipelines made it necessary to store hydrogen in underground facilities. Subsurface storages such as salt caverns, depleted oil and gas fields or aquifers have the needed potential to supply the necessary scale of energy. [4, p. 2] Underground hydrogen storage (UHS) stands out with its cost-effectiveness, scalability, vast storage capacity and safety in comparison with surface storage facilities. [7, p. 2]
Current experience in the field of hydrogen storage in the subsurface is restricted to salt caverns which are limited in potential locations and storage capacity. [8, p. 1] Only 9% of the used working gas worldwide is attributed to the storage in salt caverns. [8, p. 2] On the other hand, aquifers and depleted hydrocarbon reservoirs are widely available and have high storage capacities. The gained experiences from the past for these two types are only based on the storage of hydrogen-bearing town gas. [8, p. 1] Enough experience was gained from the storage of oil, CO_2, natural gas and compressed air, which can be used for an efficient and safe storage of hydrogen. For each storage type, parameters like working gas capacity, cushion gas requirements, site preparation, production rate, leakage risks, monitoring and maintenance cost differ depending on the storage type. [4, p. 2]

Cushion gas (base gas) is used to maintain a certain minimum pressure and given production levels of the reservoir. [8, p. 8] It is injected before the working gas to stabilise the storage formation and to isolate the hydrogen from the surrounding fluid. CH_4, N_2 and CO_2 are used as cushion gas. [9] The other component of a reservoir is the working gas, which can be withdrawn and used during a storage cycle. The percentage of cushion gas on the total volume of the reservoir is higher in pore storages than in salt caverns. [8, p. 8]

Abandoned mine shafts and lined rock caverns are two additional options to store hydrogen in the underground. Engineered caverns are built in suitable hard rock formations. Technical challenges and requirements are the reasons why these options are less interesting than salt caverns or aquifers. [4] Typical storage types for hydrogen with their stored power and discharge duration can be seen in Figure 1.

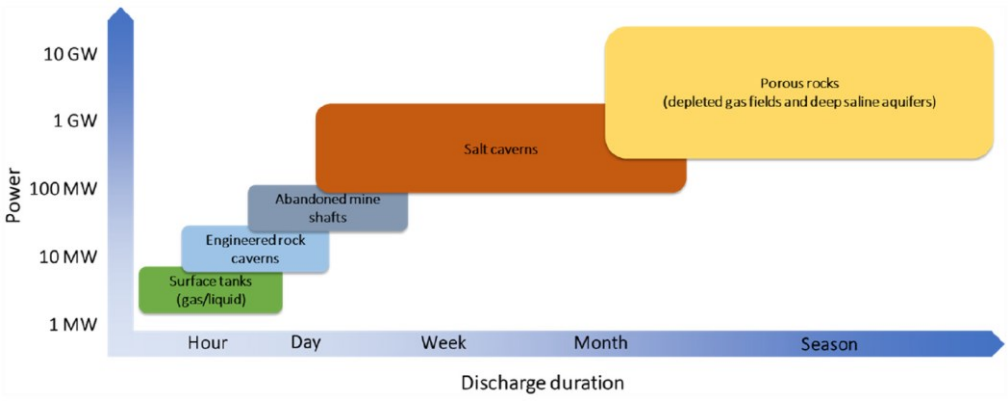

Figure 1: Hydrogen storage types like porous rock reservoirs, salt caverns, abandoned mines, engineered rock caverns or surface tanks with their storage power and discharge time [4, p. 3]

Biotic and abiotic reactions

Sandstone or limestone are typical rock formations of depleted gas fields and deep aquifers. Silicate minerals like quartz and feldspar (minerals of sandstone) do not react with hydrogen at typical reservoir conditions. Reactive components of limestones or mineral accessories in sandstones on the other hand can form toxic gases like hydrogen sulphide with hydrogen. A kinetically limited redox reactivity of hydrogen, due to its high bonding energy, has the effect that these reactions remain insignificant at low temperatures in the reservoir. [8, pp. 3-4]

Biotic processes can indeed endanger hydrogen storages by decreasing the hydrogen quality and volume in contrast to the described abiotic reactions. Microorganisms can consume hydrogen and the production of methane (CH_4) and hydrogen sulphide (H_2S) is possible. [8, pp. 3-4]

Petrophysical properties of prospective pore storage systems

There is no exact value for the optimal porosity and permeability for rock formations in gas storage systems because they depend on the application of the storage and the gas type, which is going to be stored. Higher permeability is often needed for high-pressure applications. Effective stress state, deformation state and temperature are also considered during the evaluation process of the suitability of a rock formation for storge purpose. [8, p. 5]

Storage depth, sealing capacity, and integrity of caprock

The prevention of the upward migration of the hydrogen gas through the rock above the reservoir is described with the sealing capacity, which is critical to effectively trap the gas in the reservoir. Hydrogen is trapped until the net buoyancy exceeds the capillary displacement pressure of the seal. The size of the interconnected pores, the wetting behaviour, which can be described by the brine-rock-hydrogen contact angle θ, and hydrogen-brine interfacial tension are properties influencing the capillary entry pressure. [8, p. 5]

2.2.1 Salt caverns

The fast-cycling flexibility, large storage capacity and the technological maturity make salt caverns the most promising future UHS facilities. Experience for the storage of hydrogen has been gained from one commercial storage in UK and three in USA. [4]
Benefits of salt as a storage rock mass are the: [4]

- good sealing capability due to its low permeability
- inert chemical behaviour with hydrogen
- preferable mechanical properties for cyclic acting loads

2.2.2 Depleted gas reservoirs

Depleted gas reservoirs have a very broad distribution and high storage capacity even higher than deep aquifers, which makes them more attractive than salt caverns. High requirements on the integrity and stability of the reservoir itself but also of the caprock and wellbore guarantee a safe storage and cycling of hydrogen. [7, pp. 1-2] Only two pilot studies from green methane projects in Austria and Argentina have successfully injected and recovered hydrogen from porous media since today. [4]

2.2.3 Deep aquifers

An underground hydrogen storage in aquifers gains more interest because of the large storage capacity and wide distribution in sedimentary basins. [10, p. 2] A storage in aquifers is more expensive than in depleted gas fields because of the increased preliminary work to prove that the storage is capable of holding and containing gas under high pressure. [5]
Town gas is stored in saline aquifers starting in the 1950s and the gained experience can now be used for the hydrogen storage. It is produced through the gasification from coal and contains of 50-60% hydrogen, 30% methane and 20% CO_2 and CO. [4]

2.3 Hydrogen storage facilities

Multiple UHS are currently under operation or development around the world. The United States of America has four active storage facilities which are constructed as a salt cavern. A list of the most popular facilities can be found in Table 1.

Table 1: Location, storage type, gas composition, storage volume and status of current underground hydrogen storage facilities [4]

Location	Storage type	Gas composition	Storage volume (m^3)	Status
Teesside, UK	Salt cavern	95% H_2	3 x 70,000	Active
Clemens, USA	Salt cavern	95% H_2	580,000	Active
Moss Bluff, USA	Salt cavern	H_2	566,000	Active
Spindletop, USA	Salt cavern	95% H_2	906,000	Active
Underground Sun Storage, Austria	Porous reservoir (depleted field)	10% H_2	115,000	Under development
Hychico, Argentina	Porous reservoir (aquifer)	10% H_2	750,000	Under development
HyBRIT, Sweden	Rock cavern	100% hydrogen	100	Under development

2.4 Hydrogen storage project

A pilot project to store excess renewable energy in the form of hydrogen will be carried out at the research facility Zentrum am Berg (ZaB) on the Styrian Erzberg. It is an EU-wide research project that aims to provide a planning and design basis for the implementation of underground compressed air or hydrogen storage in existing underground structures. Various potential storage locations will be evaluated through a feasibility study. The ZaB provides a suitable environment for a pilot project due to the presence of former mining tunnels at the Styrian Erzberg and the existing infrastructure of the ZaB. For logistical reasons, such as the size of the cross section of the access tunnels for transporting construction materials and prefabricated storage components, the location of the hydrogen storage facility in the "Verbindungstunnel Nord" is favoured. Like the other positions along an old mining tunnel of the mining company at the Styrian Erzberg, the so-called "Presserstollen", the overburden height of around 200 metres is sufficient. The geology in this area of ZaB is limestone and the location of the storage inside the underground infrastructure of ZaB is shown in Figure 2.

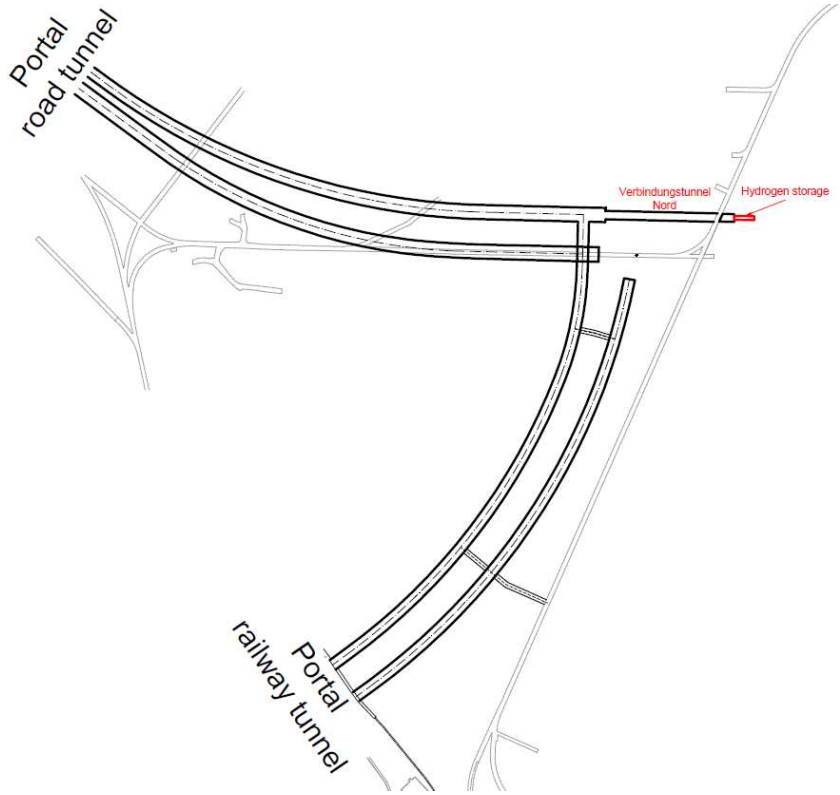

Figure 2: Overview of the existing underground infrastructure at ZaB and the location of the hydrogen storage facility at the end of the "Verbindungstunnel Nord"

The research facility ZaB consists of two single tube railway tunnels and two single tube road tunnels, which are shown in black in Figure 2. Existing galleries from previous underground mining activities are shown in grey and are also used for research purposes. "Verbindungstunnel Nord" is an extension of the northern tube of the road tunnels and the hydrogen storage with a length of 15 m and a diameter of 3 m will be built at the current location of the tunnel face.

Two different linings are being analysed for the hydrogen storage facility. Either a pre-stressed concrete lining, shown as a cross-section in Figure 3, or a steel lining, like it is displayed in Figure 4, will be constructed. Other options in the form of precast concrete segments "Tübbinge" were considered but not realised due to disadvantages in the design. Special types of steel or sealing membranes are used to ensure the tightness of the hydrogen storage. However, these are not covered in this master's thesis.

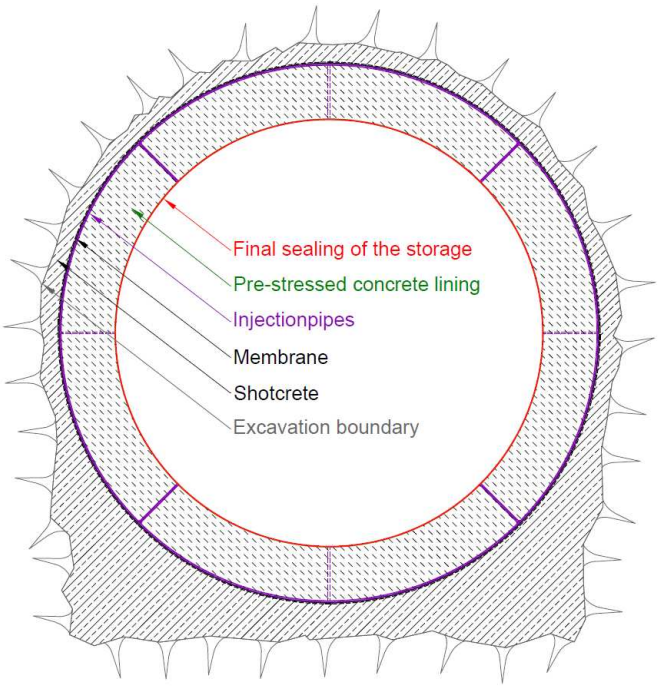

Figure 3: Cross-section of the pre-stressed concrete lining for the hydrogen storage at ZaB

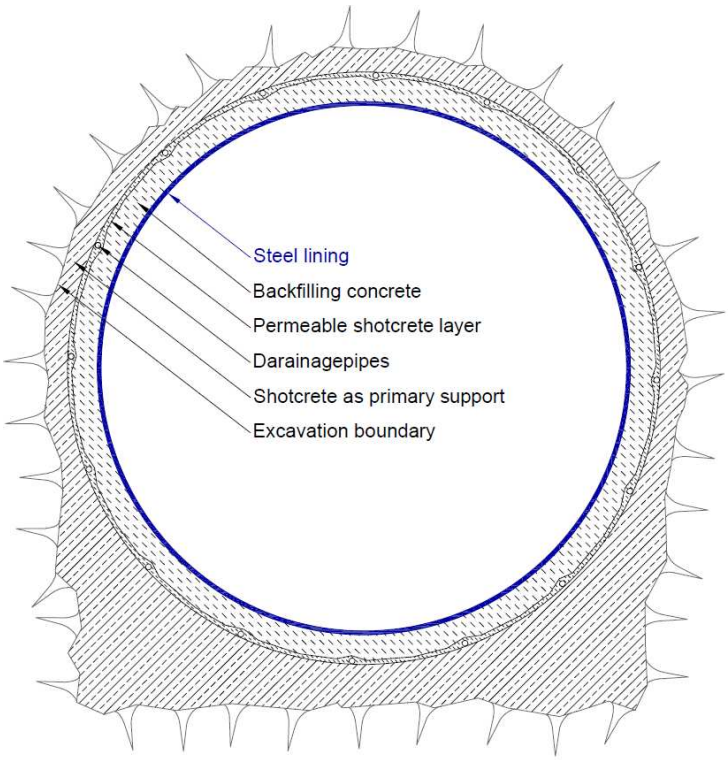

Figure 4: Cross-section of the steel lining for the hydrogen storage at ZaB

3 Compressed air energy storage

A Compressed Air Energy Storage (CAES) Gas Turbine system utilizes low-cost electric power. The compressed air is stored in an underground rock cavern and is used to generate power during the peak-demand. [11]
To achieve a certain amount of efficiency during the energy recovery, the stored gas must be under high pressure (10-30 MPa). A feasibility assessment of CAES from a geotechnical and structural point of view consists of an uplift failure of the rock mass beyond the storage, loss of tightness of the sealing layer and shear failure of the plug, which closes the cavern. As a lining concept for a CAES, a composite structure with a thin steel shell as sealing and a reinforced concrete shell on the outer side is recommended. [12, p. 1]

3.1 Past development of CAES

In large scale energy supply the concept of compressed air has never been used due to its low power density and the high losses during transportation. The development of compressed air energy storage (CAES) was not necessary in the energy supply before the 1960s. It started with the baseload energy supply from nuclear power plants and large coal fired power plants because since then it has been economically to store off-peak power and transfer the energy to the peak-load hours. Suitable geological formations like salt domes have been used in the past to store compressed natural gas and can also be used to store compressed air. A rising interest in the CAES technology started by the mid-1970s, stimulated by the Huntorf project. [1, p. 251] At the beginning of the 21st century more research and development on technologies for CAES has been conducted. [1, p. 253] A detailed timeline from the first patent until the construction of several CAES facilities with different principles is shown in Figure 5.

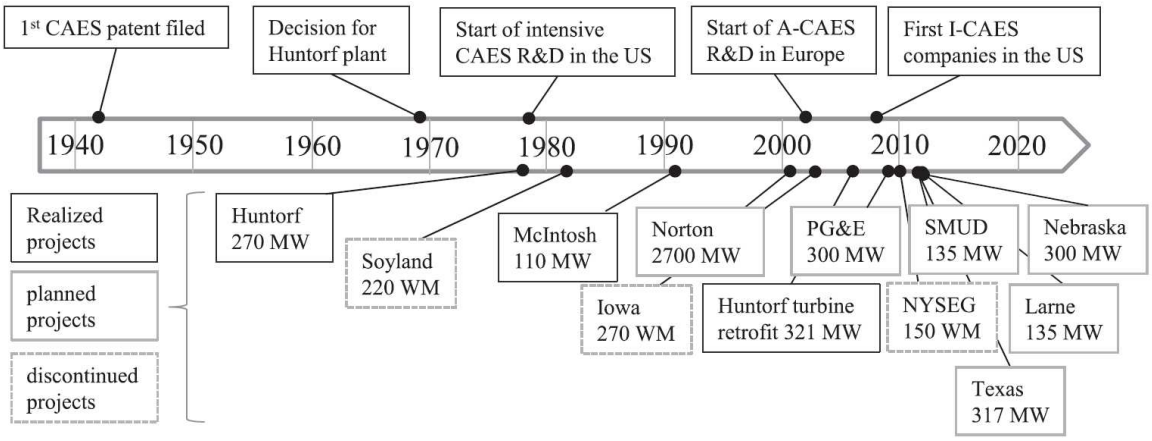

Figure 5: Stages of the past development of CAES with the realized, planned and discontinued projects [1, p. 252]

3.2 State of the art of CAES

It is possible to store compressed air at a constant volume (isochoric) or at a constant pressure (isobaric). Isochoric storages, such as salt caverns, have varying pressures and the disadvantage is the changing pressure for the compression and expansion machines, which reduces efficiency. [1, p. 264]
Existing airtight underground structures like mined salt caverns or mining shafts, which can withstand the operation pressure, can be used to store compressed air with the benefit of low investment costs and low land consumption. Salt caverns, porous reservoirs and hard rock caverns are the three main types to be used as storage volume for compressed air. [2, p. 2671]
A new system for an isobaric CAS is the subsea CAS, which uses the geodetic height of the water above and a facility has been applied in Lake Ontario. [1, pp. 264-265]
To balance the pressure of the stored gas through a representative water column above the storage, deep locations of the storage are needed. The alternative of an artificial water curtain was successfully used in Norway where leakages of gas pressures from 4 to 8 MPa could be eliminated. Larger gas pressures require an increase of the water pressure of the curtain, which can cause hydraulic fracturing at low in-situ stresses. [10, pp. 7-8]

3.2.1 Salt cavern

Salt caverns dominate as storage facility because of the experience gained from storing natural gas during the last decades. Minimum operation pressure and condensation of water are highly relevant for a salt cavern storage. [1, p. 265] A salt deposit can reach a thickness of several kilometres and therefore salt caverns can have large volumes. Salt has a high strength, uniform properties and self-repairing capability to seal fractures and prevent further crack propagation. The need of less base gas than other underground storage facilities make salt caverns best suited for the flexible operation and cycling of a CAES plant. [13]

3.2.2 Hard rock cavern

CAES projects in hard rock caverns have been completed at two test sites in Japan at depths between 200 m to 500 m. The first cavern is unlined and requires the pressure of the surrounding groundwater to be airtight and the second one is a lined cavern in an abandoned mine. An advanced adiabatic CAES pilot project was constructed in Switzerland in a mountain tunnel with an overburden of 450 m. A hard rock cavern can be sited close to the energy source, such as wind or solar, to reduce transmission costs, and at a shallow depth, which significantly reduces construction costs. [2, pp. 2671-2672]

3.2.3 Porous reservoir

Porous reservoirs are still under research due to the small number of suitable locations and the difficult control of air leakage because of the geological uncertainty. [2, p. 2672] The storage principles from natural gas in porous rock formations can also be applied to store air under high pressure. During the injection process the water is replaced by an artificial gas field. Aquifer storages need 50-80% cushion gas in contrast to 20% for salt caverns, which limits the utility. [13]

3.3 General concept of CAES

The charging process of the storage is done by an electrically driven compressor. It converts the excess electric energy into storable potential energy of compressed air. This energy can be released on demand by expanding the air in a turbine and generate electricity. Different processes to handle the heat which is generated during compression of the air can be used as an CAES technology and can be differentiated into diabatic, adiabatic and isothermal concepts. [1, p. 253]

The diabatic concept (D-CAES) has no use of the generated heat, which is wasted to the ambient. An external heat source is necessary to properly discharge the storage to avoid condensation and icing of the machine due to the expansion of the air. An adiabatic system (A-CAES) uses a thermal energy storage (TES) device to capture the generated heat and reuse it during the expansion process. In an isothermal CAES (I-CAES) the heat production during compression is prevented or minimized as low as possible. These three concepts differ in the cycle efficiency, start-up time, energy density, fields of application and status of development. [1, p. 253] An overview of all three concepts can be seen in Figure 6.

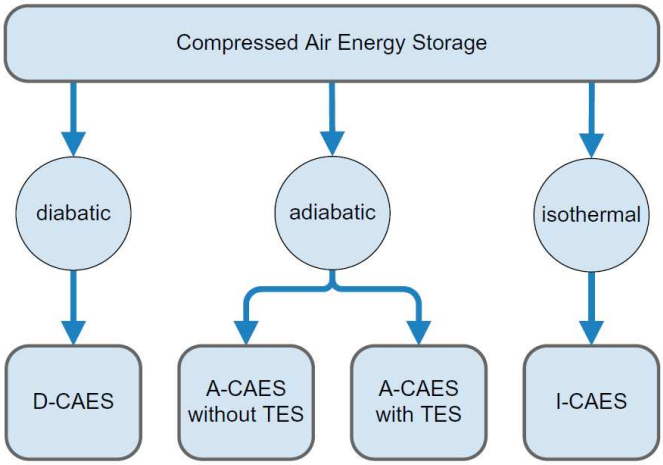

Figure 6: Overview about the current CAES concepts and their abbreviations [1, p. 253]

Adiabatic compressed air energy storage A-CAES

The storage of the generated heat during the compression can be done in two ways:

- A-CAES without TES [1, p. 260]

The compressed hot air is stored itself and the CAS acts like a "*combined thermal energy and compressed air storage volume"*. High temperature is already reached at low pressure, which restricts an A-CAES without TES to low storage pressure (10 bar). Known storage facilities are not capable to withstand the high temperature of the stored air. This type has only been realized at laboratory scale so far because of the high costs.

- A-CAES with TES [1, p. 260]

This concept is used in most of the A-CAES projects. Cooled compressed air can be stored in any CAS suitable for sealing the air. Increasing air pressure leads to higher power densities and a typical storage pressure for this type is 60 bar.

Isothermal compressed air energy storage I-CAES

By preventing the increase of the temperature during compression and a decrease during expansion this system avoids the known problems. It is based on the piston machinery because of the slow compression and expansion process, which allows enough time for the heat exchange inside the machine. An exchange surface and a liquid piston or pre-mixed foam can carry out the heat exchange. A pilot plant with 2 MW power was finished in Texas in 2012. [1, pp. 263-264]

3.4 Pilot projects

3.4.1 Underground Compressed Air Storage Facility for CAES-G/T

The storage with an operating pressure of 4 to 8 MPa is lined with a split lining structure. It transmits the pressure on to the surrounding rock and assures air tightness through an airtight lining. The split lining consists of 20 cm thick steel reinforced concrete segments and non-reinforced concrete filling between the segments and the rock mass. 3 mm thick reinforced rubber sheet and joint fillers are used for the air tightness. The imbedded mesh is necessary to prevent the entrapment of the rubber sheet into the cracks of the concrete segments. Joint fillers are made of natural rubber with a steel sheet as reinforcement to prevent the sealing from tearing as it becomes entrapped into the joint gaps. [11]

3.4.2 ANGAS (Advanced Natural Gas Storage) project

Several verification tests were conducted at an experimental LRC cavern in Japan. The ANGAS project ran from 2004 to 2007 to develop a suitable LRC system for Japan. [14, p. 1]

The main parts of the design and numerical analysis are focused on the: [14, p. 2]

- resistance against uplift failure of the rock mass
- rock mass behaviour during operation
- steel lining behaviour during operation
- concrete plug behaviour during operation
- temperature distribution around the cavern during operation

3.4.3 Pilot cavern Hunan, China

A pilot project in an exploration tunnel of Pingjiang hydroelectric storage plant in Hunan Province, China was used to explore the viability of a CAES at shallow depth. The airtightness of the fibre-reinforced plastic (FRP), stability of the cavern under high pressure and the efficiency of a thermal compensation system have been experimentally and numerically investigated. [2, p. 2672]
A pilot cavern with a design pressure of 10 MPa was built in a depth of around 110 m in the province Hunan, China. The Young's modulus of the intact rock was in the range of 47-50 GPa and the strength of the rock between 78 and 130 MPa. The cavern is a horizontal oriented cylinder with a length of 5 m, a diameter of 2.9 m and a 7 m long double-conical concrete plug with a steel door closing the storage. The cavern has a reinforced concrete liner and a 2 cm thick FRP liner for sealing. [2, p. 2673]
A heat exchanger inside the cavern and a cold/hot water pool outside the cavern are built as thermal compensation system, to prevent the temperature to be too high or too low during the charging and discharging phases. Consolidation, backfill and contact grouting were carried out to increase the capability of transferring load to the rock. [2, p. 2673]
The longitudinal section of the pilot cavern with the heat exchange system is shown in Figure 7.

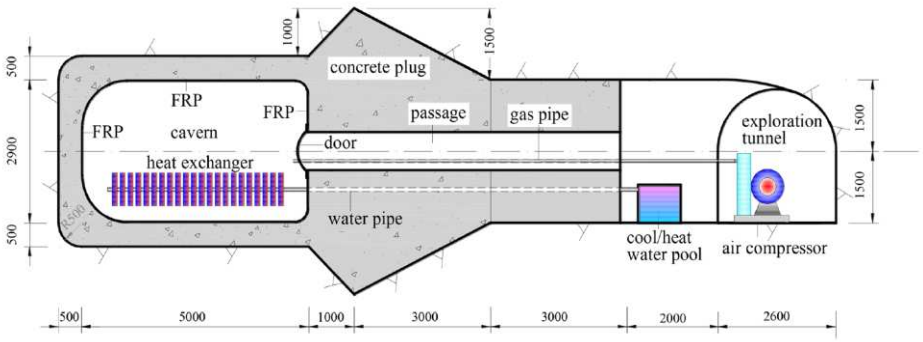

Figure 7: Longitudinal section of the pilot cavern in Hunan, China [2, p. 2673]

3.4.4 Grängesberg pilot test

Grängesberg lies 250 km northwest of Stockholm in central Sweden. The pilot facility has three test caverns (Room 1-3) and multiple access tunnels and shafts, as shown in Figure 8. Granite, with a UCS of 340 MPa and a Young's modulus of 56 GPa, is the rock type in which the caverns of the pilot facility were constructed. [15, pp. 42-43]

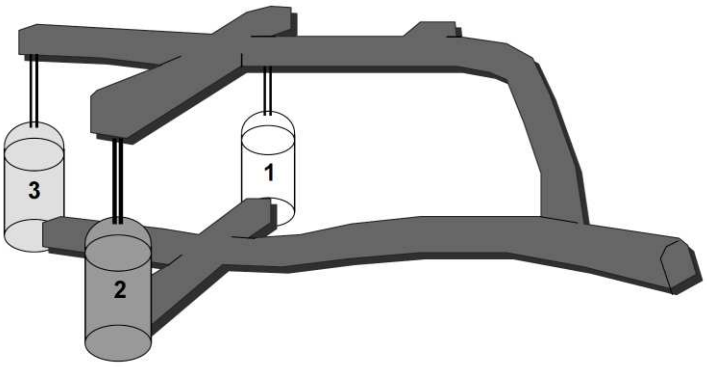

Figure 8: Layout of the Grängesberg pilot caverns with the location of the three test caverns and the access tunnels and shafts [15, p. 42]

Pilot caverns at Grängesberg were constructed to investigate the behaviour of different lining methods, different pressure and temperature regimes, rock mass failure mechanisms and leakages of the cavern. The dimensions of the caverns are 9 m in height and 4.4 m in diameter, with an overburden of 50 m. [6, p. 8]
The first cavern (room 1) had a 0.4 mm thick austenitic stainless steel as a lining. Quality problems with the lining welding method have limited the proper investigation due to leakage problems. [6, p. 8] A limited number of tests was possible in room 1 and a maximum pressure of 14 MPa was reached. [15, p. 44]
Carbon steel with a thickness of 6 mm with an asphalt sliding layer at the interface with the 0.6 m thick unreinforced concrete was used as cavern wall lining in the second cavern (room 2). A pressure of 52 MPa in the 200 load cycles was achieved for the testing which is far beyond the in-situ stress and near the concrete compressive strength. Radial displacements of 5.65 mm with fracturing of the concrete were measured because of the internal pressure. The concrete had only the function as load transfer medium and therefore the fracturing had no effect on the functionality of the cavern. [6, p. 9]
Room 3 had a lining consisting of 0.5 mm stainless steel instead of 10 mm fusion welded thermoplastic sheets because the plastic lining was too brittle and failed during construction. A reinforced concrete was installed for the load transfer. An internal pressure of 28 MPa in 91 load cycles resulted in 3.2 mm maximum displacement and only thin cracks in the concrete. [6, p. 9]

3.5 CAES power plants

Different concepts of CAES facilities have already been constructed for demonstration purpose or commercial use. An overview of some important projects with their achievable power and used storage method is given in Table 2.

Table 2: Current CAES projects with their location, project purpose, power and storage method [13]

Project	Location	Project Purpose	Power [MW]	Storage method
Pilot scale demonstration of AA-CAES	Gotthard base tunnel, Biasca, Switzerland	Demonstration	0.7	Previously excavated unlined rock cavern
Goderich A-CAES	Goderich, Ontario, Canada	Commercial	2.2	Mined cavern
Feicheng A-CAES	Feicheng, Shandong, China	Commercial	1250 (expected)	Repurposed salt and coal mine caverns
PG&E Advanced Underground CAES	San Joaquin County, California, USA	Commercial	300 (expected)	Depleted natural gas store
Angas A-CAES facility	Strathalbyn, South Australia,	Commercial	5	Repurposed zine mine

Huntorf plant

In 1978 the first CAES facility was commissioned in Huntorf, Germany. It consists of two caverns at a depth of 600 m which were used in the past for salt mining. [2, p. 2671]
Two compressors are used to store the air with an operation pressure between 46 and 72 bar. Re-cooling of the air before its stored, called an "*intercooled two-stage compression process*", limits the energy losses. Huntorf is a D-CAES without a heat storage device and 25% of the electrical energy is consumed by the cooling process. The storage caverns have a total volume of around 310,000 m³. Two caverns are necessary to guarantee a high availability even during maintenance. The Huntorf power plant has a black start capability and can also provide reactive power and frequency regulation. A small number of operational hours of 200 h per year for the generator is the result of this field of application. [1, pp. 258-259]

McIntosh plant

With a depth of 450 m, the second CAES facility with one solution mined salt cavern was finished in 1991 in McIntosh, Alabama. [2, p. 2671]
Only one cavern with a total volume of 538,000 m³ is used in McIntosh. It works similar to the CAES plant in Huntorf by using intercooling stages to reduce losses and no heat storage device. One main difference is the exhaust-heat recuperator, which has as a result a higher cycle efficiency of 54% compared to Huntorf with 42%. The charging and discharging cycle of McIntosh is longer than Huntorf because it was designed to perform weekly load shifting and not to provide blackstart capability. [1, pp. 259-260]

4 Lined rock cavern - LRC

An over many years developed lined rock cavern (LRC) lining system consists of a steel lining, a bituminous sliding layer and reinforced concrete. This concept is used to store natural gas at relatively shallow depths. [15, pp. 7, 14, 18] Lined rock caverns are a more cost-effective concept for shallow depths and can be built in a broader range of geological conditions. [6, p. 7] As part of the main principle, the surrounding rock mass takes up the internal pressure and the lining makes the storage gas tight and takes up only a negligible amount of the pressure. [15, p. 18]

A LRC concept consists of an above and below ground facility which can be seen in Figure 9. [15, p. 17] The facility at the surface consists of a compressor, control system, heating/cooling equipment, valves and piping. [6, p. 10]

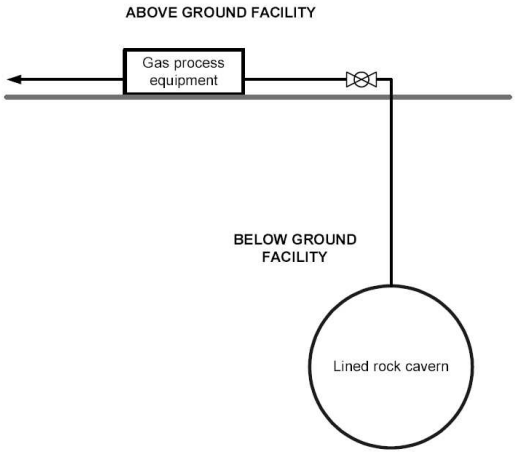

Figure 9: Layout of the LRC concept consisting of an above and below ground facility [15, p. 17]

Storage caverns, vertical shafts, gas pipelines and some access tunnels are the main part of the underground facility. The caverns are vertical cylinders (35-40 metres diameter and 60-100 metres height) with a half spherical top and bottom and are built in 100-200 metres depth. [15, pp. 17-18]
The internal pressure can reach 15-30 MPa and is higher than the in-situ stress in the rock mass, which implies that the surrounding rock mass cannot hinder a gas escape and must be strong enough to withstand the uplift failure. [15, pp. 18-19]

A typical cavern wall build up can be seen in Figure 10: [15, p. 20]

1. Steel liner
2. Sliding layer
3. Concrete lining
4. Reinforcement
5. Low strength and permeable shotcrete
6. Drainage system
7. Surrounding rock mass

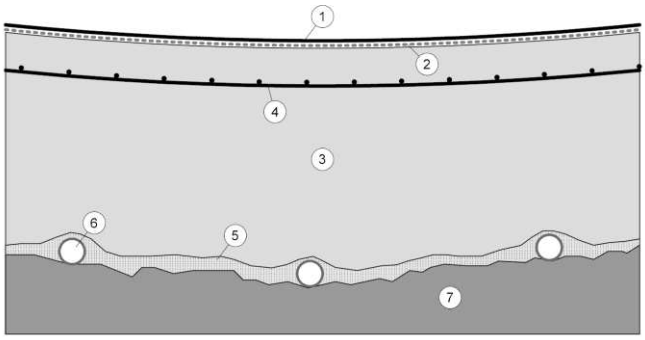

Figure 10: Cross section of the cavern wall build-up according to the LRC concept [15, p. 20]

Welded steel plates represent the ductile steel lining, and the concrete layer aims as a transition zone between the rock mass and the steel lining. Reinforcement in the concrete and the sliding layer redistribute the strain concentration from above the concrete cracks to the whole steel lining. Shotcrete is the primary support and protection of the drainage system when the cast in place concrete is built in. Water pressure from outside is prevented by the drainage system, which has also the function of a gas detector and collector of leaked gas. [16] A gas leakage is detected by a system integrated into the drainage, which is based on the detection through a pressure increase in the pipes.
[6, p. 12]

4.1 Failure modes

The following failure modes of the LRC can occur:

- Total failure of the rock mass [15, p. 21]

It is called uplift failure because the strength of the rock mass above is exceeded. A sufficient depth is an important aspect to avoid this failure.

- Rupture of the steel lining [15, p. 21]

The steel lining fails due too large deformations of the surrounding rock mass.

- Fatigue of the steel lining [15, p. 21]

Large numbers of load cycles are typical for a CAES and can cause a fatigue failure of the steel.

- Local failure of the steel lining caused by local weaknesses [15, p. 21]

A weakness zone in the rock mass or in the reinforced concrete caused by corrosion.

4.1.1 Uplift

The horizontal stress distribution is of particular interest for the uplift failure. Zero tangential stress in the crown marks the beginning of the tensile failure of the rock and the development of a plastic zone. If the inner pressure of the storage reaches the compressive strength of the rock, shear failure occurs. The critical pressure p_c of the storage can be seen as that pressure, where the entire overburden is cracked due to tensile failure. P_c increases with the rock strength and overburden as a result of the higher in-situ horizontal stress in the surrounding rock mass. [12, pp. 316-318]

4.1.2 Rock mass deformation

An excessive rock mass deformation leads to tensile failure in the steel lining and must be avoided during operation. A limit of 2% tangential deformation can be set for the steel lining. [12, pp. 318-319] The rock mass strength and the coefficient of lateral stress have an influence on the location of the maximum tangential strain. With increasing strength of the rock, the tangential strain decreases and remains the same as the rock strength is equal or higher than the inner pressure. Especially for weak rock mass conditions ($\sigma_c < 5$ MPa), an increasing overburden and K_0 factor decrease the tangential strain. [12, p. 319]

Stress anisotropy

Rock mass deformations can be anisotropic because of the in-situ stress situation and the orientation of the joints (influence on the strength and stiffness parameters). [15, p. 65]

The maximum radial deformation occurs in the direction of the minor principal stress and the maximum tangential deformation occurs in the major principal stress direction. The secondary tangential stress state controls the tangential stress generated by the storage pressure and determines the pressure at which tensile stresses occur in the surrounding rock. [15, p. 69] For example, if the secondary tangential stress at a given location is 20 MPa, no tensile cracks or joint openings will occur if the internal storage pressure is less than 20 MPa. [15, p. 71] Figure 11 shows an example of a circular storage cross section with anisotropic in-situ stress conditions with an opening of existing rock joints due to tensile conditions near the storage boundary.

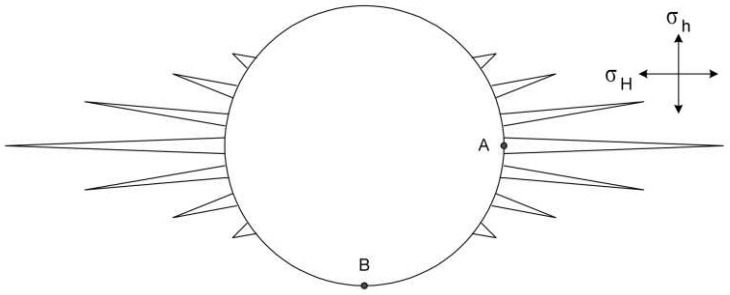

Figure 11: Location of the opening of existing joints in the rock mass around a storage depending on the anisotropic in-situ stress conditions [15, p. 71]

- Point A in Figure 11:

Tangential deformations of fractured rock mass are mainly influenced by the opening of rock joints. Local tensile conditions near the storage also affect the rock mass modulus and the radial deformations. [15, p. 71]

- Point B in Figure 11:

Compressive stress in tangential direction at this point will be even for high internal pressure. Elastic strain of the rock mass and the large-scale effect of the rock joint opening in point A generate large radial deformation. [15, p. 71]

4.1.3 Effect of joints

The cavern wall is subjected to compressive forces perpendicular to the surface and tensile forces tangential to the surface due to the expansion caused by the internal pressure. An expansion of the cavern leads to the opening and shearing of existing joints in the surrounding rock mass. Cracks in the concrete lining will concentrate above the joints and the induced stresses in the steel lining depend on the shear strength of the steel-concrete interface. [15, pp. 25-26] Unreinforced concrete has no ability to distribute the locally concentrated large cracks in the concrete over the entire steel lining, which can be seen in Figure 12. [6, p. 36]
Nearly uniform distributed tangential deformation of the steel lining is a result of a low friction coefficient of the sliding layer between the steel and concrete lining. The deformation is governed by mechanical rock mass properties like the rock mass modulus. No application of a sliding layer will cause stress and strain peaks above the concrete cracks as shown in Figure 13. [6, p. 36] The behaviour of the steel lining is now affected by the rock joints instead of the rock mass modulus. [15, p. 26]

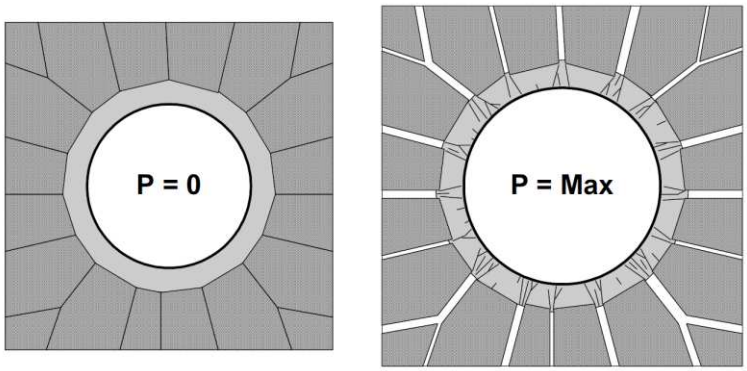

Figure 12: Impact of joints in the surrounding rock mass on the storage lining during operation with the maximal internal pressure [15, p. 25]

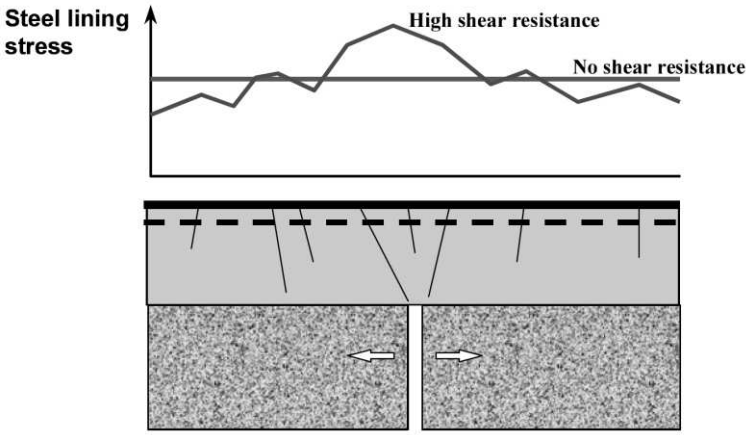

Figure 13: Stress distribution in the steel lining above an opened joint in the rock mass depending on the shear resistance of the interface between steel and concrete [15, p. 26]

4.1.4 Fatigue

The large number of load cycles during the lifetime of the storage make it necessary to control the maximum strain of the lining according to fatigue failure. [6, p. 37] Surface or internal defects can initialise fatigue failure if it is not stress (type a) or strain-controlled (type b). [15, p. 98]
Two behaviour types can be distinguished according to their strain range and are shown in Figure 14 (ε_y = yield strain of the steel lining): [15, p. 98]

a) $\varepsilon_y <$ strain range $< 2\ \varepsilon_y$
b) $> 2\ \varepsilon_y$

Type a)

The steel lining reaches its yielding strength in tension at the first loading cycle, but the strain range is lower than two times the yield limit. During the unloading cycle the tension changes to compression but the yielding point in the compressive state will not be reached. Completely elastic behaviour of the steel is set during the entire loading and unloading cycle, starting from the second cycle. This behaviour is called high-cycle fatigue (HCF) because of the large number of cycles necessary for a possible failure. [6, p. 37] A conventional HCF failure implies a stress-controlled behaviour, and the number of cycles is in the range of over 10^5. [15, p. 98]

Type b)

The second fatigue type has a strain range higher than two times the yield limit, which results in a yielding of the steel in tensional and compressional stage during every cycle. As a result of the steel yielding in every cycle, the number of cycles until failure occurs, is smaller and the behaviour is called low-cycle fatigue (LCF). For a LRC the biaxial stress state and the strain in both directions must be considered in the fatigue design. [6, pp. 38-39] For a LCF failure, the typical number of cycles until failure is in the range of 10^3, which is nearly the same as the maximum number of cycles during the life of an LRC facility and therefore more critical than HCF. [15, p. 98]

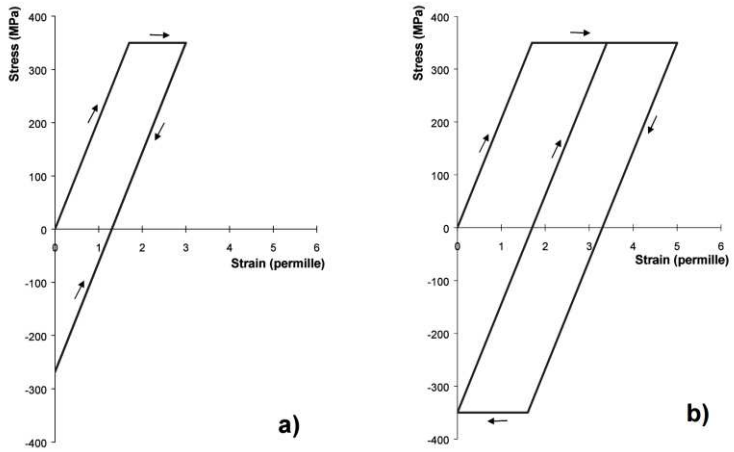

Figure 14: Stress-strain diagrams of both fatigue failure types with the loading and unloading path during operation of the storage [15, p. 98]

4.2 Drainage system

The system is designed to drain the groundwater during construction and to avoid high water pressures and damages on the lining during low pressure operation stages. Detection, collection and evacuation of leaked gases for safety reasons can be done by the drainage pipes. [6, pp. 40-41]
For a LRC the drainage system consists mainly of: [6, pp. 40-41]

- a pattern grid of perforated pipes with a spacing of 1-2 m
- two gas collector pipes which are ring shaped
- gas evacuation pipes which lead the collected gas from the collector pipes to the surface

Filling the drainage pipes with water helps to prevent chemical or biological blockages. [6, pp. 40-41]

4.3 Monitoring

Radial deformations in the surrounding rock mass were measured using multiple extensometers and the measurement of the tangential strains of the lining was done by mini extensometers in the concrete lining. Convergence lines were used for the measurement of the changes from the storage diameter. [15, p. 44]
The monitoring system can also be used to measure the thermal-mechanical response of the facility including temperature, pressure and humidity of the pressurised air, deformation and temperature of the rock mass, stress and strain of the liner and the degree of opening of the joints. [2, p. 2674]

Joint meters "J", reinforcement meters "KL", strainmeters "S", multi-point extensometers "M" and temperature meters "T" were used for the monitoring system, as shown in Figure 15. They were installed at various locations at the rock-concrete interface, within the concrete liner or in the surrounding rock mass. [2, pp. 2674-2675]

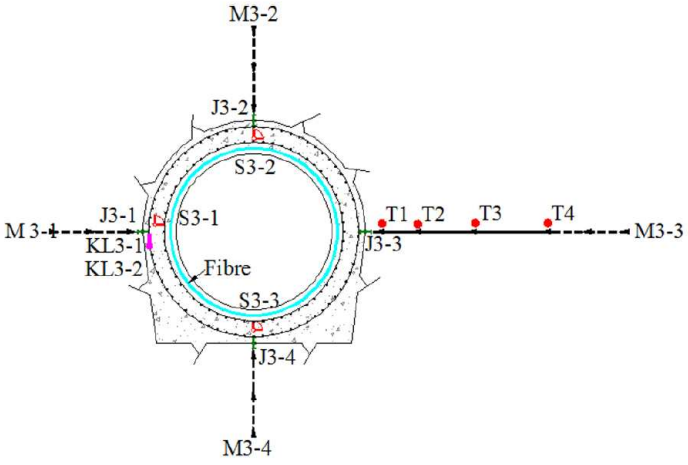

Figure 15: Monitoring system of the pilot lined rock cavern facility in Hunan province, China [2, p. 2675]

5 Pre-stressed concrete lining

Pre-stressed concrete linings have the advantage of an effective utilization of the surrounding rock mass and can obtain uncracked and watertight conditions during operation by using a membrane as a sealing layer. [17, p. 2] It can be applied for a wide range of different applications, even for large diameters with a slender lining.
[17, pp. 7-8]
The principle is based on increasing the load-bearing capacity of the in-situ concrete lining by injecting cement under high pressure into the circumferential gap between the concrete and the rock mass. The so-called passive pre-stressing process induces compressive stresses in the concrete, which increases its tensile strength. A sufficient rock mass strength and stiffness is crucial to maintain the pre-stressing effect. The grouting pressure must remain below the smallest principal stress. [18, p. 5]

5.1 Past development of pre-stressed concrete lining

Kieser has introduced a design and construction method, the so called corering, based on the thick-walled cylinder theory, to substitute the steel lined water tunnels for an operation pressure of up to 11 bar. A further development of the corering method was described by Lauffer, Seeber and Kaindl for circular tunnels and tube-a-manchette grouting systems. [17, p. 5] The so-called TIWAG gap grouting method is similar to Kieser's method and was introduced by Lauffer and Seeber 1961. [18, pp. 7-8] One major drawback of the borehole grouting, the variable pre-stressing of the lining with local stress peaks, has been overcome with this grouting system. Debonding agents and membranes help to rupture the interface between the concrete and shotcrete lining to achieve a full penetration of the interface, by minimizing the bonding forces between the two surfaces. [17, p. 5] TIWAG gap grouting was successfully applied at many pressure tunnel projects around the world and is popular because it is 30% cheaper than a steel lining and only slightly permeable. Further benefits through the injection are the continuous load transfer from the lining to the rock mass, lower permeability and homogenization of the rock mass around the tunnel. [18, pp. 7-8]

5.2 Injection

The standard injection material for joints and high-pressure injections is a cement suspension with a water to cement ratio of 1 and additional bentonite with 2% of the cement weight. [19, p. 6.9]
Injections fulfil several purposes: [19, p. 6.7]

- Close the shrinkage- and temperature gap between the lining and the rock mass
- Fill open joints and bond the rock mass
- Increase the Young's and deformation modulus of the rock mass
- Decrease the permeability of the rock mass
- Increase of the rock mass strength
- Pre-stress the concrete lining

Systematically borehole injections are carried out through radially orientated holes with approximately two to five metre distance between each other. These holes should be perpendicular to the main joint set to pump in the cement suspension with a pressure between 10 and 40 bars. [19, pp. 6.9-6.10] The holes are injected individually, but a constant pre-stressing pressure cannot be generated without special actions. A successful injection can be measured by pressure increase, communicating boreholes and deformation measurement of the lining. If the injection pressure cannot be reached, pre-injections with mortar or chemicals are used to close cavities. [19, pp. 6.10-6.11]

5.3 Pre-stressing methods

Passive pre-stressed concrete linings for tunnels are only possible because of the development of membranes and grout hoses for the high-pressure demand. Radially aligned grout lines with a defined spacing between them, ensure complete wetting of the lining circumference. [17, p. 6]

5.3.1 Maximum theoretically possible inner pressure

The strain capacity of the concrete is linked to the Young's modulus and the tensile strength by the Equation (1): [19, p. 6.19]

$$\varepsilon_b = \frac{\beta_z}{E_B} = 0{,}1\ ‰, \tag{1}$$

where ε_B is the concrete strain, β_z is the tensile strength of the concrete and E_B is the Young's modulus of concrete. The maximum possible internal pressure depends on the ratio of the rock mass deformation modulus to the concrete Young's modulus. A lower concrete modulus leads to a higher possible internal pressure. [19, p. 6.20] It is assumed that there is a gap between the rock mass and the concrete lining. If the gap is too large and the concrete tensile strength is reached before the gap is closed, the concrete fails in tension. Proper gap filling and bedding is therefore more important than a thicker lining. [19, pp. 6.19-6.20]

5.3.2 Core ring method by Kieser

Kieser's method is characterised by the fact that an annular cavity, which is kept free around the inner lining ring and is divided into individual sections in the longitudinal direction, gets injected under pressure using cement mortar. To create the cavity, the so-called core ring is either constructed from prefabricated hollow bricks or concreted in situ, with the spacing being maintained by means of hump plates that serve as outer formwork for the concrete. [20, p. 64]

Rock and support create a circular, stable and dry working area and play an important role as an abutment in the hydraulic stressing method. To maintain the external equilibrium, the rock lining and the rock may crack and get compressed until they take up the radial pressure through elastic resistance. The Barlow's formula is used to calculate the maximum injection pressure of the core ring. Five-metre-long zones are created using multi-part steel rings, which are integrated into the rock mass and serve to block the injection material. The reliable injection of the cavities and cracks represents a technical and economic advantage of this method. [21, pp. 132-149]

Backfilling procedure: [21, pp. 132-149]

1. Pneumatic backfilling until the water on the surface has been pressed out through an ejection tap in the crown.
2. Closing of the ejection tap and pressurise with 5 to 6 bar working pressure.
3. High pressure cement injection pumps are used to generate the desired pre-stressing pressure by pumping cement slurry into the soft mortar mass.
4. Water leaks into the surrounding rock mass, the tunnel tube or the adjacent zone.
5. Expansion of the cavity and cracking in the outer shell forms spaces which are continuously filled with cement slurry.
6. Components are elastically braced against each other, and a firmly pressed mass is created, which can no longer be compressed to any significant extent.
7. Relaxation processes and losses due to creep and cooling are considered by a sufficient addition to the pump pressure (approx. 1.5 times the operating pressure).

5.3.3 TIWAG gap injection method

The TIWAG method is based on the same principle as Kieser by pumping a cement suspension under high pressure into the gap between the rock mass and the concrete lining. [20, p. 64]
A precisely distributed overall injection of the gap, which can be repeated several times, is the result of the injection process. The grout seals fissures of the surrounding rock mass during the hardening process. [18, p. 7] A continuous injection pressure is reached through a system of plastic hoses which are fixed on the shotcrete inner surface with two to three metre distance in between. [19, p. 6.38] The injection ring pipes with release valves at 1.5 metre intervals and an internal diameter of 10 to 12 mm are positioned on the shotcrete. Lime milk facilitates the splitting of the construction joint and to initiate the opening of the gap, the injection hoses are inserted into 30 cm wide PVC sheathing hoses. If a membrane as separation layer is used, injection barriers of a polypropylene fleece are needed, which seal the gap by filtering out the cement grains. A sufficient pre-stressing effect can be achieved if the injection pressure ruptures the primary lining, and the grout penetrates the joints of the rock mass. [22, pp. 37-38]

5.3.4 Preservation of the pre-stressing

The pre-stress in the concrete lining is ensured by the in-situ stress, whereby the criterion is that the smallest primary in-situ stress is greater than the initial pre-stressing pressure. It is assumed that the injection restores at least partially the primary stress state, and the in-situ stress prevents the pre-stress from creeping away. Seeber estimates a 30-40% loss of pre-stress in the concrete due to creeping of the concrete and rock mass. The creep of the concrete depends on the air humidity and dimensions of the lining. [19, pp. 6.42-6.43]

5.3.5 Mechanically pre-stressed concrete lining

System Wayss & Freytag

The company Wayss & Freytag AG, from Frankfurt am Main, developed a pre-stressing system with steel wires to pre-tension the pressure tunnel for the main stage in Kaprun. Due to unfavourable geological conditions, with black phyllite as in-situ rock, the required resistance to take up the internal pressure could not be achieved, and a tension-resistant lining was necessary. The pressure tunnel with a diameter of 3.2 metres has an operating pressure of around 11.3 bar.
Prestressed concrete pipes were used as lining with a backfilling of compressed mortar between the pipe and the reinforced shotcrete shell. The concrete pipe absorbed the internal pressure and the pneumatic mortar backfill was used for bedding and frictional connection of the concrete pipe with the shotcrete shell and the rock which thus contributes to absorbing the internal pressure.
The pre-stressed concrete rings are 34 cm wide and 30 cm thick and consist of six segments, which are joined together by two spirals of wrapped 6 mm thick alloy pre-stressing steel in a horizontal position by a winding and placing machine. A maximum number of 32 turns with a prestressing of 7,000 kg/cm² results in a radial prestressing pressure of 9.38 kg/cm² and a tangential prestressing pressure of 60.2 kg/cm² in the concrete ring. [21, pp. 117-120]

System Dyckerhoff & Widmann

For the Lünerseewerk, the company Dyckerhoff & Widmann, KG from Munich developed a system for d in rings or partial rings in casing tubes. Intersecting steel rods have rolled threads at the recessed ends in the concrete for attaching the presses. A pre-stressing of around 4,500 kg/cm² in the steel and 60 kg/cm² in the concrete can be achieved. Pre-stressing steel has a breaking strength of 10,500 kg/cm², a yield strength of 8,000 kg/cm² and is stressed to 75% of the yield strength. During operation, a compressive stress of -5 kg/cm² should remain in the lining. [21, pp. 122-124]

5.3.6 Pressure losses

To use the injection pressure for pre-stressing, it is crucial to consider the right amount of pre-stressing losses. From the injection pump to the gap, a loss of 20-30% can be considered. Contact stresses between the lining and rock mass are defined by non-elastic deformations after the hardening of the gap injection material. These deformations are results of creeping, shrinkage and temperature processes. [23, pp. 30-31]

5.3.7 Tangential pre-stressing of the surrounding rock mass

An injection is an additional load and causes tangential tensional stresses in the surrounding rock mass. Discontinuities in the rock mass are injected and cause a tangential and radial compressive state which can be represented by a pre-stressed rock mass ring. An additional bonding in the discontinuities increases the rock mass modulus. The tangential compressive stress from the injection acts against the tangential tensional stresses caused by the inner pressure loading. [23, pp. 35-36]

5.4 Analytical calculation by Seeber

Rock mass and concrete lining are considered as a composite construction. The load sharing between the materials can be calculated based on the compatibility condition of deformations, where the radial deformations between the lining and rock mass are set to equal. The smallest in-situ stress is used as a support from the rock mass by Seeber (1984) in the load-line diagram, the so-called Seeber diagram method. [18, p. 8]

Seeber is a graphical solution for the system of equations for lining, rock mass and compatibility conditions. The equation for the mountain can be replaced by a measured working line. It is not based on a purely elastic behaviour because it considers the complicated stress-strain behaviour of the rock mass and the secondary stress state by a direct measurement of the working line with the TIWAG radial press in the tunnel. Anisotropy is considered by using the poorer bedding for the design. According to Seeber, the limit of rock mass entrainment is the smallest primary rock stress.
[19, pp. 3.3, 3.6-3.7]

Seeber's load-line diagram is based on the rock mass deformation modulus, which depends on the in-situ stress in the rock mass. The deformation line represents the acting load at the interface between the rock mass and the lining. Increasing compressive strength of the concrete lining lead to a higher gap injection pressure, but it should always remain below the smallest principal stress in the surrounding rock to avoid a fracturing or hydraulic jacking of the rock mass. Losses in the remaining grouting pressure due to creeping, shrinkage and temperature changes are considered in the diagram. This analytical method is dedicated to straight ahead circular tunnel with an elastic isotropic behaviour of the surrounding rock mass and a uniform in-situ stress. [18, pp. 8-9]

5.5 Monitoring

Geological inhomogeneity can cause variable bedding condition and ovalisation of the concrete lining and decreases the quality of the grouting process. The Niagara Tunnel Facility Project developed a monitoring system based on a laser system in combination with a grouting control system with a high real-time accuracy of 2/10 of a millimetre. [24, p. 6]
An aerial scan method as a monitoring system used hundreds of aerial clusters per scan. A developed software package combined the data from all the grouting activities with the deformation monitoring. Unfavourable conditions in the grouting process can be detected and prevented with the monitoring system. Two laser scanners survey 12.5m of tunnel length with a certain overlap to cover all pre- and post-deformations. [24, p. 7] The actual grout pressure in the gap between the shotcrete and the concrete can only be measured after the flow rate has stopped completely. A measurement over time of the correspondent grout pressure acting within the gap is done until the pressure magnitude is constant. Ovalisation of the lining can be used as a boundary criterion and the compressive strain as a criterion to reach the necessary pre-stressing. Different bedding in the crown and side wall can be dealt with the monitoring concept. [24, p. 7]

5.6 Niagara Tunnel Facility Project – NTFP

The pressure tunnel with a diameter of 12.8 m consist of an unreinforced concrete lining with a thickness of at least 0.5 m. A sandwich construction for the final lining consists of a passively pre-stressed concrete lining designed for a maximum operational pressure of 13 bars. The facility is located in a sedimentary formation consisting of mudstone with high swelling potential in the southern part of the Niagara escarpment. As a result of the swelling potential the lining had to be watertight and for the low-pressure regime, a waterproofing membrane is an economical and technical attractive solution. [17, p. 6] Long-term bonding of the different layers and the maintenance of an uncracked concrete lining is guaranteed by the interface grouting. Ovalisation and the large diameter lead to a difficult pre-stressing process and therefore a high sophisticated monitoring system had to be developed. [17, p. 7] The different parts of the pre-stressed concrete lining are shown in Figure 16.

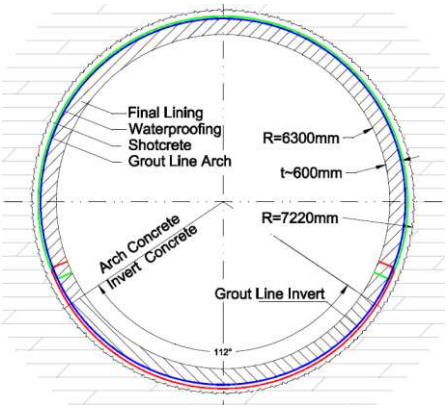

Figure 16: Cross section of the pre-stressed concrete lining of the Niagara facility [17, p. 7]

6 Steel lining

Prevention of a possible gas leakage out of the storage is the main function of the steel lining. Extensive tangential strains in the lining or fatigue phenomena because of the charging and discharging cycles during lifetime, can be seen as the critical failure mechanisms. The steel quality and factors such as strain magnitude and number of cycles effect the behaviour of the steel lining. Steel plates are welded on the construction site to build the lining and the properties of the welds are not the same as the parent material. The high temperature welding process has also an impact on the crystal structure of the nearby ground material. High-quality grade steel with high ductility, excellent weldability and a minimum yield strength between 300 and 400 MPa should be a requirement for the lining. [15, p. 96]

6.1 Thin-walled lining

Thin-walled steel linings have a wall thickness of 5-6 mm, whereby the lining is only needed to ensure tightness. Buckling failure is a risk due to the low shell thickness and a concrete inner ring is needed for support. The system of steel shell and concrete inner ring can be manufactured as a precast element with a length of 4 m. The segments are welded together, the remaining joint is cast in concrete and the necessary injection system is already integrated into the precast elements. [19, pp. 6.68-6.70]

6.2 Thick-walled lining

If the rock cannot absorb the full internal pressure, a thick-walled steel lining is necessary. The boundary between a thin-walled and thick-walled steel shell is 10 - 12 mm. The gap between the steel shell and the bedding concrete is 0.3–0.4 per mille of the inner radius. Creep deformations, cooling of the concrete and plastic deformations of the rock were thus considered. High-pressure gap injection can significantly improve the load transfer between the lining and the rock. [19, pp. 6.72-6.73]
Proof of buckling is required for the thick-walled steel shell. Radial rings or shear ribs can be welded to the outside of the steel lining and anchored in the bedding concrete, to increase the external pressure that can be taken up according to buckling failure. [19, pp. 6.72-6.73] To reduce the risk of buckling due to external water pressure, drains are used which can be opened in phases of no internal pressure. [21, p. 88]

7 Numerical simulation

7.1 Basics

7.1.1 Nature of rock mass

As a natural geological material, rock has physical properties that must be empirically established, unlike materials defined by a manufacturing process. The rock mass can be described as a discontinuous, inhomogeneous, anisotropic and not-elastic (DIANE) material. Different kinds of constituents, complex interactions and long-lasting formation processes make the mathematically representation of rock mass so difficult in a numerical simulation. [25, p. 285]
For an adequate representation of the nature of rock mass and the additional engineering consequences, the following features must be implemented in a numerical model:
[25, pp. 285-286]

- Mathematically representation of the physical processes by partial differential equations (PDEs)
- Variables for relevant mechanisms and parameters for constitutive laws
- In-situ stress conditions of the rock mass
- Pre-existing temperature and water pressure
- Naturally existing fractures
- Representation of the inhomogeneous rock mass by variation of the properties
- Consideration of possible anisotropic rock mass behaviour
- Scale dependent rock mass properties

7.1.2 Rocscience software RS2

RS2 is a software tool used for 2D finite element analysis of geotechnical structures, particularly in civil and mining applications. It can be applied for rock and soil material (RS2: Rock and Soil 2D). Several underground excavations like tunnels and mines, as well as surface excavations, foundations, slope stability, groundwater seepage and consolidation can be dealt with RS2. [26]

7.1.3 Finite Element method – FEM

Finite element method (FEM) is very popular due to its flexibility with handling inhomogeneity, anisotropy, dynamic problems and complex boundary conditions. It has a moderate efficiency in case of complex constitutive models and fractures. Discretization of the domain, local approximations and solving of the global matrix equation are the main steps for the completion of the finite element analysis (FEA). Discretizing the domain means to divide the area into a finite number of elements with regular shapes and a fixed number of nodes. [25, p. 295]

The basic of a FEA is an unknown function, u^e_i for each element of the grid, which can be solved by using a trial function of the nodal values of the system, shown in Equation (2): [25, p. 295]

$$u_i^e = \sum_{j=1}^{M} N_{ij} * u_i^j, \tag{2}$$

where N_{ij} are the shape or interpolation functions, M is the order of the elements and u_i^j are the nodal values.
The use of the shape functions replaces Equation (3): [25, p. 295]

$$\sum_{i=1}^{N} \left[K_{ij}^e\right] * \left\{u_j^e\right\} = \sum_{i=1}^{N} \{f_i^e\} \; or \; \boldsymbol{Ku} = \boldsymbol{F} \tag{3}$$

where $[K_{ij}^e]$ is the coefficient matrix, $\{u^e_j\}$ is the nodal value vector of the unknown variables, $\{f_i^e\}$ is the body force vector and in case of an elastic behaviour, $[K_{ij}^e]$ is the element stiffness matrix.

Rock mechanics has many challenges, including fractures, anisotropy, and scale effects. There is a lot of potential for developing numerical methods to address these challenges. FEM is the most used numerical method in the field of civil engineering because the traditional finite difference method (FDM) with regular grids cannot effectively solve the rock mechanical problems. [25, pp. 295-296]

7.1.4 Calculation of pre-stressed tunnels by Simanjuntak

Pre-stressed concrete linings have a bearing capacity, which depends on the support capacity of the surrounding rock mass. Anisotropic rock mass material behaviour is the case for most of the rock mechanics' tasks. [18, pp. 10-11]
Only a few numerical analyses have been conducted in the past on the topic of pre-stressed concrete-linings for pressure tunnels with either an elastic isotropic or elasto-plastic isotropic rock mass behaviour. [18, pp. 10-11]

If an elastic isotropic material behaviour of the rock mass is assumed, analytical solutions can be used to calculate the induced strains of a pre-stressed tunnel. A non-elastic and anisotropic rock mass behaviour has a different deformation behaviour and a non-linear constitutive law like Hoek Brown must be considered. Laminated anisotropic rock mass with non-uniform in-situ stress have not yet been investigated and is ignored sometimes during the tunnel design of pressurized tunnels. [18, p. 11]

7.2 Tasks for the numerical analysis

The numerical analysis of the hydrogen storage at the ZaB facility is part of a research series of several master's and bachelor's theses. In May 2024, Gabriel Loucky has finished his master's thesis about the investigation of lining solutions for a lined rock cavern. He used the analytical solution from Seeber to design the lining. Steel or pre-stressed concrete have been chosen as lining for the storage. As part of his thesis, he prepared an excel-sheet based on the Seeber calculation, which makes it possible to carry out a dimensioning of the lining with different input parameters.
Deformation modulus (V_F), Poisson's ratio (ν) and rock mass modulus (E_{rm}) are the most important rock mass input parameters for the analytical calculation according to Seeber. V_F cannot be implemented in the numerical model and is therefore not considered in the calibration and comparison process.

7.2.1 Calibration of the pre-stressed concrete model on Seeber

Building up on the results from Seeber, the calibration process aims to combine the advantages of a numerical simulation in the field of rock mechanics and the quick calculation tool given by the analytical design method from Seeber.
The magnitudes of the gap injection and pre-stressing pressure are taken from [27], after selecting the necessary input parameters, as shown in Figure 17, in the prepared excel-sheet from Gabriel Loucky. Rock mass and concrete parameters as well as the internal pressure (p_i) are changed for every calibration.
A certain gap injection pressure is necessary for a successful pre-stressing process. It depends on the thickness, strength and stiffness of the lining as well as on the stiffness of the surrounding rock mass. A curing temperature of 35°C was fixed to get the needed creeping, shrinkage and temperature losses of the gap injection pressure according to the analytical solution from Seeber.

Identical concrete strength, stiffness and thickness as well as the same rock mass strength and stiffness are crucial for the calibration. A 5 mm thick layer between the concrete lining and the surrounding rock mass is necessary to simulate the gap injection process. This interlayer is representing the gap injection material and the calibration is carried out through a variation of the stiffness of the gap injection material (E_{gap}). An internal storage pressure (p_i) of 4, 7 and 10 MPa and concrete lining thickness of 0.1 m, 0.2 m and 0.3 m were fixed for the design of the pre-stressed concrete storage. Assumptions from Seeber about the rock mass behaviour and in-situ stress conditions can be found under Chapter 5.4 and are adapted for the numerical model.

The calibration is intended to provide a tool for the creation of a numerical model, which can determine the same necessary value of the pre-stressing pressure (p_v) for the concrete lining as Seeber. In addition, the numerical model makes it possible to investigate certain failure scenarios of the surrounding rock mass and lining as well as the influence of the in-situ stress on the success of the pre-stressing and the load bearing capacity of the lining.

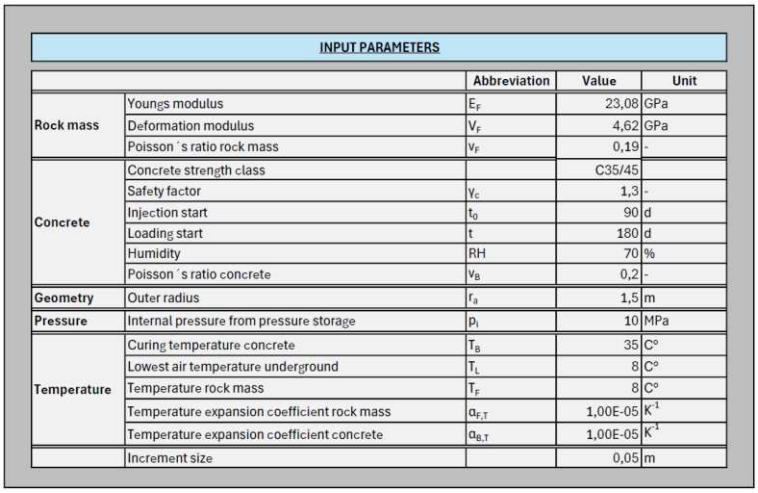

INPUT PARAMETERS				
		Abbreviation	Value	Unit
Rock mass	Youngs modulus	E_F	23,08	GPa
	Deformation modulus	V_F	4,62	GPa
	Poisson´s ratio rock mass	v_F	0,19	-
Concrete	Concrete strength class		C35/45	
	Safety factor	γ_c	1,3	-
	Injection start	t_0	90	d
	Loading start	t	180	d
	Humidity	RH	70	%
	Poisson´s ratio concrete	v_B	0,2	-
Geometry	Outer radius	r_a	1,5	m
Pressure	Internal pressure from pressure storage	p_i	10	MPa
Temperature	Curing temperature concrete	T_B	35	C°
	Lowest air temperature underground	T_L	8	C°
	Temperature rock mass	T_F	8	C°
	Temperature expansion coefficient rock mass	$\alpha_{F,T}$	1,00E-05	K^{-1}
	Temperature expansion coefficient concrete	$\alpha_{B,T}$	1,00E-05	K^{-1}
	Increment size		0,05	m

Figure 17: Input parameters for the calibration of the pre-stressed concrete lining [27]

Depending on the chosen input parameters, the calculation from Seeber results in different gap injection pressures. A maximum gap injection pressure ($p_{v,0}$) leads to the potential damage of the surrounding rock mass. The residual pre-stressing pressure (p_v), where the losses of the gap injection pressure are excluded, is needed for the effective long-term pre-stressing of the concrete lining.

All the necessary pressures and the resulting strains of the pre-stressed concrete lining according to the analytical method from Seeber are taken from the generated excel-sheet from [27] and can be found in Table 3, where γ_c is the safety factor of the concrete, r_a is the outer radius of the storage, r_i is the inner radius of the storage, d is the concrete lining thickness, ΔT is the temperature difference for the temperature gap, pi is the internal pressure of the storage, pi' internal pressure in the contact joint, p_F is the internal pressure share of the rock mass, $\Delta p_{v,Kr}$ is the pre-stressing pressure loss of the concrete lining due to creeping, $\Delta p_{v,\Delta T}$ is the pre-stressing pressure loss of the concrete lining due to temperature influence, E_F is the Young's modulus of the rock mass, p_v is the required injection pressure exclusive losses, $p_{v,0}$ is the required injection pressure inclusive losses, $\varepsilon_{B,Kr}$ is the strain due to creeping, $\varepsilon_{B,\Delta T}$ is the strain due to temperature influence, V_F is the deformation modulus of the rock mass, ε_V is the strain due to pre-stressing pressure of the concrete lining exclusive losses, $\varepsilon_{V,0}$ is the strain due to pre-stressing pressure of the concrete lining inclusive losses and E_{cm} is the Young's modulus of the concrete.

Table 3: Results of the analytical method from Seeber for a pre-stressed concrete lining [27]

γ_c	1.3	p_i	10.00 MPa	E_F	23.08 GPa	V_F	4.62 GPa
r_a	1.50 m	p_i'	9.33 MPa	p_V	3.54 MPa	ε_V	0.00149
r_i	1.40 m	p_F	5.79 MPa	$p_{v,0}$	8.54 MPa	$\varepsilon_{V,0}$	0.00360
d	0.10 m	$\Delta p_{v,Kr}$	4.24 MPa	$\varepsilon_{B,Kr}$	0.000179	Concrete quality C35/45	
ΔT	27 K	$\Delta p_{v,\Delta T}$	0.75 MPa	$\varepsilon_{B,\Delta T}$	0.000317	E_{cm}	34 GPa

Plastic numerical simulation

The calibrated value for E_{gap} is used to carry out a realistic numerical simulation with shotcrete as primary support and plastic material behaviour of the lining and rock mass. This aims to investigate the accuracy of the results from Seeber with the calibrated numerical models considering plastic material behaviour, possible failure scenarios and the behaviour of the pre-stressed concrete lining under realistic conditions.

7.2.2 Comparison of the results from the steel lining design

A comparison of the results from Seeber and the numerical model was carried out for the steel lining. Steel can take up higher tensile forces than concrete and the p_i for the design was therefore fixed with 10, 15 and 20 MPa. The assumptions from Seeber about the rock mass behaviour and in-situ stress conditions can be found under Chapter 5.4 and were adapted for the numerical model. Rock mass parameters, steel grade and p_i are the constantly changed input parameters for the comparison. An overview of the input parameters is given in Figure 18.

INPUT PARAMETERS

		Abbreviation	Value	Unit
Rock mass	Youngs modulus	E_F	23,08	GPa
	Modulus of deformation	V_F	4,62	GPa
	Poisson´s ratio rock mass	v_F	0,19	-
Steel	Steel grade		S460	
	Youngs modulus	E_s	210	GPa
	Safety factor	γ_S	1,25	-
	Poisson´s ratio steel	v_S	0,3	-
Geometry	Outer radius	r_a	1,5	m
Pressure	Internal pressure from pressure storage	p_i	15	MPa
	Overburden	h	200	m
	Safety factor	γ_h	1,5	-
Temperature	Curing temperature fill concrete	T_B	35	C°
	Lowest air temperature underground	T_L	8	C°
	Temperature rock mass	T_F	8	C°
	Temperature expansion coefficient rock mass	$\alpha_{F,T}$	1,00E-05	K^{-1}
	Temperature expansion coefficient steel	$\alpha_{S,T}$	1,00E-05	K^{-1}
	Increment size		0,001	m

Figure 18: Input parameters for the design of the steel lining according to Seeber [27]

A given p_i of the storage results in a minimum thickness of the steel lining for a given geology. The thickness depends on p_i, V_F and the maximum allowable strain of the steel (ε_{zul}), which depends on the steel grade and is listed in Table 12. Seeber's load-line diagram and the results from the analytical steel lining design can be seen in **Fehler! Verweisquelle konnte nicht gefunden werden.**.
The achieved results depending on the chosen input parameters according to the analytical method from Seeber for the design of a steel lining, which are calculated by the generated excel-sheet from [27], can be seen in Table 4, where γ_s is the safety factor of steel, r_a is the outer radius of the storage, t is the calculated steel lining thickness, ΔT is the temperature difference for the temperature gap, $\varepsilon_{\Delta T}$ is the strain at ΔT , h is the rock overburden above the storage, $p_{i,plan}$ is the planned internal pressure, $p_{S,plan}$ is the planned internal pressure share of the steel lining, $p_{F,plan}$ is the planned internal pressure share of the rock mass, ε_{plan} is the strain at $p_{i,plan}$, $p_{i,max}$ is the maximum allowed internal pressure

to be taken up by the steel lining, $p_{S,max}$ is the maximum internal pressure share of the steel lining, $p_{F,max}$ is the maximum internal pressure share of the rock mass, ε_{zul} is the maximum allowed strain of the steel lining, E_s is the Young's modulus of steel, E_F is the Young's modulus of the rock mass and V_F is the deformation modulus of rock mass.

Table 4: Achieved results and chosen input parameters according to the analytical method from Seeber for a steel lining [27]

γ_s	1.25	h	200 m	relevant for dimensioning: internal pressure			
r_a	1.50 m	$p_{i,plan}$	15.00 MPa	$p_{i,max}$	15.10 MPa	E_s	210 GPa
t	42 mm	$p_{S,plan}$	10.24 MPa	$p_{S,max}$	10.30 MPa	E_F	23.08 GPa
ΔT	27 K	$p_{F,plan}$	4.76 MPa	$p_{F,max}$	4.79 MPa	V_F	4.62 GPa
$\varepsilon_{\Delta T}$	0.00036	ε_{plan}	0.00159	ε_{zul}	0.00159	steel grade S460	

Steel lining thickness (t) is a combination of the necessary thickness to take up p_i and an additional thickness (Δt) because of the temperature difference between the curing temperature of the concrete and the lowest air temperature of the storage. A contraction of the steel results in a gap between the concrete and the steel and Δt is needed to take up the extra deformation of the steel to bridge the gap. [3]
The thickness t is calculated using the following Equation (4): [3]

$$t = \frac{p_i - (V_F * \frac{m}{1+m} - \varepsilon_{zul})}{\frac{f_{y,k}}{\gamma_s} * r_a} + \Delta t, \tag{4}$$

where p_i is the internal pressure, V_F is the deformation modulus of the rock mass, m is the transverse strain number (Querdehnungszahl), ε_{zul} is the maximum allowable strain of the steel, $f_{y,k}$ is the characteristic yield strength of the steel, γ_s is the safety factor for steel, r_a is the outer radius of the storage and Δt is the additional steel lining thickness.
The additional thickness Δt is calculated with Equation (5): [3]

$$\Delta t = \frac{r_a}{\frac{f_{y,k}}{\gamma_s}} * (\varepsilon_{\Delta T} * V_F * \frac{m}{1+m}), \tag{5}$$

where r_a is the outer radius of the storage, $f_{y,k}$ is the characteristic yield strength of the steel, γ_s is the safety factor for steel, $\varepsilon_{\Delta T}$ is the total temperature strain, V_F is the deformation modulus of the rock mass and m is the transverse strain number.
The numerical simulation neglects the temperature influence, therefore, Δt is not considered.

The purpose of the comparison is to make a statement about the Seeber steel lining thickness requirements in terms of meeting the given criterion for ε_{zul}.

Plastic numerical simulation

The comparison process was also done for a steel lining with plastic material behaviour under uniform in-situ stress with a magnitude of 5 MPa and the generated results were compared with the results of the elastic steel lining.

7.2.3 Gap injection influence on the surrounding rock mass

The gap injection acts as a hydrostatic pressure in the gap between the concrete lining and the surrounding rock mass or primary support and is needed to induce compressive forces into the concrete lining. At the same time, it strains the surrounding rock mass and changes the secondary stress state of the rock depending on the magnitude of $p_{v,0}$.

A certain magnitude of p_v is needed to achieve a necessary pre-stressing of the concrete. Losses of the pre-stressing pressure must be added to p_v to get $p_{v,0}$. [3]

E_{rm} and the in-situ stress conditions influence the deformation behaviour of the rock mass, caused by $p_{v,0}$. An exceedance of the principal stress as well as the tensile strength of the rock mass during the gap injection process causes a failure of the rock mass. Failure scenarios like fracturing, hydraulic jacking or opening of existing joints can occur. A potential rock mass failure during the injection process is simulated using $p_{v,0}$ as internal pressure of the unlined storage. RS2 simulates the rock mass as a continuum and therefore only fracturing of the surrounding rock mass can be simulated.
The maximum $p_{v,0}$ for each p_i of 4, 7 and 10 MPa and each rock type are chosen for the simulation and listed in Table 5. Tuff 2 is neglected in the simulation of the gap injection influence because a necessary unexcavated storage has already some plastic failure without implementing $p_{v,0}$, due to the low rock mass strength.

Table 5: Summary of the maximum $p_{v,0}$ for each rock type and p_i

Rock type	Maximum value of $p_{v,0}$ for each magnitude of p_i and rock type		
	p_i: 4 MPa	p_i: 7 MPa	p_i: 10 MPa
Sauberger Kalk	6.50 MPa	9.09 MPa	11.67 MPa
Ankerit	6.28 MPa	7.92 MPa	9.56 MPa
Tuff 1	6.14 MPa	8.72 MPa	11.31 MPa
Rock mass 1	6.54 MPa	8.70 MPa	10.86 MPa
Rock mass 2	6.56 MPa	8.94 MPa	11.32 MPa

7.2.4 In-situ stress influence on the design of the storage lining

Different in-situ stress conditions influence the behaviour of the lining during operation. The significance of the influence is determined for the pre-stressed concrete and steel lining. Seeber assumes that the in-situ stress and deformation conditions are determined by the TIWAG radial press during the excavation of the tunnel [3]. If these in-situ tests are not available, the influence on the dimensioning of the lining must be determined in the design because an accurate prediction of the in-situ stress conditions is not possible. Excavation of the storage changes the state of the in-situ stress from primary to secondary. The tangential stress at the boundary of the excavation (σ_t) is of main interest for the design of the storage. Low magnitudes of σ_t after excavation of the tunnel can lead to tensile failure of the rock mass during the gap injection process or operation of the storage. Equation (6) from Kirsch is a simplified version of the equation 6.18 from Brady and Brown [28]. It is used to calculate σ_t for a circular tunnel with elastic isotropic rock mass behaviour. Input parameters for Equation (6) can be seen in Figure 19.

$$\sigma_\theta = \frac{(\sigma_1+\sigma_2)}{2} * \left(1+\frac{a^2}{r^2}\right) - \frac{(\sigma_1-\sigma_2)}{2} * \left(1+3*\frac{a^4}{r^4}\right) * \cos 2\theta, \qquad (6)$$

In Equation (6) σ_θ is the tangential stress at the tunnel boundary, σ_1 is the major principal stress, σ_2 is the minor principal stress, a is the outer tunnel radius, r is the considered distance from the centre of the tunnel and θ is the angle from the principal stress field.

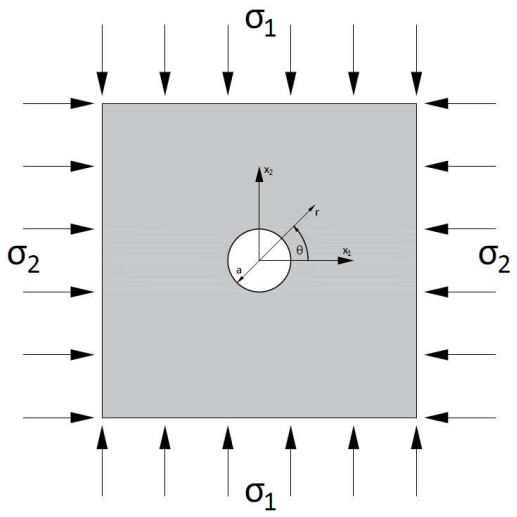

Figure 19: Graphical display of the input parameters for the Kirsch equations

Equation (6) is used to calculate σ_t with different side pressure coefficients (K_0) and a fixed vertical stress (σ_v) of 5 MPa and the results are presented in Figure 20.

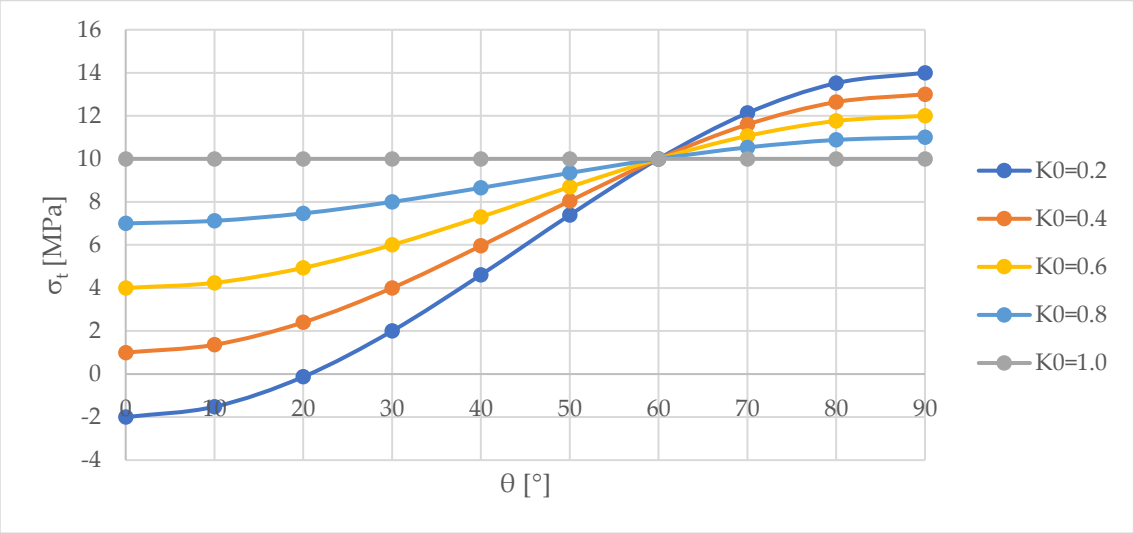

Figure 20: Tangential stress at the boundary of the storage (σ_t) for different side pressure coefficients (K_0) and a fixed primary vertical stress (σ_v)

For a K_0 with a magnitude smaller than 0.5, σ_t in the crown gets negative or nearly zero. The outwards acting component of $p_{v,0}$ during the gap injection process and p_i during the operation of the storage will further change the magnitude of σ_t and can cause an opening of existing joints if σ_t gets negative and cause tensile cracks if σ_t in the crown exceeds the tensile strength of the rock. Failed rock mass with residual strength and stiffness parameters should be avoided in the design of the storage because it prevents a uniform pre-stressing of the concrete lining and a unform strain of the steel lining.

Pre-stressed concrete lining

Depending on the tensile strength of the rock as well as on the ratio between σ_3 and the summed up radial loading of p_i and $p_{v,0}$, failure of the rock mass can occur. The residual stiffness in the plastic zone of the rock mass causes a peak value of the total displacement in this area. A non-uniform deformation of the pre-stressed concrete lining during operation can lead to a failure of the lining because concrete has a strain capacity of only 0.1 ‰ before it fails. The behaviour of the concrete lining was investigated for seven different in-situ stress conditions and a p_i of 4, 7 and 10 MPa for every rock type

Steel lining

Seeber does not consider a sliding layer between the steel lining and the backfilling concrete of the storage. Therefore, a non-uniform deformation of the storage boundary will lead to peaks of the strain and loading of the steel in the areas of higher radial displacements, which can possibly exceed the strength capacity of the steel lining. Three different in-situ stress conditions were considered to investigate the resistance of the steel lining against a potential failure due to excessive elongation.

7.3 Geotechnical data

A constitutive model for intact rock and rock mass is important for a numerical analysis in the field of rock engineering. Mohr-Coulomb and Hoek-Brown are typically used as failure criteria in a numerical model. [25, p. 320]
Sauberger Kalk, Tuff 1, Tuff 2, Ankerit, Rock mass 1 and Rock mass 2 are used as rock types in the numerical analysis of the hydrogen storage. Peak strength and stiffness parameters for each rock type are taken from different resources expected Rock mass 1 and Rock mass 2, which are invented for the calibration process. Residual strength parameters are chosen to represent the failed rock mass realistically.
The input parameter E_{rm} was calculated for Sauberger Kalk, Ankerit, Rock mass 1 and Rock mass 2 using Equation (7) from Hoek and Diederichs: [29]

$$E_{rm} = E_i * (0.02 + \frac{1-{}^{D}/_{2}}{1+e^{({}^{(60+15D-GSI)}/_{11})}}, \tag{7}$$

where GSI is the geological strength index, D is the disturbance factor (Auflockerungsfaktor) and E_i is the intact rock modulus. The calculation of E_{rm} for the named rock types can be found in the appendix Chapter A.
Hoek (1994) and Hoek et al. (1995) introduced the geological strength index (GSI) for the rock mass classification. [30, p. 6] Hoek et al. introduced 2002 the disturbance factor D to estimate the rock mass damage caused by blasting and stress relief. [29, p. 210]

Sauberger Kalk

The rock mechanical data for Sauberger Kalk can be found in Table 6 and is taken from the geomechanically report, which was prepared for the tender project of the ZaB research facility [31].
Used abbreviations for the rock mechanical parameters are:

- UCS for uniaxial compressive strength
- GSI for geological strength index
- m_i for the Hoek-Brown intact rock material constant for intact rock
- ν for the Poisson's ratio
- c for the cohesion (input for Mohr-Coulomb failure criterion)
- φ for the internal friction angle (input for Mohr-Coulomb failure criterion)
- E_i for the Young's modulus of the intact rock
- E_{rm} for the rock mass modulus

Damaged samples for testing have a large effect on the measured values of the intact rock modulus but do not significantly affect the intact rock strength. Therefore, the strength can be considered as more reliable and is used for the calculation of the Young's modulus of the intact rock (E_i) for Sauberger Kalk by using Equation (8): [29, p. 208]

$$E_i = MR * \sigma_{ci} = 500 * 63 = 31.5, \tag{8}$$

where σ_{ci} is the uniaxial compressive strength of the intact rock, from [31], and MR is the expected modulus ratio for limestone, from [32].

Table 6: Intact rock and rock mass parameters for Sauberger Kalk

Sauberger Kalk					
Intact rock parameters			Rock mass parameters		
UCS	63	[MPa]	GSI	70	[-]
m_i	14	[-]	c	12	[MPa]
ν	0.19	[-]	φ	36	[°]
E_i	31.5	[GPa]	E_{rm}	23.08	[GPa]
Residual strength parameters for the Hoek Brown criterion					
m_i	10	[-]	GSI	50	[-]

Tuff 1 and Tuff 2

The intact rock and rock mass parameters for Tuff 1 and Tuff 2 are listed in Table 7 and are taken from the Global – Geotechnical – Technical Report for the Brisbane Airport Link [33].

Table 7: Intact rock and rock mass parameters for Tuff 1 and Tuff 2

Tuff 1					
Intact rock parameters			Rock mass parameters		
UCS	65	[MPa]	GSI	80	[-]
m_i	13	[-]	c	4.5	[MPa]
ν	0.2	[-]	φ	60	[°]
E_i	22	[GPa]	E_{rm}	17.5	[GPa]
Residual strength parameters for the Hoek Brown criterion					
m_i	8	[-]	GSI	70	[-]
Tuff 2					
Intact rock parameters			Rock mass parameters		
UCS	50	[MPa]	GSI	70	[-]
m_i	13	[-]	c	-	[MPa]
ν	0.2	[-]	φ	-	[°]
E_i	15	[GPa]	E_{rm}	8	[GPa]
Residual strength parameters for the Hoek Brown criterion					
m_i	8	[-]	GSI	50	[-]

Rock mass 1 and Rock mass 2

These rock types were chosen for a higher accuracy of the calibration of the numerical model based on the calculation method from Seeber. Strength and stiffness parameters from Rock mass 1 and Rock mass 2 can be found in Table 8 and lay between those from Sauberger Kalk and Ankerit, to guarantee an adequate distribution of the geotechnical input parameters.

Table 8: Intact rock and rock mass parameters for Rock mass 1 and Rock mass 2

Rock mass 1					
Intact rock parameters			Rock mass parameters		
UCS	80	[MPa]	GSI	75	[-]
m_i	12	[-]	c	-	[MPa]
ν	0.19	[-]	φ	-	[°]
E_i	50	[GPa]	E_{rm}	40.82	[GPa]
Residual strength parameters for the Hoek Brown criterion					
m_i	8	[-]	GSI	55	[-]
Rock mass 2					
Intact rock parameters			Rock mass parameters		
UCS	70	[MPa]	GSI	70	[-]
m_i	11	[-]	c	-	[MPa]
ν	0.25	[-]	φ	-	[°]
E_i	45	[GPa]	E_{rm}	32.98	[GPa]
Residual strength parameters for the Hoek Brown criterion					
m_i	7	[-]	GSI	50	[-]

Ankerit

The geotechnical data for Ankerit is shown in Table 9 and is taken from the geomechanically report, which was prepared for the tender project of the ZaB research facility [31].

Table 9: Intact rock and rock mass parameters for Ankerit

Ankerit					
Intact rock parameters			Rock mass parameters		
UCS	140	[MPa]	GSI	82.5	[-]
m_i	14	[-]	c	16	[MPa]
ν	0.21	[-]	φ	40	[°]
E_i	81	[GPa]	E_{rm}	73.34	[GPa]
Residual strength parameters for the Hoek Brown criterion					
m_i	10	[-]	GSI	60	[-]

The program RS Data is used for the analysis of strength data from rock and soil. Linear and non-linear strength envelopes and multiple physical parameters can be determined. Principal stress envelopes are used to simulate the behaviour of an underground excavation. Generalized Hoek-Brown and Mohr-Coulomb are two of the utilized strength models in RS Data, which can be used for rock strength envelopes. Determined strength properties from RS Data are suitable input parameters for numerical analysis programs like RS2. [34] The principal stress plot for all six rock types is shown in Figure 21 and the determined tensile strength for each rock can be taken from Table 10.

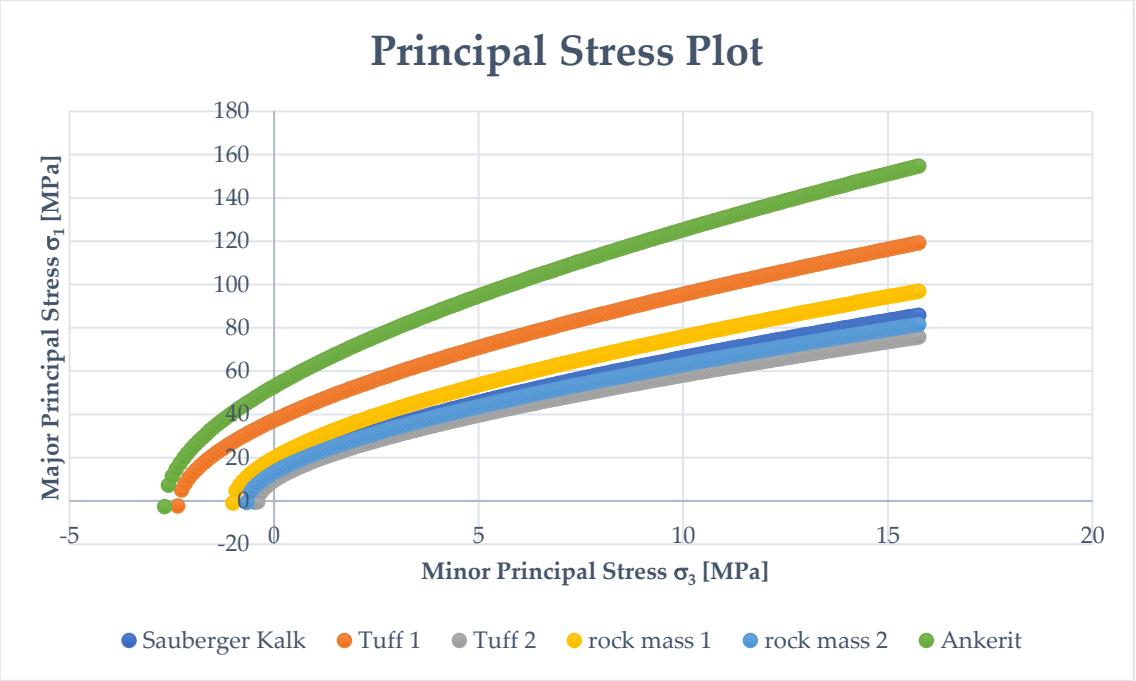

Figure 21: Hoek-Brown failure curves shown in a principal stress plot for all used rock types

Table 10: Tensile strength of the intact rock according to the Hoek-Brown criterion for all used rock types

Tensile strength of the intact rock		
Sauberger Kalk	0.47	[MPa]
Ankerit	2.67	[MPa]
Tuff 1	2.35	[MPa]
Tuff 2	0.40	[MPa]
Rock mass 1	1.01	[MPa]
Rock mass 2	0.66	[MPa]

Hoek-Brown failure criterion

Research about the brittle failure of intact rock (Hoek, 1965) and model studies of jointed rock mass behaviour (Brown, 1970) resulted in the Hoek-Brown criterion. The rock mass characterisation is based on the GSI, which was developed from Hoek (1994) and Hoek et al. (1995), to link field gained engineering geology observations to the failure criterion. The estimation of the strength and deformation of a jointed rock mass with the Hoek-Brown failure criterion and the GSI value is widely accepted and used. [35, p. 445]
Defects like micro-cracks in the material are the origin of the failure from brittle material like rock, concrete and ceramic. Based on the nonlinear failure criterion from Griffith, Hoek and Brown (1980a, b) developed an empirical Equation (9), which fits to a wide range of intact rock triaxial tests: [35, p. 446]

$$\sigma_1 = \sigma_3 + \sigma_{ci} * \sqrt{m_i * \frac{\sigma_3}{\sigma_1} + 1}, \quad (9)$$

where σ_1 is the major principal stress, σ_3 is the minor principal stress, σ_{ci} is the unconfined compressive strength and m_i is a material constant for intact rock.

Generalized Hoek-Brown criterion

Hoek (1994) and Hoek et al. (1995) developed the Generalized Hoek-Brown criterion to estimate the strength of rock mass by using the following Equation (10): [35, p. 446]

$$\sigma_1 = \sigma_3 + \sigma_{ci} * (m_b * \frac{\sigma_3}{\sigma_{ci}} + s)^a, \tag{10}$$

where σ_1 and σ_3 are the major and minor principal stresses, σ_{ci} is the unconfined compressive strength and m_b, s and a are material constants for the rock mass.

The rock mass material constants m_b, s, and a can be calculated with Equations (11), (12) and (13): [35, p. 446]

$$m_b = m_i * e^{\left[\frac{GSI-100}{28-14D}\right]} \tag{11}$$

$$s = e^{\left[\frac{GSI-100}{9-3D}\right]} \tag{12}$$

$$a = \frac{1}{2} + \frac{1}{6} * (e^{-\frac{GSI}{15}} - e^{-\frac{20}{3}}), \tag{13}$$

where m_i is a material constant for intact rock, GSI is the geological strength index and D is the disturbance factor.

The disturbance factor (D) depends on the damage, which is caused by blasting and stress relaxation. Equations for m_b, s and a are suitable for rock masses with low to moderate confining stress. [35, p. 446] The scale of the failure curve in a σ_1 - σ_3 diagram is dominated by σ_{ci} and the shape of the curve is defined by the constants m_b, s and a. [35, p. 447]
The Hoek-Brown criterion can only be applied for shear and ductile rock mass failure. A massive rock with high confinement stress or a high GSI value is not suitable for the application of the failure criterion. [35, pp. 447-449]

7.4 Liner properties

7.4.1 Parameters for the concrete lining

The strength and stiffness parameters of the used concrete were taken from [36], can be found in Table 11 and must be the same as used for the analytical calculation from Seeber. A peak tensile strength of 1 MPa was chosen for every concrete quality, to avoid failure of the concrete in the lining installation stage of the numerical analysis.

Residual strength of the concrete is fixed with zero and is therefore neglected. A partial safety factor for the concrete (γ_c) with 1.3 is fixed by Seeber and considered in the simulation [3].

Used abbreviations for the concrete parameters are:

- f_{ck} for the characteristic value of the cylinder compressive strength of the concrete
- f_{cd} for the design value of the cylinder compressive strength of the concrete
- f_{cm} for the mean value of the cylinder compressive strength of the concrete
- E_{cm} for the value of the Young's modulus of the concrete

Table 11: Concrete compressive strength and stiffness parameters for the concrete qualities C25/30, C30/37, C35/45 and C40/50

Concrete parameters				
Concrete quality	C25/30	C30/37	C35/45	C40/50
f_{ck} [MPa]	25.00	30.00	35.00	40.00
f_{cd} [MPa]	16.70	20.00	23.30	26.70
f_{cm} [MPa]	33.00	38.00	43.00	48.00
f_{cm}/γ_c [MPa]	25.38	29.23	33.08	36.92
E_{cm} [GPa]	31	33	34	35

Three different concrete thicknesses of 0.1 m, 0.2 m and 0.3 m were chosen for the simulation of the storage with an outer diameter of 3.0 m.

7.4.2 Parameters for the steel lining

Three different high strength steel grades were chosen for the comparison of the lining thickness from Seeber and the numerical analysis. The strength of each steel grade was taken from [37] and stiffness and Poisson's ratio were taken from [38].
Design values for the yield strength of the steel ($f_{y,d}$) were calculated by dividing the characteristic yield strength ($f_{y,k}$) with the safety factor (γ_s), which has a fixed value of 1.25. [3]

The maximum allowable strain of the steel (ε_{zul}) is calculated with Hooke's law, which is described in Equation (14):

$$\sigma = E * \varepsilon \rightarrow \varepsilon = \frac{\sigma}{E} = \frac{f_{y,d}}{E}, \tag{14}$$

where E is the Young's modulus from steel, σ is the normal stress, $f_{y,d}$ is the design yield strength of the steel and ε is the normal strain. All the calculations for the steel lining can be found in the appendix Chapter B.1 and the steel parameters for the steel grades S460, S550 and S690 can be found in Table 12.

Table 12: Design value of the yield strength, Young's modulus, ν and ε_{zul} of steel for the high strength steel grades S690, S550 and S460

Steel grade	$f_{y,d}$ [MPa]	Young's modulus [GPa]	ν [-]	ε_{zul} [‰]
S690	552	210	0.3	2.63
S550	440	210	0.3	2.10
S460	368	210	0.3	1.75

7.4.3 Parameters of the gap injection material

A cement suspension is pumped into the gap during the gap injection process. The injection material is considered as elastic and has fluid-like properties in the gap injection stage and pre-stressing stage of the numerical analysis. At the time, where p_i is applied during operation, the gap injection material can be regarded as solid with different properties. The calibration of the model is done through a variation of E_{gap} in the gap injection and pre-stressing stage and fixation of the solid gap injection material stiffness ($E_{gap,hardened}$) with 2000 MPa. Strength parameters like cohesion (c) and friction angle (φ) are not relevant due to the elastic behaviour of the gap injection material but are also fixed for the gap injection material and can be seen in Table 13, as well as stiffness and ν of the material.

Table 13: Strength parameters c and φ as well as stiffness parameters Young's modulus and ν for the soft and hardened gap injection material

Soft gap injection material			Hardened gap injection material		
c	0.1	[MPa]	c	2	[MPa]
φ	10	[°]	φ	25	[°]
ν	0.49	[-]	ν	0.2	[-]
E_{gap}	variable	[MPa]	$E_{gap,hardened}$	2,000	[MPa]

The variable E_{gap} depends on the stiffness (E_{cm}) and thickness of the concrete lining, E_{rm} as well as on p_i. A determined E_{gap} for a rock type, p_i and concrete quality through the calibration process is used for the plastic model to find out the in-situ stress influence.

7.4.4 Parameters for the shotcrete lining

Simulation of the in-situ stress influence was carried out with a numerical simulation considering plastic material behaviour of the lining. The real build-up of the lining, with a shotcrete as primary support for the excavation, was therefore taken into account. A plastic behaviour is chosen for the shotcrete to avoid unrealistic tensile forces inside the shotcrete. Selected parameters for the shotcrete are listed in Table 14.

Table 14: UCS, Young's modulus, thickness and ν for shotcrete

UCS [MPa]	Young's modulus [MPa]	Thickness [m]	ν [-]
25	15,000	0.1	0.2

7.5 Procedure of the numerical analysis

A Pseudo-model is the basic of every numerical model and consists of a hand drawn sketch of the model, in which all the gathered information about the project is visualized. Geotechnical data like core data from a geotechnical site investigation program are converted into material boundaries of the model as well as possible fault zones and joints. Knowledge about the construction and excavation method is used for the implementation as stages.

7.5.1 Modell set up

Model geometry, grid generation and discretisation

The external boundaries of the model are typically three to five times of the diameter away from the excavation boundary. The distance of the external boundary for the simulation of the hydrogen storage was chosen with six times of the diameter because of the high internal pressure, which results in a deep influencing zone in the surrounding rock mass.

Boundary Conditions

The restraints of the external boundaries for deep tunnels are standardised fixed on every site. A necessary movement of the boundary like a subsidence is not foreseen and does not have to be taken care of.

Geometry

An outer diameter of the circular cross-section of the storage with 3.0 m is fixed from the pre-defined design of the pilot hydrogen storage at ZaB.

Material Properties

The material properties for every rock type can be found in Chapter 7.3. Seeber considered the rock mass as elastic, which is also implemented in the calibration models for the pre-stressed concrete and the comparison models for the steel lining. Plastic material behaviour for the rock mass is necessary to find out the in-situ stress and gap injection influence.

Stresses

The field stress acts on the external boundaries of the numerical model and simulates the in-situ stress condition. Different values of the K_0-factor as well as magnitudes of the stresses are chosen for the investigation of the in-situ stress influence.
With an overburden of approximately 200 m for the location of the hydrogen storage and an average unit weight of 25 kN/m³, the vertical stress (σ_v) at the depth of the storage can be assumed with 5 MPa. Additional body forces of the elements are not considered.

7.5.2 Running of the simulation

The set up of the RS2 model is fixed in the project settings of the model. Stress analysis, units, solver options and stages are sections of the project settings, which must be defined before running the simulation. [39] Most of the settings for the stress analysis are set by default like the maximum number of iterations with 500, number of load steps with automatic and convergence type with comprehensive. Only the tolerance is changed from the default value of 0.001 to 0.01. [40]
The tolerance is a dimensionless parameter, which defines the allowable unbalanced energy in the model. A suggested range of the value is between 0.001 and 0.01 and with an increase of the tolerance, the needed time to achieve convergence and accuracy of the solution will decrease. Elastic analyses do not use the tolerance because the solution can be seen as exact and only plasticity analyses need a defined tolerance. [40]
The excavation of the storage is not considered in the numerical simulation because a proper stiffness of the rock mass is required by Seeber to maintain the gap injection pressure. Displacements which occur due to the excavation of the storage are reset to avoid an influence on the results.

Calibration of the pre-stressed concrete model on Seeber

A uniform in-situ stress of 5 MPa is fixed for the calibration. Nevertheless, different in-situ stress magnitudes have no significant influence on the calibration process. Values for the gap injection pressure are calculated with Seeber, like it is described in Chapter 7.2.1. Strength and stiffness parameters for the concrete, gap injection material and rock mass can be found in Chapter 7.3 and 7.4. The whole model was considered as elastic, and an overview of the model set-up is shown in Figure 22.

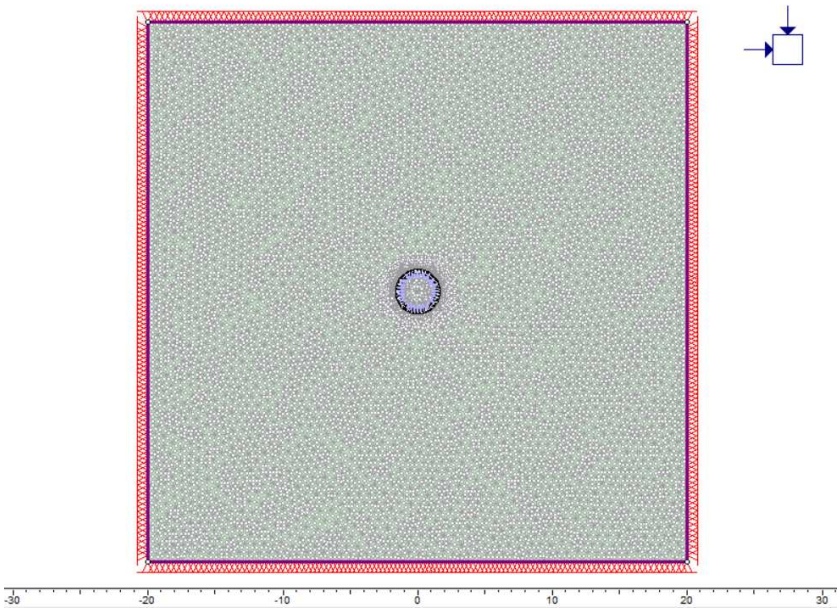

Figure 22: Set up of the numerical model to carry out the calibration process of the pre-stressed concrete lining for Tuff 1

The construction process of the storage, starting with the building of the concrete lining, continuing with the pre-stressing of the lining, through the gap injection and up to the operation of the storage with a certain p_i, was simulated in different stages of the model:

1. **Initial stage:** initialise the stress conditions in the model
2. **Excavation stage:** excavate the tunnel without support
3. **Implementation of the gap injection stage:** install the gap injection material
4. **Lining stage:** installation of the concrete liner
5. **Gap injection stage:** application of the gap injection pressure $p_{v,0}$
6. **Pre-stressing stage:** replacement of $p_{v,0}$ through p_v
7. **Pressurisation stage:** application of p_i

The pre-defined 5 mm thick layer (light blue coloured layer), which can be seen in Figure 23, is modelled between the rock mass (green area) the concrete lining (dark blue coloured dashed line). It represents the pumped in gap injection material and allows two separate loads to act on the outer and inner boundary of the layer, as it can be seen in Figure 26, for a realistic simulation of the gap injection pressure. A uniform load represents the gap injection pressure and the internal pressure of the storage in the numerical simulation, as it is shown in Figure 24 and Figure 25. P_i with a magnitude of 4, 7 and 10 MPa was used for the calibration.

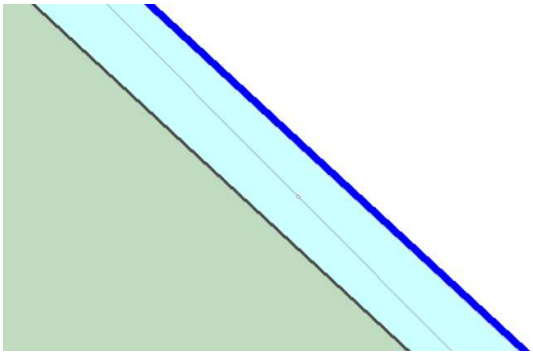

Figure 23: Detail of the pre-defined gap between the concrete lining and the rock mass with the soft gap injection material in the lining stage of the numerical model

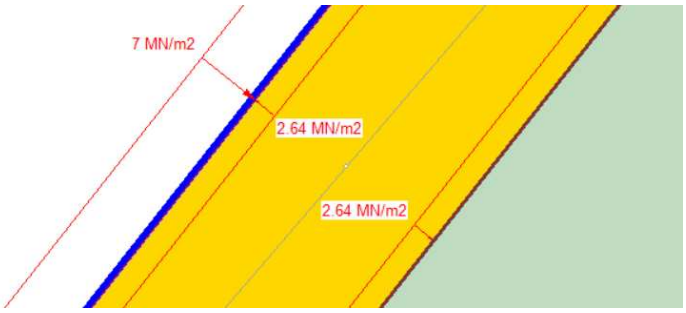

Figure 24: Simulation of p_v with a magnitude of 2.64 MPa inside the pre-defined layer of the hardened gap injection material (yellow coloured layer) and p_i with a magnitude of 7 MPa at the inner surface of the concrete lining of the numerical model

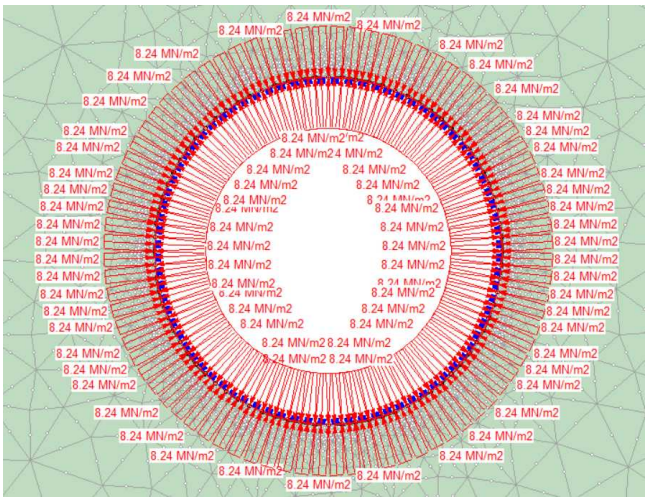

Figure 25 Implementation of $p_{v,0}$ with a magnitude of 8.24 MPa in the gap injection stage

Concrete lining properties like the thickness, strength and stiffness as wells as p_i, $p_{v,0}$, p_v and $E_{gap,hardened}$ are fixed input parameters for each calibration cycle. Only E_{gap} is varied and optimized in the gap injection and pre-stressing stage of the model during the calibration process. Nearly zero but still compressive axial force of the liner after the application of p_i in the pressurisation stage, like it can be seen in Figure 26, is the aim of the calibration. Figure 26 shows the axial force of the modelled liner in the numerical simulation for each stage. The y-axis shows the axial force of each node of the liner and the x-axis shows the position of the node at the unwinding of the circumference as a distance of the liner. E_{gap} has an influence on the deformation behaviour of the pre-defined gap injection material layer and therefore on the amount of induced compressive stress inside the concrete lining caused by the gap injection pressure. Figure 26 shows the different magnitudes of axial force of the pre-stressed concrete lining and every stage after installation. It is clearly visible that a higher value of the acting gap injection pressure leads to an increase of the axial force. P_i reduces the axial force in the pressurisation stage but the calibrated value of E_{gap}, for a given p_v according to Seeber, assures that the axial force remains in a compressive state.

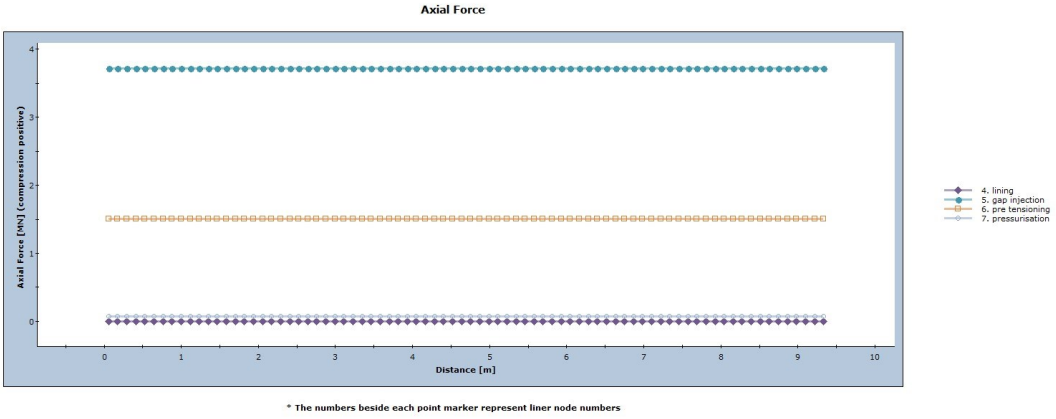

Figure 26: Axial force of the concrete liner at the lining (purple), gap injection (turquoise), pre-stressing (orange) and pressurisation stage (light blue) of the numerical simulation considering uniform in-situ stress conditions and elastic material behaviour

Comparison of the results from the steel lining design

A 3.0 m outer diameter of the circular storage was fixed for every model. Seeber's result is a minimum thickness of the steel lining for a given geology and a certain ε_{zul}. Strength and stiffness parameters of the steel lining and rock mass can be found in Chapter 7.3 and 7.4. The whole model was considered as elastic, and an overview of the model is shown in Figure 27. Uniform in-situ stress with a magnitude of 0.01 MPa was used for the comparison of the results between the numerical simulation and the analytical calculation from Seeber.

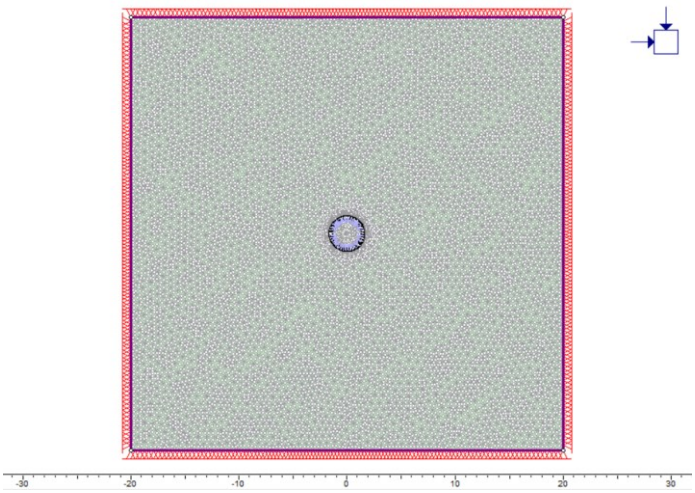

Figure 27: Set up of the numerical model for the comparison of the results from the steel lining design

Construction and operation of the storage are simulated in four stages:

1. **Initial stage:** initialise the stress conditions in the model
2. **Excavation stage:** excavate the tunnel without support
3. **Lining stage:** installation of the steel liner
4. **Pressurisation stage:** application of p_i

The maximum p_i of 10, 15 and 20 MPa was implemented in the pressurisation stage, as it is shown in Figure 30 for a p_i of 15 MPa and the resulting radial displacement of the storage lining was used to calculate a hoop strain (Umfangsdehnung) of the lining and compare it with ε_{zul}.

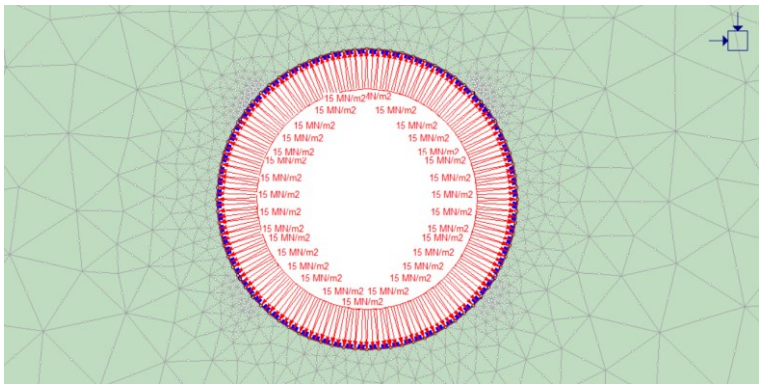

Figure 28: Implementation of p_i with a magnitude of 15 MPa in the pressurisation stage of the numerical model for Tuff 1

Gap injection influence on the surrounding rock mass

The primary function of the gap injection is achieved by the cement suspension, which penetrates the gap between the concrete lining and the rock mass and pre-stresses the concrete lining. On the other hand, the rock mass gets deformed and probably fails due to an exceedance of the tensile or shear strength by the induced stresses in the surrounding rock mass.

An unlined circular storage with a diameter of 3.0 m was pressurised with $p_{v,0}$, which was calculated using the equations from Seeber. The rock mass was modelled with a plastic material behaviour to determine a failed zone around the storage caused by the injection pressure. Uniform and non-uniform in-situ stresses with different magnitudes were used to investigate the gap injection influence on the surrounding rock mass.
The minor principal stress (σ_3) is not allowed to be exceeded by $p_{v,0}$ according to Seeber. To analyse this criterion, additional numerical simulations with different in-situ stress conditions were carried out to investigate a possible exceedance of σ_3 by $p_{v,0}$.

Simulation of the gap injection influence is done in three stages:

1. **Initial stage:** initialise the stress conditions in the model
2. **Excavation stage:** excavate the tunnel without support
3. **Gap injection stage:** application of the gap injection pressure of the storage

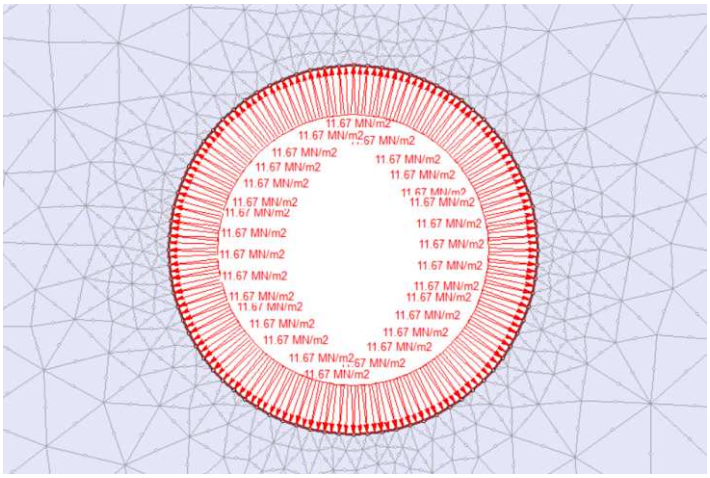

Figure 29: Simulation of the gap injection influence by an unlined storage and an internal pressure with the magnitude of $p_{v,0}$ acting at the storage boundary

In-situ stress influence on the design of the storage lining

The in-situ stress marks an uncertainty in every design and the importance of an accurate estimation must be determined in the design stage. A model sensitivity according to the in-situ stress was the result of a detailed analysis. Variation of the K_0-factor and the magnitude of the in-situ stress was carried out for several numerical models with a steel or pre-stressed concrete lining. Stages of the models were identical to the models, which were used for the calibration of the pre-stressed concrete lining and the comparison of the steel lining. Lining materials and the rock mass were simulated with plastic material behaviour with a certain residual strength, which can be found in Chapter 7.4.

7.6 Confirmation process

Confirmation consists of the interpretation, verification, validation and calibration of the model. It is crucial that the achieved results are interpreted according to their plausibility. Basic knowledge about the expected behaviour is assumed while working with a numerical program. The confirmation process aims to make the model as accurate and realistic as possible by testing the model and compare and observe the results.

7.6.1 Verification

Numerical simulations are employed to address complex systems that cannot be accurately solved using analytical methods. Comparing the results from a numerical model with those obtained from an alternative calculation method, such as an analytical solution, is referred to as verification. It is crucial to understand that only the region where the analytical and numerical solutions align can be considered as verified.

Verification of the elastic numerical models

The σ_1 and σ_3 plots of the numerical simulations were compared with the results from the analytical solution from Kirsch, whereby σ_3 of the numerical model represents σ_2 of the Kirsch equation. Elastic and isotropic rock mass behaviour as well as a circular shaped cross section of the tunnel are the requirements for the application of the Kirsch solution. Equation (6) can be applied to calculate the radial distribution of σ_t and Equation (15) is used to calculate the radial distribution of the radial stress (σ_r) and is a simplification of equation 6.18 from Brady and Brown [28]:

$$\sigma_r = \frac{(\sigma_1+\sigma_2)}{2} * \left(1 - \frac{a^2}{r^2}\right) + \frac{(\sigma_1-\sigma_2)}{2} * \left(1 + 3 * \frac{a^4}{r^4} - 4 * \frac{a^2}{r^2}\right) * \cos 2\theta, \qquad (15)$$

where σ_r is the radial stress around the tunnel, σ_1 is the major principal stress, σ_2 is the minor principal stress, a is the outer tunnel radius, r is the considered distance from the centre of the tunnel and θ is the angle from the principal stress field.

Non-uniform in-situ stress with a magnitude of σ_1 with 5 MPa and σ_2 with 2.5 MPa was chosen for the verification. The resulting radial distribution of σ_r and σ_t in the crown and sidewall until the distance of 5 m from the centre of the storage is shown in Table 15.

Table 15: Distribution of σ_r and σ_t in the crown and sidewall of the storage until a radial distance of 5 m from the centre of the storage according to the Kirsch equations

Stress distribution from σ_r and σ_t in the crown and sidewall of the storage				
Distance r	$\sigma_{r,crown}$	$\sigma_{r,sidewall}$	$\sigma_{t,crown}$	$\sigma_{t,sidewall}$
1.5 m	0.00 MPa	0.00 MPa	2.50 MPa	12.50 MPa
2.0 m	1.26 MPa	2.02 MPa	3.42 MPa	8.30 MPa
2.5 m	2.34 MPa	2.46 MPa	3.36 MPa	6.84 MPa
3.0 m	3.05 MPa	2.58 MPa	3.20 MPa	6.17 MPa
3.5 m	3.52 MPa	2.60 MPa	3.06 MPa	5.82 MPa
4.0 m	3.84 MPa	2.60 MPa	2.95 MPa	5.60 MPa
4.5 m	4.07 MPa	2.59 MPa	2.87 MPa	5.46 MPa
5.0 m	4.24 MPa	2.58 MPa	2.81 MPa	5.37 MPa

A verification was done through an elastic numerical simulation of the excavation of the storage and a primary stress with a σ_1 of 5 MPa and a σ_2 of 2.5 MPa. The resulting secondary stress plot of σ_1 is shown in Figure 30 and of σ_3 can be seen in Figure 31. As the resulting secondary stress plots of the numerical model show almost identical values to those calculated by the Kirsch equations, the verification can be considered successful.

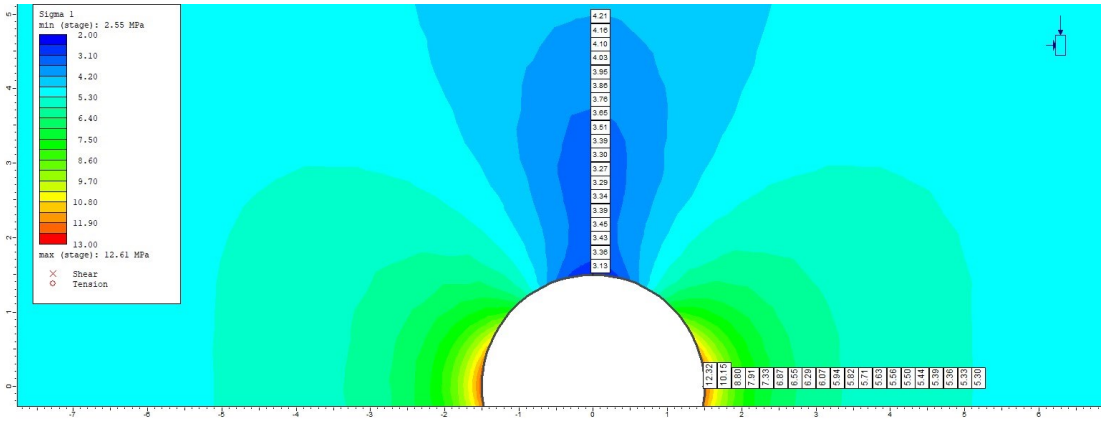

Figure 30: Display of the major principal stress σ_3 of the secondary stress state after excavation of the storage for a primary stress with a σ_1 of 5 MPa and a σ_3 of 2.5 MPa

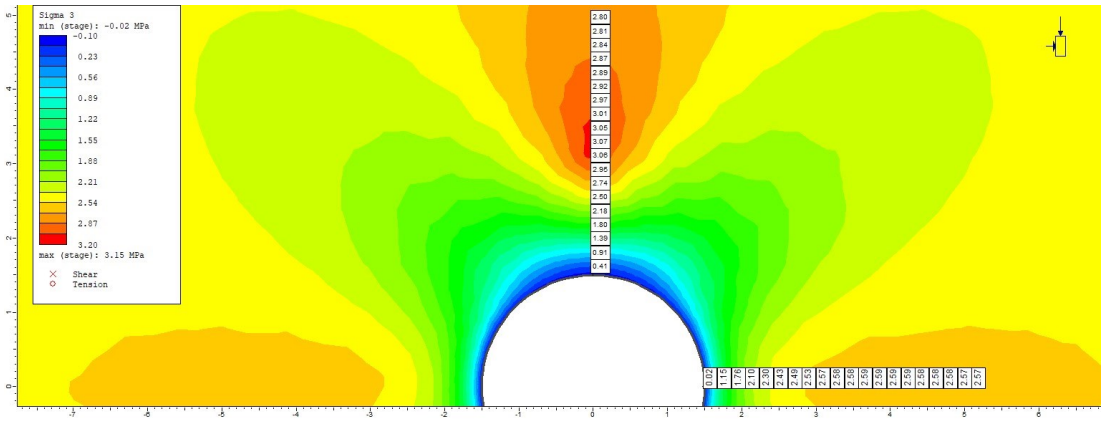

Figure 31: Display of the minor principal stress σ_3 of the secondary stress state after excavation of the storage for a primary stress with a σ_1 of 5 MPa and a σ_3 of 2.5 MPa

7.6.2 Validation

The validation process shows that the model is legitimate by proving that there are no errors in the model and it is consistent. However, only the set-up can be validated and not the results. A change of the model set-up like the used mesh size and boundary conditions should have no significant influence on the results to prove the model as valid.

Mesh-size

A change of the gradation factor as a mesh set-up option was carried out for the numerical model in Rock mass 2 and the resulting strength factor at the excavation boundary and in a depth of 0.3 m can be seen in Figure 32 for a gradation factor of 0.1 and in Figure 33 for a gradation factor of 0.05. The results show no significant difference, and the numerical model can therefore be seen as valid.

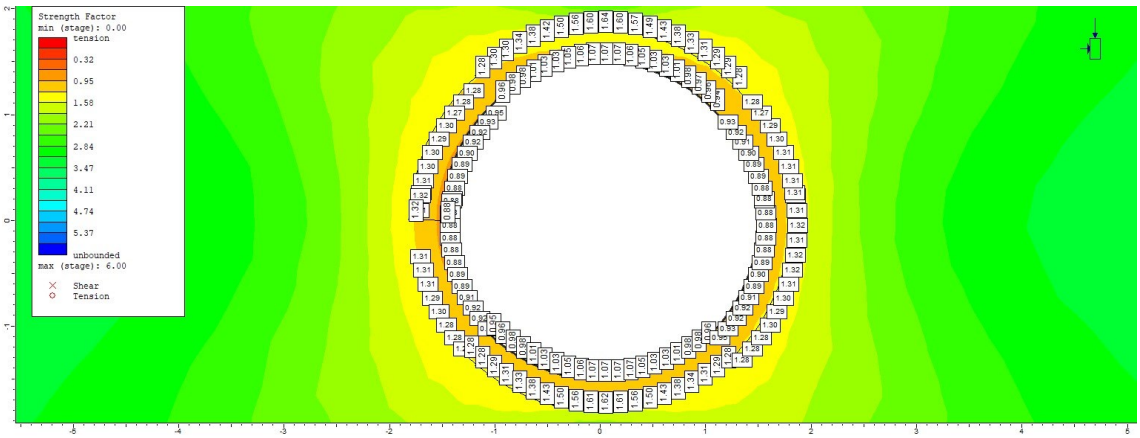

Figure 32: Strength factor at the storage boundary and 0.3 m inside the rock mass around the excavated storage in Rock mass 2 for a non-uniform in-situ stress with a σ_1 of 5 MPa and σ_3 of 2.5 MPa and a mesh set-up with a gradation factor of 0.1

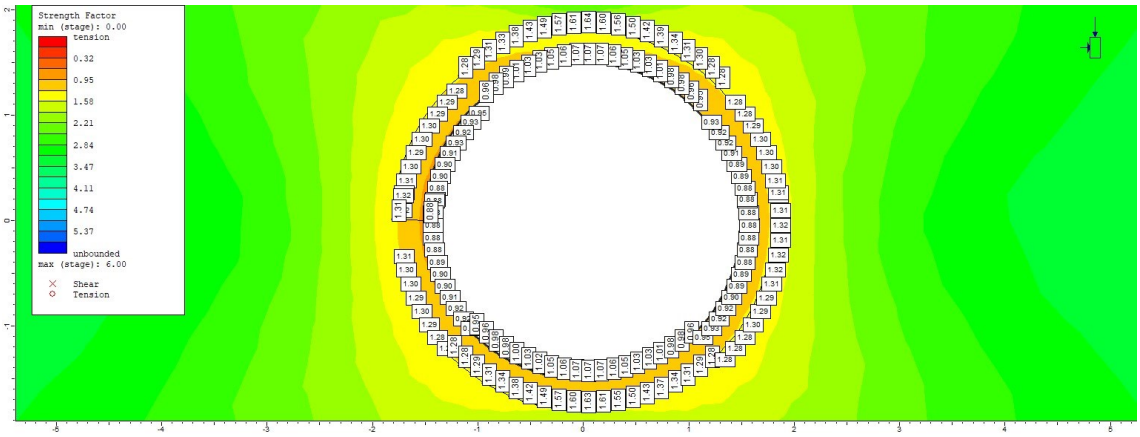

Figure 33: Strength factor at the storage boundary and 0.3 m inside the rock mass around the excavated storage in Rock mass 2 for a non-uniform in-situ stress with a σ_1 of 5 MPa and σ_3 of 2.5 MPa and a mesh set-up with a gradation factor of 0.05

External boundary conditions

The external boundary conditions of all four sides of the numerical model of a deep underground infrastructure facility are standardised fixed because no settlement of the surface is expected and has to be simulated. A comparison of the strength factor in the surrounding rock mass of the storage was carried out for different external boundary conditions. Figure 34 shows the resulting strength factor of the rock mass after excavation from a numerical model with fixed external boundaries.

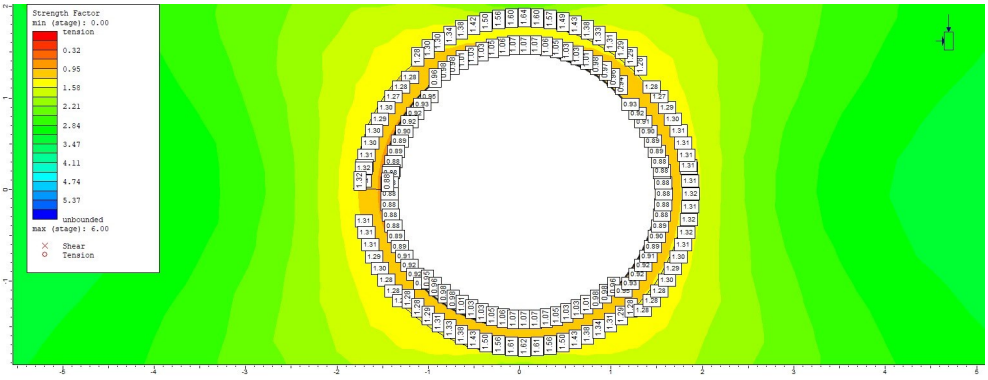

Figure 34: Strength factor for the excavated storage in Rock mass 2 for a non-uniform in-situ stress with a σ_1 of 5 MPa and σ_3 of 2.5 MPa and fixed external boundary of the model

A fixed external boundary at the bottom side of the numerical model and three external boundaries, which allow tangential sliding of the element nodes at the external boundary result in the strength factor distribution shown in Figure 35.

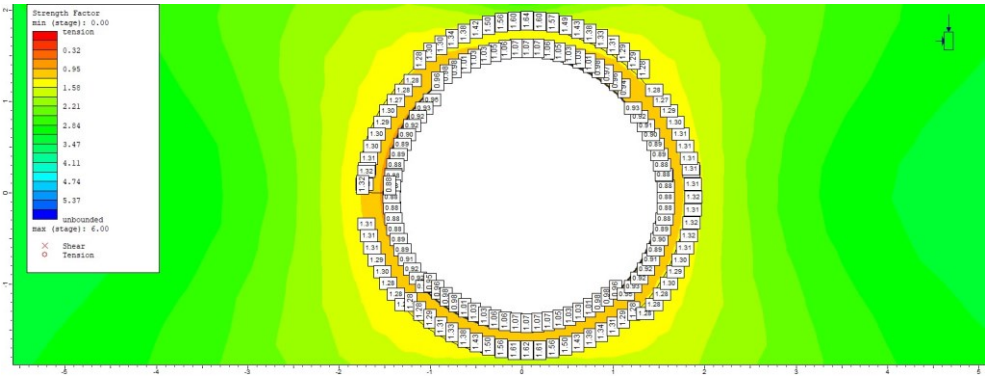

Figure 35: Strength factor for the excavated storage in Rock mass 2 for a non-uniform in-situ stress with a σ_1 of 5 MPa and σ_3 of 2.5 MPa and three roller and on fixed external boundary of the model

The strength factor distributions are identical for both external boundary conditions, confirming the validation of the numerical model.

7.6.3 Calibration

Results of a monitoring concept during the construction and operation of the storage facility can be used to calibrate the numerical model. Adjustments of the model can be done through the interpretation of the differences between the reality and the model, which has advantages for future projects.

7.7 Sensitivity analysis

In the design process of engineering structures, the capacity C and the demand D of an element are linked via the factor of safety (FOS), which is defined as FOS=C/D. If FOS is less than unity, failure of the designed structure is likely to occur.
A sensitivity study is used to give a broader assessment of the risk of failure according to the FOS for a particular design. Significant parameters are varied systematically in multiple calculations over a defined range to investigate their influence on the FOS. Parameters like φ, UCS and the orientation of discontinuities have a range of possible values. These input parameters cannot be predicted precisely and the relative likelihood of a magnitude can be described in a probability density function (PDF). Gaussian distribution is a common PDF for many variables and is therefore mainly used in geotechnical engineering for probabilistic studies. [41]

The aleatory and epestimic uncertainty in geomechanics is the result of the natural variation of the rock properties. Material properties, geometry or external loads can be seen as key parameters for the sensitivity of the model. Input parameters like material boundaries, dilation, mesh size or the failure criterion can be simplified because they have no significant influence. [41]

A sensitivity analysis can be done in a deterministic way by changing the parameters manually. One or multiple parameters can be changed from the medium value to the best and worst case and different combinations can be analysed. Single parameters or combinations can be missed out in the deterministic method. [41]
The probabilistic way is based on statistical methods and needs more and better input parameter sets. Nothing can be missed out with this method and the results are more accurate and robust. [41]

Sensitivity analysis for the calibration process of the pre-stressed concrete lining

The calibration process of the pre-stressed concrete was carried out using elastic numerical models and was build up on a systematic variation of the key parameters like E_{rm}, p_i and the thickness of the concrete lining, to determine the necessary value for E_{gap}. An additional sensitivity analysis for these models was therefore not necessary. The description of the results from the calibration process can be found in Chapter 8.1.

Sensitivity analysis for the comparison of the results from the steel lining design

The comparison of the results of the steel lining between Seeber and the numerical analysis was executed through numerical simulations with an elastic behaviour of the rock mass and lining. Stiffness parameters influence the results of the simulations and can be seen as key parameters of the numerical model. A deterministic change of E_{rm} was done for the sensitivity analysis to investigate the occurred changes of the results. Young's modulus of the steel lining can be seen as fixed, because the properties of the used steel grade are guaranteed to be constant as a result of a standardised manufacturing process.

Rock mass 1, Sauberger Kalk and Tuff 2 were chosen to carry out a sensitivity analysis of the key parameter E_{rm}. The magnitude of E_{rm} was varied by 20% and the changes of the radial displacement was evaluated in Figure 36 and Figure 37.

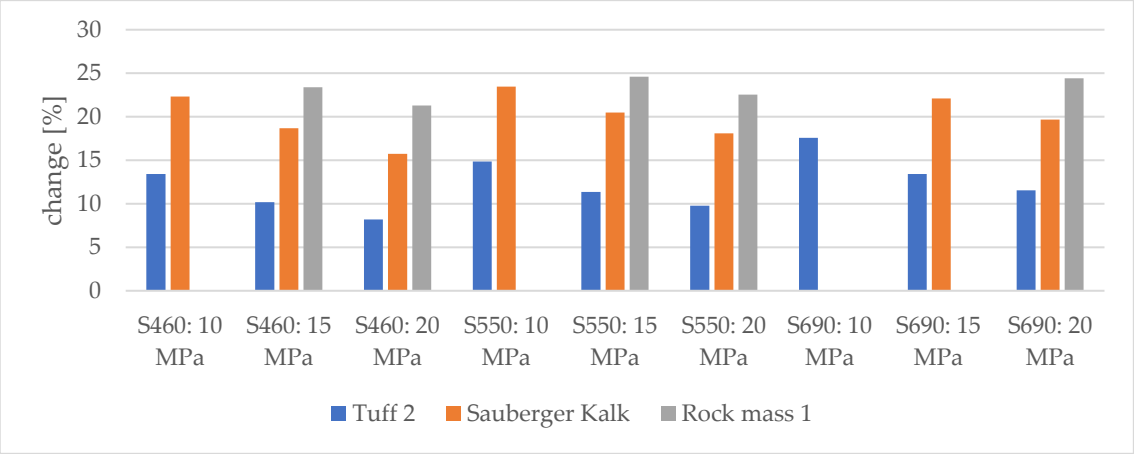

Figure 36: Change of the radial displacement of the steel lined storage boundary after decreasing the magnitude of E_{rm} by 20% for Rock mass 1, Sauberger Kalk and Tuff 2, using steel grades S460, S550 and S690 as well as a p_i of 10, 15 and 20 MPa

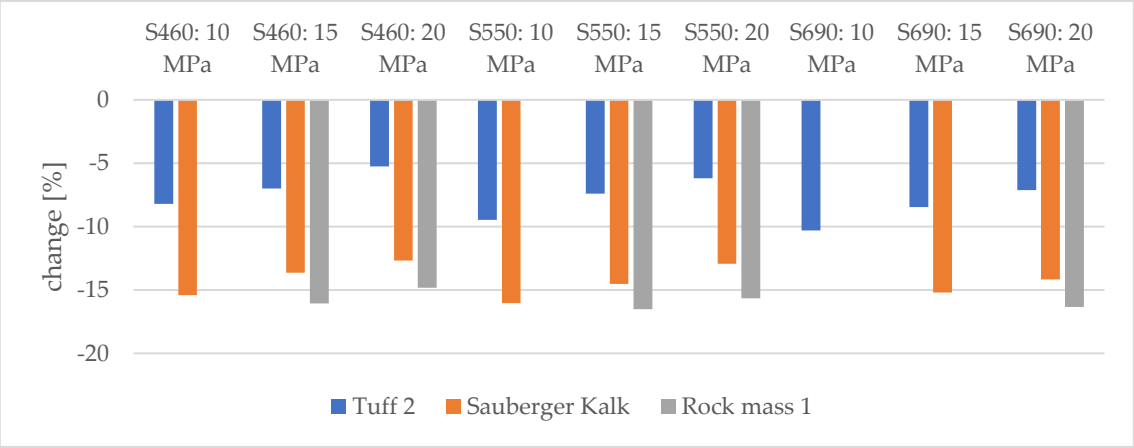

Figure 37: Change of the radial displacement of the steel lined storage boundary after increasing the magnitude of E_{rm} by 20% for Rock mass 1, Sauberger Kalk and Tuff 2, using steel grades S460, S550 and S690 as well as a p_i of 10, 15 and 20 MPa

Increasing radial displacements lead to higher values of the steel strain and higher values of the utilization (μ) of the steel strength capacity. The results for Rock mass 1, Sauberger Kalk and Tuff 2 are presented in Figure 38, Figure 39 and Figure 40 for 80, 100 and 120 percentage of the design value of E_{rm}.
The utilization is calculated by Equation (16)

$$\mu = \frac{\varepsilon_{steel}}{\varepsilon_{zul}}, \tag{16}$$

where μ is the utilization of the steel strength capacity, ε_{steel} is the calculated strain of the steel lining in the numerical simulation, which is shown in the appendix Chapter B.2 and ε_{zul} is the maximum allowable steel strain for each steel grade from Table 12.

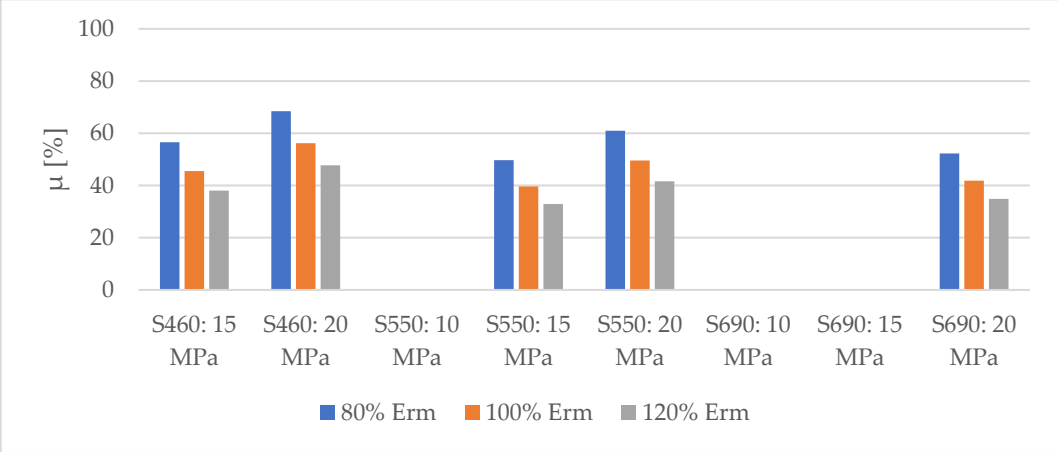

Figure 38: Utilization of the strength capacity of the steel lining for 80%, 100% and 120% of the design value of E_{rm} for Rock mass 1, steel grades S460, S550 and S690 as well as a p_i of 10, 15 and 20 MPa

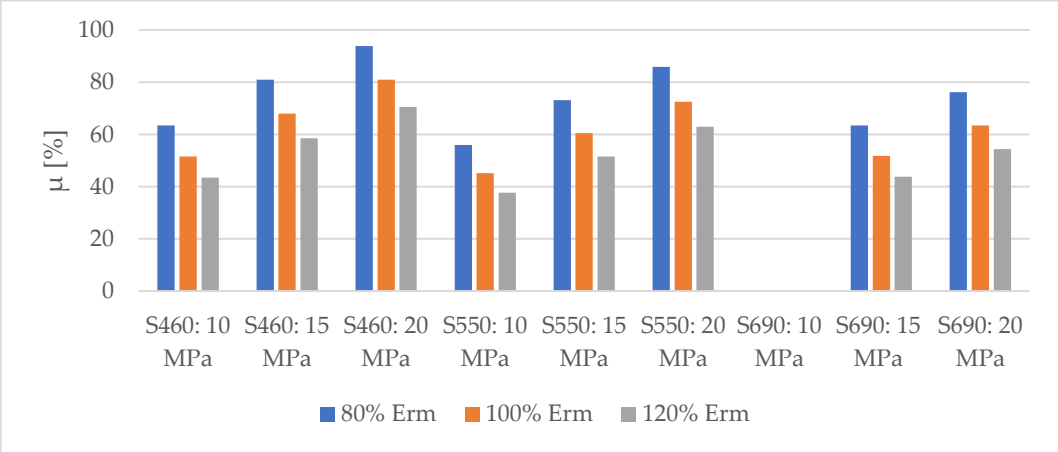

Figure 39: Utilization of the strength capacity of the steel lining for 80%, 100% and 120% of the design value of E_{rm} for Sauberger Kalk, steel grades S460, S550 and S690 as well as a p_i of 10, 15 and 20 MPa

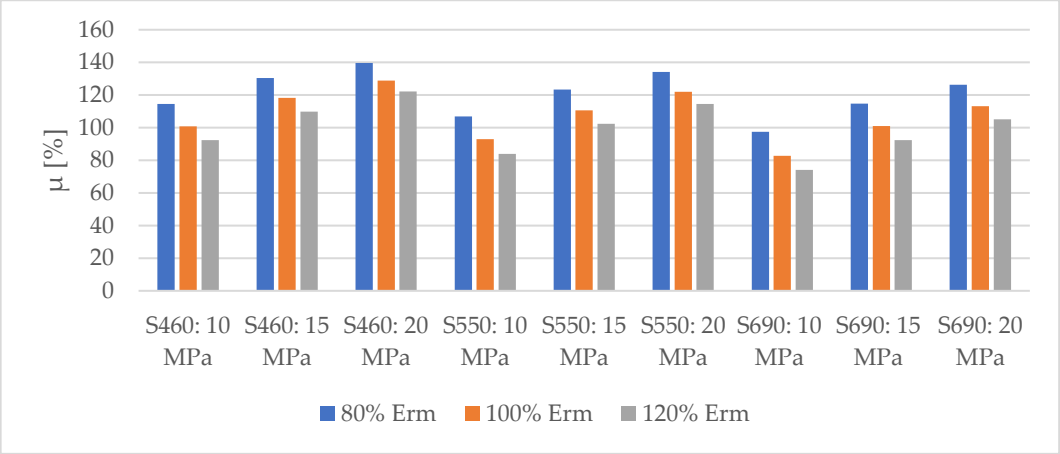

Figure 40: Utilization of the strength capacity of the steel lining for 80%, 100% and 120% of the design value of E_{rm} for Tuff 2, steel grades S460, S550 and S690 as well as a p_i of 10,15 and 20 MPa

A variation of E_{rm} by 20% leads to a change of μ by approximately 10% for every rock type. An increase of μ by 10% can possibly exceed the maxed out capacity of a steel lining and therefore, a systematic change of E_{rm} during the design process is crucial for a successful design.

Sensitivity analysis for the gap injection influence on the surrounding rock mass

The determination of the gap injection influence was performed with several numerical models for each rock type with different in-situ stress conditions and plastic material behaviour. Strength and stiffness parameters of the surrounding rock mass are the key input parameters of the simulation. A separate sensitivity analysis to investigate the influence of the key parameters and in-situ stress was not necessary because the affect of different magnitudes of E_{rm} has already been investigated.

Sensitivity analysis for the in-situ stress influence on the design of the storage

The gained knowledge about the rock mass behaviour for different in-situ stress conditions from the numerical simulations to investigate the gap injection influence can also be applied for the investigation of the in-situ stress influence and substitutes the sensitivity analysis.

8 Results

8.1 Calibration of the pre-stressed concrete

The calibration for a 3.0 m diameter circular storage aims to find the right magnitude of E_{gap} for a given rock mass, p_i and concrete lining thickness. Necessary values for $p_{v,0}$ and p_v are taken from Seeber depending on each rock type, p_i, concrete quality and concrete thickness. An overview of the necessary input parameters as well as the resulting E_{gap} is given in Table 16 for Rock mass 2 and a p_i of 4 MPa. It can be seen that E_{gap} is only changing with the thickness of the concrete lining.

Table 16: Calibrated E_{gap} for Rock mass 2, p_i of 4 MPa, different concrete input parameters like concrete quality, E_{cm} and thickness as well as the Seeber input parameters of $p_{v,0}$ and p_v

Rock mass 2 – p_i of 4 MPa						
Concrete input parameters			Seeber input		gap injection material	
Quality [-]	E_{cm} [GPa]	thickness [m]	$p_{v,0}$ [MPa]	p_v [MPa]	E_{gap} [MPa]	$E_{gap,hardened}$ [MPa]
C25/30	31	0.1	4.32	1.09	**0.95**	2000
	31	0.2	5.78	1.60	**1.35**	2000
	31	0.3	6.56	1.84	**1.35**	2000
C30/37	33	0.1	4.16	1.13	**0.95**	2000
	33	0.2	5.63	1.66	**1.35**	2000
	33	0.3	6.44	1.89	**1.35**	2000
C35/45	34	0.1	3.92	1.16	**0.95**	2000
	34	0.2	5.40	1.68	**1.35**	2000
	34	0.3	6.23	1.91	**1.35**	2000
C40/50	35	0.1	3.76	1.18	**0.95**	2000
	35	0.2	5.24	1.71	**1.35**	2000
	35	0.3	6.09	1.93	**1.35**	2000

All rock types are considered in the calibration process and the resulting magnitudes of E_{gap} for every concrete lining thickness are presented in Table 17 for a p_i of 4 MPa. The results for a pi of 7 and 10 MPa can be found in the appendix in Chapter C.1. Considering E_{rm} from Chapter 7.3 for each rock type, shows that the magnitude of E_{gap} is increasing with higher values of E_{rm} and a possible linear dependency is investigated in the next step.

Table 17: Calibrated E_{gap} for Ankerit, Rock mass 1, Rock mass 2, Sauberger Kalk, Tuff 1 as well as Tuff 2 and a concrete lining thickness of 0.1 m, 0.2 m and 0.3 m with a p_i of 4 MPa

Rock type	Thickness of the concrete lining		
	0.1 m	0.2 m	0.3 m
Ankerit	1.40 MPa	2.20 MPa	2.50 MPa
Rock mass 1	1.05 MPa	1.50 MPa	1.60 MPa
Rock mass 2	0.95 MPa	1.35 MPa	1.35 MPa
Sauberger Kalk	0.85 MPa	1.05 MPa	1.00 MPa
Tuff 1	0.65 MPa	0.75 MPa	0.65 MPa
Tuff 2	0.35 MPa	0.30 MPa	0.20 MPa

The resulting E_{gap} for a p_i of 4 MPa are plotted in a graph, which can be seen in Figure 41, for every rock type and lining thickness. A linear regression line is used for every lining thickness to generate an equation, which can be used to calculate the calibrated value of E_{gap} for a given E_{rm} and lining thickness. Two equations are generated for every thickness. The first equation is generated from a linear regression line, which includes the calibrated result of the high stiffness rock type Ankerit. Due to its high value of E_{rm}, with 73.34 GPa in contrast to the other rock types, Ankerit has a major influence on the resulting final equation for the chosen thickness. The achieved accuracy with the equation, which includes Ankerit, is more accurate for the calculation of E_{gap} for high stiffness rock types and a scope of application is therefore necessary.

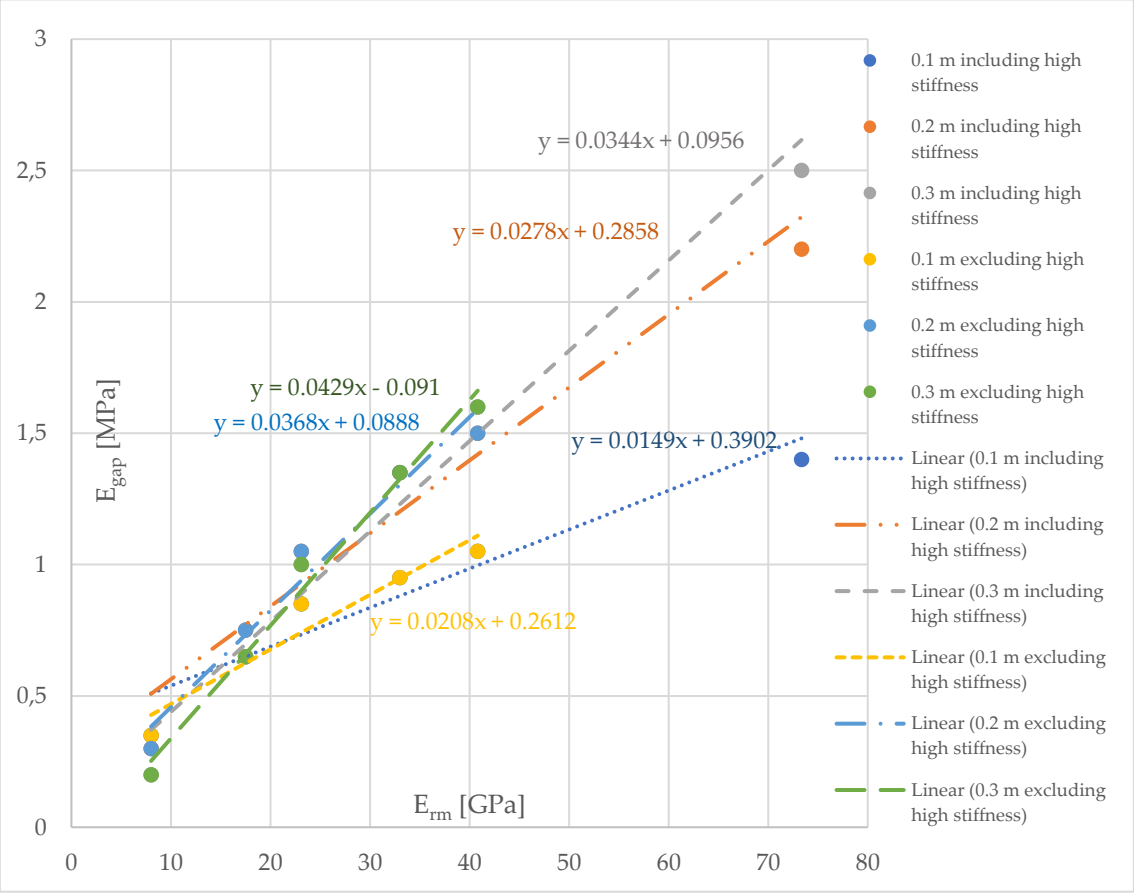

Figure 41: Graphical display of the resulting equations to calculate the necessary value of E_{gap} depending on E_{rm} for a p_i of 4 MPa and concrete lining thicknesses of 0.1 m, 0.2m and 0.3 m

Test of the generated equations

A medium p_v was determined for four concrete qualities using the Seeber method for a chosen E_{rm} between 5 GPa and 50 GPa, with a given concrete lining thickness and p_i magnitude. The value of p_v from Seeber was compared in the next step with the numerically determined p_v. The numerical simulation was carried out with the calculated E_{gap} for a given E_{rm}, concrete lining thickness and p_i, using the equations from Figure 41. An analysis of the difference between p_v from Seeber and p_v from the numerical simulation for a p_i of 4 MPa and lining thickness of 0.3 m is shown in Table 18 and Table 19. Achieved accuracies of the determined p_v for different values of E_{rm} can be seen in Figure 42 depending on the used equations.

Table 18: Comparison of the achieved result of the value for p_v from the calibrated numerical model with the method from Seeber for a 0.3 m thick concrete lining, a p_i of 4 MPa and the use of the calibrated equation including Ankerit

Equation: excluding high stiffness y = 0.0429x – 0.091			Seeber: Medium pressure p_v	Analysis Numerical versus Seeber	
E_{rm} [GPa]	stiffness [MPa]	numerical p_v [MPa]	Seeber p_v [MPa]	Difference [MPa]	Difference [%]
5	0.12	3.10	2.83	0.27	**9.4**
10	0.34	2.70	2.54	0.17	**6.5**
20	0.77	2.10	2.10	0.00	**0.0**
30	1.20	1.85	1.79	0.06	**3.2**
40	1.63	1.70	1.56	0.14	**8.8**
50	2.05	1.55	1.39	0.16	**11.9**

Table 19: Comparison of the achieved result of the value for p_v from the calibrated numerical model with the method from Seeber for a 0.3 m thick concrete lining, a p_i of 4 MPa and the use of the calibrated equation excluding Ankerit

Equation: including high stiffness y = 0.0344x + 0.0956			Seeber: Medium p_v	Analysis Numerical versus Seeber	
E_{rm} [GPa]	stiffness [MPa]	numerical p_v [MPa]	Seeber p_v [MPa]	Difference [MPa]	Difference [%]
5	0.27	3.85	2.83	1.02	**35.9**
10	0.44	2.90	2.54	0.36	**14.4**
20	0.78	2.15	2.10	0.05	**2.4**
30	1.13	1.85	1.79	0.06	**3.2**
40	1.47	1.60	1.56	0.04	**2.4**
50	1.82	1.45	1.39	0.06	**4.7**

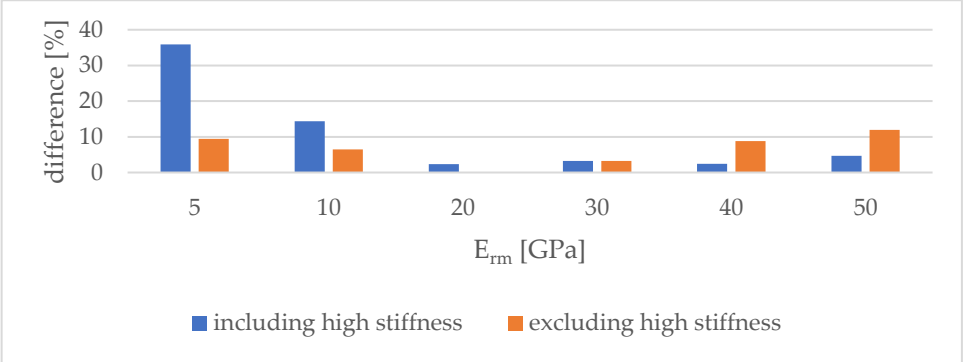

Figure 42: Achieved accuracy from the application of the necessary E_{gap} in a numerical simulation calculated by the calibrated equations for a thickness of 0.3 m and p_i of 4 MPa

The possibility to calculate E_{gap} and implement it in the numerical simulation to achieve nearly the same p_v as with the anlytical method from Seeber is the result of the calibration process. An inclusion of the rock type Ankerit in the calibration process makes it possible to get more accurate results for higher values of E_{rm}. On the other hand, for lower values of E_{rm}, it can be seen in Figure 42 that the results are less accurate than with the equation in which the high stiffness results are excluded.
As a result of the gained accuracies, a scope of application was fixed for the different equations to calculate E_{gap} as an input parameter for the calibrated numerical model:

- For a magnitude of E_{rm} between 5 GPa and 20 GPa, the resulting equation with an exclusion of the high stiffness results should be used
- For a higher magnitude of E_{rm} than 20 GPa, the resulting equation with an inclusion of the high stiffness results should be used

The design of a pre-stressed concrete lining in a rock mass with an E_{rm} lower than 5 GPa would be not sensible because a certain magnitude of E_{rm} is necessary to maintain the pre-stressing of the lining over the life span of the storage. Large differences from the magnitude of p_v between Seeber and the numerical method, like it is visible for low and high values of E_{rm} in Figure 42, have to be considered in the design process. A certain range for p_v can be used to investigate the stability of the concrete lining as well as a potential rock mass failure for the extreme values of p_v during the design process. The range of p_v should be integrated in a sensitivity analysis to guarantee a stable storage facility and rock mass in the design.
Losses of the magnitude of the gap injection pressure must be calculated by equations from guidelines, standards or another calculation method like Seeber and added up to the value of p_v to get $p_{v,0}$. The following numerical simulation, like it is described in Chapter 7.2.3, is needed to investigate a potential rock mass failure during the gap injection process.

The generated equations for a storage facility with an outer diameter of 3.0 m, a p_i of 4, 7 and 10 MPa and a concrete lining thickness of 0.1 m, 0.2 m and 0.3 m are listed in Table 20. All the achieved results for the values of E_{gap} and accuracies of the calibration can be found in the appendix in Chapter C.1.

Table 20: Determined equations to calculate the calibrated magnitude of E_{gap} for the usage in a numerical simulation for a p_i of 4, 7 and 10 MPa

Equation for E_{gap}; y = E_{gap} and x = E_{rm}			
excluding high stiffness (E_{rm} between 5 to 20 GPa)		including high stiffness (E_{rm} higher than 20 GPa)	
4 MPa and 0.1 m	y = 0.0208x + 0.2612	4 MPa and 0.1m	y = 0.0149x + 0.3902
4 MPa and 0.2 m	y = 0.0368x + 0.0888	4 MPa and 0.2m	y = 0.0278x + 0.2858
4 MPa and 0.3 m	y = 0.0429x - 0.091	4 MPa and 0.3m	y = 0.0344x + 0.0956
7 MPa and 0.1 m	y = 0.0202x + 0.2757	7 MPa and 0.1m	y = 0.0132x + 0.4284
7 MPa and 0.2 m	y = 0.0356x + 0.1091	7 MPa and 0.2m	y = 0.0238x + 0.3661
7 MPa and 0.3 m	y = 0.0398x - 0.0448	7 MPa and 0.3m	y = 0.0325x + 0.1144
10 MPa and 0.1 m	y = 0.0201x + 0.2882	10 MPa and 0.1 m	y = 0.0107x + 0.4928
10 MPa and 0.2 m	y = 0.0356x + 0.1091	10 MPa and 0.2 m	y = 0.0238x + 0.3661
10 MPa and 0.3 m	y = 0.0423x - 0.1265	10 MPa and 0.3 m	y = 0.0304x + 0.134

Investigation of different storage diameters

A further step of the calibration of the numerical model by Seeber through a determination of the necessary values of E_{gap}, was an expansion on larger storage diameters than 3.0 m. The increase of the simulated storage volume was done to achieve a higher storage capacity. This was taken into consideration by carrying out the expansion of the calibration process for a p_i of 10 MPa. Tuff 1, Rock mass 1 and Ankerit were chosen as rock types and C30/37 as well as C35/45 were chosen as concrete qualities for the investigation of higher storage diameters. An increase of the diameter was done in steps of 1.0 m up to the maximum diameter of 7.0 m. Table 21 shows the calculated results of E_{gap} for different storage diameters, a concrete quality C30/37, different concrete lining thicknesses of 0.1, 0.2 and 0.3 m as well as p_v and $p_{v,0}$ according to Seeber

Table 21: Calibrated E_{gap} for a pre-stressed concrete lining built in Ankerit with storage diameters of 4, 5, 6 and 7 m, concrete quality C30/37, lining thickness of 0.1, 0.2 and 0.3 m as well as a p_i of 10 MPa

Ankerit – p_i of 10 Mpa							
Storage diameter [m]	Concrete			Seeber		gap injection material	
	Quality [-]	E_{cm} [GPa]	thickness [m]	$p_{v,0}$ [MPa]	p_v [MPa]	E_{gap} [MPa]	$E_{gap,hardened}$ [MPa]
4	C30/37	33	0.1	4.06	1.17	**0.75**	2000
		33	0.2	6.26	2.03	**1.30**	2000
		33	0.3	7.82	2.65	**1.60**	2000
5	C30/37	33	0.1	3.33	0.97	**0.50**	2000
		33	0.2	5.24	1.72	**0.90**	2000
		33	0.3	6.66	2.31	**1.15**	2000
6	C30/37	33	0.1	2.83	0.82	**0.35**	2000
		33	0.2	4.51	1.49	**0.65**	2000
		33	0.3	5.80	2.03	**0.90**	2000
7	C30/37	33	0.1	2.45	0.71	**0.25**	2000
		33	0.2	3.95	1.31	**0.50**	2000
		33	0.3	5.13	1.82	**0.70**	2000

The determined magnitudes of E_{gap} for the rock type Ankerit are summarized in Table 22 for every diameter and concrete lining thickness. A graphical display of the resulting E_{gap} depending on the storage diameter for Ankerit can be seen in Figure 43. A linear regression line was drawn for the results of every lining thickness to achieve the necessary equations to calculate E_{gap} for a given storage diameter. This procedure was also done for Tuff 1 and Rock mass 1 and can be found in the appendix Chapter C.2.

Table 22: Calibrated values of E_{gap} for the numerical simulation of a pre-stressed concrete lining in Ankerit with a p_i of 10 MPa, storage diameters of 3, 4, 5, 6 and 7 m as well as a concrete lining thickness of 0.1, 0.2 and 0.3 m

Storage diameter	Thickness of the concrete lining		
	0.1 m	0.2 m	0.3 m
3 m	1.15 MPa	1.95 MPa	2.20 MPa
4 m	0.75 MPa	1.30 MPa	1.60 MPa
5 m	0.50 MPa	0.90 MPa	1.15 MPa
6 m	0.35 MPa	0.65 MPa	0.90 MPa
7 m	0.25 MPa	0.50 MPa	0.70 MPa

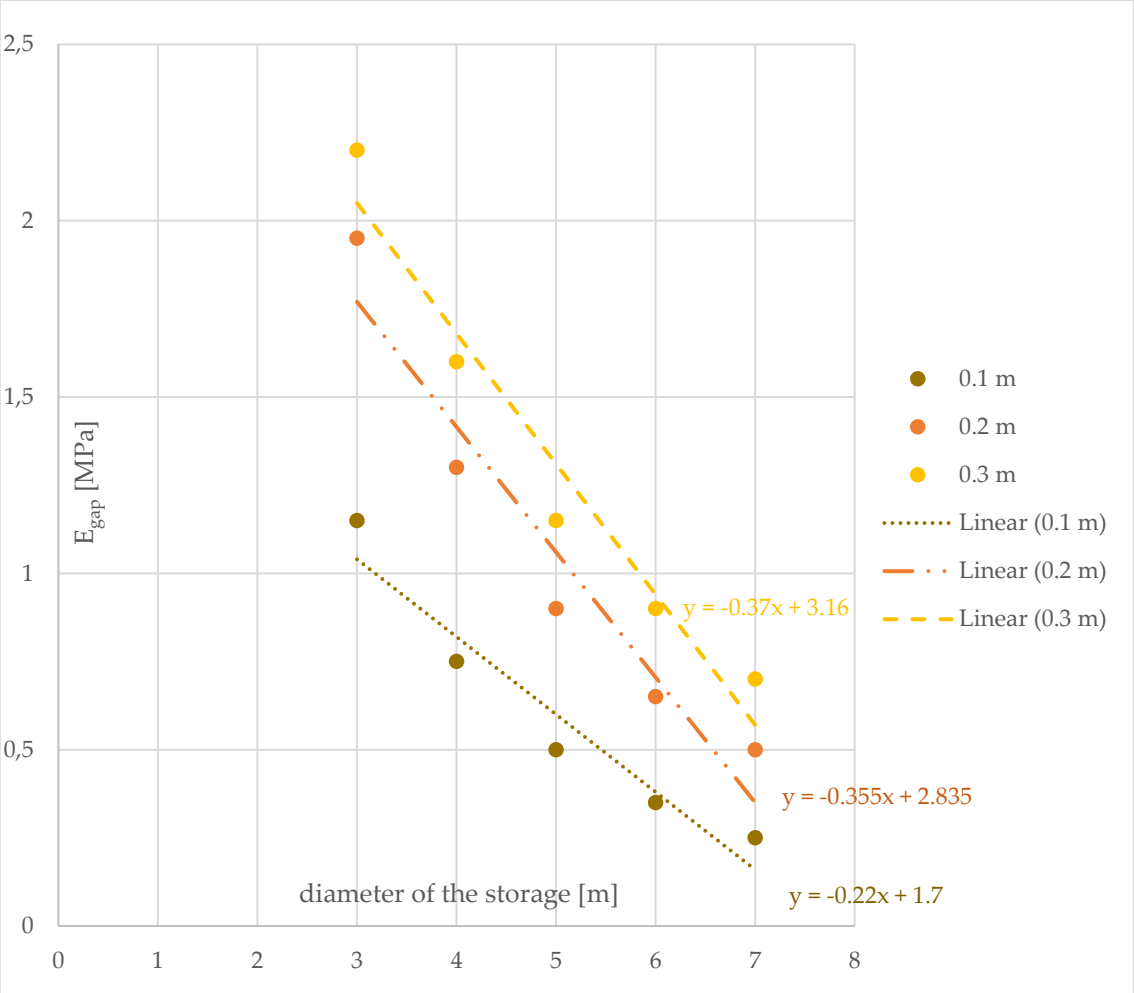

Figure 43: Graphical display of the calibrated values of E_{gap} for Ankerit and a p_i of 10 MPa depending on the storage diameter as well as on the lining thickness of 0.1, 0.2 and 0.3 m

The determined equations to calculate the calibrated value of E_{gap} for a given storage diameter are different for the rock types Tuff 1, Rock mass 1 and Ankerit. Slope and y-intercept of the equations depend on the magnitude of E_{rm} and thickness of the concrete lining. A medium value of the parts slope and y-intercept of every equation for a certain concrete lining thickness would decrease the accuracy of the calibration results significantly. It was therfore decided to develop secondary equations to calculate slope and y-intercept of the final equation separately for a defined scope of application.
This procedure guarantees maximum accuracy and makes it possible to determine E_{gap}:

- for a given storage diameter
- for a given E_{rm}
- for a given concrete lining thickness

Slope and y-intercept of each calibrated equation are listed in Table 23 for the concrete lining thickness of 0.1, 0.2 and 0.3 m as well as E_{rm} of each rock type. The secondary equation for the calculation of slope and y-intercept of the final equation for a certain E_{rm} between 15 and 40 GPa as well as a concrete lining thickness of 0.1 m can be seen in Figure 44. The other diagrams for the determination of the secondary equations to calculate slope and y-intercept of the final equation can be found in the appendix Chapter C.2.
With all the generated secondary equations it is possible to calculate the necessary E_{gap} following the steps:

1. Choose the concrete lining thickness of 0.1, 0.2 or 0.3 m
2. Choose the storage outer diameter
3. Select the proper scope of application depending on the given E_{rm} between 15 and 40 GPa or 40 and 75 GPa
4. Use the right secondary equation to calculate the slope and y-intercept of the final equation
5. Insert the calculated value of the slope and y-imtercept in the final quation
6. Calculate the necessary value of E_{gap} as an input parameter for the calibrated numerical model with the final equation

Determined slope and y-intercept of the equations to calculate E_{gap} for a storage built in Tuff 1, Rock mass 1 and Ankerit with a p_i of 10 MPa as well as a concrete lining thickness of 0.1, 0.2 and 0.3 m are listed in Table 23. The necessary magnitudes of E_{rm} for each rock type can be found in Chapter 7.3.

Table 23: Determined slope and y-intercept of the final equations to calculate the calibrated E_{gap} for a p_i of 10 MPa, different storage diameters and a lining thickness of 0.1, 0.2 and 0.3 m

0.1 m thickness			0.2 m thickness			0.3 m thickness		
E_{rm} [GPa]	slope [-]	y-intercept [-]	E_{rm} [GPa]	slope [-]	y-intercept [-]	E_{rm} [GPa]	slope [-]	y-intercept [-]
17.50	-0.12	0.94	17.50	-0.08	0.85	17.50	-0.12	1.04
40.82	-0.19	1.49	40.82	-0.25	2.10	40.82	-0.24	2.15
73.34	-0.22	1.70	73.34	-0.36	2.84	73.34	-0.37	3.16

The distribution of the values for the slope and y-intercept between each magnitude of E_{rm} is fixed to be linear. It is therefore possible, to achieve the secondary equations for the slope and y-intercept of the final equation by inserting the values of two different magnitudes of E_{rm}. The generated function of this line is used as secondary equation. For a magnitude of E_{rm} between 15 and 40 GPa and a lining thickness of 0.1 m the secondary equations can be found in Figure 44.

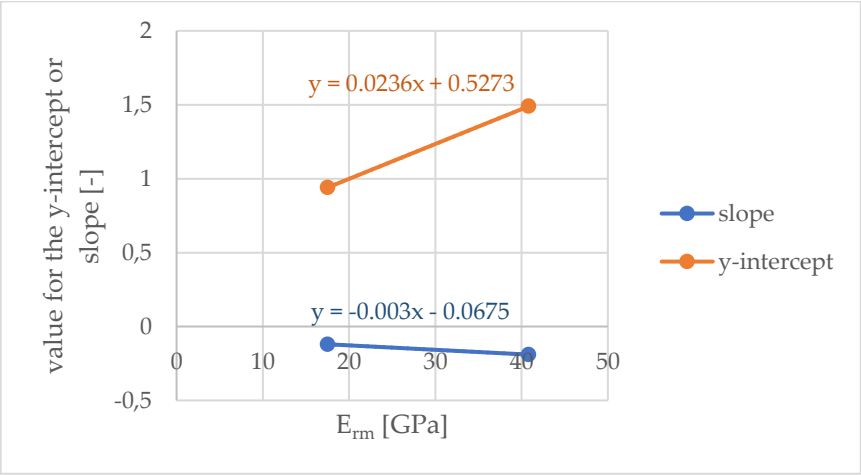

Figure 44: Determined secondary equations to calculate the slope and y-intercept of the calibrated final equation for the E_{gap} of the numerical model of the storage with a p_i of 10 MPa, a concrete lining thickness of 0.1 m and a value of E_{rm} between 15 GPa and 40 GPa

Determined secondary equations for every concrete lining thickness and range of the magnitude for E_{rm} can be seen in Table 24 and are used to calculate the calibrated E_{gap} for a storage diameter between 3.0 m and 7.0 m as well as a magnitude of E_{rm} between 15 GPa and 75 GPa.

Table 24: Determined secondary equations to calculate the y-intercept and slope of the final equations depending on E_{rm} for a p_i of 10 MPa, a magnitude of E_{rm} between 15 and 75 GPa and a concrete lining thickness of 0.1, 0.2 and 0.3 m

Equation for the y-intercept; y = y-intercept and x = E_{rm}			
E_{rm} between 15 GPa and 40 GPa		E_{rm} between 40 GPa and 75 Gpa	
Lining thickness [m]	Equation	Lining thickness [m]	Equation
0.1 m	y = 0.0236x + 0.5273	0.1 m	y = 0.0065x + 1.2264
0.2 m	y = 0.0536x – 0.0880	0.2 m	y = 0.0226x + 1.1774
0.3 m	y = 0.0474x + 0.2108	0.3 m	y = 0.0312x + 0.8709
Equation for the slope; y = slope and x = E_{rm}			
E_{rm} between 15 GPa and 40 GPa		E_{rm} between 40 GPa and 75 Gpa	
Lining thickness [m]	Equation	Lining thickness [m]	Equation
0.1 m	y = -0.0030x – 0.0675	0.1 m	y = -0.0009x – 0.1523
0.2 m	y = -0.0073x + 0.0476	0.2 m	y = -0.0032x – 0.1182
0.3 m	y = -0.0049x – 0.0337	0.3 m	y = -0.0042x – 0.0655

The achieved results of the calibration process for different storage diameters can be seen in Table 25 for four different magnitudes of E_{rm} and a storage diameter of 4.0 m. Necessary secondary equations for slope and y-intercept were taken from Table 24 for the specific scope of application and the final equations were used to calculate the calibrated value of E_{gap}. Additional examinations for a storage diameter of 5.0 m with 0.2 m thick concrete lining and a diameter of 6.0 m with 0.3 m thick concrete lining were also carried out and all the achieved accuracies are displayed in Figure 45.

Table 25: Comparison of the resulting value of p_v from the calibrated numerical simulation with p_v from Seeber for a storage diameter of 4.0 m and a lining thickness of 0.1 m

Calibrated numerical simulation			Seeber: Medium p_v	Analysis Numerical versus Seeber	
E_{rm} [GPa]	E_{gap} [MPa]	numerical p_v [MPa]	Seeber p_v [MPa]	Difference [MPa]	Difference [%]
20	0.49	3.00	2.86	0.14	**5.1**
30	0.61	2.35	2.12	0.23	**10.8**
50	0.76	1.70	1.40	0.30	**21.9**
60	0.79	1.35	1.19	0.16	**13.2**

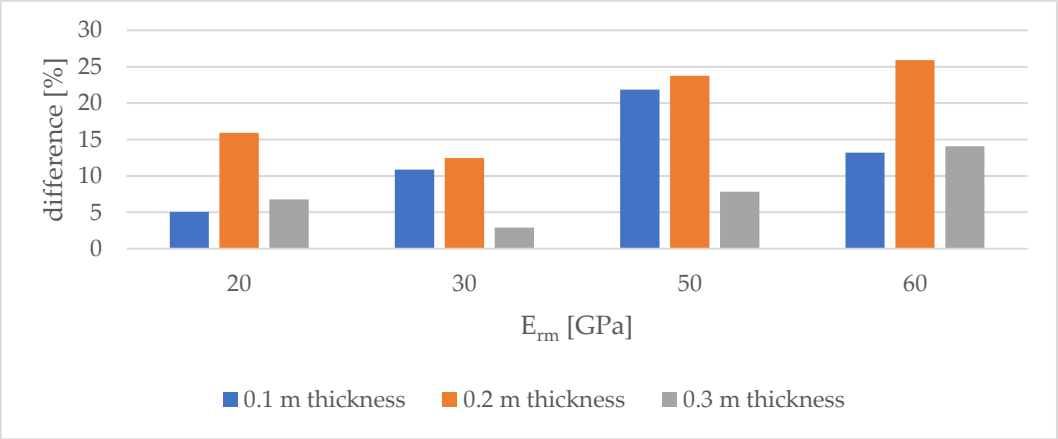

Figure 45: Analysis of the achieved accuracy of the calibration for different storage diameters, concrete lining thicknesses of 0.1, 0.2 and 0.3 m and a p_i of 10 MPa

It can be seen in Figure 45 that the accuracy of the achieved results for p_v are lower than for the calibration process with a fixed storage diameter. Large differences between Seeber and the numerical model have to be taken into account in a future design by a detailed sensitivity analysis. The additional tables and figures, which were necessary to achieve the results and needed to understand the results can be found in the appendix Chapter C.2.

Plastic behaviour of the pre-stressed concrete lining and rock mass

Failure of the lining or rock mass was not investigated by the calibrated models because the material behaviour in the model was considered as elastic following the principles from Seeber. In the next step, the calibrated E_{gap} was used in a numerical simulation of the pre-stressed concrete lining with plastic lining and rock mass behaviour. The in-situ stress was fixed as uniform with a magnitude of 5 MPa. An additional shotcrete layer was installed between the gap injection material and rock mass. It has been investigated how Seeber's results and calibrated numerical models behave if plastic material behaviour is taken into account. The state of the concrete lining and rock mass as the results can be found in the appendix Chapter C.3 and the summarized conclusions are:

- Numerical models of the pre-stressed concrete lining with a thickness of 0.1 m did not achieve equilibrium in the gap injection stage for most of the rock types and magnitudes of p_i. For that reason, it can be said that the resulting magnitude of $p_{v,0}$ for a thickness of 0.1 m is too high to be taken up by the concrete lining.

- **For Ankerit:**

Stable conditions of the rock mass and concrete lining could be achieved for a lining with 0.2 and 0.3 m thickness and a p_i of 4 MPa. With higher magnitudes of p_i only the 0.3 m thick concrete linings were stable and the models could reach equilibrium. A plot of the induced σ_3 in the surrounding rock mass and axial force of the 0.3 m thick concrete lining (purple coloured dashed line) for a p_i of 10 MPa can be seen in Figure 46.

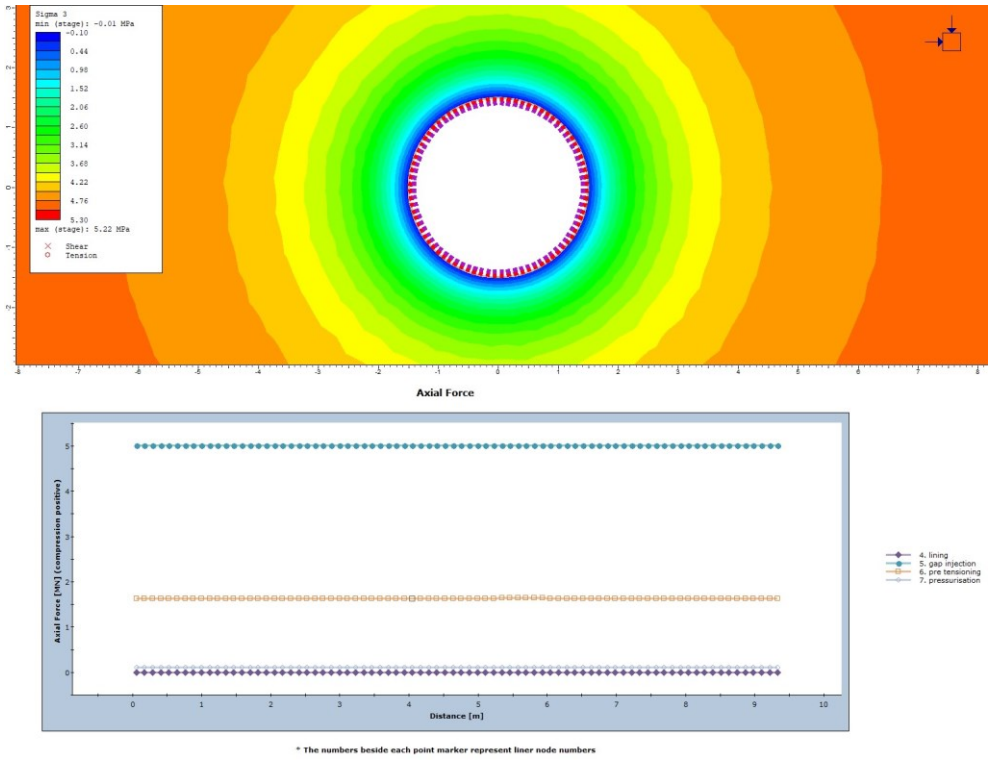

Figure 46: Display of the stable pre-stressed concrete lining at the pressurisation stage of the numerical model (top image) and axial force of the lining (bottom image) for Ankerit with a p_i of 10 MPa and a 0.3 m thick concrete lining with a concrete quality of C30/37

- **For Sauberger Kalk:**

Every model which consisted of a 0.2 or 0.3 m thick concrete lining could reach equilibrium. A p_i of 4 MPa leads to stable conditions of the rock mass as well as of the concrete and the total displacement of a 0.3 m thick C35/45 concrete lining (purple coloured dashed line) as well as a stable shotcrete lining (light blue coloured dashed line) during the gap injection process can be seen in Figure 47.

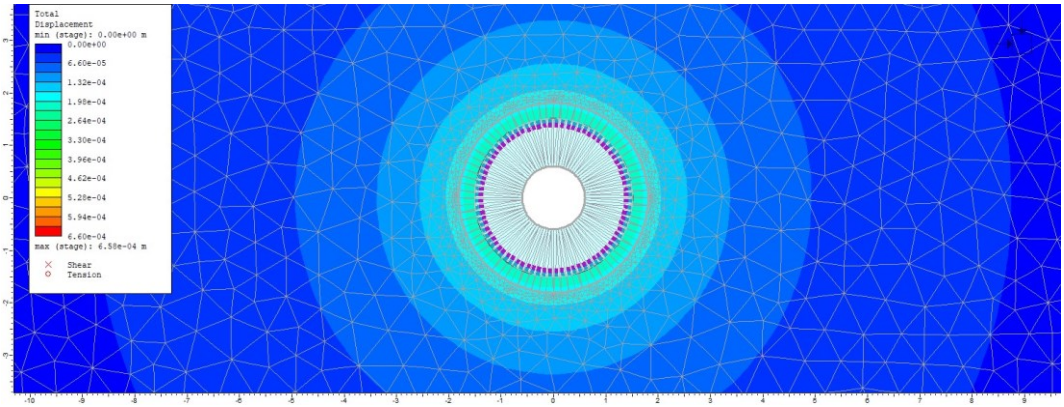

Figure 47: Total displacement of the pre-stressed concrete lining with a thickness of 0.3 m and a concrete quality C35/45 at the gap injection stage for Sauberger Kalk and a p_i of 4 MPa

A lining thickness of 0.2 m requires a concrete quality of at least C30/37 for a p_i of 7 MPa and a concrete quality of at least C35/45 for a p_i of 10 MPa to take up the induced compressive forces by $p_{v,0}$ at the gap injection stage. The failure of the 0.2 m thick C25/30 concrete lining (red coloured dashed line) for a p_i of 7 MPa is displayed in Figure 48.

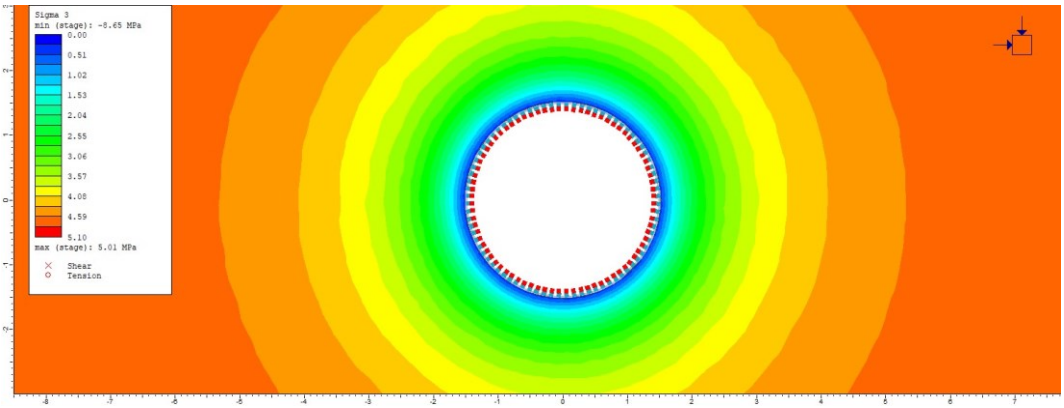

Figure 48: Display of the failed pre-stressed concrete lining at the gap injection stage for a storage built in Sauberger Kalk with a p_i of 7 MPa, a 0.2 m thick concrete lining and a concrete quality of C25/30

Concrete linings with a thickness of 0.3 m were always stable for a p_i of 4 MPa and 7 MPa. A p_i of 10 MPa required concrete qualities of at least C30/37 quality to achieve stable lining conditions, which is displayed in Figure 49.

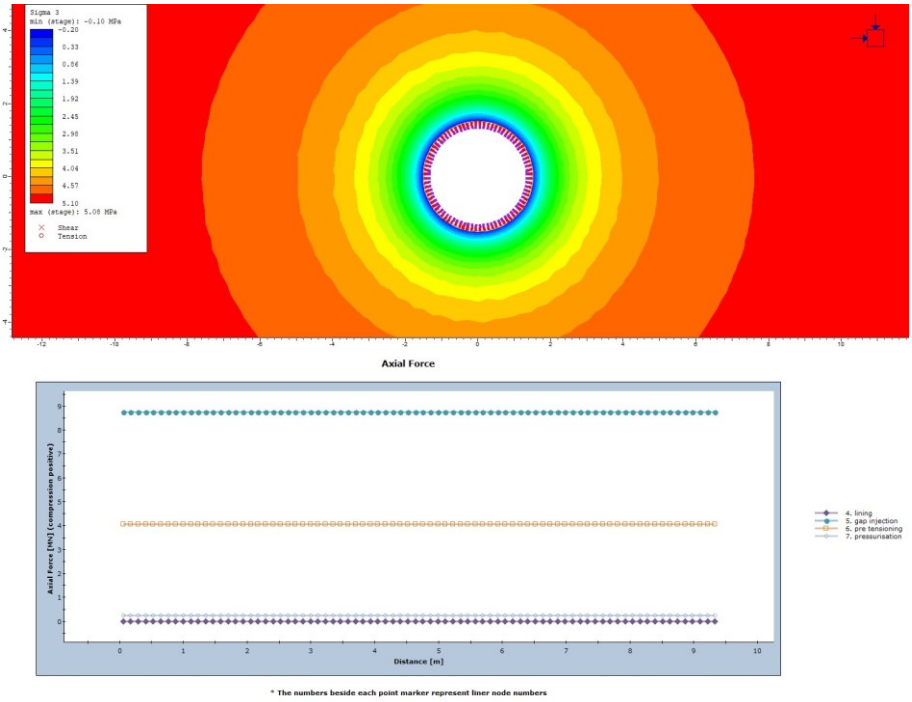

Figure 49: Induced σ_3 in the rock mass at the pressurisation stage of the numerical model (top image) and axial force of the concrete liner at every stage (bottom image) for Sauberger Kalk with a p_i of 10 MPa, a thickness of 0.3 m and a concrete quality C30/37

- **For Rock mass 1:**

100% of the simulations with a lining thickness of 0.1 m and 87.5% of the simulations with a lining thickness of 0.2 m could not reach equilibrium in the gap injection stage. A storage with a 0.3 m thick pre-stressed concrete lining had always stable rock mass and lining conditions for a p_i of 7 MPa and 10 MPa. The gap injection process compresses the concrete lining and after excluding the reduction of the compression due to the pre-stressing losses, an amount of inwards displacement is still left. Operation of the storage with p_i will reduce the compression to the smallest value, but the concrete should not be strained because of its small strain capacity to prevent failure. The remaining compression of the lining at the pressurisation stage is shown in Figure 50.

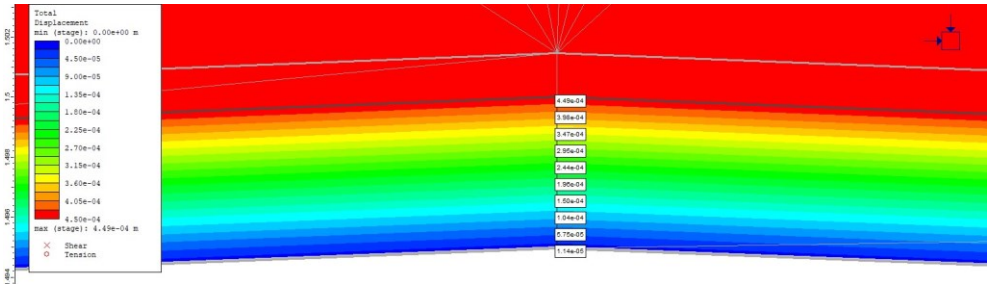

Figure 50: Radial displacement inside the gap injection material at the pressurisation stage for Rock mass 1 with a 0.3 m thick C25/30 concrete lining and a p_i of 10 MPa

The comparison of the induced σ_3 in the surrounding rock mass between the pre-stressing and pressurisation stage is shown in Figure 51 for a C25/30 concrete lining with a thickness of 0.3 m and a p_i of 7 MPa.

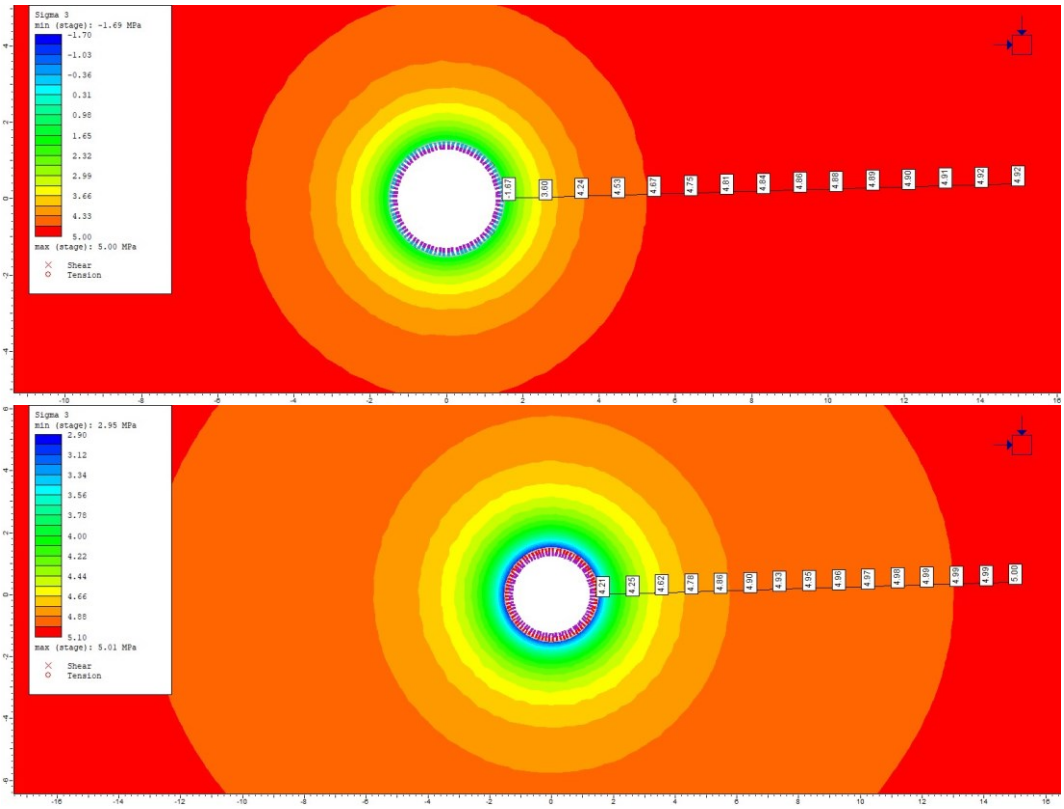

Figure 51: Distribution of the induced σ_3 in the surrounding rock mass for a storage built in Rock mass 1 with a concrete quality of C25/30, a lining thickness of 0.3 m and a p_i of 7 MPa at the pre-stressing stage (top image) and the pressurisation stage (bottom image)

- **For Rock mass 2:**

Only 47% of the simulated pre-stressed concrete linings of the storage could reach equilibrium. Storage facilities with a concrete lining thickness of 0.3 m achieved stable conditions of the lining and rock mass in ten out of twelve simulations. The resulting $p_{v,0}$ according to Seeber for a p_i of 10 MPa and a concrete lining thickness of 0.2 m exceeded the compressive strength of the lining for nearly every concrete quality. Stable conditions of the surrounding rock mass could be achieved in every successful simulation.

- **for Tuff 1:**

It could be investigated that the necessary $p_{v,0}$ according to Seeber for a concrete lining thickness of 0.2 m can be taken up by every concrete quality for a p_i of 4 MPa and a concrete quality from at least C35/45 for a p_i of 7 MPa. Necessary magnitudes of $p_{v,0}$ for a p_i of 10 MPa could not be taken up by a 0.2 m thick concrete lining. The state of the 0.2 m thick C40/50 concrete lining for a p_i of 7 MPa and 10 MPa can be seen in Figure 52 and the radial displacement of the concrete lining inside the gap injection material is visible in Figure 53. Simulations of the pre-stressed concrete lining with a thickness of 0.3 m could achieve equilibrium in 92% of the cases and were stable in 90% of the cases. Stable conditions of the surrounding rock mass could be achieved in every successful simulation.

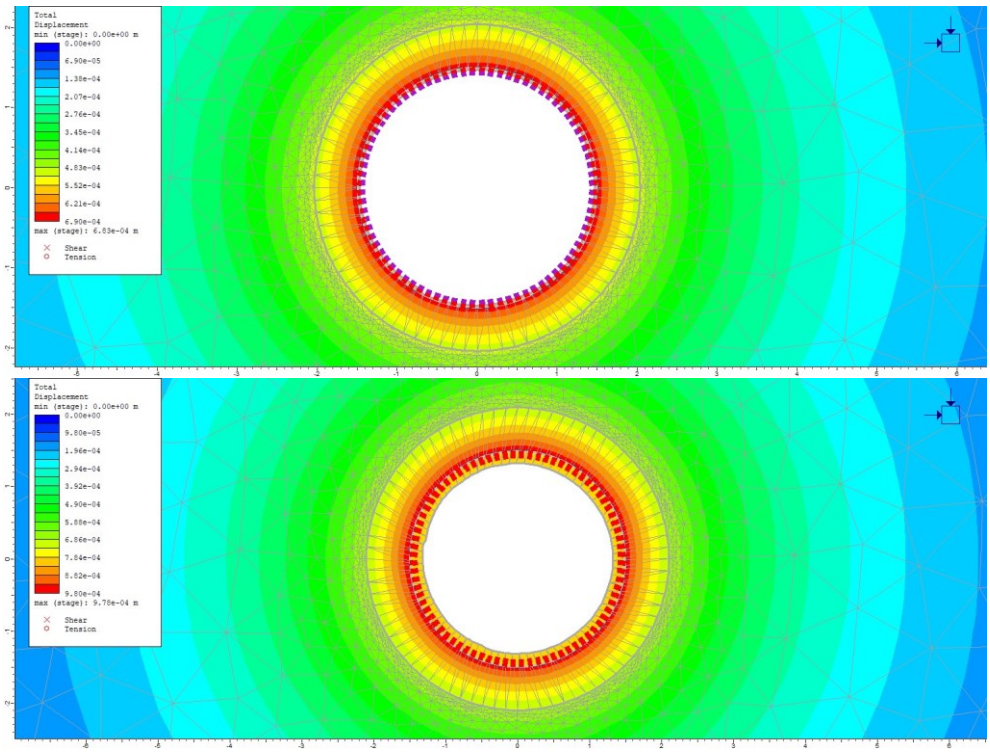

Figure 52: Comparison of the total displacement and state of the pre-stressed concrete lining at the pressurisation stage for Tuff 1 with a concrete quality C40/50, thickness of 0.2 m as well as a p_i of 7 MPa (top image) and p_i of 10 MPa (bottom image)

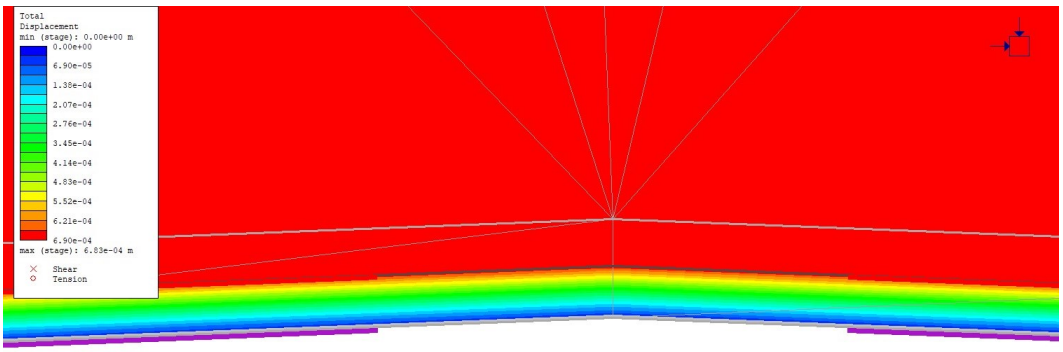

Figure 53: Total radial displacement inside the gap injection material at the pressurisation stage of the numerical model for Tuff 1 with a p_i of 7 MPa, a 0.2 m thick lining and a concrete quality of C40/50

The gap injection process induces high tensile stresses into the gap injection material due to the simulation of the gap opening. This 5 mm thick layer has elastic material behaviour and can take up the tensile stresses with no limit. Induced σ_3 caused by $p_{v,0}$ at the gap injection stage of the numerical model can be seen in Figure 54 for a p_i of 7 MPa and a 0.2 m thick concrete lining with a quality of C40/50.

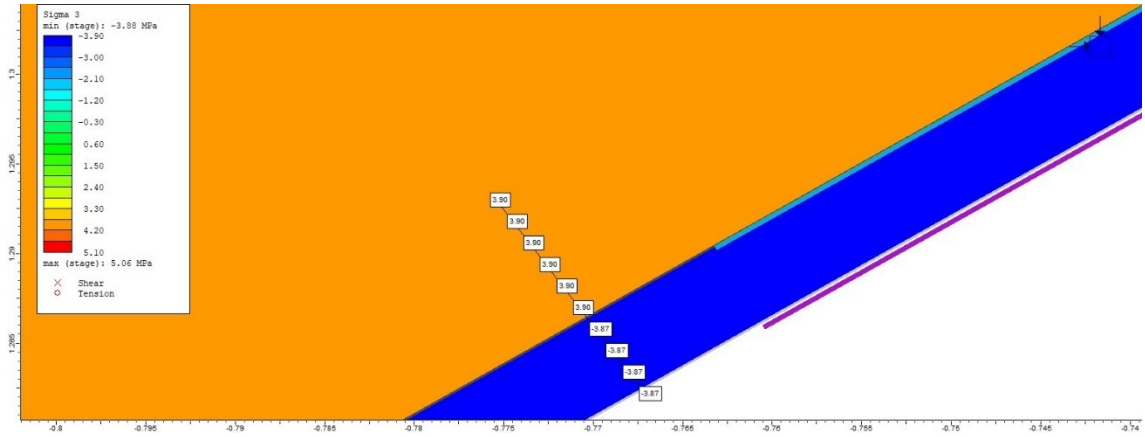

Figure 54: Induced σ_3 inside the 5 mm thick layer of the gap injection material at the gap injection stage of the numerical model for Tuff 1 with a p_i of 7 MPa, a 0.2 m thick concrete lining and a concrete quality of C40/50

- **for Tuff 2:**

A concrete quality of C40/50 was necessary to achieve stable conditions for a 0.1 m thick concrete lining at the gap injection stage with a p_i of 4 MPa. The induced σ_3 in the surrounding rock mass and stable conditions of the shotcrete (light blue coloured dashed line) and concrete lining (purple coloured dashed line) is shown in Figure 55. Successful numerical simulations of 0.2 and 0.3 m thick linings were always stable for a p_i of 4 MPa.

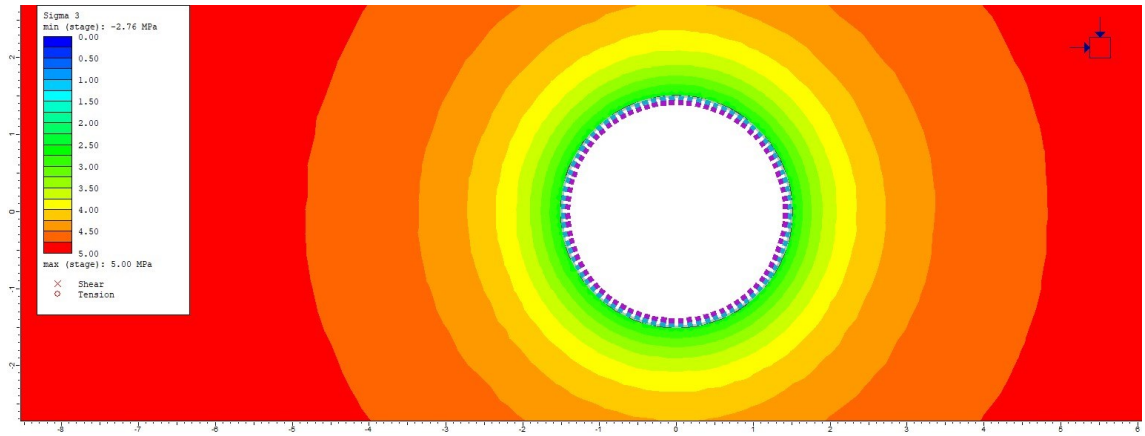

Figure 55: Induced σ_3 in the rock mass at the gap injection stage of the pre-stressed concrete lining with a thickness of 0.1 m and a concrete quality C40/50 for Tuff 2 and a p_i of 4 MPa

Pre-stressed concrete linings with a p_i of 7 MPa have required a minimum thickness of 0.3 m and a concrete quality of C35/45 to take up the induced compressive stresses by $p_{v,0}$. Figure 56 shows the radial displacement of the storage boundary and an intact 0.3 m thick concrete lining at the gap injection stage.

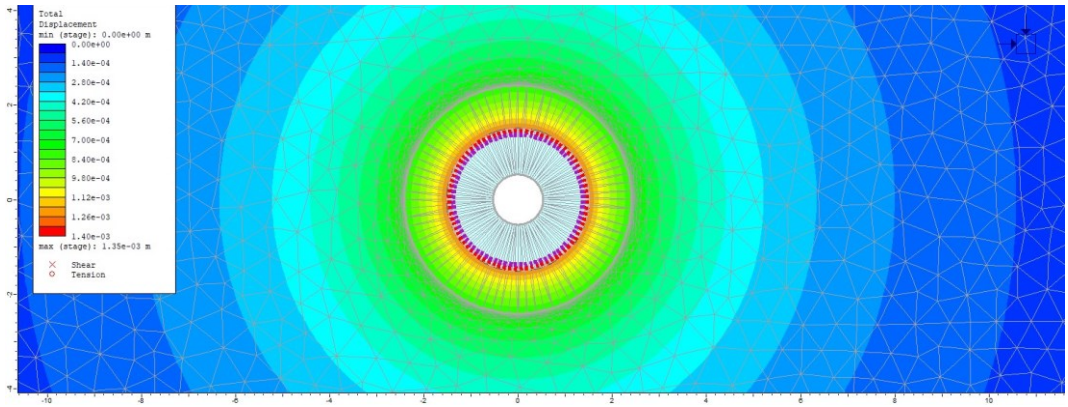

Figure 56: Total displacement of the pre-stressed concrete lining with a thickness of 0.3 m and a concrete quality C35/45 at the gap injection stage for Tuff 2 and a p_i of 7 MPa

Every lining thickness for every concrete quality failed in the gap injection stage for a numerical simulation of the storage with a p_i of 10 MPa. The failed 0.3 m thick lining for a p_i of 10 MPa as well as the associated axial force plot are shown in Figure 57.

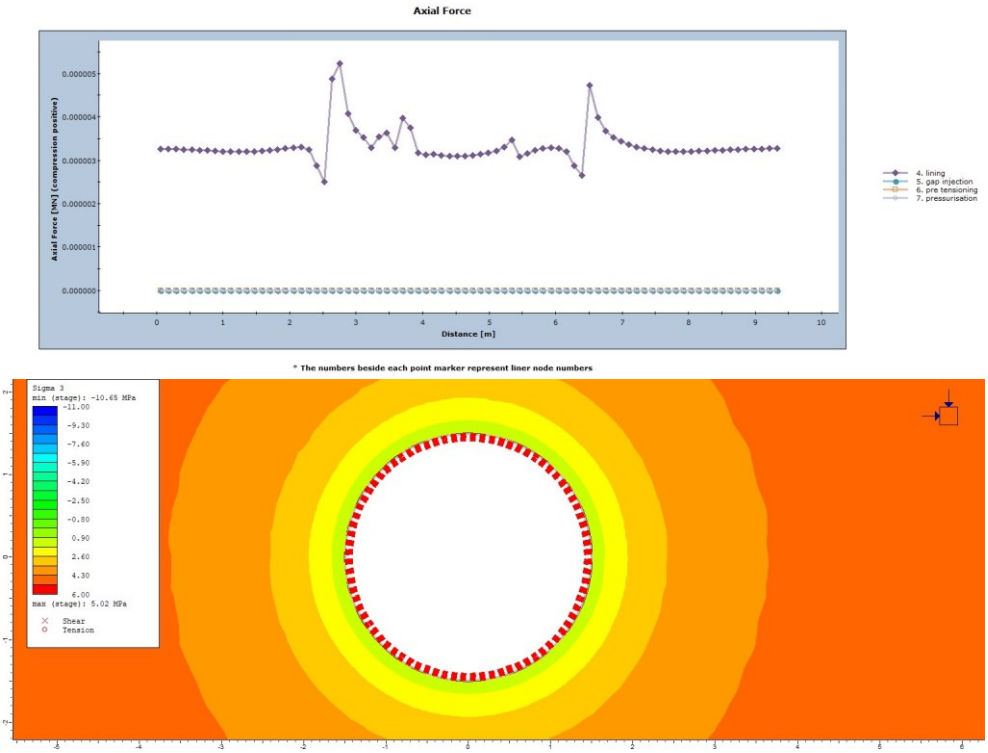

Figure 57: Axial force of the liner (top image) as well as display of the failed pre-stressed concrete lining and induced σ_3 in the surrounding rock mass at the gap injection stage (bottom image) of the numerical model for Tuff 2 with a p_i of 10 MPa and a 0.3 m thick concrete lining of C30/37 concrete quality

A comparison is carried out between the concrete qualities C30/37 and C40/50 with a lining thickness of 0.3 m and a p_i of 10 MPa by the induced σ_3 as well as failed rock mass in Figure 58 and the total radial displacement of the storage boundary in Figure 59.

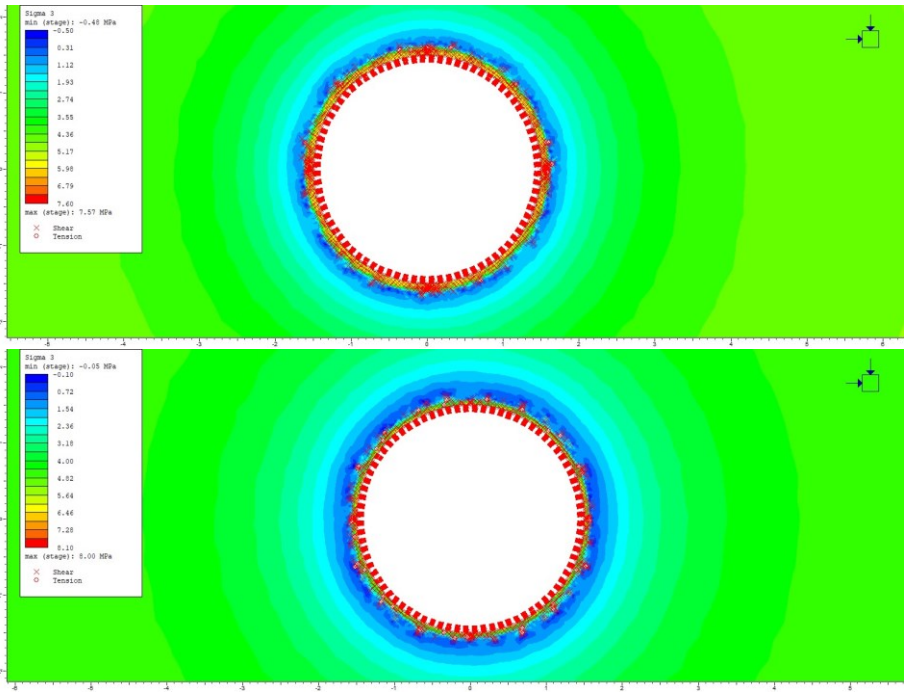

Figure 58: Comparison of the induced σ_3 and failed rock mass at the pressurisation stage of the pre-stressed concrete lining for Tuff 2 with a lining thickness of 0.3 m and a p_i of 10 MPa between a concrete quality C30/37 (top image) and a concrete quality C40/50 (bottom image)

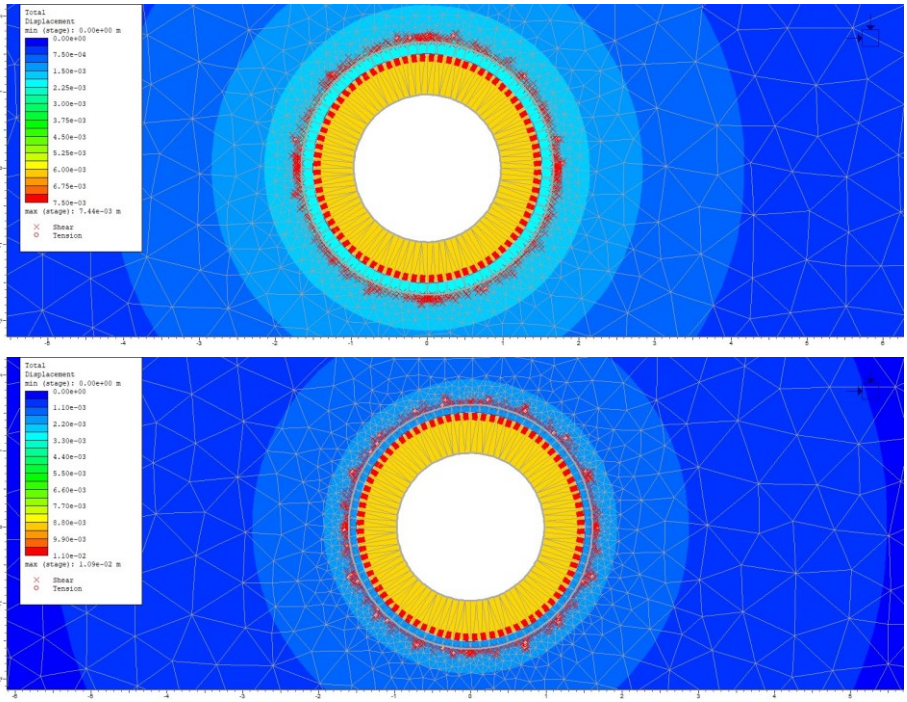

Figure 59: Comparison of the radial displacement of the storage boundary at the pressurisation stage of the pre-stressed concrete lining for Tuff 2 with a lining thickness of 0.3 m and a p_i of 10 MPa between a concrete quality C30/37 (top image) and a concrete quality C40/50 (bottom image)

8.2 Comparison of the results from the steel lining design

Seeber's criterion for the steel lining is based on a maximum allowable strain (ε_{zul}) of the lining caused by the loading with p_i. The resulting thickness of the steel lining for every rock type can be seen in the appendix Chapter D.1. It is needed to assure that the steel strain during operation does not exceed ε_{zul} for a certain steel grade. ε_{zul} is calculated with the Hooke's law and can be found in Table 12 with all the necessary steel properties.

A valid comparison requires certain conditions to be preserved:

- Nearly zero in-situ stress to avoid an influence on the deformation behaviour of the steel lining from the in-situ conditions
- Circular shape of the storage with a diameter of 3.0 m
- Simulation with the calculated thickness from Seeber for a certain steel grade
- Elastic lining and rock mass behaviour

The evaluation of the results from the numerical analysis for the comparison is carried out by converting the uniform total/radial displacement at the storage boundary in the pressurisation stage, as shown in Figure 60, into a tangential strain of the steel lining. RS2 made it possible to query the values for the radial displacement at the boundary, transfer the achieved data into an excel-sheet and calculate the medium value.

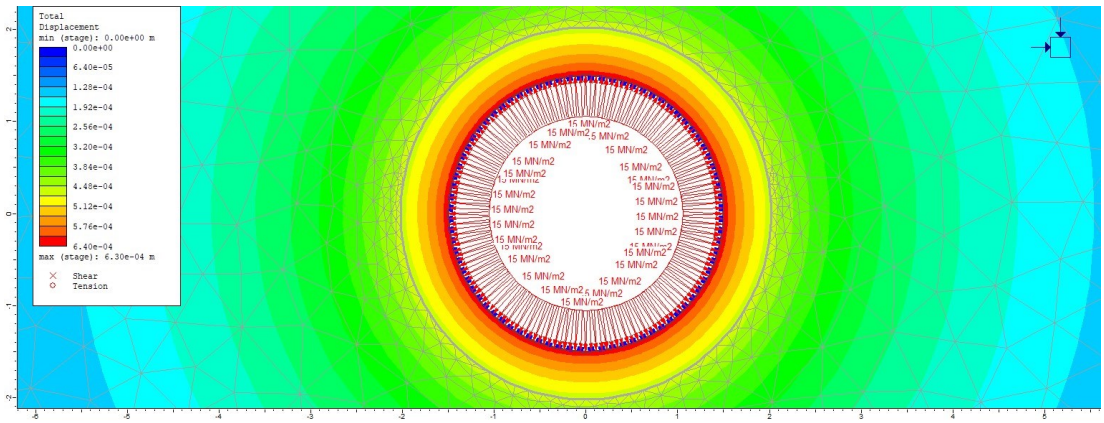

Figure 60: Total displacement of a steel lined storage boundary for Rock mass 1 with a p_i 15 MPa, using steel grade S550

For each rock type, a summary of the maximum strain, achieved by the steel lining in the numerical simulation, is provided. Some of the rock types are strong and stiff enough to take up p_i without a required steel lining. ε_{zul} and the achieved strain for Tuff 2, Rock mass 2, every p_i and steel grade are listed in Table 26 and
Table 27. The utilization (μ) of steel capacity as a factor of ε_{zul} is shown in Figure 61 and is calculated using Equation (17):

$$\mu = \frac{\varepsilon_{steel}}{\varepsilon_{zul}} [\%], \tag{17}$$

where ε_{steel} is the strain of the steel lining from the numerical simulation and ε_{zul} is the maximum allowable strain of the steel.

Table 26: Calculated strain of the steel lining from the numerical simulation for Tuff 2, a p_i of 10, 15 and 20 MPa as well as steel grades S460, S550 and S690

Strain of the steel lining for Tuff 2									
Steel grade	S690			S550			S460		
p_i [MPa]	10	15	20	10	15	20	10	15	20
radial displacement [mm]	1.60	1.96	2.22	1.44	1.72	1.92	1.31	1.54	1.69
New circumference [m]	9.45	9.45	9.45	9.44	9.44	9.45	9.44	9.44	9.45
Old circumference [m]	9.43	9.43	9.43	9.43	9.43	9.43	9.43	9.43	9.43
ε_{steel} [‰]	2.13	2.62	2.96	1.92	2.3	2.55	1.75	2.06	2.26
ε_{zul} [‰]	**2.63**	**2.63**	**2.63**	**2.10**	**2.10**	**2.10**	**1.75**	**1.75**	**1.75**

Table 27: Calculated strain of the steel lining from the numerical simulation for Rock mass 2, a p_i of 10, 15 and 20 MPa as well as steel grades S460, S550 and S690

Strain of the steel lining for Rock mass 2									
Steel grade	S690			S550			S460		
p_i [MPa]	10	15	20	10	15	20	10	15	20
radial displacement [mm]	no lining	0.77	0.96	no lining	0.73	0.90	0.52	0.70	0.85
New circumference [m]		9.43	9.44		9.43	9.44	9.43	9.43	9.44
Old circumference [m]		9.43	9.43		9.43	9.43	9.43	9.43	9.43
ε_{steel} [‰]		1.03	1.28		0.98	1.2	0.69	0.93	1.13
ε_{zul} [‰]	**2.63**	**2.63**	**2.63**	**2.10**	**2.10**	**2.10**	**1.75**	**1.75**	**1.75**

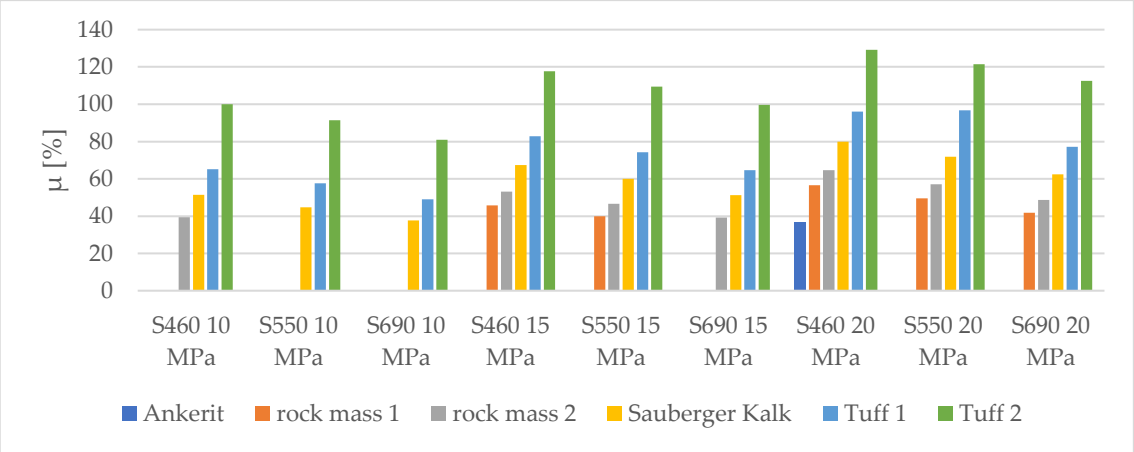

Figure 61: Utilization of the steel strain capacity for every rock type, a p_i of 10, 15 and 20 MPa as well as for steel grades S460, S550 and S690

Only rock types with a low E_{rm}, like Tuff 2, can reach or exceed the strain capacity of the steel lining in the numerical simulation, considering an elastic steel and rock mass behaviour with negligible uniform in-situ stress conditions of 0.01 MPa.
After assessing the results, a numerical simulation without considering any steel lining was done to find out, if ε_{zul} can even be reached for each rock type and p_i. The radial displacement for an unlined storage built in the rock type Tuff 1 with 5 MPa uniform in-situ stress and a p_i of 20 MPa is shown in Figure 62. The resulting tangential strain can be found in Table 28.

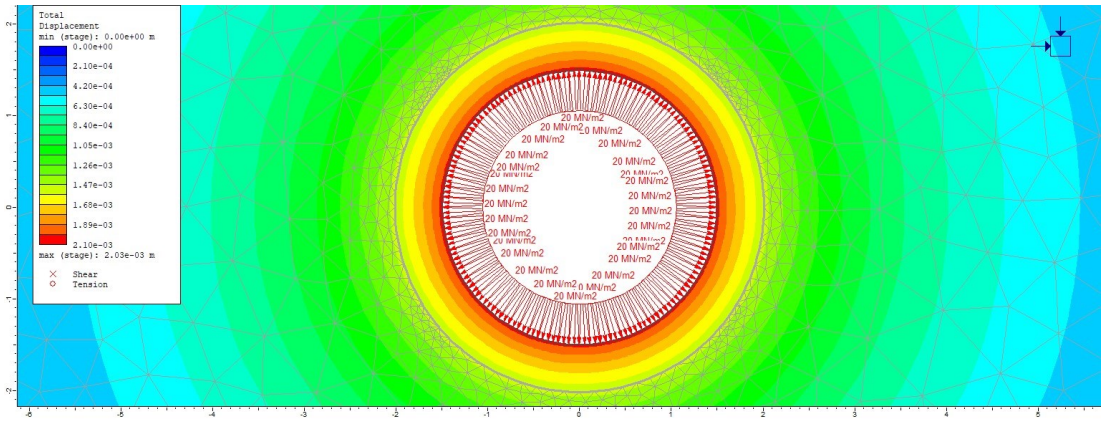

Figure 62: Total displacement of the unlined storage boundary in Tuff 1 with a p_i of 20 MPa

Table 28: Calculated tangential strain of the unlined storage boundary from the numerical simulation for Tuff 1 as well as for a p_i of 10, 15 and 20 MPa

p_i [MPa]	10	15	20
Radial displacement [mm]	1.02	1.52	2.03
New circumference [m]	9.438	9.444	9.450
Old circumference [m]	9.425	9.425	9.425
Tangential strain [‰]	1.36	2.03	2.71

A calculation of the tangential strain of the unlined storage boundary is carried out for every rock type with a p_i of 10, 15 and 20 MPa and the results can be looked up in the appendix Chapter D.2 and D.3. The graphical display of all tangential strains, shown in Figure 63, indicates that only a steel lining built in the following rock types can exceed ε_{zul}:

- Sauberger Kalk with a p_i of 20 MPa and a lining with a steel grade S460
- Tuff 1 with a p_i of 15 MPa and a lining with a steel grade S460
- Tuff 1 with a p_i of 20 MPa and a lining with a steel grade S460 and S550
- Tuff 2 with every p_i and for every steel grade

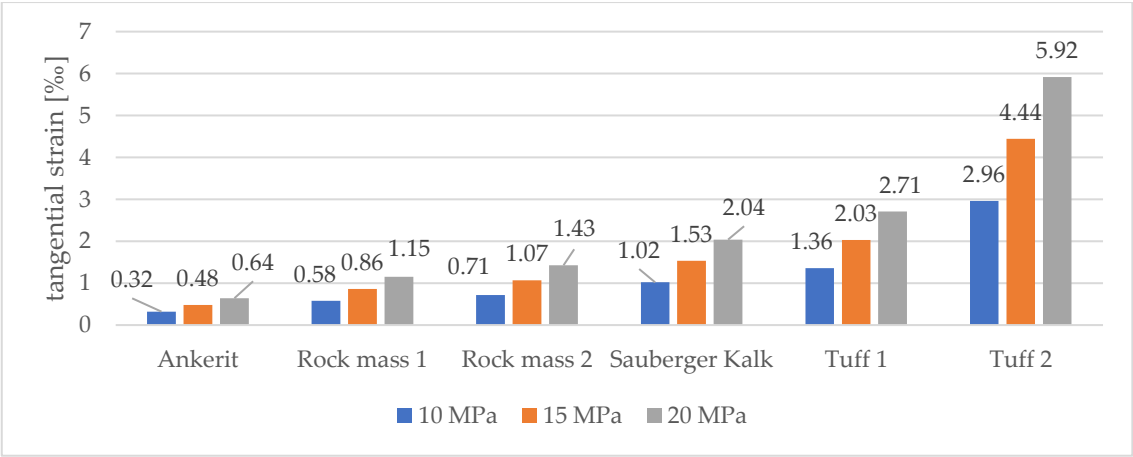

Figure 63: Tangential strain of the unlined storage boundary for each rock type and a p_i of 10, 15 and 20 MPa

Based on this knowledge, the use of a high strength steel lining for load bearing tasks of a storage is only meaningful for rock types with a low E_{rm} because the radial displacement of the storage can be reduced significantly, as shown in Figure 64.

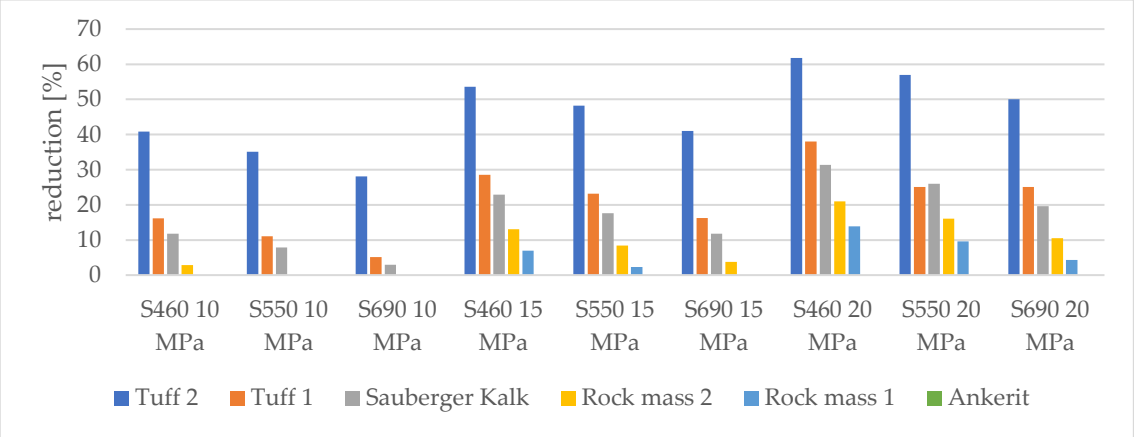

Figure 64: Reduction of the radial displacement of the storage boundary due to a constructed steel lining for a p_i of 10, 15 and 20 MPa and steel grades S460, S550 and S690

Plastic behaviour of the steel lining and rock mass

If the rock mass is allowed to fail and plastic zones can potentially develop, the strain of the steel lining is going to increase. The rock types of Tuff 1, Sauberger Kalk and Rock mass 2 with a p_i of 15 and 20 MPa were used in a series of numerical simulations to investigate this topic. Tuff 2 was neglected because the necessary unlined excavation is not stable and plastic zones are already existing after the excavation. Uniform in-situ stress with a magnitude of 5 MPa was chosen for the comparison and the results are presented in Figure 65 and can be seen in the appendix Chapter D.4.

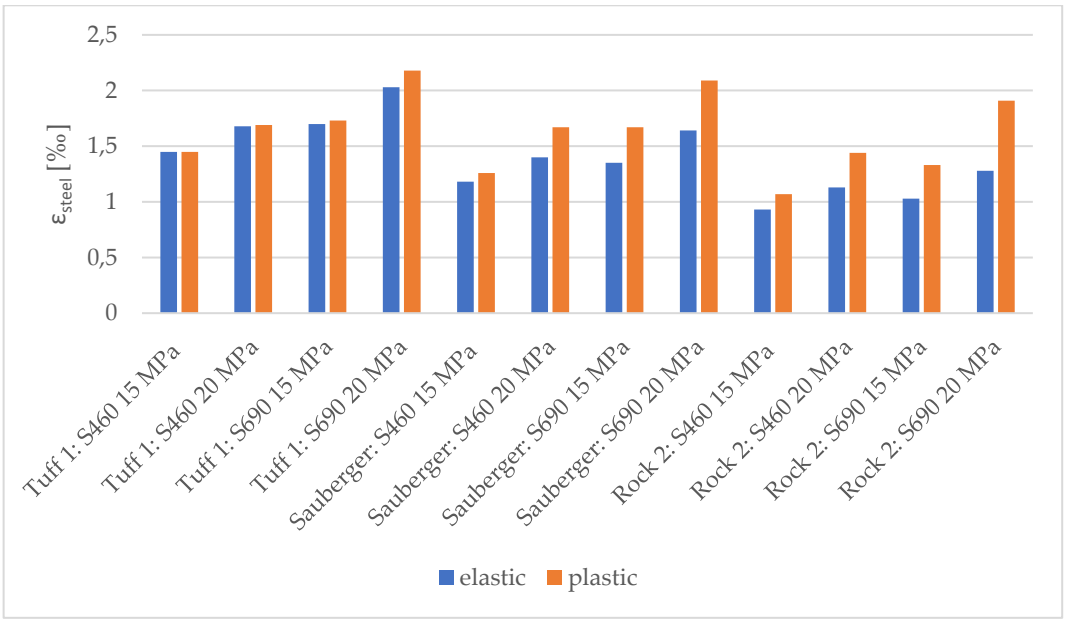

Figure 65: Strain of the steel lining ε_{steel} for Tuff 1, Sauberger Kalk and Rock mass 2 for the steel grades S460 and S690 and magnitudes of p_i with 15 MPa and 20 MPa

Figure 61 makes it clear that, with the exception of Tuff 2, with its very low value of E_{rm}, the steel strength capacity is not effectively utilized and that the lining is in general over-dimensioned. Even after considering plastic rock mass behaviour, the maximum strain of the steel lining and therefore the utilization of the steel capacity did not increase significantly, as it can be seen in Figure 65. Regarding cost-efficiency and CO_2 consumption, the design with the analytical calculation from Seeber is not favourable and must be optimized.

A comparison of the magnitude of radial displacement is carried out for a steel lined storage in Rock mass 1, a p_i of 20 MPa and steel grade S550 between the elastic and plastic model in Figure 66. The increase of 0.39 mm to a maximum displacement of 1.17 mm of the storage boundary from the elastic model to the plastic model shows, that even with a failed rock mass around the storage, caused by p_i, the criterion from Seeber with ε_{zul} of 2.10‰ for a S550 cannot be reached by a resulting ε_{steel} of 1.56‰.

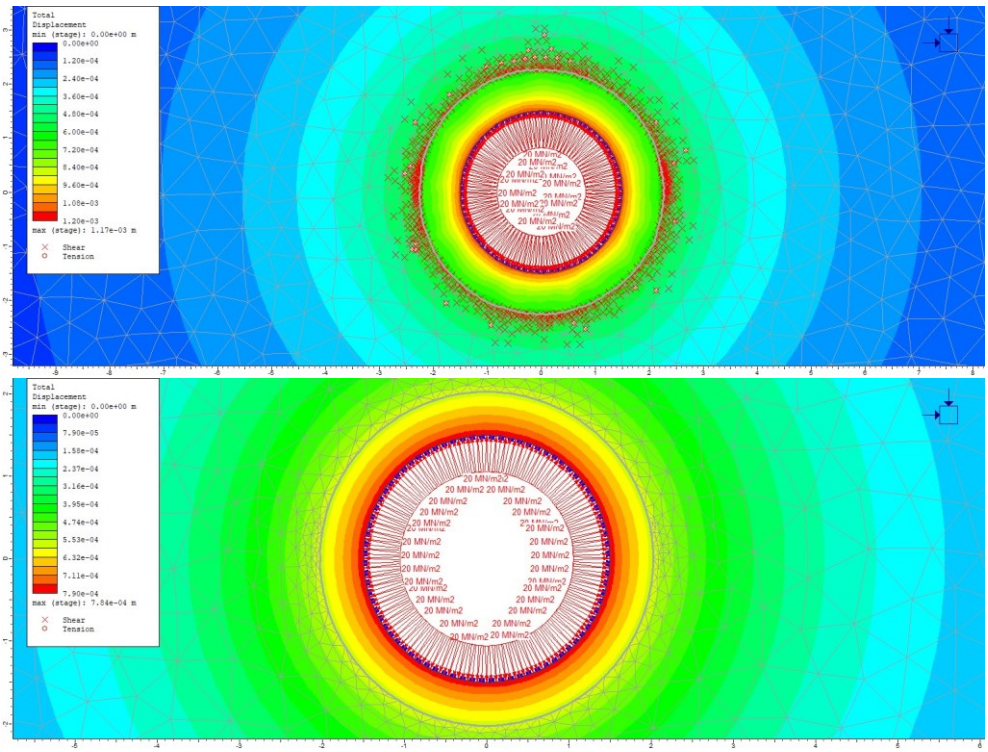

Figure 66: Comparison of the radial displacement of the steel lined storage boundary in Rock mass 1 with a p_i of 20 MPa and steel grade S550 between the plastic numerical model (top image) and the elastic numerical model (bottom image)

The rock mass failure is caused by an exceedance of the tensile strength of 1.01 MPa for Rock mass 1, which can be seen in Figure 67, by comparing the σ_3 plots of the elastic and plastic model for a p_i of 20 MPa and steel grade S550. A plastic zone, like it is visible in Figure 67, must be avoided in the design process of the storage facility and an optimization of the steel lining was therefore carried out for the rock types Tuff 1 and Sauberger Kalk.

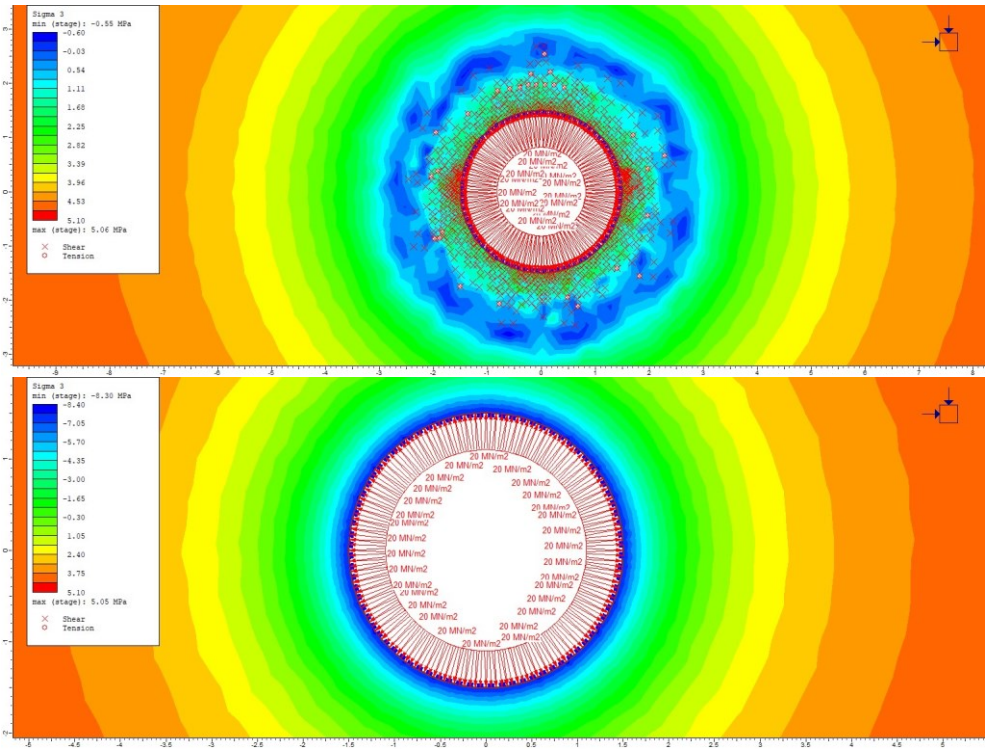

Figure 67: Comparison of σ_3 in the surrounding rock mass of the steel lined storage boundary in Rock mass 1 with a p_i of 20 MPa and the steel grade S550 between the plastic numerical model (top image) and the elastic numerical model (bottom image)

Optimization of the steel lining

Failed rock mass will also cause a failure of the backfilling concrete of the steel lining. Cracked concrete provides no sufficient bedding of the lining and will lead to a reduction of the life span and damage on the drainage system. Stress peaks can lead to a partially yielding of the steel lining due to an exceedance of the tensile strength. Therefore, the integrity of the surrounding rock must be maintained by an adequate design. A numerical simulation was carried out for Tuff 1 and Sauberger Kalk and uniform in-situ stress of 5 MPa to determine the necessary thickness of the steel lining for a p_i of 15 and 20 MPa without causing any rock mass failure. Resulting maximum axial forces of the liner are divided through the steel lining thickness from the numerical simulation to get the peak normal stress (σ_n), by using Equation (18). The σ_n is compared with $f_{y,d}$ of each steel grade to calculate the utilized steel strength capacity (μ) with the Equation (19).

$$\sigma_n = \frac{axial\ force}{lining\ thickness}\ [MPa] \tag{18}$$

$$\mu = \frac{\sigma_n}{f_{y,d}}\ [\%] \tag{19}$$

The calculated thickness according to the analytical method from Seeber can be found in the appendix Chapter D.1 and had to be increased to prevent the occurrence of any rock mass failure. Optimized values of the thickness as well as the achieved μ of each steel grade are shown in Table 29 for Tuff 1 and in Table 30 for Sauberger Kalk.

Table 29: Optimization of the steel lining thickness of the storage built in Tuff 1 and the associated σ_n and μ for a p_i of 15 and 20 MPa as well as for steel grades S460, S550 and S690

Steel grade	p_i	Optimized thickness	Axial force	σ_n	μ
S460	15 MPa	28 mm	**5 MN**	179 MPa	49 %
S550	15 MPa	28 mm	**5 MN**	179 MPa	41 %
S690	15 MPa	28 mm	**5 MN**	179 MPa	32 %
S460	20 MPa	65 mm	**12 MN**	185 MPa	50 %
S550	20 MPa	65 mm	**12 MN**	185 MPa	42 %
S690	20 MPa	65 mm	**12 MN**	185 MPa	33 %

Table 30: Optimization of the steel lining thickness of the storage built in Sauberger Kalk and the associated σ_n and μ for a p_i of 15 and 20 MPa as well as for steel grades S460, S550 and S690

Steel grade	p_i	Optimized thickness	Axial force	σ_n	μ
S460	15 MPa	63 mm	**7.4 MN**	117 MPa	32 %
S550	15 MPa	63 mm	**7.4 MN**	117 MPa	27 %
S690	15 MPa	63 mm	**7.4 MN**	117 MPa	21 %
S460	20 MPa	125 mm	**15.0 MN**	120 MPa	33 %
S550	20 MPa	125 mm	**15.0 MN**	120 MPa	27 %
S690	20 MPa	125 mm	**15.0 MN**	120 MPa	22 %

It can be seen in Table 29 and Table 30, that the maximum value of μ is 50%. As a result, high-strength steel grades are not needed for the steel lining of the storage, which is also proven by the achieved ε_{steel} for Tuff 1 and Sauberger Kalk in comparison with ε_{zul} listed in Table 31.

Table 31: Comparison of the achieved ε_{steel} from the lining in the numerical simulation with ε_{zul} for each steel grade S460, S550 and S690 as well as for a p_i of 15 and 20 MPa

Steel grade	p_i [MPa]	ε_{zul} [‰]	Tuff 1	Sauberger Kalk
			ε_{steel} [‰]	ε_{steel} [‰]
S460	15	1.75	1.54	0.998
S550	15	2.10	1.54	0.998
S690	15	2.63	1.54	0.998
S460	20	1.75	1.59	1.000
S550	20	2.10	1.59	1.000
S690	20	2.63	1.59	1.000

The success of the optimization to prevent rock mass failure can be seen in Figure 68 for the rock type Tuff 1 and a p_i of 20 MPa and the caused increase of the axial force in the steel lining is shown in Figure 69.

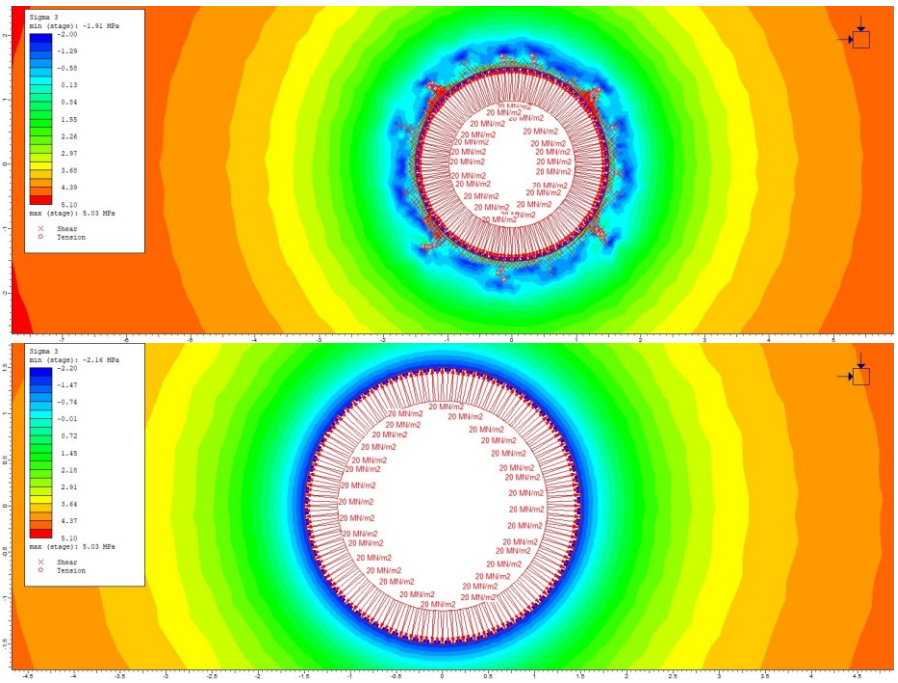

Figure 68: Comparison of the resulting induced σ_3 and plastic zone from the numerical simulation of a steel lined storage built in Tuff 1 for a p_i of 20 MPa and the steel grade S550 between the original steel lining (top image) and the optimized steel lining (bottom image)

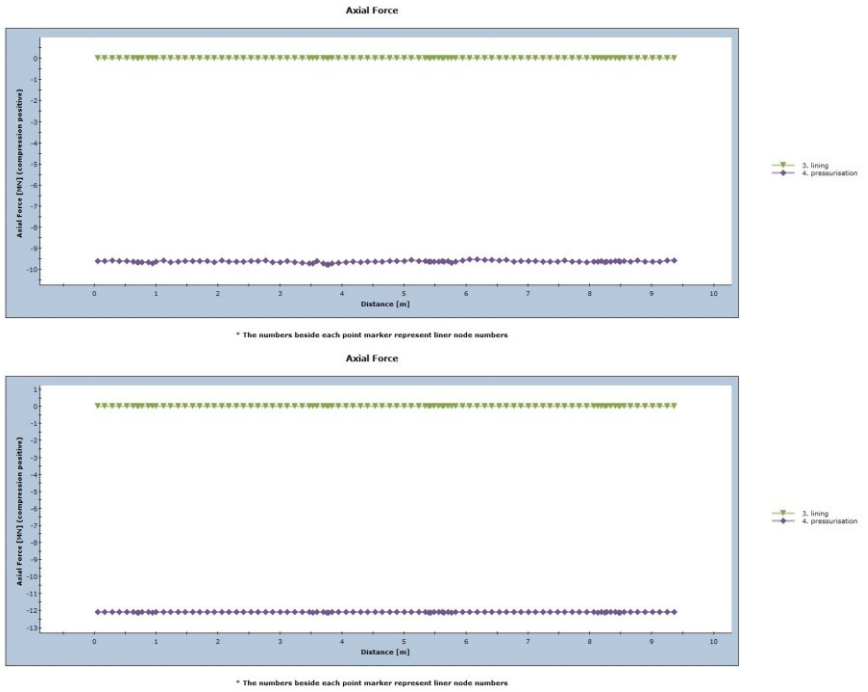

Figure 69: Comparison of the axial force of the steel lining from the numerical simulation of a storage built in Tuff 1 for a p_i of 20 MPa and the steel grade S550 between the original steel lining (top image) and the optimized steel lining (bottom image)

8.3 Gap injection influence on the surrounding rock mass

The maximum values of $p_{v,0}$ for every rock type and magnitude of p_i, which are listed in Table 5, were applied as an internal pressure at the excavation boundary of an unlined storage facility, as described in Chapter 7.5.2. Different in-situ stress conditions, leaned on the given overburden of the storage facility, were chosen to investigate the importance for a given rock type by an analysis of the generated results.

The following in-situ stress conditions were chosen for the numerical analyses:

- Uniform in-situ stress with a magnitude of 5 MPa (second most likely to occur in reality)
- Uniform in-situ stress with a magnitude of 2 MPa (to investigate the behaviour of the rock mass under low uniform in-situ stress conditions compared with the injection pressure)
- Non-uniform in-situ stress with a magnitude of 5 MPa for σ_1 and a magnitude of 2.5 MPa for σ_3 (most likely to occur in reality)
- Non-uniform in-situ stress with a magnitude of 2 MPa for σ_1 and a magnitude of 1 MPa for σ_3 (to investigate the behaviour of the rock mass under low non-uniform in-situ stress conditions compared with the injection pressure)

Comparison of the results was carried out with the total displacement of the excavated storage boundary and a visual analysis of the failed zones of the surrounding rock mass, due to the applied internal pressure with the magnitude of $p_{v,0}$.
Resulting total displacements for the same rock type and $p_{v,0}$ were compared between the different magnitudes of uniform or non-uniform in-situ stresses. A decrease of in-situ stress led to an increase of the total displacement and depth of the plastic zone. The percentages of increase of the total displacement for every rock type and uniform in-situ stress after reducing the uniform in-situ stress with a magnitude of 5 MPa to 2 MPa is shown in Figure 70 and for a reduction of the magnitude of the non-uniform in-situ stress in Figure 71.

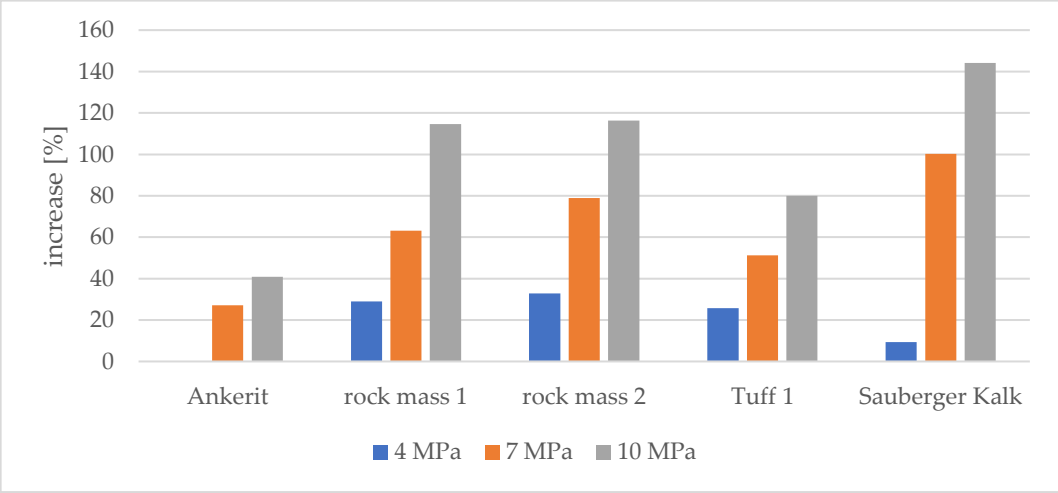

Figure 70: Increase of the total radial displacement of the storage boundary for uniform in-situ stress, every investigated rock type and the maximum $p_{v,0}$ for a p_i of 4, 7 and 10 MPa

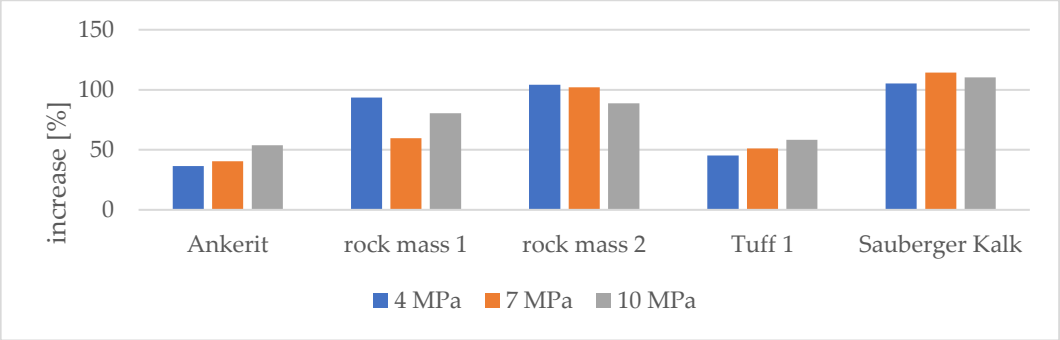

Figure 71: Increase of the total radial displacement of the storage boundary for non-uniform in-situ stress, every investigated rock type and the maximum $p_{v,0}$ for a p_i of 4, 7 and 10 MPa

A clear difference of the increase of the total displacement can be seen in Figure 70 for uniform in-situ stress conditions. Higher magnitudes of $p_{v,0}$ result in a higher increase after decreasing the in-situ stress of the total displacement because of the occurrence of a deeper plastic zone. The amount of increase is linked with the depth of the plastic zone and therefore with the magnitude of the in-situ stress. This result is displayed in the comparison of the application of the same $p_{v,0}$ for uniform in-situ stresses of 5 MPa and 2 MPa in Figure 72 and Figure 73.
Maximum displacements for non-uniform in-situ stresses occur in the direction of σ_1 because the occurring tensile and shear failure in that area reduces E_{rm} from the peak to the residual value and increases the possible displacement. The increase of the maximum radial displacement is therefore nearly constant for every $p_{v,0}$ because a rock mass failure occurs already after implementing a low magnitude of $p_{v,0}$ as internal pressure. This result is displayed in the comparison of the application of the same $p_{v,0}$ for both non-uniform in-situ stresses in Figure 74 and Figure 75.

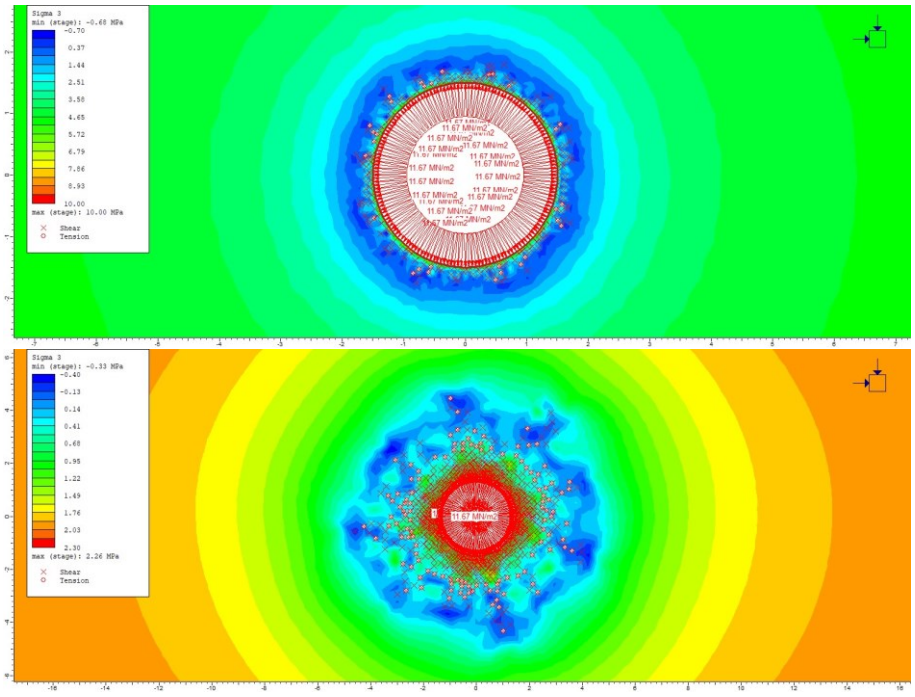

Figure 72: Comparison of σ_3 and occuring plastic zone in Sauberger Kalk with a $p_{v,0}$ of 11.67 MPa between a uniform in-situ stress of 5 MPa (top image) and 2 MPa (bottom image)

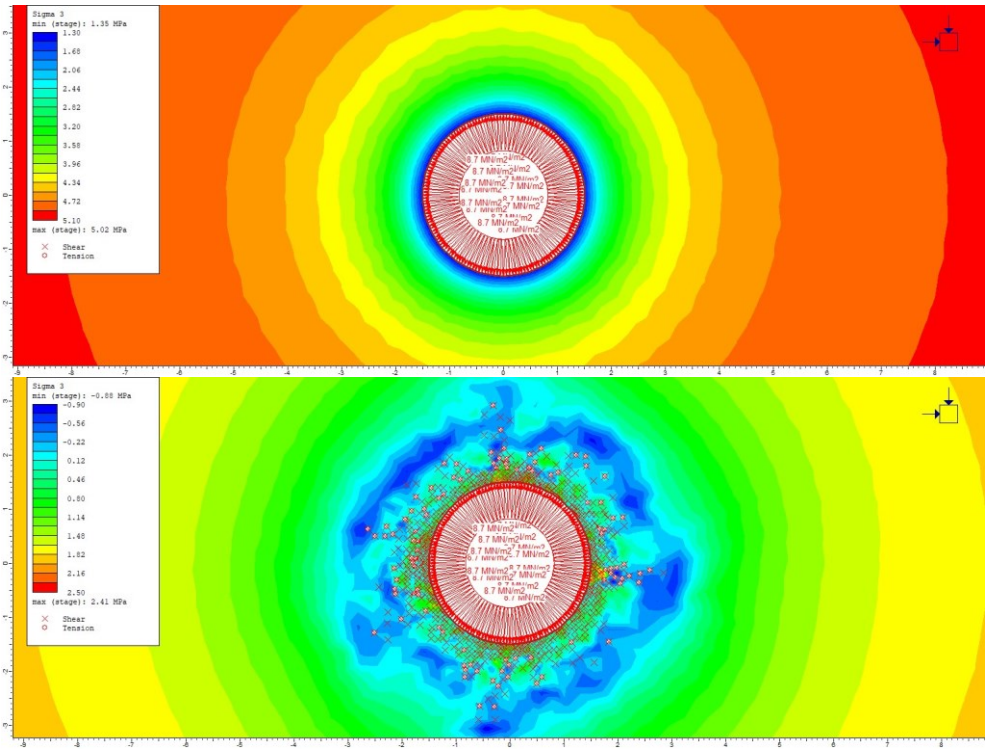

Figure 73: Comparison of σ_3 and occuring plastic zone in Rock mass 1 with a $p_{v,0}$ of 8.7 MPa between a uniform in-situ stress of 5 MPa (top image) and of 2 MPa (bottom image)

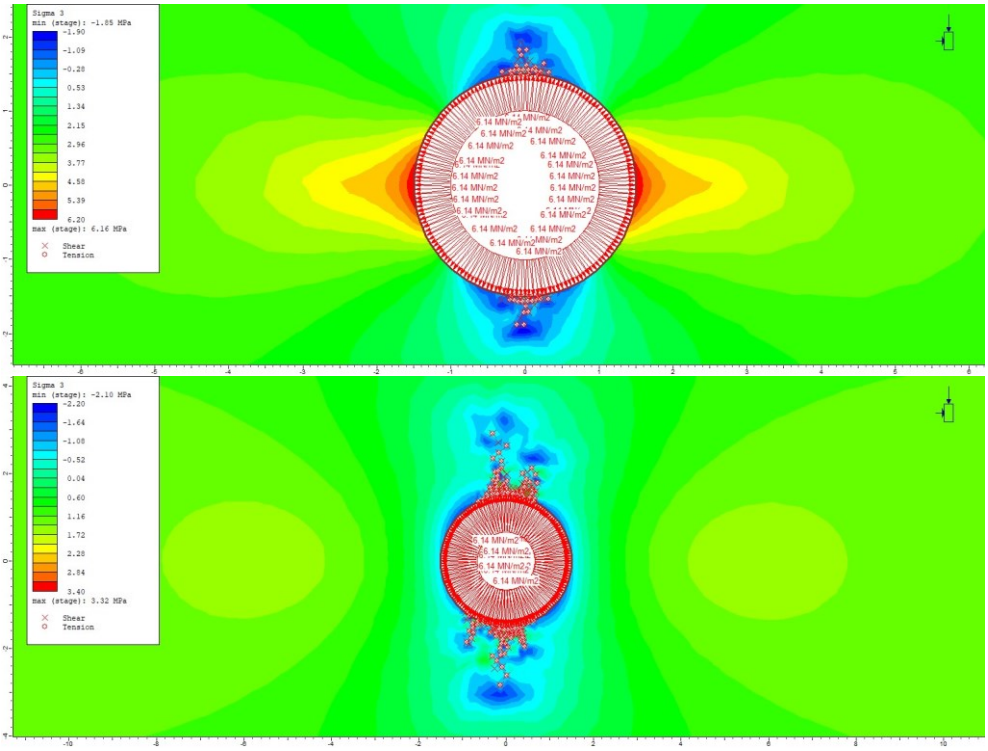

Figure 74: Comparison of σ_3 and occuring plastic zone for Tuff 1 with a $p_{v,0}$ of 6.14 MPa between a non-uniform in-situ stress with σ_1 of 5 MPa and σ_3 of 2.5 MPa (top image) and a non-uniform in-situ stress with σ_1 of 2 MPa and σ_3 of 1 MPa (bottom image)

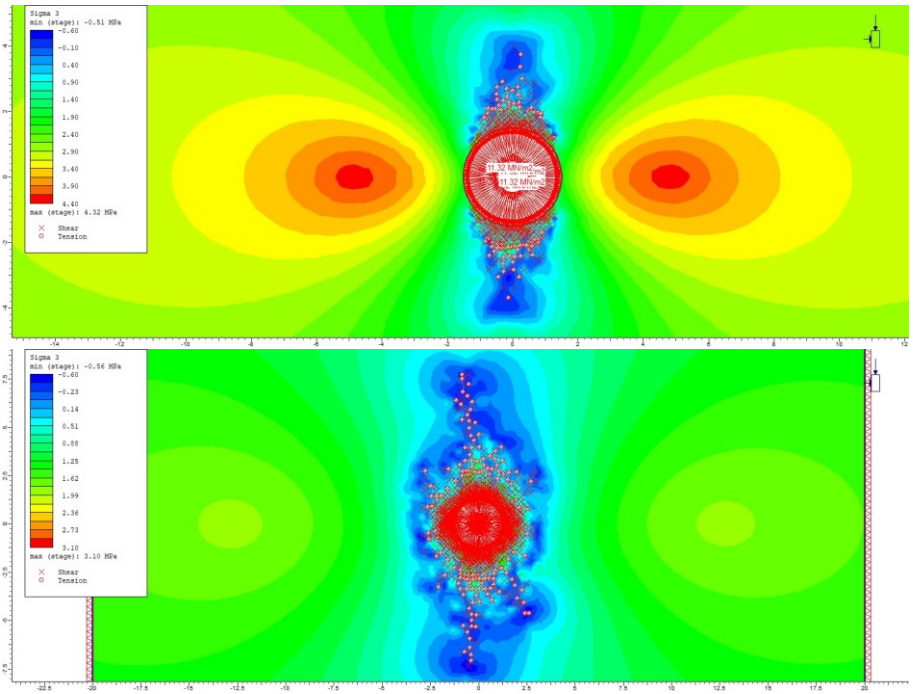

Figure 75: Comparison of σ_3 and occurring plastic zone in Rock mass 2 with a $p_{v,0}$ of 11.32 MPa between a non-uniform in-situ stress with σ_1 of 5 MPa and σ_3 of 2.5 MPa (top image) and a non-uniform in-situ stress with σ_1 of 2 MPa and σ_3 of 1 MPa (bottom image)

Non-uniform radial displacement of the storage boundary, which are caused by a non-uniform in-situ stress and rock mass failure, is shown in Figure 76.

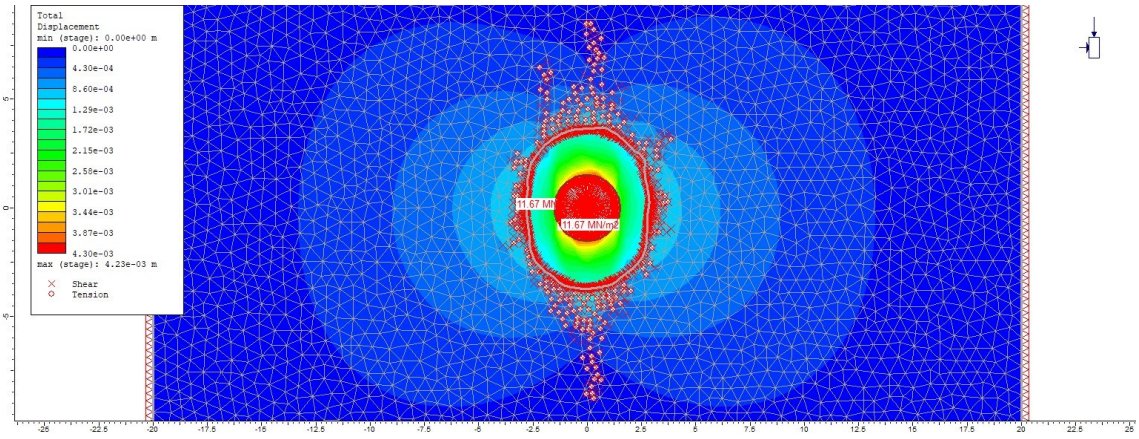

Figure 76: Distribution of the radial displacement for Sauberger Kalk with a $p_{v,0}$ of 11.67 MPa and a non- uniform in-situ stress with a σ_1 of 2 MPa and a σ_3 of 1 MPa

A certain stiffness and magnitude of in-situ stress is necessary to maintain the pre-stressing of the concrete lining over the whole life span of the storage. The decrease of the strength and stiffness of the surrounding rock mass caused by rock mass failure from the peak to residual values has several negative consequences:

- a decrease of the rock mass stiffness and deformation modulus, which was considered in the calculation according to Seeber in the plastic zone
- a decrease of the possible gap injection pressure in reality
- non-uniform plastic zones lead to a non-uniform pre-stressing of the concrete

As mentioned in Chapter 5.4, σ_3 should always be higher than $p_{v,0}$ to avoid rock mass failure. [3] An investigation of this statement was carried out through a numerical simulation in which $p_{v,0}$ was increased in multiple stages until a failure of the surrounding rock mass starts to develop. The determined magnitude of $p_{v,0}$ for each rock type and different in-situ stress, which are shown in Figure 77, was compared with the actual σ_3 and the possible exceedance of σ_3 by $p_{v,0}$ can be seen in Figure 78.

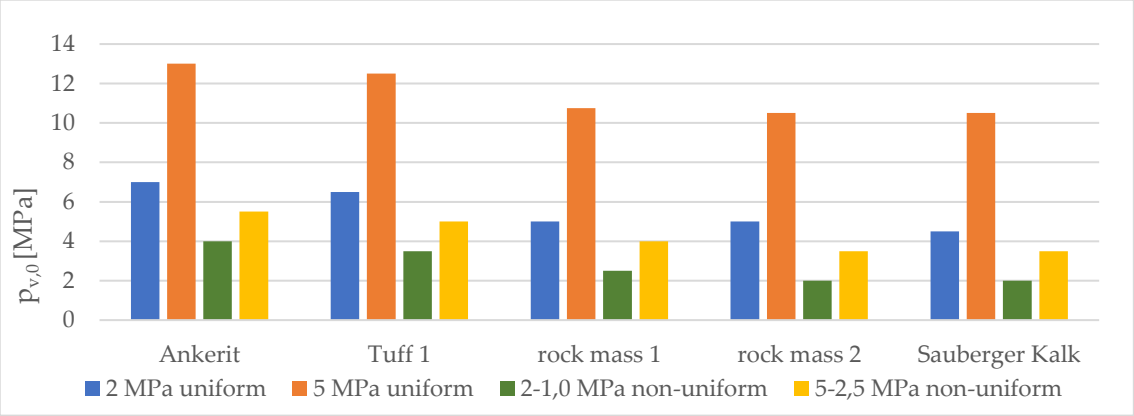

Figure 77: Maximum $p_{v,0}$ to cause failure for every rock type and for two different uniform in-situ stress magnitudes as wells as two different non-uniform in-situ stress conditions

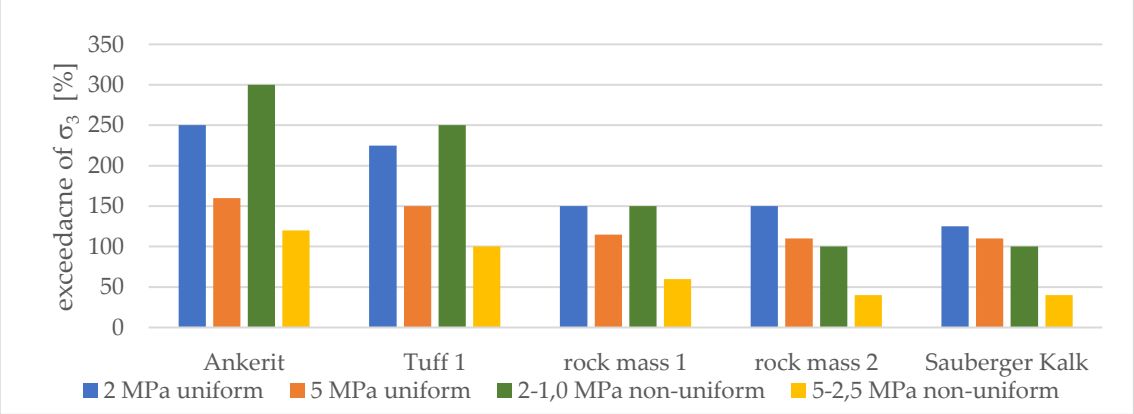

Figure 78: Exceedance of σ_3 by $p_{v,0}$ for every rock type and for two different uniform in-situ stress magnitudes as wells as two different non-uniform in-situ stress conditions

The rock types in Figure 78 are distributed according to their tensile strength, which are listed in Table 10 starting with Ankerit with the highest value. A possible exceedance gets higher with an increasing tensile strength because a higher magnitude of induced tensile stresses can be taken up by the surrounding rock mass. Even for rock mass with low tensile strength capacity, like Sauberger Kalk, σ_3 can be exceeded by 40%.
An optimized design of the gap injection pressure for a pre-stressed concrete lining should consider a possible exceedance of σ_3 by $p_{v,0}$ especially for rock types with high tensile strength and a storage facility location with a low magnitude of the in-situ stress.

The additional tables and figures, which were necessary to achieve and understand the results can be found found in the appendix Chapter E.

8.4 In-situ stress influence on the lining

8.4.1 In-situ stress influence on the pre-stressed concrete lining

Concrete has a low tensile strength, with around 1/10 of the compressive strength and a low strain capacity of 0.1 ‰. Only an increase of the radial displacement of slightly higher than 0.075 mm, lead to an exceedance of the strain capacity and cracking of the concrete lining. Such a magnitude of radial displacement leads to an increase of the circumference of 0.001 m and the concrete strain can be calculated with Equation (20):

$$concrete\ strain: \frac{\Delta C}{C} = \frac{0.001}{9.425} = 0.1\ ‰\,, \tag{20}$$

where ΔC is the increase of the circumference of the storage and C is the original circumference with 9.425 m.

The determination of the in-situ stress influence on the pre-stressed concrete lining (purple coloured lining in the following plots) was done by multiple numerical simulations of a pre-stressed concrete lining with:

- different in-situ stress conditions,
- a thickness of the concrete lining of 0.3 m,
- a concrete quality of C30/37,
- a p_i of 4, 7 and 10 MPa including the required p_v and $p_{v,0}$ according to Seeber
- as well as the calibrated value of E_{gap}.

Shotcrete as primary support (turquoise coloured lining in the following plots) was implemented in the model to also investigate a potential failure of the primary support. Lining and rock mass had a plastic post-peak behaviour with residual strength and stiffness according to Chapter 7.3 and 7.4. Yielded parts of the lining are marked red in the following plots of the results from the numerical simulation.

The following in-situ stress magnitudes were chosen for the numerical simulations:

- σ_1 with 10 MPa and σ_3 with 5 MPa
- σ_1 with 8 MPa and σ_3 with 4 MPa
- σ_1 with 6 MPa and σ_3 with 3 MPa
- σ_1 with 5 MPa and σ_3 with 2.5 MPa
- σ_1 with 4 MPa and σ_3 with 2 MPa
- σ_1 with 2 MPa and σ_3 with 1 MPa

Maximum radial displacement of the storage boundary and the lowest value of the induced σ_3 of the surrounding rock mass were determined. The results for Ankerit and Tuff 1 can be seen in Table 32 and Table 33.

Table 32: Resulting maximum radial displacement and lowest value of σ_3 for Ankerit, a p_i of 10 MPa and different magnitudes of in-situ stress

Ankerit – p_i of 10 MPa							
In-situ stress [MPa]	5 uniform	10-5	8-4	6-3	5-2.5	4-2	2-1
σ_3 [MPa]	-0.01	-2.55	-2.98	-2.94	-5.27	-3.91	-10.46
max. displacement [mm]	0.243	0.254	0.274	0.32	0.377	0.384	0.536

Table 33: Resulting maximum radial displacement and lowest value of σ_3 for Tuff 1, a p_i of 10 MPa and different magnitudes of in-situ stress

Tuff 1 – p_i of 10 MPa							
In-situ stress [MPa]	5 uniform	10-5	8-4	6-3	5-2.5	4-2	2-1
σ_3 [MPa]	0.09	-1.75	-2	not stable	not stable	not stable	not stable
max. displacement [mm]	1.7	1.74	1.72				

The difference between the maximum radial displacement between the different magnitudes of in-situ stress is less than 0.075 mm and therefore bottom image the crack criterion of concrete until the in-situ stress reaches a certain magnitude. For Ankerit a reduction of σ_3 of the primary in-situ stress from 2 MPa to 1 MPa leads to an exceedance of the strain capacity of concrete by the difference of the maximum radial displacement. Crack patterns are going to occur and will damage the sealing layer of the hydrogen storage. A decrease of σ_3 4 MPa to 3 MPa for Tuff 1 leads to an unstable model, which could not reach equilibrium. Figure 79 shows an overview of the maximum radial displacements of every converged numerical simulation of all rock types for a p_i of 10 MPa and different in-situ stress magnitudes.

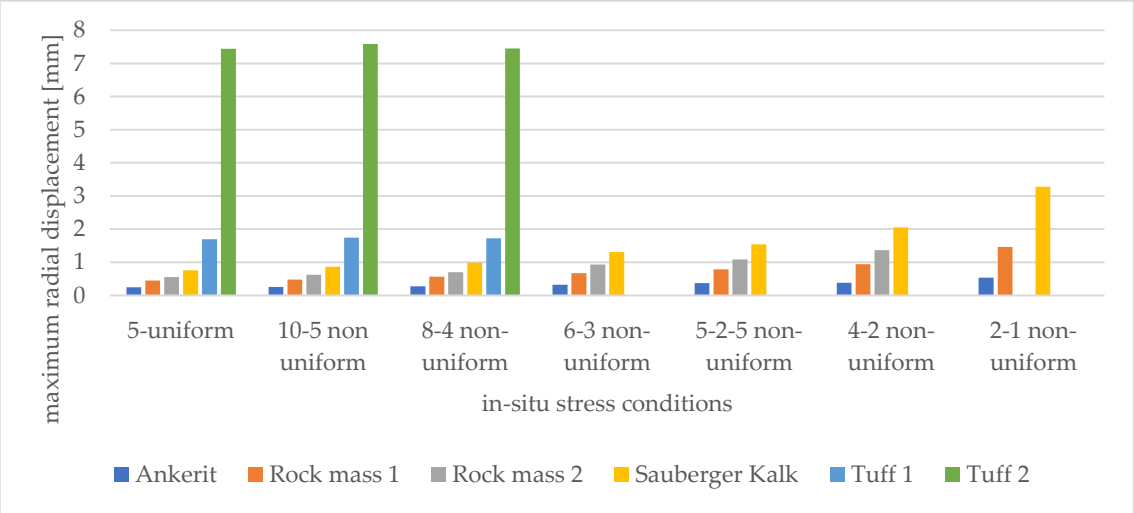

Figure 79: Maximum radial displacements of the storage boundary constructed with a pre-stressed concrete lining for every rock type, a p_i of 10 MPa and different in-situ stress magnitudes

An increase of p_i and decrease of the magnitude of the in-situ stress led to an increase of the number of yielded elements of the shotcrete and concrete liner as well as the number of yielded elements in the surrounding rock mass. In Figure 80 the total displacement of the storage boundary is compared between different non-uniform in-situ stress conditions for Rock mass 2 and a p_i of 4 MPa. The concrete lining fails in the numerical simulation with lower in-situ stress due to the concentrated displacement peaks in the crown and invert caused by the increased depth of the failed rock mass zone. Results for an increased magnitude of p_i with 10 MPa and a higher difference between the values of the in-situ stress can be seen for Ankerit in Figure 81. Clearly visible fractures in the rock mass and nearly a completely failed concrete lining mark an unsuccessful design of the storage.

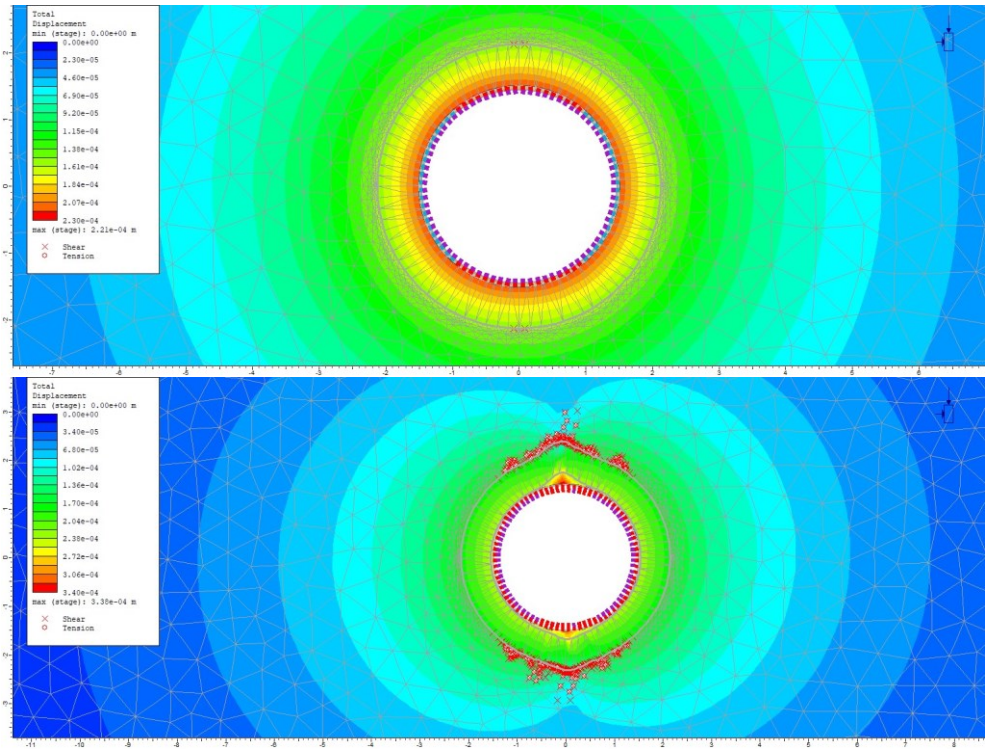

Figure 80: Total displacement the storage boundary constructed with a 0.3 m thick C30/37 pre-stressed concrete in Rock mass 2 with a p_i of 4 MPa, a non-uniform in-situ stress with a σ_1 of 6 MPa and a σ_3 of 3 MPa (top image) and a σ_1 of 2 MPa and a σ_3 of 1 MPa (bottom image)

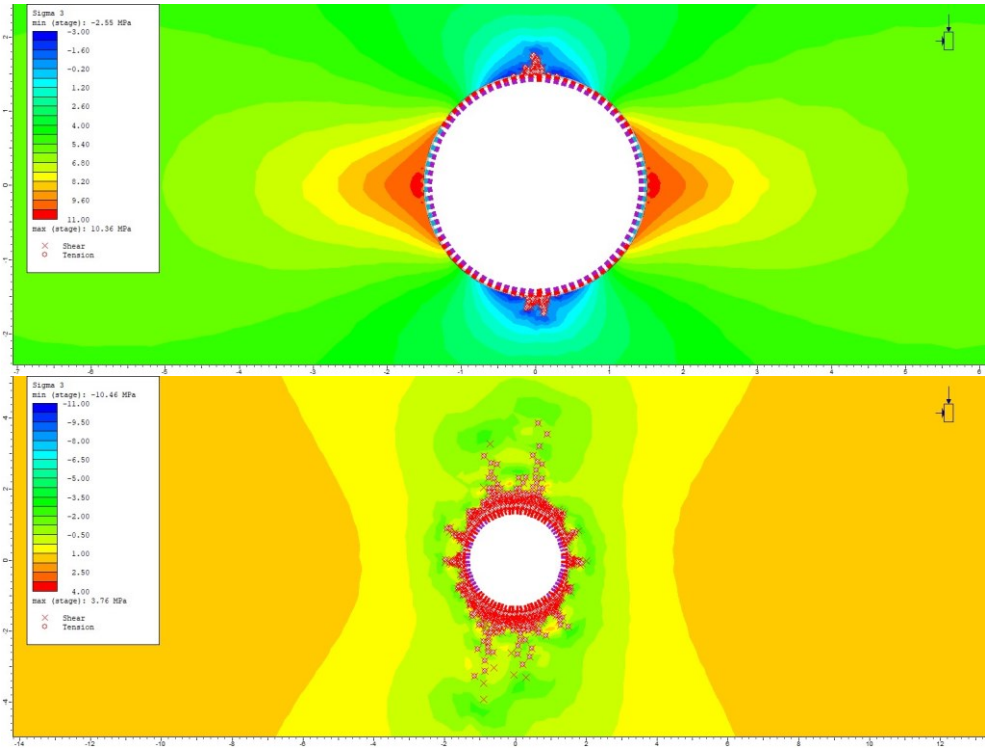

Figure 81: Failure of the rock mass and 0.3 m thick C30/37 concrete lining for Ankerit with a p_i of 10 MPa, a non-uniform in-situ stress with a σ_1 of 10 MPa and a σ_3 of 5 MPa (top image) and a σ_1 of 2 MPa and σ_3 of 1 MPa (bottom image)

Figure 82 shows the difference of the failed rock mass as well as the yielded parts of the lining for Rock mass 2 and a p_i of 7 MPa. It can be seen that $p_{v,0}$ already causes rock mass failure and yielding of the shotcrete, but the concrete lining partly yields only by the increased plastic zone in the pressurization stage.

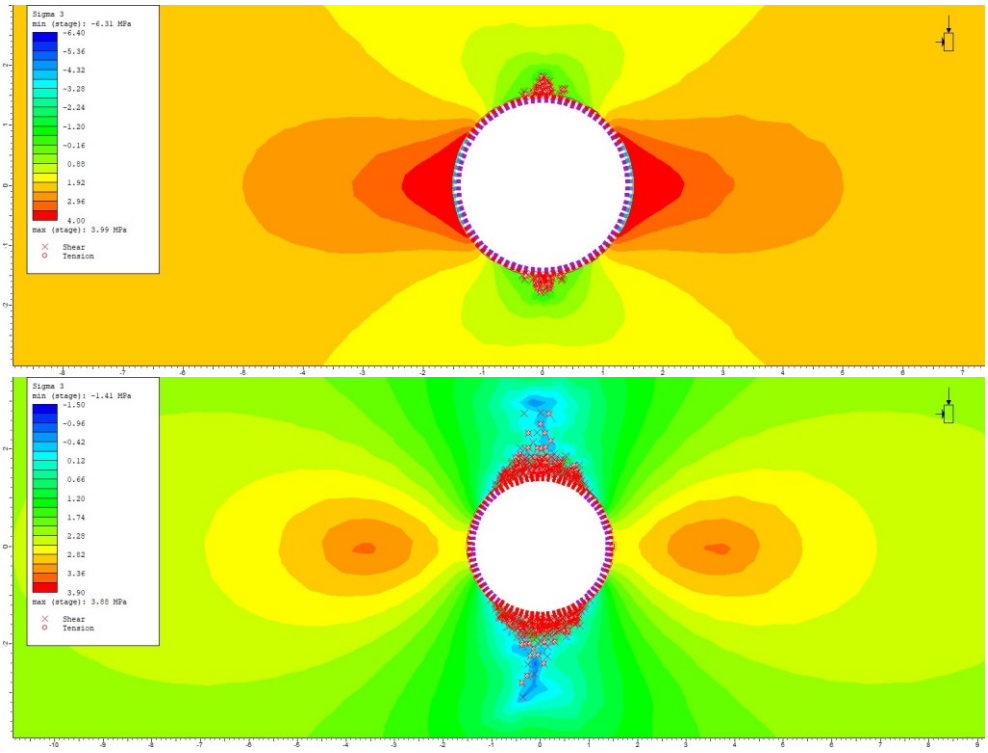

Figure 82: Failure of the rock mass and pre-stressed 0.3 m thick C30/37 concrete lining in Rock mass 2 with a p_i of 7 MPa and a non-uniform in-situ stress with a σ_1 of 4 MPa and a σ_3 of 2 MPa in the gap injection stage (top image) and the pressurisation stage (bottom image)

A proof that the high tensile stresses of the σ_3 plots only occur in the gap injection material during the gap injection stage, is given in Figure 83.

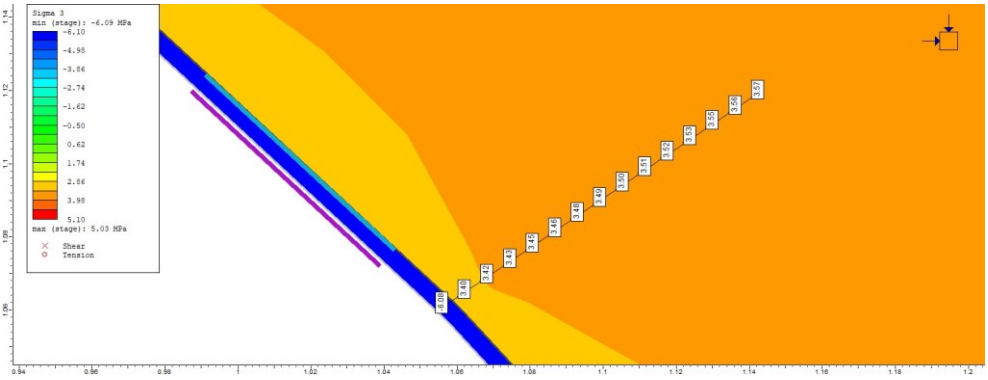

Figure 83: σ_3 plot with a query of the nodal values near the gap injection material in the gap injection stage for Ankerit, a p_i of 10 MPa and an in-situ stress with a magnitude of 5 MPa

The additional tables and figures, which were necessary to achieve and understand the results can be found found in the appendix Chapter F.

8.4.2 In-situ stress influence on the steel lining

The influence of the in-situ stress conditions on the behaviour of the steel lining is carried out by numerical simulations with a p_i of 15 and 20 MPa for every steel grade and the rock types Tuff 1, Sauberger Kalk, Rock mass 1 and Rock mass 2. These rock types are chosen because they represent a broad range of stiffness and strength capacities. Following in-situ stress conditions were chosen for the investigation:

- uniform in-situ stress with a magnitude of 5 MPa
- non-uniform in-situ stress with a σ_1 of 6 MPa and a σ_3 of 3 MPa
- non-uniform in-situ stress with a σ_1 of 6 MPa and a σ_3 of 2 MPa

For non-uniform in-situ stress conditions with a σ_1 in vertical direction, a peak radial displacement is expected in the crown and invert, which can cause a failure of the steel lining due to excessive elongation. The maximum radial displacement of the storage boundary is compared for every rock type and the results for Sauberger Kalk are shown in Figure 84. Figure 85 shows the total displacement plot for Rock mass 1 and a non-uniform in-situ stress with a σ_1 of 6 MPa and a σ_3 of 3 MPa.

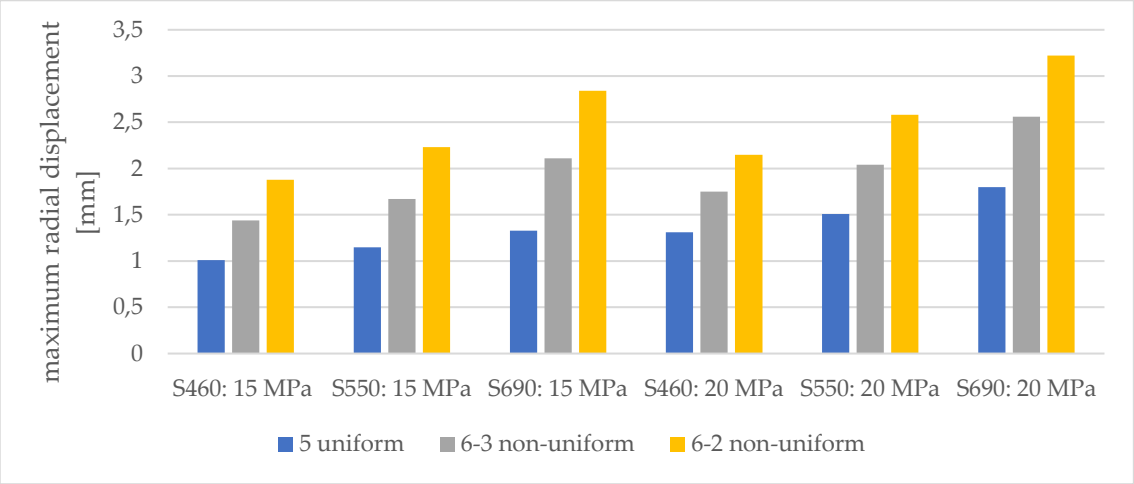

Figure 84: Maximum radial displacement of the steel lined storage boundary with steel grades S460, S550 and S690 for Sauberger Kalk, different uniform and non-uniform in-situ stress conditions as well as a p_i of 15 and 20 MPa

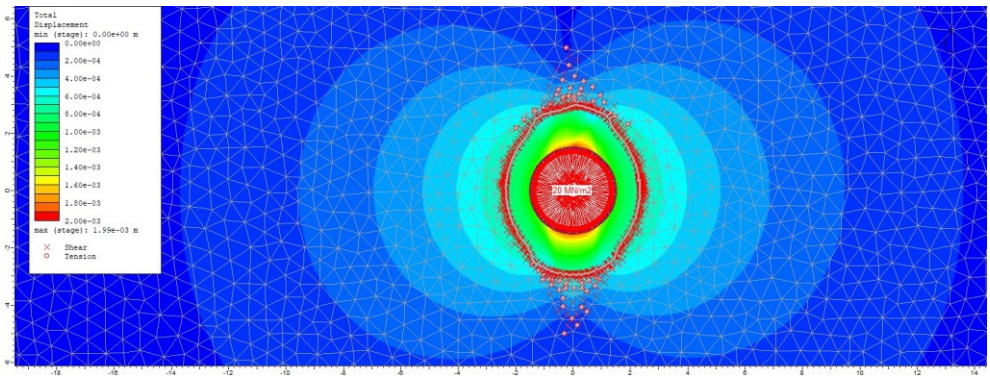

Figure 85: Total displacement of the steel lined storage boundary with steel grade S550 in Rock mass 1, non-uniform in-situ stress with σ_1 of 6 MPa and σ_3 of 3 MPa and a p_i of 20 MPa

Peaks in the radial displacement of the storage boundary also lead to peak loads in the axial force of the steel lining. Resulting maximum normal forces in the liner are converted into peak normal stresses (σ_n), by using Equation (18) and compared with $f_{y,d}$ of each steel grade to calculate the utilized strength capacity (μ) with the Equation (19).

The calculation is carried out for every rock type and the resulting σ_n and μ for Tuff 1 and different in-situ stress conditions are listed in Table 34, Table 35 and Table 36. A graphical display of the results can be seen in Figure 86 and Figure 87.

Table 34: Calculated σ_n and μ of the storage steel lining in Tuff 1, for a p_i of 15 MPa and 20 MPa, using steel grades S460, S550 and S690 and 5 MPa uniform in-situ stress

Tuff 1					
in-situ stress: 5 MPa uniform					
steel grade	p_i	lining thickness	axial force	σ_n	μ
S460	15 MPa	0.03614 m	6.15 MN	170 MPa	46%
S550	15 MPa	0.02614 m	4.80 MN	184 MPa	42%
S690	15 MPa	0.01576 m	3.30 MN	209 MPa	38%
S460	20 MPa	0.05652 m	11.25 MN	199 MPa	54%
S550	20 MPa	0.04318 m	9.50 MN	220 MPa	50%
S690	20 MPa	0.02935 m	7.70 MN	262 MPa	48%

Table 35: Calculated σ_n and μ of the storage steel lining in Tuff 1, for a p_i of 15 MPa and 20 MPa, using steel grades S460, S550 and S690 as well as a non-uniform in-situ stress with a σ_1 of 6 MPa and a σ_3 of 3 MPa

Tuff 1					
in-situ stress: 6-3 MPa non-uniform					
steel grade	p_i	lining thickness	axial force	σ_n	μ
S460	15 MPa	0.03614 m	7.50 MN	208 MPa	56%
S550	15 MPa	0.02614 m	6.25 MN	239 MPa	54%
S690	15 MPa	0.01576 m	4.70 MN	298 MPa	54%
S460	20 MPa	0.05652 m	12.60 MN	223 MPa	61%
S550	20 MPa	0.04318 m	11.50 MN	266 MPa	61%
S690	20 MPa	0.02935 m	9.85 MN	336 MPa	61%

Table 36: Calculated σ_n and μ of the storage steel lining in Tuff 1, for a p_i of 15 MPa and 20 MPa, using steel grades S460, S550 and S690 as well as a non-uniform in-situ stress with a σ_1 of 6 MPa and a σ_3 of 2 MPa

Tuff 1					
in-situ stress: 6-2 MPa non-uniform					
steel grade	p_i	lining thickness	axial force	σ_n	μ
S460	15 MPa	0.03614 m	8.70 MN	241 MPa	65%
S550	15 MPa	0.02614 m	7.30 MN	279 MPa	63%
S690	15 MPa	0.01576 m	5.70 MN	362 MPa	66%
S460	20 MPa	0.05652 m	14.50 MN	257 MPa	70%
S550	20 MPa	0.04318 m	13.25 MN	307 MPa	70%
S690	20 MPa	0.02935 m	11.40 MN	388 MPa	70%

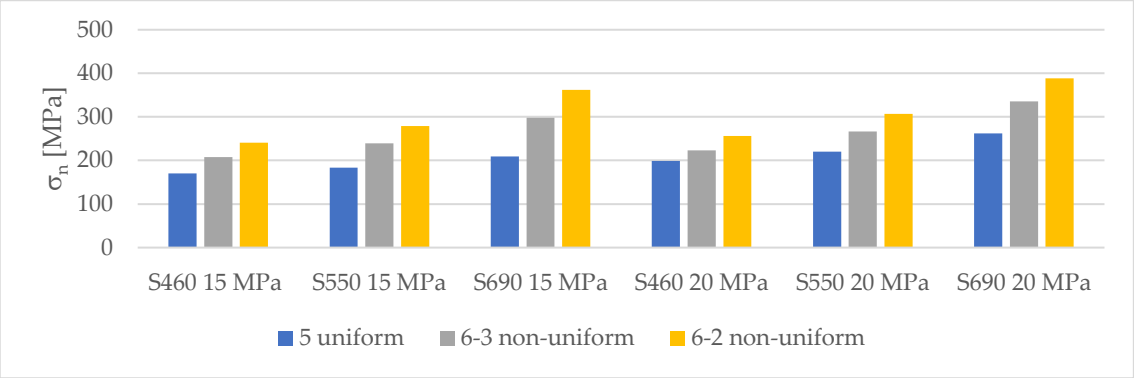

Figure 86: Normal stress of the storage steel lining in Tuff 1, different in-situ stress conditions, steel grades S460, S550 and S690 as well as a p_i of 15 MPa and 20 MPa

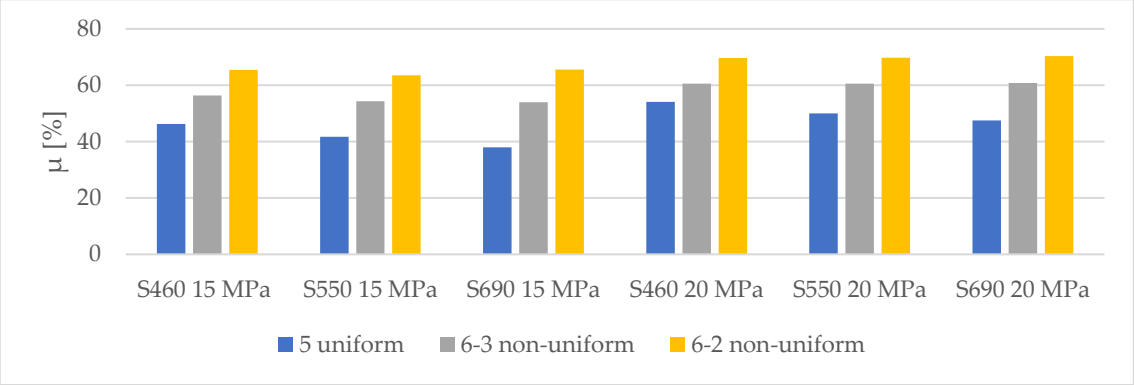

Figure 87: Utilization of the strength capacity of the storage steel lining in Tuff 1, different in-situ stress conditions, steel grades S460, S550 and S690 as well as a p_i of 15 and 20 MPa

The maximum utilization of 70 % of the steel strength capacity for the non-uniform in-situ stress with a magnitude of 6 and 2 MPa implies that the calculated thickness for the steel lining by Seeber is over dimensioned. This result of the analysis of the in-situ stress influence emphasizes the achieved resume about the steel lining design in Chapter 8.2.

An evenly distributed radial displacement of the storage boundary and axial force of the steel lining can be achieved for uniform in-situ stress, like it is shown in Figure 88 for Sauberger Kalk and a p_i of 15 MPa. The maximum radial displacement of 1.52 mm leads to a strain of 2.03‰, which is under ε_{zul} of S550 with 2.10‰.

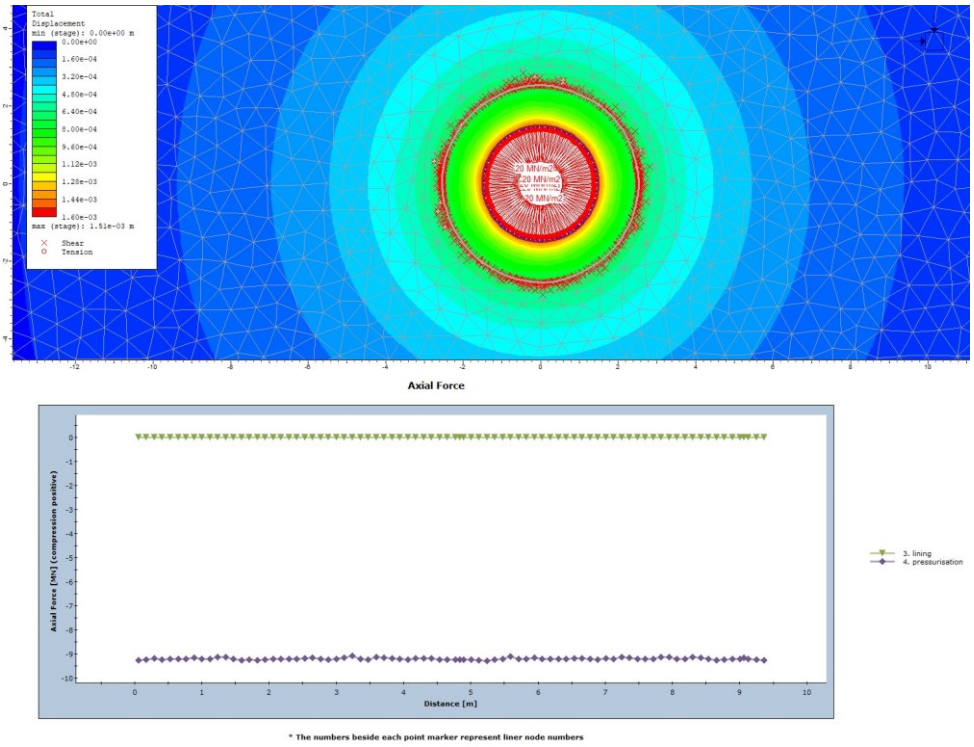

Figure 88: Total displacement of the storage boundary (top image) and axial force of the steel lining (bottom image) in Sauberger Kalk with a p_i of20 MPa, steel grade S550 and 5 MPa uniform in-situ stress

The tensile strength of Rock mass 1 is high enough to take up the induced tensile stresses by the internal storage pressure for a uniform in-situ stress of 5 MPa, a p_i of 15 MPa and a steel grade S460, without causing any rock mass failure. Low total radial displacements of the storage boundary are the result, which can be seen in Figure 89.

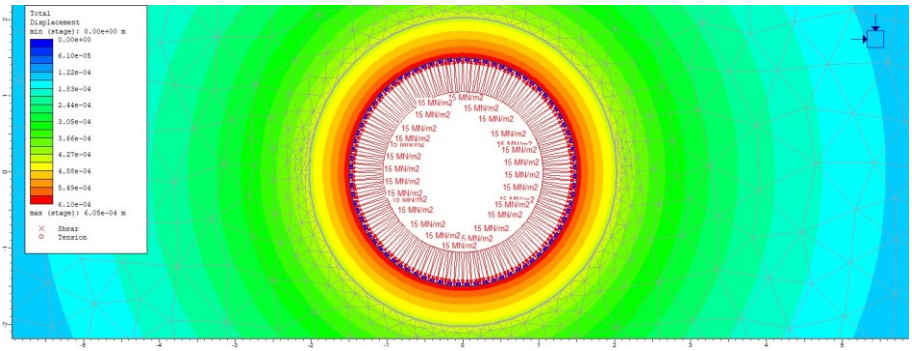

Figure 89: Total displacement of the storage boundary for Rock mass 1 with a p_i of15 MPa, steel grade S460 and 5 MPa uniform in-situ stress

Non-uniform in-situ stress has the effect that a potential rock mass failure has a preferred orientation like it is visible in Figure 90. It shows the total displacement as well as the axial force of the steel lining of a storage in Rock mass 2 with a p_i of 15 MPa and non-uniform in-situ stress. Tensile and shear failure starts in the direction of σ_1 in the crown and invert and develops around the storage with an increasing magnitude of p_i. Peak displacements lead to a peak axial force and σ_n of the lining. The utilization of the strength capacity of the steel lining has a maximum at this location.

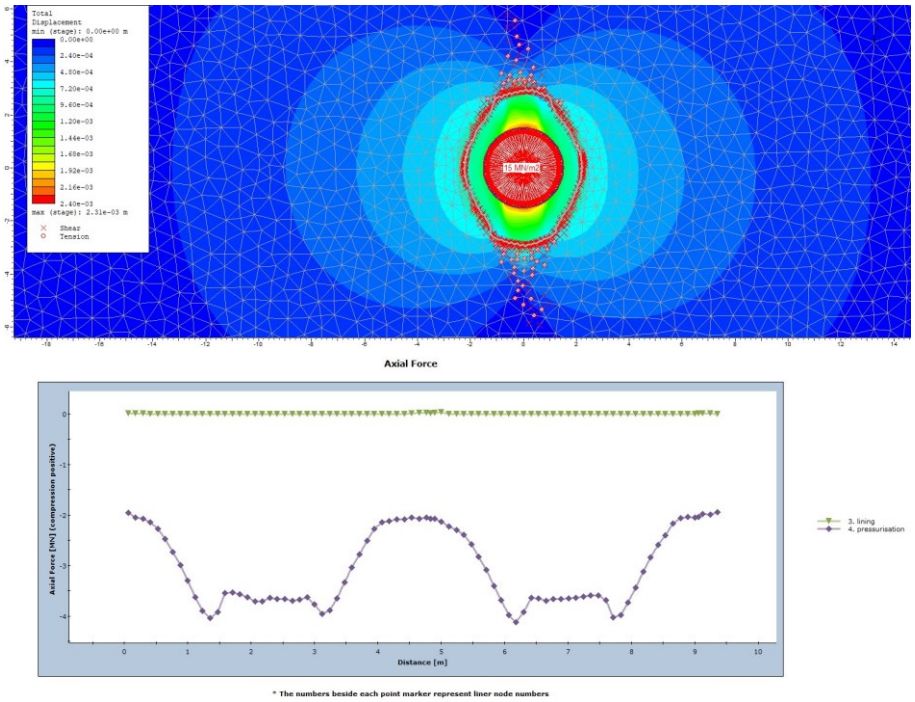

Figure 90: Total displacement of the storage boundary (top image) and axial force of the steel lining (bottom image) in Rock mass 2 with a p_i of 15 MPa, steel grade S550 and non-uniform uniform in-situ stress with a σ_1 of 6 MPa and a σ_3 of 2 MPa

The extent of the plastic zone of the rock mass can be seen in Figure 91 for a steel lined storage in Rock mass 1 with p_i of 20 MPa and non-uniform in-situ stress conditions.

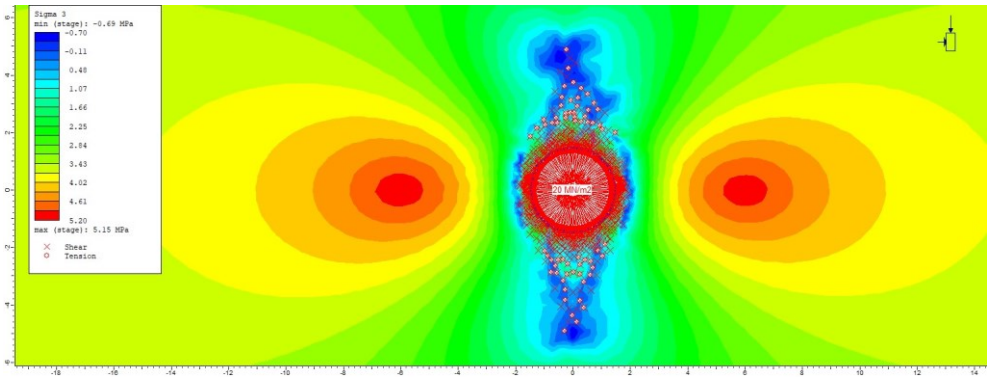

Figure 91: σ_3 and failure of the surrounding rock mass of the steel lined storage in Rock mass 1 with a p_i of 20 MPa, steel grade S550 and non-uniform uniform in-situ stress with a σ_1 of 6 MPa and a σ_3 of 3 MPa

The additional tables and figures, which were necessary to achieve and understand the results can be found in the appendix Chapter G.

9 Discussion

Detailed design is still required for the construction of the hydrogen storage facility at ZaB. This master's thesis and the thesis of Gabriel Loucky [27] provide important knowledge for making a decision about the lining method. The dimensions and components of the storage facility are based on the pilot project in Hunan described in Chapter 3.4.3 and the built up of the storage is visible in Figure 7. A detailed design of the concrete plug and the whole facility including the face of the storage must be carried out by a 3D numerical simulation. Further geotechnical site investigations have to be carried out in order to be able to accurately predict the rock mass and its behaviour.

3D numerical-simulation

Separate consideration of the load transfer of the internal storage pressure into the rock mass is not sufficient for detailed planning due to the storage length of 15 m, as the induced stresses caused by the lateral surface, the face and the concrete plug are overlapping. In addition to the necessary three-dimensional consideration of the load transfer of the internal storage pressure into the rock mass, the compact shape of the hydrogen storage facility at the ZaB also requires consideration of the load transfer of the lining in the longitudinal direction. Stress peaks occur at the transition zones between the face of the storage facility and the lateral surface as well as from the lateral surface to the concrete plug due to the different directions of deformation caused by the internal pressure. Numerical structural analysis programs such as Dlubal or high sophisticated programs such as Abaqus allow an analysis of the internal stress distribution of the lining and therefore an appropriate design.

9.1 Calibration of the pre-stressed concrete lining

A major part of this thesis was the development of a model in RS2 that represents the gap injection process in a realistic way. In reality, the gap between the shotcrete and concrete lining, which is pre-defined by a membrane, opens up due to the penetrating cement suspension and generates a load acting inwards onto the concrete lining and outwards onto the surrounding rock mass. During injection, the concrete lining gets compressed and therefore pre-stressed, and the in-situ stress state in the surrounding rock mass gets changed. Secondary stress peaks at the excavation boundary will be reduced and, depending on the previous primary stress state, negative σ_3 stresses will occur at a certain position of the excavation boundary and at a specific injection pressure. Low tensile stresses at the excavation boundary can lead to the opening of joints in the rock mass. Intact rock is able to take up some tensile stresses without failing as a result of its low tensile strength. The aim of uniform pre-stressing of the concrete lining cannot be achieved if the surrounding rock mass fails as described.

By adding an additional layer in the numerical model for the gap injection material between the rock mass and concrete lining, it was possible to ensure that two uniform stresses of the same magnitude but in opposite directions could be applied at the outer and inner boundary of that layer to simulate the gap injection pressure. It was therefore possible to pre-stress the concrete lining on the one hand and induce stresses in the surrounding rock mass on the other hand. A separate installation stage of the gap injection material before implementing the concrete lining is crucial for a realistic simulation. FEM programs are based on the calculation of the unknown nodal forces by solving the so-called stiffness matrix, which is explained in Chapter 7.1.3 [25, p. 295]. The additional layer for the gap injection material leads to a change in the stiffness matrix and therefore to a re-calculation of the nodal forces in the model. As a result, existing axial forces in the installed liners of the model also change. However, the concrete lining has no internal stress or axial force during installation, with the exception of the internal stresses that occur due to the curing process of the concrete. The additional layer of the gap injection material must therefore be implemented before the installation stage of the concrete lining, in order to prevent loading of the concrete lining because of simultaneous installation.
Physically, the gap injection material is described as a cement suspension during the pre-stressing process and a cement stone after hardening and therefore during the operation of the storage facility. The numerical model is calibrated according to Seeber by varying the stiffness of the gap injection material (E_{gap}). Cement suspension has no Young's modulus and therefore the calibrated stiffness represents a theoretical value with no actual relation to reality. According to Hooke's law, the stiffness of a material has an influence on the deformation behaviour of a material. Therefore, this fact could be used to induce different pre-stressing forces in the concrete lining for the same magnitude of acting pre-stressing pressure in the gap.

Considering plastic material behaviour, the calibrated numerical simulation makes it possible to investigate an exceedance of the compressive strength of the concrete lining during the gap injection process. Together with the investigation of the in-situ stress influence, these possibilities mark the gained advantages from the calibration.
A drawback of this method is the influence of the two gap injection pressures on each other. It is therefore not possible to simulate the induced stresses in the rock mass realistically. Assumptions can be made if the gap injection process leads to low tangential stresses at the excavation boundary and therefore to a potential tensile failure. The effect of the inwards pressure was simulated for a 0.3 m thick C40/50 concrete lining of a storage in Rock mass 2. A constant outwards acting pressure of 10 MPa and varying inwards acting pressure of 6 MPa and 1 MPa were simulated. A comparison of the resulting induced σ_3 stresses in the surrounding rock mass is shown in Figure 92 and the radial displacement of the storage boundary can be seen in Figure 93.

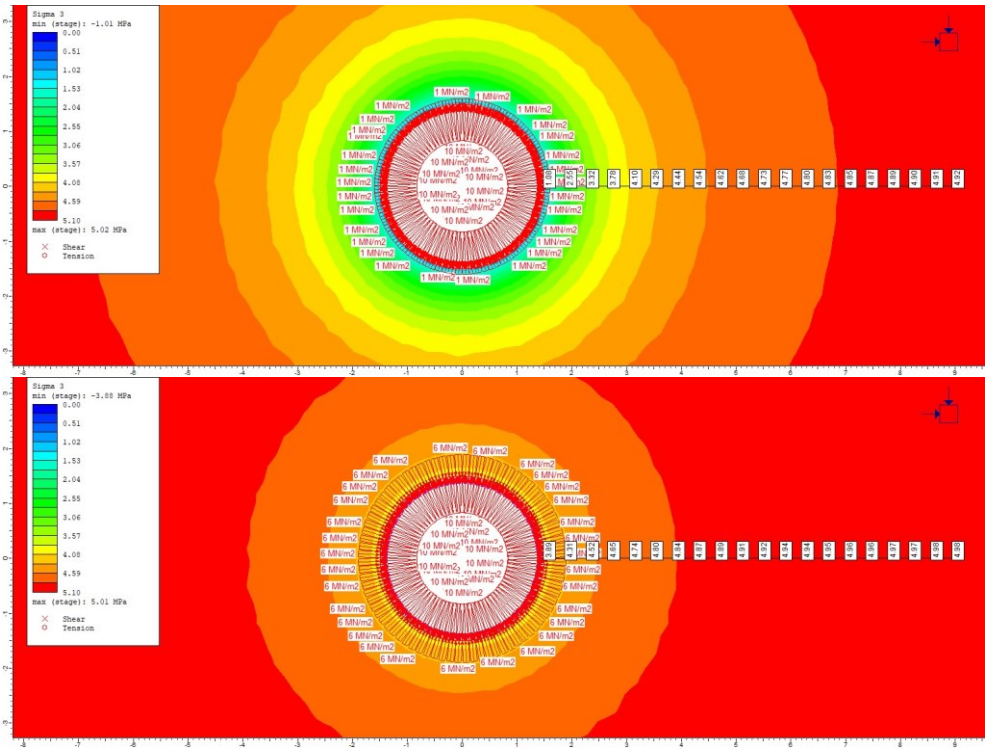

Figure 92: Comparison of the induced σ_3 stresses in the rock mass for 0.3 m thick C40/50 concrete lining of the storage in Rock mass 2 with a constant inwards acting pressure in the gap injection material of 10 MPa and an outwards acting pressure of 1 MPa (top image) and 6 MPa (bottom image)

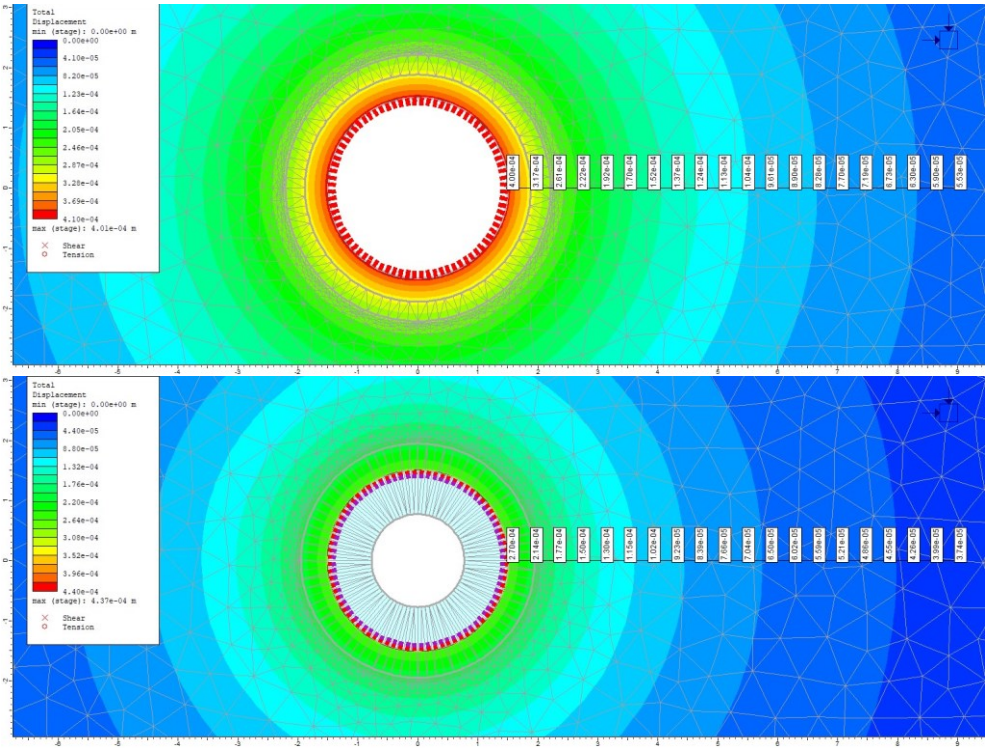

Figure 93: Comparison of the displacement of the storage boundary for 0.3 m thick C40/50 concrete lining of the storage in Rock mass 2 with a constant inwards acting pressure in the gap injection material of 10 MPa and an outwards acting pressure of 1 MPa (top image) and 6 MPa (bottom image)

For the actual evaluation of failure processes in the surrounding rock mass, a separate numerical model must be used, which was described in Chapter 7.2.3. Further investigations on the technique to simulate the pre-stressing of the concrete lining in RS2 should be carried out by a further thesis.
All in all, the aim to develop a tool to calibrate a numerical model to Seeber's analytical results could be achieved in this thesis and the benefits of the combined use could be demonstrated. Nevertheless, it is important to mention that according to the achieved accuracy, the described numerical method to simulate the pre-stressing of the concrete is a rough calculation tool and should only be used to estimate the success of the result from Seeber or to conduct a feasibility study for the decision of the proper lining. The monitoring of the success of the pre-stressing, as described in Chapter 5.5, guarantees sufficient pre-stressing of the concrete lining. A sensitivity analysis in the design process makes it possible to predict with a certain accuracy whether the pre-stressing pressure may cause any damage to the surrounding rock mass.
Due to its easy and fast usage, the calibrated numerical tool has its proper field of application in the determination of the in-situ stress influence and possible exceedance of the minor principal stress in the surrounding rock mass.

Continuing work for future theses

The calibration was carried out for a concrete lining thickness of 0.1, 0.2 and 0.3 m. Increasing lining thickness for higher storage diameters would make sense and the calibration process can also be carried out using the presented principle. This thesis has shown that it is also possible to find a correlation between different storage diameters, which can be used for the calibration. It may also be possible to determine a correlation between different internal pressures in order to expand the field of application for a combined use of a numerical simulation and the analytical method from Seeber in the future. The numerical analysis of the calibrated pre-stressed concrete lining model considering plastic material behaviour could sometimes not achieve equilibrium and did not generate results. This part must be further investigated according to the reasons for the unstable model conditions.

9.2 Comparison of the results from the steel lining design

The resulting minimum steel thickness according to Seeber for internal storage pressures of 10, 15 and 20 MPa and high-strength steel grades S460, S550 and S690 was used in several numerical simulations under different in-situ conditions. The aim was to determine the steel lining elongation using numerical simulation in order to compare it with the maximum allowable steel strain (ε_{zul}) according to Seeber. In combination with the determination of the utilisation of the steel strength capacity, it was found that the steel lining is over-dimensioned in regard to strength and grade. Due to possible failure of the rock mass before the steel lining is completely utilised, an optimisation of the steel lining was carried out, which led to an increase of the steel thickness. High-strength steel grades with good ductility and weldability are recommended for the steel lining of underground high-pressure storage facilities. [15, p. 96] A further investigation of the steel lining with lower strengths and a numerical analysis with plastic material behaviour is recommended as part of a future bachelor's or master's thesis.

9.3 Pre-stressed concrete lining

Verification of Seeber's results and also of the calibrated numerical simulation with the use of other numerical programs can be considered as the next step. Abaqus is a numerical program which provides the possibility to treat geotechnical and engineering tasks together due to its broad field of application. It can therefore be used to represent the pre-stressing process of the concrete lining as well as the impact on the rock mass.

Simulation of the lining as thick layer

The simulation of the concrete lining by a material layer with the actual thickness of the lining has the benefit of visualizing the distribution of the hoop and radial stresses inside the concrete. Different hoop stresses on the inner and outer surface of the lining occur, caused by the loading scenarios. A pre-stressed concrete lining must have a low remaining compressive stress at the inner surface during operation of the storage to achieve safe conditions. The overview of a numerical model to test out an analysis with a simulated material layer of the concrete lining is displayed in Figure 94.

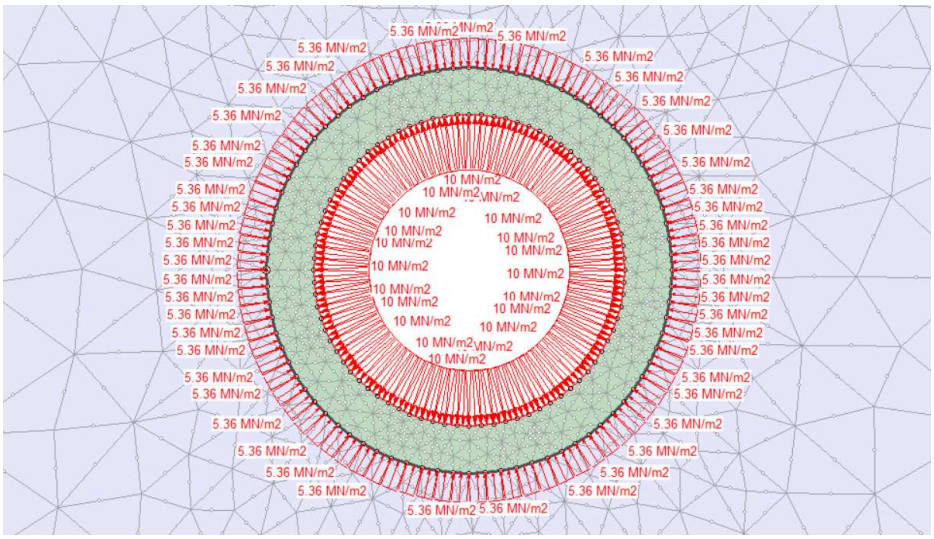

Figure 94: Overview of a pre-stressed concrete lining modelled as a material layer with 0.3 m thickness in Sauberger Kalk with a p_i of 10 MPa

The concrete lining can be simulated using the Mohr-Coulomb failure criterion. Unfortunately, this version of the pre-stressed concrete lining could not be further investigated, as a stress-free installation of the concrete lining in the model was not possible with this method in RS2. Various interface options between the concrete and the surrounding rock mass could reduce the stress in the concrete layer. However, changing the shear and normal stiffness as well as the shear strength of the interface between the concrete and rock mass also led to a reduction of the transferable pre-stressing force in the concrete and influenced the contact condition between the rock mass and the concrete. The induced stresses in the rock mass were reduced and the in-situ stress influence on the pre-stressing of the lining was disturbed.

In-situ stress influence

A uniform pre-stressing of the concrete lining can only be achieved by isotropic bedding conditions in the surrounding rock mass. Anisotropic rock mass behaviour or in-situ stress conditions will cause a non-uniform pre-stressing of the lining. Simanjuntak [18] has mentioned and investigated these influencing parameters in his thesis. Non-uniform hoop stresses in the pre-stressed concrete lining can be seen in Figure 95 caused by anisotropic in-situ stress conditions during the gap injection process.

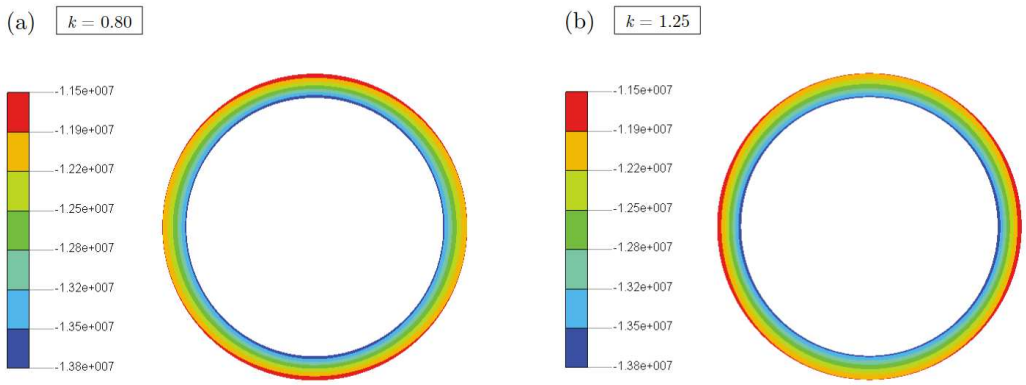

Figure 95: Induced hoop stresses in the pre-stressed concrete lining with a thickness of 0.3 m for a side pressure coefficient K_0 of 0.8 (left) and 1.25 (right) [18, p. 61]

The direction of the major principal stress in the rock mass will lead to the position of the maximum induced compressive stress in the lining. Locations of low induced hoop stresses are going to fail at first because the hoop stresses get negative at these locations at lower magnitudes of the internal storage pressure. The influence of anisotropic in-situ stress on the pre-stressing process can therefore be seen as a critical aspect to achieve stable conditions of the lining during operation of the storage. A sensitivity analysis with different in-situ stress conditions, magnitudes of the internal pressure and lining thicknesses is crucial for a successful design.

9.4 Steel lining

Effect of joints

The effect of opening joints on the steel lining is described in Chapter 4.1.3. Opening of joints caused by a negative σ_3 stress at the excavation boundary, which cannot be taken up by the missing tensile strength in the joint surface, leads to cracks in the concrete and therefore to an insufficient bedding of the steel lining. This is not a failure of the rock mass caused by exceeding the intact rock strength capacity, but a kinematic failure of the rock mass discontinuum at the joint surfaces. In particular, the bedding planes of sedimentary rock such as limestone can open as a result of the induced stresses from the internal storage pressure. Numerical programs using a discontinuum code can be used to investigate this topic. Joints can also be simulated in RS2, but since RS2 is a continuum program, it is not possible to represent the opening of joints.

A numerical simulation of the effect of joints would improve knowledge about:

- influence of different opening widths
- influence of different spacing of joint sets and bedding planes
- influence of different dipping angles and dip directions of the joints in relation to the storage boundary
- induced crack pattern in the backfilling concrete depending on the joint width
- advantages of injection in advance to the construction of the lining on the joint surface properties and their behaviour during pressurisation

Application of a sliding layer

The static friction coefficient between steel and concrete can reach a magnitude of 0.6 under high pressure. A thin sliding layer in between can decrease the friction coefficient to a magnitude of 0.1. To consider the irregularities during construction (sliding layer does not cover the whole interface) an average value of 0.35 is taken into account for the friction coefficient. [16]
Reduction of the interactions at the steel/concrete interface can be done with the sliding layer. Strain peaks in the steel lining due to concrete cracks can be avoided. Corrosion protection and concrete sealing of potential small gas leaks are some of the minor tasks of the sliding layer. [15, pp. 91-92]
An asphalt paint with a thickness of 1-2 mm can be used as a sliding layer. The application of paint makes it different to guarantee a certain uniform thickness and quality. Figure 96 shows an exemplary build-up of a sliding layer with a textile reinforced modified bitumen. Improvements in terms of durability, shear resistance, deformability, ageing and application methods can be achieved by a bitumen membrane, which is currently used as waterproofing membrane. [15, pp. 91-92]

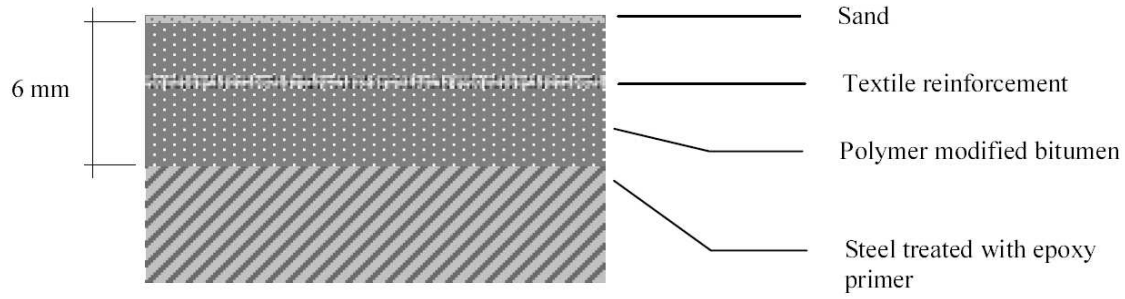

Figure 96: Build-up of the sliding layer [15, p. 92]

The application of the sliding layer in RS2 is possible by simulating the storage lining by a composite liner. At the interface between the concrete and steel layer a joint can simulate the sliding layer. Stiffness parameters like the normal and shear stiffness as well as strength parameters like the friction angle and cohesion must be chosen in the joint properties. Strain peaks of the stee lining can be avoided by the sliding layer and a simulation of the scope of application and advantages can be useful. The sliding layer will have benefits on the behaviour of the steel lining, particularly where the previously described effect of joints has to be reduced.

10 Summary

Underground high-pressure storage facilities for hydrogen or compressed air can be dimensioned using numerical programs or analytical calculation methods.
This thesis is intended to explain the advantages of a combined approach of a two-dimensional numerical simulation, using the program RS2, and Seeber's analytical method for the design of an underground hydrogen storage. Seeber's calculation method offers the advantages of a quick and easy dimensioning of the static load transfer of the storage lining by using a steel or a pre-stressed concrete lining. The method from Seeber is based on determining the necessary deformation behaviour of the rock mass after the excavation of the storage facility using large-scale in-situ tests, such as the TIWAG radial press. If no data from such in-situ tests is available for the design of the pre-stressed concrete or steel lining, the parameters must be determined using laboratory tests and equations. This inaccuracy in determining the actual deformation behaviour of the rock mass on the basis of laboratory tests can be reduced by combining the analytical calculation method with a numerical simulation.

Numerical analyses in the field of rock mechanics offer advantages in the representation of complex stress, deformation and failure mechanisms during the excavation of underground structures. Together with a numerical sensitivity analysis of the required input parameters for the calculation method from Seeber, the advantages of a numerical simulation can be used as a complement to increase the meaningfulness and reliability of the design.

The calibration of the numerical model of the pre-stressed concrete lining to Seeber's results makes it possible to determine the influences of the in-situ stress state and the variation of the deformation behaviour of the surrounding rock mass on the design process of the pre-stressed concrete lining. Additional numerical simulations can be used to determine a potential failure of the surrounding rock mass, due to the pre-stressing gap injection and make it possible to provide a reliable statement on the uptake of the injection pressure by the rock mass.

According to Seeber, steel linings require a minimum thickness to absorb the tensile forces occurring in the lining due to the internal pressure of the storage. Based on the results of the numerical calculation of this thesis, the steel thickness is over-dimensioned regarding the strength capacity and can therefore be optimised through further numerical simulations. High-strength steel grades are not necessary as the strength and deformation properties are not utilised because the surrounding rock mass remains intact in case of a successful design. The calculated steel lining thickness according to Seeber did not always prevent rock mass failure in the numerical simulation and had to be optimised to assure stable storage conditions. An optimised lining thickness to achieve intact rock conditions over the lifetime of the storage is the design objective and can be achieved by the numerical simulation for different in-situ stress conditions.

References

[1] M. Budt, D. Wolf, R. Span and J. Yan, "A review on compressed air energy storage: Basic principles, past milestones and recent developments," *Elsevier,* no. 170, pp. 250-268, 2016.

[2] Z. Jiang, P. Li, D. Tang, H. Zhao and Y. Li, "Experimental and Numerical Investigations of Small-Scale Lined Rock Cavern at Shallow Depth for Compressed Air Energy Storage," *Rock Mechanics and Rock Engineering,* no. 53, p. 2671–2683, 2020.

[3] G. Seeber, Druckstollen und Druckschächte – Bemessung - Konstruktion - Ausführung, Stuttgart: ENKE im Georg Thime Verlag, 1999.

[4] J. Miocic, N. Heinemann, K. Edlmann, J. Scafidi, F. Molaei and J. Alcalde, "Underground hydrogen storage: a review," Geological Society, London, 2023.

[5] I. Zelenika, D. Pavlovic, P. Rajic, T. Kovacic and M. Srpak, "Hydrogen Underground Storage as a Critical Factor in the Energy Transition Period," https://doi.org/10.17559/TV-20200605130232, 2021.

[6] F. Johansson, "Investigation of research needs regarding the storage of hydrogen gas in lined rock caverns: Prestudy for Work Package 2.3 in HYBRIT Research Program 1," Stockholm, 2018.

[7] L. Zeng, M. Sarmadivaleh, A. Saeedi, Y. Chen, Z. Zhong and Q. Xie, "Storage integrity during underground hydrogen storage in depleted gas reservoirs," *Earth-Science Reviews,* no. 247, 2023.

[8] K. Alms, B. Ahrens, M. Graf and N. Mathias, "Linking geological and infrastructural requirements for large-scale underground hydrogen storage in Germany," Frontiers in Energy Research, doi: 10.3389/fenrg.2023.1172003, 2023.

[9] M. Saeed and P. Jadhawar, "Optimizing underground hydrogen storage in aquifers: The impact of cushion gas type," *international journal o f hydrogen energy,* no. https://doi.org/10.1016/j.ijhydene.2023.08.352, 2023.

[10] K. Lubon, R. Tarkowski and B. Uliasz-Misiak, "Impact of Depth on Underground Hydrogen Storage Operations in Deep Aquifers," *Energies,* no. 17, 2024.

[11] T. Ishihata, "Underground Compressed Air Storage Facility for CAES-G/T Power Plant Utilizing an Airtight Lining," New Energy Foundation, Tokyo.

[12] P. Perazzelli and G. Anagnostou, "Design issues for compressed air energy storage in sealed underground cavities," *Journal of Rock Mechanics and Geotechnical Engineering,* vol. 8, pp. 314-328, 2016.

[13] M. King, A. Jain, R. Bhakar, J. Mathur and J. Wang, "Overview of current compressed air energy storage projects and analysis of the potential underground storage capacity in India and the UK," *Renewable and Sustainable Energy Reviews,* no. 139, 2021.

[14] T. Okuno, N. Wakabayashi, K. Niimi, Y. Kurihara, M. Iwano and T. Komatsubara, "Advanced natural gas storage system and verification tests of lined rock cavern - ANGAS project in Japan -," *J-STAGE*, vol. 5, no. 2, pp. 95-102, 2009.

[15] J. Johansson, "High Pressure Storage of Gas in Lined Rock Caverns CAVERN WALL DESIGN PRINCIPLES," Division of Soil & Rock Mechanics, Royal Institute of Technology, Stockholm, 2003.

[16] D. R. Damasceno and F. J. Johan Spross, "Effect of rock joints on lined rock caverns subjected to high internal gas pressure," *Journal of Rock Mechanics and Geotechnical Engineering*, no. https://doi.org/10.1016/j.jrmge.2022.11.011, 2022.

[17] H. Wannenmacher, M. Bauert and A. Heizmann, "Aspects of pressure tunnel lining; with special focus on pre-stressed pressure tunnels," DOI: 10.13140/2.1.1933.9048, 2013.

[18] Y. Simanjuntak, "Prestressed concrete-lined pressure tunnels," CRC Press/Balkema, Delft, 2015.

[19] S. Jürgen, Druckstollen und Druckschächte - Bemessung und Konstruktion, München: Dissertations- und Fotodruck Frank GmbH, 1985.

[20] P. Matt, F. Thurnherr and I. Uherkovich, "Vorgespannte Druckstollen," *Schweizerische Bauzeitung*, pp. 63-72, 2 Februar 1978.

[21] A. Kieser, Druckstollenbau, Wien-Bregenz: Springer Verlag, 1960.

[22] B. Bonapace, "Prestress Grouting of Tunnel Linings," *Druckstollen und Druckschächte, Vorträge zum 38. Salzburger Kolloquium für Geomechanik 1989*, no. 38, pp. 33-50, 1989.

[23] J. Schwarz, Berechnung von Druckstollen - Entwicklung und Anwendung eines mathematischen Modells und Ermittlung der felsmechanischen Parameter, München: Dissertations- und Fotodruck Frank GmbH, 1987.

[24] H. Wannenmacher, M. Bauert, H. Krenn, F. Engel and N. Komma, "Improved Pressure Tunnel Lining Methods, A Case Study of the Niagara Tunnel Facility Project," WTC, Geneva, 2013.

[25] L. Jing, "A review of techniques, advances and outstanding issues in numerical modelling for rock mechanics and rock engineering," *International Journal of Rock Mechanics & Mining Sciences*, no. 40, p. 283–353, 2003.

[26] Rocscience, "rocscience," 1996. [Online]. Available: https://www.rocscience.com/help/rs2/documentation. [Accessed 9 Mai 2024].

[27] G. Loucky, "Investigation of lining solutions for a lined rock cavern at the site of Zentrum am Berg," Montanuniversität Leoben, Leoben, 2024.

[28] B. H. G. Brady and E. Brown, Rock Mechanics for undeground mining, Dordrecht: Springer Science + Business Media, Inc., 2004.

[29] E. Hoek and M. Diederichs, "Empirical estimation of rock mass modulus," *International Journal of Rock Mechanics & Mining Sciences*, no. 43, pp. 203-215, 2006.

[30] E. Hoek and E. T. Brown, "Practical estimates of rock mass strength," *International Journal of Rock Mechanics and Mining Science,* vol. 8, no. 34, pp. 1165-1186, 1997.

[31] "Geomechanischer Bericht," Research@ZaB - Forschung im Zentrum am Berg, Leoben, 2017.

[32] L. Gonzalez de Vallejo, Geological Engineering, CRC Press, 2011.

[33] P. B. A. J. Venture, "Global - Geotechnical - Technical Report, BC-PBA-GLGTR100-RPT-0003-G-01," Airport Link, 2010.

[34] "rocscience," [Online]. Available: https://www.rocscience.com/help/rsdata/documentation/program-overview/rsdata-overview. [Accessed 2 August 2024].

[35] E. Hoek and E. T. Brown, "The Hoek - Brown failure criterion and GSI - 2018 edition," *Journal of Rock Mechanics and Geotechnical Engineering,* no. 11, pp. 445-463, 2019.

[36] R. Fritze, G. F. Kidéry and W. Potucek, STAHLBETONBAU Teil 2: Bemessungstabellen auf Basis des Eurocodes 2 (ÖNORM EN 1992-1-1 und nationaler Anhang ÖNORM B 1992-1-1), Wien: MANZ Verlag Schulbuch GmbH, 2016.

[37] Austrian Standards International, ÖNORM EN 10025-6, Austrian Standards plus GmbH, 2023.

[38] G. Luza und M. Palka, STAHLBAU - Formeln und Tabellen, Wien: MANZ Verlag Schulbuch GmbH, 2011.

[39] Rocscience, "Rocscience," 1996. [Online]. Available: https://www.rocscience.com/help/rs2/documentation/rs2-model/project-settings. [Accessed 8 August 2024].

[40] Rocscience, "Rocscience," 1996, [Online]. Available: https://www.rocscience.com/help/rs2/documentation/rs2-model/project-settings/stress-analysis/stress-analysis-2. [Accessed 8 August 2024].

[41] E. Hoek, Practical rock engineering, Vancouver: Evert Hoek Consulting Engineer Inc..

Figures

Tables

Appendix

Appendix A for Chapter 7.3 Geotechnical data

Calculation of E_{rm} with the Equation (7):

- Sauberger Kalk:
  - E_i= 31.5 GPa
  - D= 0
  - GSI= 70

$$E_{rm} = 31.5 * (0.02 + \frac{1}{1 + e^{\left((60-70)/11\right)}} = \mathbf{23.08\ GPa}$$

- Ankerit:
  - E_i= 81 GPa
  - D= 0
  - GSI= 82.5

$$E_{rm} = 81 * (0.02 + \frac{1}{1 + e^{\left((60-82.5)/11\right)}} = \mathbf{73.34\ GPa}$$

- Rock mass 1:
  - E_i= 50 GPa
  - D= 0
  - GSI= 75

$$E_{rm} = 50 * (0.02 + \frac{1}{1 + e^{\left((60-75)/11\right)}} = \mathbf{40.82\ GPa}$$

- Rock mass 2:
  - E_i= 45 GPa
  - D= 0
  - GSI= 70

$$E_{rm} = 45 * (0.02 + \frac{1}{1 + e^{\left((60-70)/11\right)}} = \mathbf{32.98\ GPa}$$

Appendix B.1 for Chapter 7.4.2 Parameters for the steel lining

Calculation of the design value of the yield strength $f_{y,d}$:

- Safety factor γ_s: 1.25

$$\text{S690: } f_{y,d} = \frac{f_{y,k}}{\gamma_s} = \frac{690}{1.25} = 552\ MPa$$

$$\text{S550: } f_{y,d} = \frac{f_{y,k}}{\gamma_s} = \frac{550}{1.25} = 440\ MPa$$

$$\text{S460: } f_{y,d} = \frac{f_{y,k}}{\gamma_s} = \frac{460}{1.25} = 368\ MPa$$

Calculation of the maximum allowable strain ε_{zul}:

- Young's modulus from steel: 210,000 GPa

$$S690: \varepsilon_{zul} = \frac{f_{y,d}}{E} = \frac{552}{210{,}000} = 2{,}63\ ‰$$

$$S550: \varepsilon_{zul} = \frac{f_{y,d}}{E} = \frac{440}{210{,}000} = 2.1\ ‰$$

$$S460: \varepsilon_{zul} = \frac{f_{y,d}}{E} = \frac{368}{210{,}000} = 1.75\ ‰$$

Appendix B.2 for Chapter 7.7 Sensitivity analysis

Strain and utilization of the steel lining in the numerical simualtion for 80, 100 and 120% of E_{rm} of the rock types Rock mass 1, Sauberger Kalk and Tuff 2

Steel grade and p_i	Rock mass 1			Sauberger Kalk			Tuff 2		
	Percentage of E_{rm}			Percentage of E_{rm}			Percentage of E_{rm}		
	80%	100%	120%	80%	100%	120%	80%	100%	120%
	Strain of the steel lining [‰]								
S690: 10 MPa	No lining			No lining			2.56	2.18	1.95
S550: 10 MPa	No lining			1.18	0.95	0.79	2.24	1.95	1.76
S460: 10 MPa	No lining			1.11	0.90	0.76	2.00	1.76	1.62
S690: 15 MPa	No lining			1.67	1.36	1.15	3.02	2.66	2.43
S550: 15 MPa	1.04	0.83	0.69	1.54	1.27	1.08	2.59	2.32	2.15
S690: 15 MPa	0.99	0.80	0.67	1.42	1.19	1.02	2.28	2.07	1.92
S460: 20 MPa	1.38	1.10	0.92	2.00	1.67	1.43	3.32	2.98	2.76
S550: 20 MPa	1.28	1.04	0.87	1.80	1.52	1.32	2.82	2.56	2.40
S460: 20 MPa	1.20	0.98	0.84	1.64	1.42	1.23	2.44	2.26	2.14
Steel grade and p_i	Utilization of the steel lining [%]								
S690: 10 MPa	No lining			No lining			97	83	74
S550: 10 MPa	No lining			56	45	38	107	93	84
S460: 10 MPa	No lining			63	52	43	114	101	92
S690: 15 MPa	No lining			63	52	44	115	101	92
S550: 15 MPa	50	40	33	73	61	52	123	111	102
S690: 15 MPa	57	46	38	81	68	59	130	118	110
S460: 20 MPa	52	42	35	76	63	54	126	113	105
S550: 20 MPa	61	50	42	86	73	63	134	122	114
S460: 20 MPa	69	56	48	94	81	70	140	129	122

Appendix C.1 for Chapter 8.1 Calibration of the pre-stressed concrete

Calibration results for a p_i of 4 MPa:

Calibrated E_{gap} for Sauberger Kalk, p_i of 4 MPa, different concrete input parameters like concrete quality, E_{cm} and thickness as well as the Seeber input parameters $p_{v,0}$ and p_v

Sauberger Kalk - p_i of 4 MPa						
Concrete in put parameters			Seeber input		stiffness gap injection material	
Quality	E_{cm} [GPa]	thickness [m]	$p_{v.0}$ [MPa]	p_v [MPa]	E_{gap} [MPa]	$E_{gap.hardened}$ [MPa]
C25/30	31	0.1	4.77	1.34	**0.85**	2000
	31	0.2	5.98	1.87	**1.05**	2000
	31	0.3	6.50	2.07	**1.00**	2000
C30/37	33	0.1	4.57	1.39	**0.85**	2000
	33	0.2	5.81	1.92	**1.05**	2000
	33	0.3	6.36	2.12	**1.00**	2000
C35/45	34	0.1	4.31	1.42	**0.85**	2000
	34	0.2	5.57	1.95	**1.05**	2000
	34	0.3	6.15	2.14	**1.00**	2000
C40/50	35	0.1	4.13	1.44	**0.85**	2000
	35	0.2	5.40	1.97	**1.05**	2000
	35	0.3	6.01	2.16	**1.00**	2000

Calibrated E_{gap} for Ankerit, p_i of 4 MPa, different concrete input parameters like concrete quality, E_{cm} and thickness as well as the Seeber input parameters $p_{v,0}$ and p_v

Ankerit - p_i of 4 MPa						
Concrete in put parameters			Seeber input		stiffness gap injection material	
Quality	E_{cm} [GPa]	thickness [m]	$p_{v.0}$ [MPa]	p_v [MPa]	E_{gap} [MPa]	$E_{gap.hardened}$ [MPa]
C25/30	31	0.1	3.27	0.57	**1.4**	2000
	31	0.2	5.00	0.94	**2.2**	2000
	31	0.3	6.28	1.18	**2.5**	2000
C30/37	33	0.1	3.16	0.6	**1.4**	2000
	33	0.2	4.91	0.99	**2.2**	2000
	33	0.3	6.22	1.23	**2.5**	2000
C35/45	34	0.1	2.98	0.61	**1.4**	2000
	34	0.2	4.72	1.01	**2.2**	2000
	34	0.3	6.02	1.25	**2.5**	2000
C40/50	35	0.1	2.86	0.63	**1.4**	2000
	35	0.2	4.58	1.03	**2.2**	2000
	35	0.3	5.89	1.28	**2.5**	2000

Calibrated E_{gap} for Tuff 1, p_i of 4 MPa, different concrete input parameters like concrete quality, E_{cm} and thickness as well as the Seeber input parameters $p_{v,0}$ and p_v

Tuff 1 - p_i of 4 MPa						
Concrete in put parameters			Seeber input		stiffness gap injection material	
Quality	E_{cm} [GPa]	thickness [m]	$p_{v.0}$ [MPa]	p_v [MPa]	E_{gap} [MPa]	$E_{gap.hardened}$ [MPa]
C25/30	31	0.1	4.8	1.43	**0.65**	2000
	31	0.2	5.8	1.96	**0.75**	2000
	31	0.3	6.14	2.15	**0.65**	2000
C30/37	33	0.1	4.6	1.48	**0.65**	2000
	33	0.2	5.63	2.01	**0.75**	2000
	33	0.3	6	2.19	**0.65**	2000
C35/45	34	0.1	4.35	1.51	**0.65**	2000
	34	0.2	5.41	2.03	**0.75**	2000
	34	0.3	5.82	2.21	**0.65**	2000
C40/50	35	0.1	4.16	1.54	**0.65**	2000
	35	0.2	5.25	2.06	**0.75**	2000
	35	0.3	5.69	2.23	**0.65**	2000

Calibrated E_{gap} for Tuff 2, p_i of 4 MPa, different concrete input parameters like concrete quality, E_{cm} and thickness as well as the Seeber input parameters $p_{v,0}$ and p_v

Tuff 2 - p_i of 4 MPa						
Concrete in put parameters			Seeber input		stiffness gap injection material	
Quality	E_{cm} [GPa]	thickness [m]	$p_{v.0}$ [MPa]	p_v [MPa]	E_{gap} [MPa]	$E_{gap.hardened}$ [MPa]
C25/30	31	0.1	5.62	2.15	**0.35**	2000
	31	0.2	5.67	2.56	**0.30**	2000
	31	0.3	5.43	2.61	**0.20**	2000
C30/37	33	0.1	5.35	2.20	**0.35**	2000
	33	0.2	5.48	2.60	**0.30**	2000
	33	0.3	5.30	2.64	**0.20**	2000
C35/45	34	0.1	5.06	2.23	**0.35**	2000
	34	0.2	5.28	2.62	**0.30**	2000
	34	0.3	5.16	2.66	**0.20**	2000
C40/50	35	0.1	4.86	2.26	**0.35**	2000
	35	0.2	5.14	2.64	**0.30**	2000
	35	0.3	5.06	2.67	**0.20**	2000

Calibrated E_{gap} for Rock mass 1, p_i of 4 MPa, different concrete input parameters like concrete quality, E_{cm} and thickness as well as the Seeber input parameters $p_{v,0}$ and p_v

Rock mass 1 - p_i of 4 MPa						
Concrete in put parameters			Seeber input		stiffness gap injection material	
Quality	E_{cm} [GPa]	thickness [m]	$p_{v.0}$ [MPa]	p_v [MPa]	E_{gap} [MPa]	$E_{gap.hardened}$ [MPa]
C25/30	31	0.1	3.95	0.90	**1.05**	2000
	31	0.2	5.56	1.38	**1.50**	2000
	31	0.3	6.54	1.63	**1.60**	2000
C30/37	33	0.1	3.81	0.94	**1.05**	2000
	33	0.2	5.43	1.43	**1.50**	2000
	33	0.3	6.43	1.68	**1.60**	2000
C35/45	34	0.1	3.60	0.96	**1.05**	2000
	34	0.2	5.21	1.46	**1.50**	2000
	34	0.3	6.22	1.70	**1.60**	2000
C40/50	35	0.1	3.45	0.98	**1.05**	2000
	35	0.2	5.06	1.48	**1.50**	2000
	35	0.3	6.08	1.73	**1.60**	2000

Calibrated E_{gap} for Rock mass 2, p_i of 4 MPa, different concrete input parameters like concrete quality, E_{cm} and thickness as well as the Seeber input parameters $p_{v,0}$ and p_v

Rock mass 2 - p_i of 4 MPa						
Concrete in put parameters			Seeber input		stiffness gap injection material	
Quality	E_{cm} [GPa]	thickness [m]	$p_{v.0}$ [MPa]	p_v [MPa]	E_{gap} [MPa]	$E_{gap.hardened}$ [MPa]
C25/30	31	0.1	4.32	1.09	**0.95**	2000
	31	0.2	5.78	1.6	**1.35**	2000
	31	0.3	6.56	1.84	**1.35**	2000
C30/37	33	0.1	4.16	1.13	**0.95**	2000
	33	0.2	5.63	1.66	**1.35**	2000
	33	0.3	6.44	1.89	**1.35**	2000
C35/45	34	0.1	3.92	1.16	**0.95**	2000
	34	0.2	5.4	1.68	**1.35**	2000
	34	0.3	6.23	1.91	**1.35**	2000
C40/50	35	0.1	3.76	1.18	**0.95**	2000
	35	0.2	5.24	1.71	**1.35**	2000
	35	0.3	6.09	1.93	**1.35**	2000

Calibration results for a p_i of 4 MPa:

Calibrated value of E_{gap} for Ankerit, Rock mass 1, Rock mass 2, Sauberger Kalk, Tuff 1 as well as Tuff 2 and a concrete lining thickness of 0.1 m, 0.2 m and 0.3 m with a p_i of 4 MPa

Rock type	Thickness of the concrete lining		
	0.1 m	0.2 m	0.3 m
Sauberger Kalk	0.85 MPa	1.05 MPa	1.00 MPa
Ankerit	1.40 MPa	2.20 MPa	2.50 MPa
Tuff 1	0.65 MPa	0.75 MPa	0.65 MPa
Tuff 2	0.35 MPa	0.30 MPa	0.20 MPa
Rock mass 1	1.05 MPa	1.50 MPa	1.60 MPa
Rock mass 2	0.95 MPa	1.35 MPa	1.35 MPa

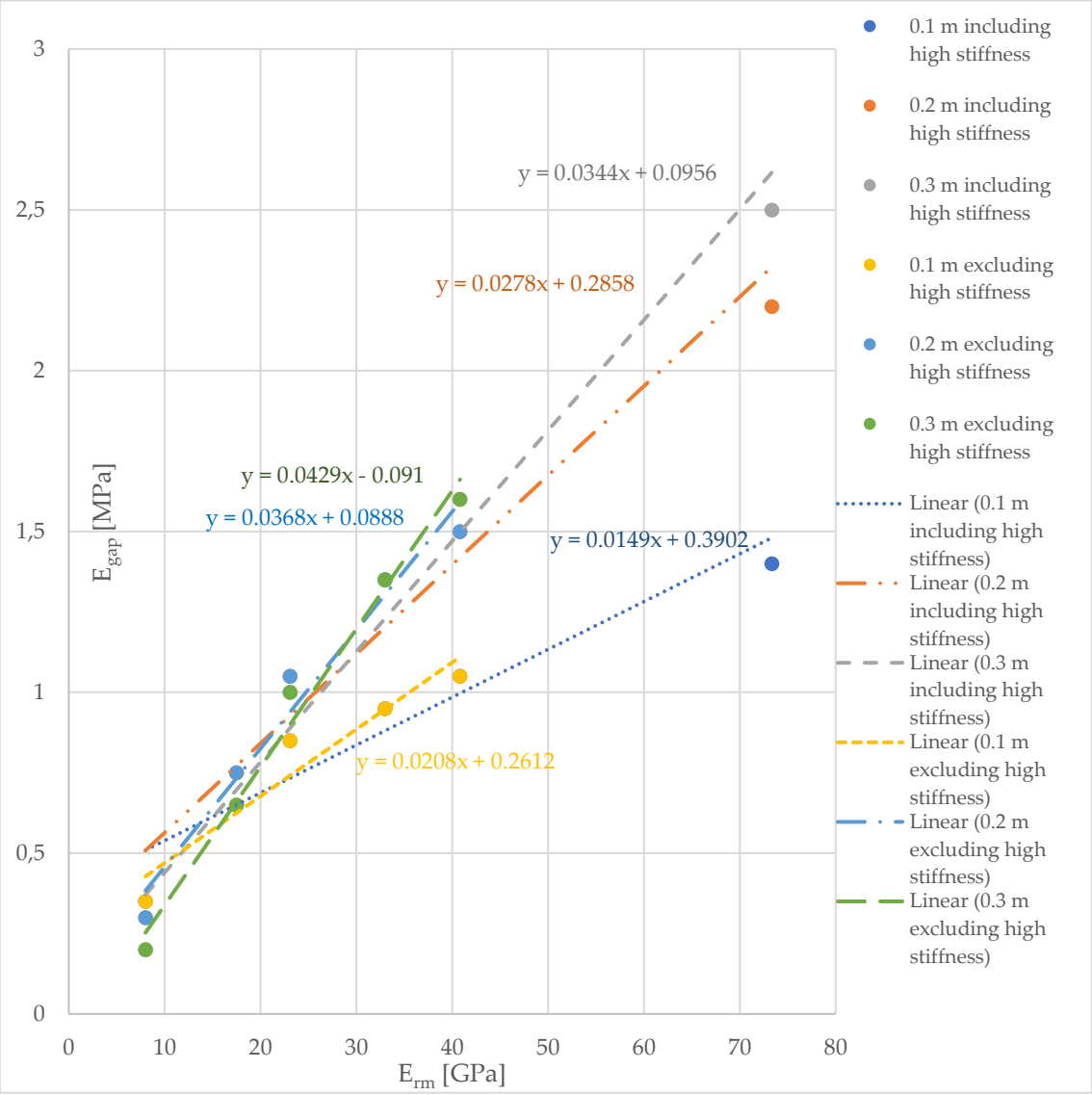

Graphical display of the resulting equations to calculate the necessary value of E_{gap} depending on E_{rm} for a concrete lining thickness of 0.1 m, 0.2m and 0.3 m and a p_i of 4 MPa

Calibration results for a p_i of 4 MPa and 0.1 m thickness of the concrete lining:

Comparison of the achieved result of the value for p_v from the calibrated numerical model with Seeber for a 0.1 m thick concrete lining, a p_i of 4 MPa and the use of the calibrated equation excluding Ankerit

Equation excluding Ankerit: y = 0.0208x + 0.2612			Seeber: Medium p_v	Analysis Numerical versus Seeber	
E_{rm} [GPa]	E_{gap} [MPa]	numerical p_v [MPa]	Seeber p_v [MPa]	Difference [-]	Difference [%]
5	0.37	3.25	2.61	0.64	**24.6**
10	0.47	2.10	2.01	0.10	**4.7**
20	0.68	1.40	1.37	0.03	**2.2**
30	0.89	1.10	1.04	0.06	**5.5**
40	1.09	0.95	0.84	0.11	**13.1**
50	1.30	0.90	0.70	0.20	**28.1**

Comparison of the achieved result of the value for p_v from the calibrated numerical model with Seeber for a 0.1 m thick concrete lining, a p_i of 4 MPa and the use of the calibrated equation including Ankerit

Equation including Ankerit: y = 0.0149x + 0.3902			Seeber: Medium p_v	Analysis Numerical versus Seeber	
E_{rm} [GPa]	E_{gap} [MPa]	numerical p_v [MPa]	Seeber p_v [MPa]	Difference [-]	Difference [%]
5	0.46	3.70	2.61	1.09	**41.9**
10	0.54	2.20	2.01	0.20	**9.7**
20	0.69	1.40	1.37	0.03	**2.2**
30	0.84	1.10	1.04	0.06	**5.5**
40	0.99	0.90	0.84	0.06	**7.1**
50	1.14	0.80	0.70	0.10	**13.9**

Calibration results for a p_i of 4 MPa and 0.2 m thickness of the concrete lining:

Comparison of the achieved result of the value for p_v from the calibrated numerical model with Seeber for a 0.2 m thick concrete lining, a p_i of 4 MPa and the use of the calibrated equation excluding Ankerit

Equation excluding Ankerit: y = 0.0368x + 0.0888			Seeber: Medium p_v	Analysis Numerical versus Seeber	
E_{rm} [GPa]	E_{gap} [MPa]	numerical p_v [MPa]	Seeber p_v [MPa]	Difference [-]	Difference [%]
5	0.27	3.45	2.88	0.58	**20.0**
10	0.46	2.60	2.46	0.15	**5.9**
20	0.82	1.90	1.90	0.00	**0.1**
30	1.19	1.60	1.55	0.05	**3.1**
40	1.56	1.45	1.31	0.14	**10.9**
50	1.93	1.35	1.13	0.22	**19.2**

Comparison of the achieved result of the value for p_v from the calibrated numerical model with Seeber for a 0.2 m thick concrete lining, a p_i of 4 MPa and the use of the calibrated equation including Ankerit

Equation including Ankerit: y = 0.0278x + 0.2858			Seeber: Medium pressure p_v	Analysis Numerical versus Seeber	
E_{rm} [GPa]	E_{gap} [MPa]	numerical p_v [MPa]	Seeber p_v [MPa]	Difference [-]	Difference [%]
5	0.42	4.15	2.88	1.28	**44.3**
10	0.56	2.80	2.46	0.35	**14.1**
20	0.84	1.95	1.90	0.05	**2.5**
30	1.12	1.60	1.55	0.05	**3.1**
40	1.40	1.35	1.31	0.04	**3.3**
50	1.68	1.20	1.13	0.07	**6.0**

Calibration results for a p_i of 4 MPa and 0.3 m thickness of the concrete lining:

Comparison of the achieved result of the value for p_v from the calibrated numerical model with Seeber for a 0.3 m thick concrete lining, a p_i of 4 MPa and the use of the calibrated equation excluding Ankerit

Equation excluding Ankerit: y = 0.0429x - 0.091			Seeber: Medium p_v	Analysis Numerical versus Seeber	
E_{rm} [GPa]	E_{gap} [MPa]	numerical p_v [MPa]	Seeber p_v [MPa]	Difference [-]	Difference [%]
5	0.12	3.10	2.83	0.27	**9.4**
10	0.34	2.70	2.54	0.17	**6.5**
20	0.77	2.10	2.10	0.00	**0.0**
30	1.20	1.85	1.79	0.06	**3.2**
40	1.63	1.70	1.56	0.14	**8.8**
50	2.05	1.55	1.39	0.17	**11.9**

Comparison of the achieved result of the value for p_v from the calibrated numerical model with Seeber for a 0.3 m thick concrete lining, a p_i of 4 MPa and the use of the calibrated equation including Ankerit

Equation including Ankerit: y = 0.0344x + 0.0956			Seeber: Medium pressure p_v	Analysis Numerical versus Seeber	
E_{rm} [GPa]	E_{gap} [MPa]	numerical p_v [MPa]	Seeber p_v [MPa]	Difference [-]	Difference [%]
5	0.27	3.85	2.83	1.02	**35.9**
10	0.44	2.90	2.54	0.37	**14.4**
20	0.78	2.15	2.10	0.05	**2.4**
30	1.13	1.85	1.79	0.06	**3.2**
40	1.47	1.60	1.56	0.04	**2.4**
50	1.82	1.45	1.39	0.06	**4.7**

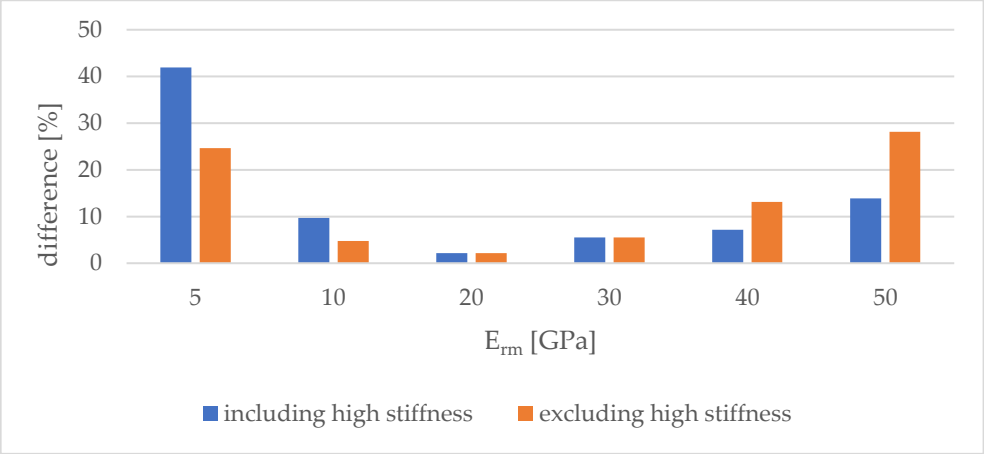

Analysis of the achieved accuracy for the calibration of the 0.1 m thick pre-stressed concrete lining and a p_i of 4 MPa

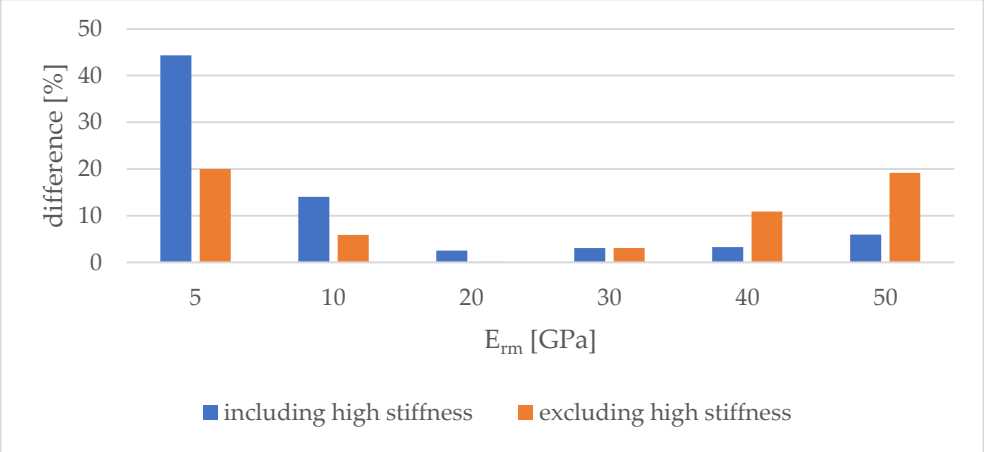

Analysis of the achieved accuracy for the calibration of the 0.2 m thick pre-stressed concrete lining and a p_i of 4 MPa

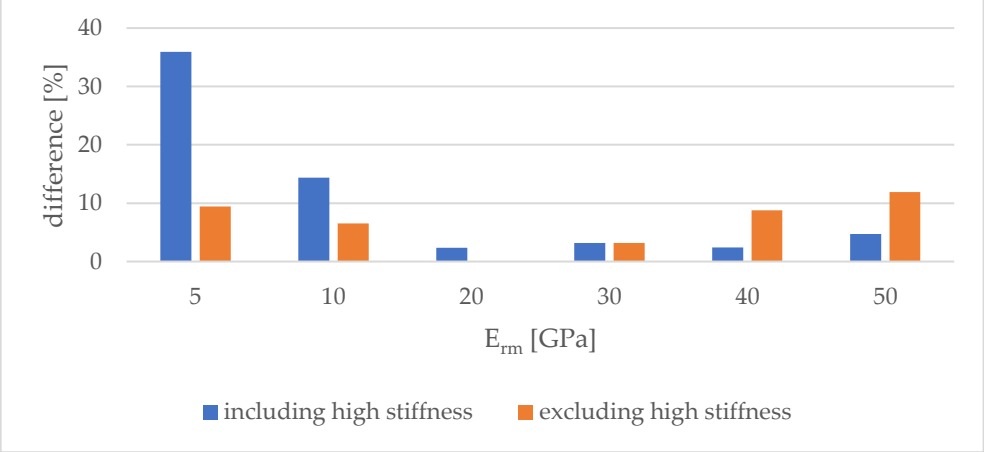

Analysis of the achieved accuracy for the calibration of the 0.3 m thick pre-stressed concrete lining and a p_i of 4 MPa

Calibration results for a p_i of 7 MPa:

Calibrated E_{gap} for Sauberger Kalk, p_i of 7 MPa, different concrete input parameters like concrete quality, E_{cm} and thickness as well as the Seeber input parameters $p_{v,0}$ and p_v

Sauberger Kalk – p_i of 7 MPa						
Concrete in put parameters			Seeber input		stiffness gap injection material	
Quality	E_{cm} [GPa]	thickness [m]	$p_{v.0}$ [MPa]	p_v [MPa]	E_{gap} [MPa]	$E_{gap.hardened}$ [MPa]
C25/30	31	0.1	7.13	2.34	**0.85**	2000
	31	0.2	8.63	3.27	**1.05**	2000
	31	0.3	9.09	3.62	**1.00**	2000
C30/37	33	0.1	6.82	2.43	**0.85**	2000
	33	0.2	8.35	3.36	**1.05**	2000
	33	0.3	8.86	3.70	**1.00**	2000
C35/45	34	0.1	6.43	2.48	**0.85**	2000
	34	0.2	8.00	3.41	**1.05**	2000
	34	0.3	8.56	3.74	**1.00**	2000
C40/50	35	0.1	6.15	2.52	**0.85**	2000
	35	0.2	7.75	3.45	**1.05**	2000
	35	0.3	8.35	3.78	**1.00**	2000

Calibrated E_{gap} for Ankerit, p_i of 7 MPa, different concrete input parameters like concrete quality, E_{cm} and thickness as well as the Seeber input parameters $p_{v,0}$ and p_v

Ankerit - p_i of 7 MPa						
Concrete in put parameters			Seeber input		stiffness gap injection material	
Quality	E_{cm} [GPa]	thickness [m]	$p_{v.0}$ [MPa]	p_v [MPa]	E_{gap} [MPa]	$E_{gap.hardened}$ [MPa]
C25/30	31	0.1	4.32	0.99	**1.30**	2000
	31	0.2	6.46	1.65	**1.95**	2000
	31	0.3	7.92	2.07	**2.40**	2000
C30/37	33	0.1	4.18	1.04	**1.30**	2000
	33	0.2	6.33	1.73	**1.95**	2000
	33	0.3	7.82	2.15	**2.40**	2000
C35/45	34	0.1	3.95	1.07	**1.30**	2000
	34,	0.2	6.07	1.76	**1.95**	2000
	34	0.3	7.56	2.19	**2.40**	2000
C40/50	35	0.1	3.79	1.10	**1.30**	2000
	35	0.2	5.90	1.80	**1.95**	2000
	35	0.3	7.39	2.23	**2.40**	2000

Calibrated E_{gap} for Tuff 1, p_i of 7 MPa, different concrete input parameters like concrete quality, E_{cm} and thickness as well as the Seeber input parameters $p_{v,0}$ and p_v

Tuff 1 - p_i of 7 MPa						
Concrete in put parameters			Seeber input		stiffness gap injection material	
Quality	E_{cm} [GPa]	thickness [m]	$p_{v.0}$ [MPa]	p_v [MPa]	E_{gap} [MPa]	$E_{gap.hardened}$ [MPa]
C25/30	31	0.1	7.25	2.50	**0.65**	2000
	31	0.2	8.48	3.42	**0.75**	2000
	31	0.3	8.72	3.75	**0.65**	2000
C30/37	33	0.1	6.94	2.59	**0.65**	2000
	33	0.2	8.21	3.52	**0.75**	2000
	33	0.3	8.50	3.83	**0.65**	2000
C35/45	34	0.1	6.54	2.64	**0.65**	2000
	34	0.2	7.87	3.56	**0.75**	2000
	34	0.3	8.23	3.87	**0.65**	2000
C40/50	35	0.1	6.27	2.69	**0.65**	2000
	35	0.2	7.63	3.60	**0.75**	2000
	35	0.3	8.04	3.9	**0.65**	2000

Calibrated E_{gap} for Tuff 2, p_i of 7 MPa, different concrete input parameters like concrete quality, E_{cm} and thickness as well as the Seeber input parameters $p_{v,0}$ and p_v

Tuff 2 - p_i of 7 MPa						
Concrete in put parameters			Seeber input		stiffness gap injection material	
Quality	E_{cm} [GPa]	thickness [m]	$p_{v.0}$ [MPa]	p_v [MPa]	E_{gap} [MPa]	$E_{gap.hardened}$ [MPa]
C25/30	31	0.1	8.93	3.76	**0.35**	2000
	31	0.2	8.76	4.48	**0.30**	2000
	31	0.3	8.21	4.57	**0.20**	2000
C30/37	33	0.1	8.49	3.86	**0.35**	2000
	33	0.2	8.45	4.56	**0.30**	2000
	33	0.3	7.99	4.62	**0.20**	2000
C35/45	34	0.1	8.03	3.90	**0.35**	2000
	34	0.2	8.14	4.59	**0.30**	2000
	34	0.3	7.78	4.65	**0.20**	2000
C40/50	35	0.1	7.70	3.95	**0.35**	2000
	35	0.2	7.92	4.62	**0.30**	2000
	35	0.3	7.62	4.67	**0.20**	2000

Calibrated E_{gap} for Rock mass 1, p_i of 7 MPa, different concrete input parameters like concrete quality, E_{cm} and thickness as well as the Seeber input parameters $p_{v,0}$ and p_v

Rock mass 1 - p_i of 7 MPa						
Concrete in put parameters			Seeber input		stiffness gap injection material	
Quality	E_{cm} [GPa]	thickness [m]	$p_{v.0}$ [MPa]	p_v [MPa]	E_{gap} [MPa]	$E_{gap.hardened}$ [MPa]
C25/30	31	0.1	5.59	1.57	**1.00**	2000
	31	0.2	7.62	2.42	**1.45**	2000
	31	0.3	8.70	2.85	**1.50**	2000
C30/37	33	0.1	5.38	1.64	**1.00**	2000
	33	0.2	7.43	2.51	**1.45**	2000
	33	0.3	8.53	2.94	**1.50**	2000
C35/45	34	0.1	5.08	1.68	**1.00**	2000
	34	0.2	7.11	2.55	**1.45**	2000
	34	0.3	8.24	2.98	**1.50**	2000
C40/50	35	0.1	4.86	1.72	**1.00**	2000
	35	0.2	6.90	2.59	**1.45**	2000
	35	0.3	8.05	3.02	**1.50**	2000

Calibrated E_{gap} for Rock mass 2, p_i of 7 MPa, different concrete input parameters like concrete quality, E_{cm} and thickness as well as the Seeber input parameters $p_{v,0}$ and p_v

Rock mass 2 - p_i of 7 MPa						
Concrete in put parameters			Seeber input		stiffness gap injection material	
Quality	E_{cm} [GPa]	thickness [m]	$p_{v.0}$ [MPa]	p_v [MPa]	E_{gap} [MPa]	$E_{gap.hardened}$ [MPa]
C25/30	31	0.1	6.28	1.90	**1.00**	2000
	31	0.2	8.12	2.80	**1.35**	2000
	31	0.3	8.94	3.21	**1.30**	2000
C30/37	33	0.1	6.03	1.99	**1.00**	2000
	33	0.2	7.89	2.90	**1.35**	2000
	33	0.3	8.74	3.30	**1.30**	2000
C35/45	34	0.1	5.68	2.03	**1.00**	2000
	34	0.2	7.56	2.94	**1.35**	2000
	34	0.3	8.45	3.34	**1.30**	2000
C40/50	35	0.1	5.44	2.07	**1.00**	2000
	35	0.2	7.32	2.99	**1.35**	2000
	35	0.3	8.24	3.38	**1.30**	2000

Calibration results for a p_i of 7 MPa:

Calibrated value of E_{gap} for Ankerit, Rock mass 1, Rock mass 2, Sauberger Kalk, Tuff 1 as well as Tuff 2 and a concrete lining thickness of 0.1 m, 0.2 m and 0.3 m with a p_i of 7 MPa

Rock type	Thickness of the concrete lining		
	0.1 m	0.2 m	0.3 m
Sauberger Kalk	0.85 MPa	1.05 MPa	1.00 MPa
Ankerit	1.30 MPa	1.95 MPa	2.40 MPa
Tuff 1	0.65 MPa	0.75 MPa	0.65 MPa
Tuff 2	0.35 MPa	0.30 MPa	0.20 MPa
Rock mass 1	1.00 MPa	1.45 MPa	1.50 MPa
Rock mass 2	1.00 MPa	1.35 MPa	1.30 MPa

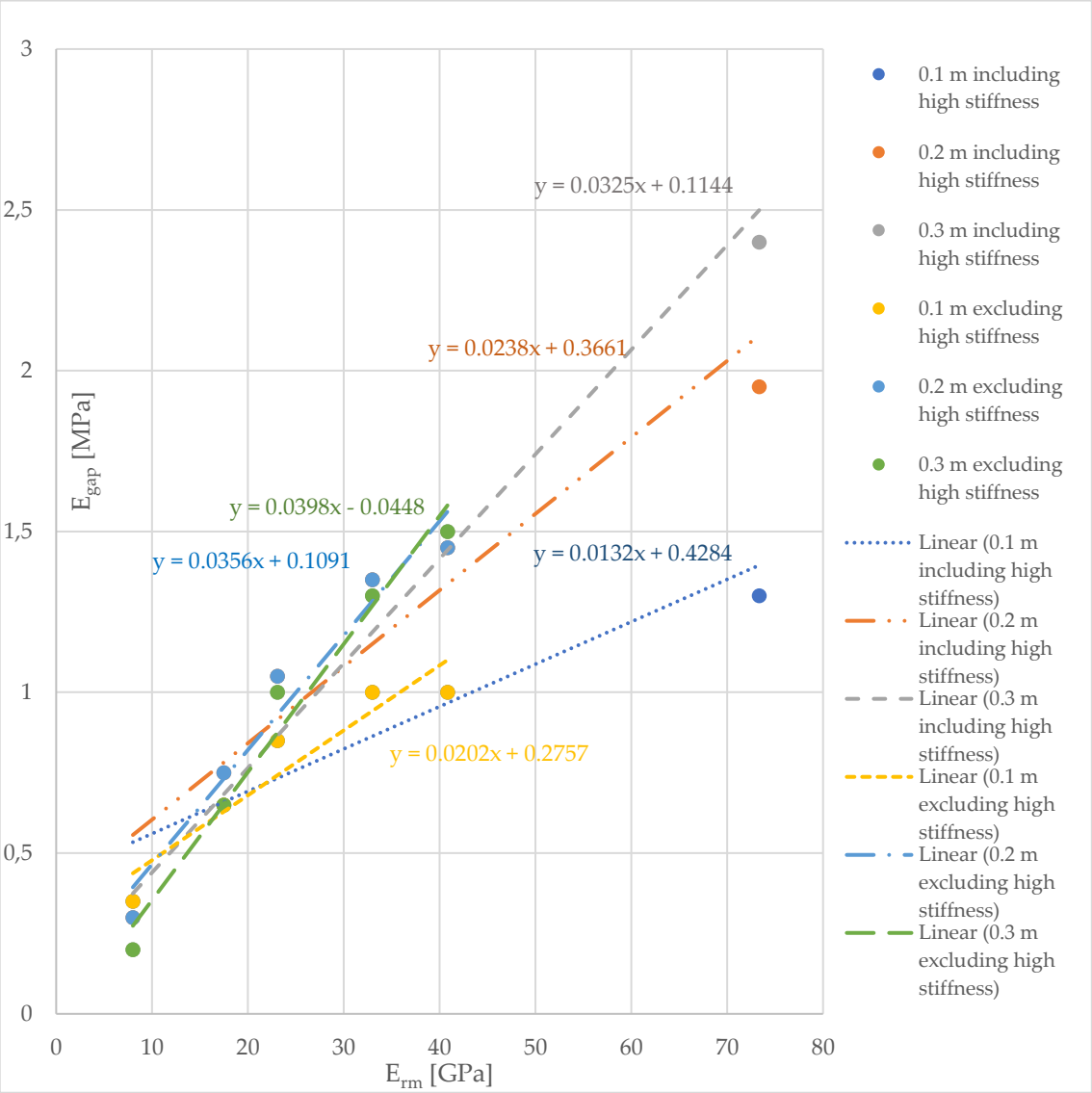

Graphical display of the resulting equations to calculate the necessary value of E_{gap} depending on E_{rm} for a concrete lining thickness of 0.1 m, 0.2m and 0.3 m and a p_i of 7 MPa

Calibration results for a p_i of 7 MPa and 0.1 m thickness of the concrete lining:

Comparison of the achieved result of the value for p_v from the calibrated numerical model with Seeber for a 0.1 m thick concrete lining, a p_i of 7 MPa and the use of the calibrated equation excluding Ankerit

Equation excluding Ankerit: y = 0.0202x + 0.2757			Seeber: Medium p_v	Analysis Numerical versus Seeber	
E_{rm} [GPa]	E_{gap} [MPa]	numerical p_v [MPa]	Seeber p_v [MPa]	Difference [-]	Difference [%]
5	0.39	5.90	4.57	1.33	**29.2**
10	0.49	3.60	3.51	0.09	**2.6**
20	0.69	2.40	2.40	0.00	**0.1**
30	0.89	1.85	1.82	0.03	**1.6**
40	1.09	1.60	1.47	0.13	**8.8**
50	1.29	1.50	1.23	0.27	**22.2**

Comparison of the achieved result of the value for p_v from the calibrated numerical model with Seeber for a 0.1 m thick concrete lining, a p_i of 7 MPa and the use of the calibrated equation including Ankerit

Equation including Ankerit: y = 0.0132x + 0.4284			Seeber: Medium p_v	Analysis Numerical versus Seeber	
E_{rm} [GPa]	E_{gap} [MPa]	numerical p_v [MPa]	Seeber p_v [MPa]	Difference [-]	Difference [%]
5	0.49	6.70	4.57	2.13	**46.7**
10	0.56	3.95	3.51	0.44	**12.5**
20	0.69	2.40	2.40	0.00	**0.1**
30	0.82	1.80	1.82	0.02	**1.1**
40	0.96	1.55	1.47	0.08	**5.4**
50	1.09	1.35	1.23	0.12	**10.0**

Calibration results for a p_i of 7 MPa and 0.2 m thickness of the concrete lining:

Comparison of the achieved result of the value for p_v from the calibrated numerical model with Seeber for a 0.2 m thick concrete lining, a p_i of 7 MPa and the use of the calibrated equation excluding Ankerit

Equation excluding Ankerit: y = 0.0356x + 0.1091			Seeber: Medium p_v	Analysis Numerical versus Seeber	
E_{rm} [GPa]	E_{gap} [MPa]	numerical p_v [MPa]	Seeber p_v [MPa]	Difference [-]	Difference [%]
5	0.29	6.15	5.03	1.12	**22.2**
10	0.47	4.50	4.30	0.20	**4.7**
20	0.82	3.35	3.33	0.02	**0.7**
30	1.18	2.80	2.71	0.09	**3.2**
40	1.53	2.50	2.29	0.21	**9.1**
50	1.89	2.35	1.99	0.37	**18.4**

Comparison of the achieved result of the value for p_v from the calibrated numerical model with Seeber for a 0.2 m thick concrete lining, a p_i of 7 MPa and the use of the calibrated equation including Ankerit

Equation including Ankerit: y = 0.0238x + 0.3661			Seeber: Medium p_v	Analysis Numerical versus Seeber	
E_{rm} [GPa]	E_{gap} [MPa]	numerical p_v [MPa]	Seeber p_v [MPa]	Difference [-]	Difference [%]
5	0.49	7.85	5.03	2.82	**56.0**
10	0.60	5.05	4.30	0.75	**17.5**
20	0.84	3.40	3.33	0.07	**2.2**
30	1.08	2.70	2.71	0.01	**0.5**
40	1.32	2.30	2.29	0.01	**0.3**
50	1.56	2.10	1.99	0.12	**5.8**

Calibration results for a p_i of 7 MPa and 0.3 m thickness of the concrete lining:

Comparison of the achieved result of the value for p_v from the calibrated numerical model with Seeber for a 0.3 m thick concrete lining, a p_i of 7 MPa and the use of the calibrated equation excluding Ankerit

Equation excluding Ankerit: y = 0.0398x - 0.0448			Seeber: Medium p_v	Analysis Numerical versus Seeber	
E_{rm} [GPa]	E_{gap} [MPa]	numerical p_v [MPa]	Seeber p_v [MPa]	Difference [-]	Difference [%]
5	0.09	5.20	4.95	0.25	**5.1**
10	0.30	4.50	4.44	0.06	**1.5**
20	0.72	3.70	3.68	0.03	**0.7**
30	1.14	3.20	3.14	0.06	**2.0**
40	1.57	2.90	2.74	0.17	**6.0**
50	1.99	2.75	2.43	0.33	**13.4**

Comparison of the achieved result of the value for p_v from the calibrated numerical model with Seeber for a 0.3 m thick concrete lining, a p_i of 7 MPa and the use of the calibrated equation including Ankerit

Equation including Ankerit: y = 0.0325x + 0.1144			Seeber: Medium p_v	Analysis Numerical versus Seeber	
E_{rm} [GPa]	E_{gap} [MPa]	numerical p_v [MPa]	Seeber p_v [MPa]	Difference [-]	Difference [%]
5	0.28	6.80	4.95	1.85	**37.4**
10	0.44	5.05	4.44	0.61	**13.9**
20	0.76	3.75	3.68	0.08	**2.0**
30	1.09	3.15	3.14	0.01	**0.4**
40	1.41	2.75	2.74	0.01	**0.5**
50	1.74	2.55	2.43	0.13	**5.2**

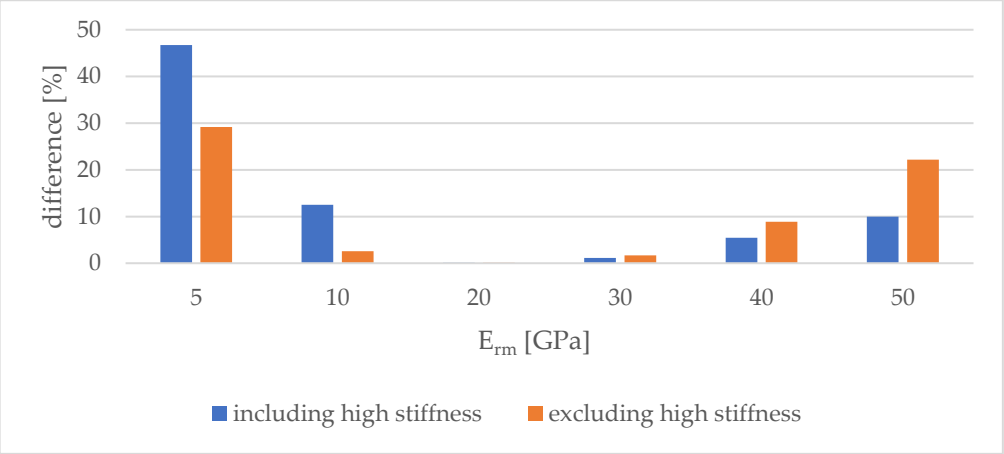

Achieved accuracy from the application of the calibrated value of E_{gap} in a numerical simulation for a thickness of 0.1 m and p_i of 7 MPa

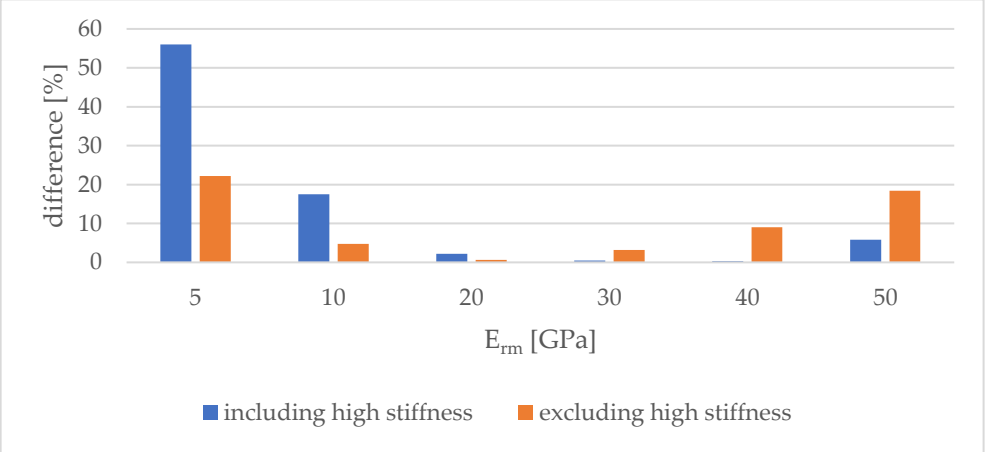

Achieved accuracy from the application of the calibrated value of E_{gap} in a numerical simulation for a thickness of 0.2 m and p_i of 7 MPa

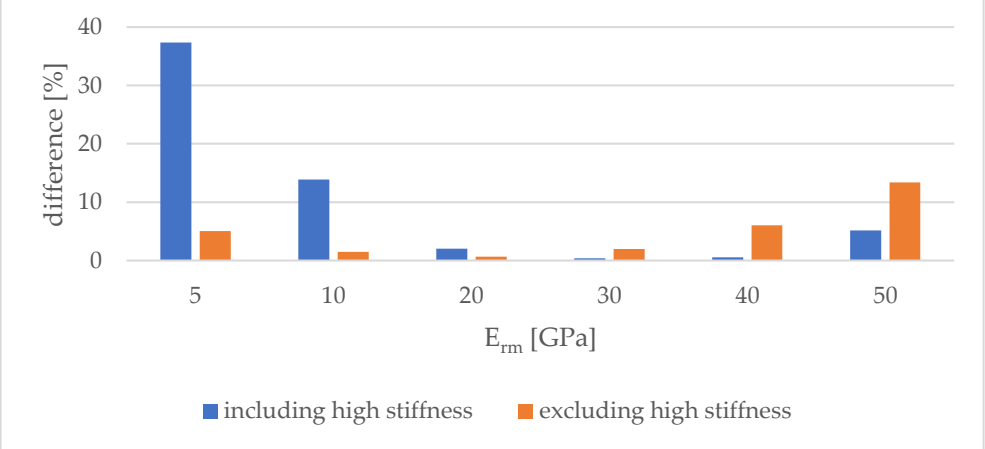

Achieved accuracy from the application of the calibrated value of E_{gap} in a numerical simulation for a thickness of 0.3 m and p_i of 7 MPa

Calibration results for a p_i of 10 MPa:

Calibrated E_{gap} for Sauberger Kalk, p_i of 10 MPa, different concrete input parameters like concrete quality, E_{cm} and thickness as well as the Seeber input parameters $p_{v,0}$ and p_v

Sauberger Kalk – p_i of 10 MPa						
Concrete in put parameters			Seeber input		stiffness gap injection material	
Quality	E_{cm} [GPa]	thickness [m]	$p_{v.0}$ [MPa]	p_v [MPa]	E_{gap} [MPa]	$E_{gap.hardened}$ [MPa]
C25/30	3	0.1	9.48	3.34	**0.90**	2000
	31	0.2	11.28	4.67	**1.05**	2000
	31	0.3	11.67	5.18	**0.95**	2000
C30/37	33	0.1	9.07	3.48	**0.90**	2000
	33	0.2	10.90	4.80	**1.05**	2000
	33	0.3	11.36	5.29	**0.95**	2000
C35/45	34	0.1	8.54	3.54	**0.90**	2000
	34	0.2	10.43	4.87	**1.05**	2000
	34	0.3	10.97	5.34	**0.95**	2000
C40/50	35	0.1	8.17	3.61	**0.90**	2000
	35	0.2	10.10	4.93	**1.05**	2000
	35	0.3	10.69	5.39	**0.95**	2000

Calibrated E_{gap} for Ankerit, p_i of 10 MPa, different concrete input parameters like concrete quality, E_{cm} and thickness as well as the Seeber input parameters $p_{v,0}$ and p_v

Ankerit - p_i of 10 MPa						
Concrete in put parameters			Seeber input		stiffness gap injection material	
Quality	E_{cm} [GPa]	thickness [m]	$p_{v.0}$ [MPa]	p_v [MPa]	E_{gap} [MPa]	$E_{gap.hardened}$ [MPa]
C25/30	31	0.1	5.38	1.41	**1.15**	2000
	31	0.2	7.92	2.36	**1.95**	2000
	31	0.3	9.56	2.96	**2.20**	2000
C30/37	33	0.1	5.20	1.49	**1.15**	2000
	33	0.2	7.75	2.47	**1.95**	2000
	33	0.3	9.42	3.08	**2.20**	2000
C35/45	34	0.1	4.91	1.53	**1.15**	2000
	34	0.2	7.43	2.52	**1.95**	2000
	34	0.3	9.10	3.13	**2.20**	2000
C40/50	35	0.1	4.71	1.57	**1.15**	2000
	35	0.2	7.21	2.57	**1.95**	2000
	35	0.3	8.89	3.19	**2.20**	2000

Calibrated E_{gap} for Tuff 1, p_i of 10 MPa, different concrete input parameters like concrete quality, E_{cm} and thickness as well as the Seeber input parameters $p_{v,0}$ and p_v

Tuff 1 - p_i of 10 MPa						
Concrete in put parameters			Seeber input		stiffness gap injection material	
Quality	E_{cm} [GPa]	thickness [m]	$p_{v.0}$ [MPa]	p_v [MPa]	E_{gap} [MPa]	$E_{gap.hardened}$ [MPa]
C25/30	31	0.1	9.70	3.57	**0.65**	2000
	31	0.2	11.16	4.89	**0.75**	2000
	31	0.3	11.31	5.36	**0.60**	2000
C30/37	33	0.1	9.27	3.71	**0.65**	2000
	33	0.2	10.79	5.02	**0.75**	2000
	33	0.3	11	5.47	**0.60**	2000
C35/45	34	0.1	8.74	3.77	**0.65**	2000
	34	0.2	10.34	5.09	**0.75**	2000
	34	0.3	10.64	5.52	**0.60**	2000
C40/50	35	0.1	8.37	3.84	**0.65**	2000
	35	0.2	10.02	5.15	**0.75**	2000
	35	0.3	10.39	5.57	**0.60**	2000

Calibrated E_{gap} for Tuff 2, p_i of 10 MPa, different concrete input parameters like concrete quality, E_{cm} and thickness as well as the Seeber input parameters $p_{v,0}$ and p_v

Tuff 2 - p_i of 10 MPa						
Concrete in put parameters			Seeber input		stiffness gap injection material	
Quality	E_{cm} [GPa]	thickness [m]	$p_{v.0}$ [MPa]	p_v [MPa]	E_{gap} [MPa]	$E_{gap.hardened}$ [MPa]
C25/30	31	0.1	12.24	5.37	**0.35**	2000
	31	0.2	11.68	6.41	**0.30**	2000
	31	0.3	10.99	6.53	**0.15**	2000
C30/37	33	0.1	11.63	5.51	**0.35**	2000
	33	0.2	11.43	6.51	**0.30**	2000
	33	0.3	10.68	6.61	**0.15**	2000
C35/45	34	0.1	10.99	5.58	**0.35**	2000
	34	0.2	11	6.56	**0.30**	2000
	34	0.3	10.39	6.64	**0.15**	2000
C40/50	35	0.1	10.53	5.64	**0.35**	2000
	35	0.2	10.69	6.6	**0.30**	2000
	35	0.3	10.17	6.67	**0.15**	2000

Calibrated E_{gap} for Rock mass 1, p_i of 10 MPa, different concrete input parameters like concrete quality, E_{cm} and thickness as well as the Seeber input parameters $p_{v,0}$ and p_v

Rock mass 1 - p_i of 10 MPa						
Concrete in put parameters			Seeber input		stiffness gap injection material	
Quality	E_{cm} [GPa]	thickness [m]	$p_{v.0}$ [MPa]	p_v [MPa]	E_{gap} [MPa]	$E_{gap.hardened}$ [MPa]
C25/30	31	0.1	5.59	1.57	**1.00**	2000
	31	0.2	7.62	2.42	**1.45**	2000
	31	0.3	8.7	2.85	**1.50**	2000
C30/37	33	0.1	5.38	1.64	**1.00**	2000
	33	0.2	7.43	2.51	**1.45**	2000
	33	0.3	8.53	2.94	**1.50**	2000
C35/45	34	0.1	5.08	1.68	**1.00**	2000
	34	0.2	7.11	2.55	**1.45**	2000
	34	0.3	8.24	2.98	**1.50**	2000
C40/50	35	0.1	4.86	1.72	**1.00**	2000
	35	0.2	6.9	2.59	**1.45**	2000
	35	0.3	8.05	3.02	**1.50**	2000

Calibrated E_{gap} for Rock mass 2, p_i of 10 MPa, different concrete input parameters like concrete quality, E_{cm} and thickness as well as the Seeber input parameters $p_{v,0}$ and p_v

Rock mass 2 - p_i of 10 MPa						
Concrete in put parameters			Seeber input		stiffness gap injection material	
Quality	E_{cm} [GPa]	thickness [m]	$p_{v.0}$ [MPa]	p_v [MPa]	E_{gap} [MPa]	$E_{gap.hardened}$ [MPa]
C25/30	31	0.1	8.23	2.71	**1.00**	2000
	31	0.2	10.47	4	**1.35**	2000
	31	0.3	11.32	4.59	**1.35**	2000
C30/37	33	0.1	7.9	2.84	**1.00**	2000
	33	0.2	10.15	4.14	**1.35**	2000
	33	0.3	11.05	4.71	**1.35**	2000
C35/45	34	0.1	7.44	2.9	**1.00**	2000
	34	0.2	9.72	4.2	**1.35**	2000
	34	0.3	10.66	4.77	**1.35**	2000
C40/50	35	0.1	7.12	2.95	**1.00**	2000
	35	0.2	9.41	4.27	**1.35**	2000
	35	0.3	10.39	4.83	**1.35**	2000

Calibration results for a p_i of 10 MPa:

Calibrated value of E_{gap} for Ankerit, Rock mass 1, Rock mass 2, Sauberger Kalk, Tuff 1 as well as Tuff 2 and a concrete lining thickness of 0.1 m, 0.2 m and 0.3 m with a p_i of 10 MPa

Rock type	Thickness of the concrete lining		
	0.1 m	0.2 m	0.3 m
Sauberger Kalk	0.90 MPa	1.05 MPa	0.95 MPa
Ankerit	1.15 MPa	1.95 MPa	2.20 MPa
Tuff 1	0.65 MPa	0.75 MPa	0.60 MPa
Tuff 2	0.35 MPa	0.30 MPa	0.15 MPa
Rock mass 1	1.00 MPa	1.45 MPa	1.50 MPa
Rock mass 2	1.00 MPa	1.35 MPa	1.35 MPa

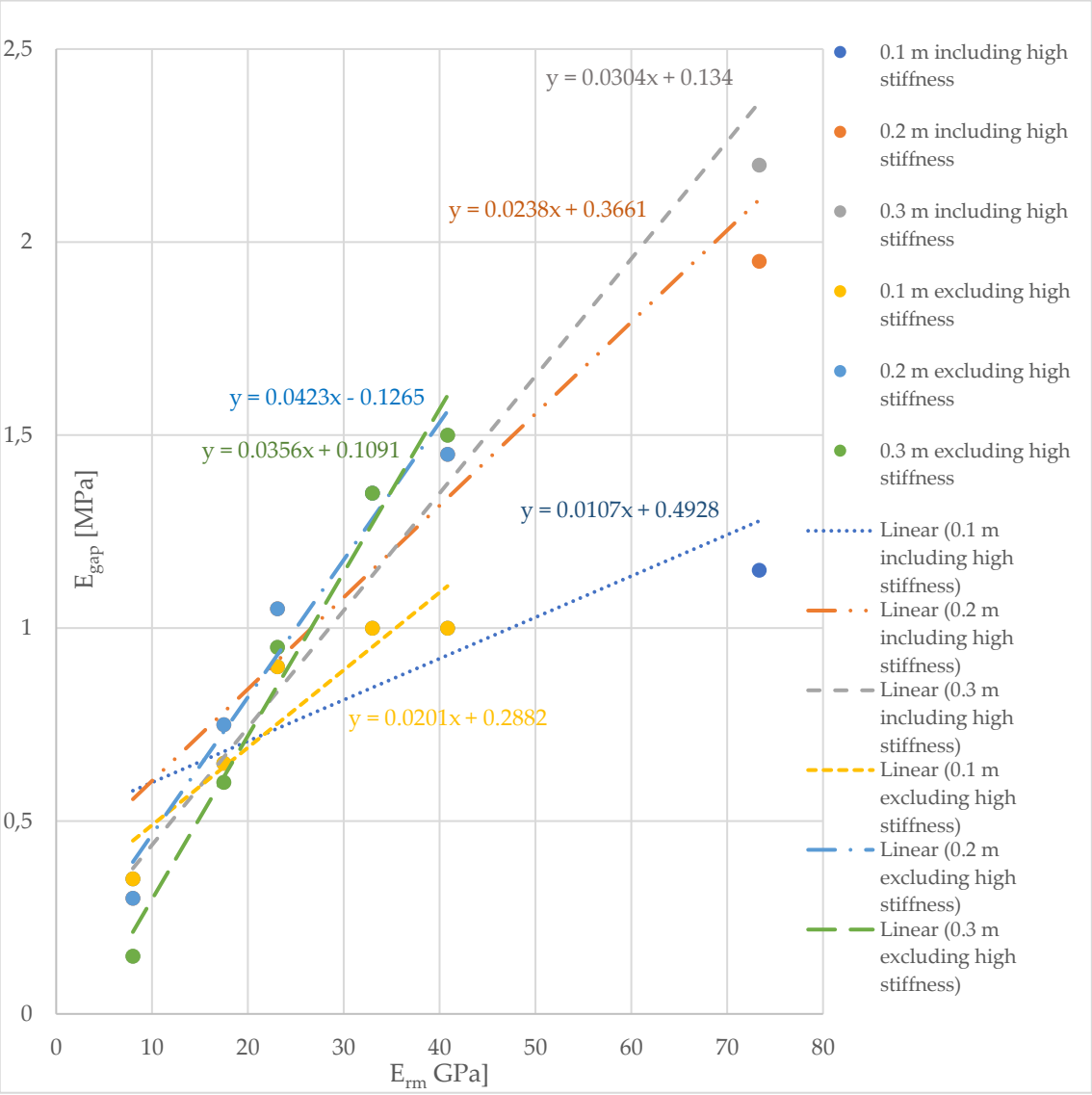

Graphical display of the resulting equations to calculate the necessary value of E_{gap} depending on E_{rm} for a concrete lining thickness of 0.1 m, 0.2m and 0.3 m and a p_i of 10 MPa

Calibration results for a p_i of 10 MPa and 0.1 m thickness of the concrete lining:

Comparison of the achieved result of the value for p_v from the calibrated numerical model with Seeber for a 0.1 m thick concrete lining, a p_i of 10 MPa and the use of the calibrated equation including Ankerit

Equation including Ankerit: y = 0.0107x + 0.4928			Seeber: Medium p_v	Analysis Numerical versus Seeber	
E_{rm} [GPa]	E_{gap} [MPa]	numerical p_v [MPa]	Seeber p_v [MPa]	Difference [-]	Difference [%]
5	0.55	10.4	6.52	3.88	**59.5**
10	0.60	5.85	5.01	0.84	**16.7**
20	0.71	3.50	3.43	0.07	**2.1**
30	0.81	2.60	2.60	0.00	**0.1**
40	0.92	2.15	2.10	0.05	**2.4**
50	1.03	1.85	1.76	0.09	**5.3**

Comparison of the achieved result of the value for p_v from the calibrated numerical model with Seeber for a 0.1 m thick concrete lining, a p_i of 10 MPa and the use of the calibrated equation excluding Ankerit

Equation excluding Ankerit: y = 0.0201x + 0.2882			Seeber: Medium p_v	Analysis Numerical versus Seeber	
E_{rm} [GPa]	E_{gap} [MPa]	numerical p_v [MPa]	Seeber p_v [MPa]	Difference [-]	Difference [%]
5	0.38	8.30	6.52	1.78	**27.3**
10	0.48	5.15	5.01	0.14	**2.7**
20	0.68	3.45	3.43	0.02	**0.7**
30	0.88	2.75	2.60	0.15	**5.7**
40	1.08	2.40	2.10	0.30	**12.5**
50	1.29	2.20	1.76	0.44	**20.1**

Calibration results for a p_i of 10 MPa and 0.2 m thickness of the concrete lining:

Comparison of the achieved result of the value for p_v from the calibrated numerical model with Seeber for a 0.2 m thick concrete lining, a p_i of 10 MPa and the use of the calibrated equation including Ankerit

Equation including Ankerit: y = 0.0238x + 0.3661			Seeber: Medium p_v	Analysis Numerical versus Seeber	
E_{rm} [GPa]	E_{gap} [MPa]	numerical p_v [MPa]	Seeber p_v [MPa]	Difference [-]	Difference [%]
5	0.49	11.20	7.19	4.01	**55.8**
10	0.60	7.20	6.14	1.06	**17.3**
20	0.84	4.85	4.75	0.10	**2.1**
30	1.08	3.90	3.88	0.02	**0.6**
40	1.32	3.30	3.28	0.02	**0.8**
50	1.56	2.95	2.83	0.12	**4.1**

Comparison of the achieved result of the value for p_v from the calibrated numerical model with Seeber for a 0.2 m thick concrete lining, a p_i of 10 MPa and the use of the calibrated equation excluding Ankerit

Equation excluding Ankerit: y = 0.0356x + 0.1091			Seeber: Medium p_v	Analysis Numerical versus Seeber	
E_{rm} [GPa]	E_{gap} [MPa]	numerical p_v [MPa]	Seeber p_v [MPa]	Difference [-]	Difference [%]
5	0.29	8.80	7.19	1.61	**22.4**
10	0.47	6.40	6.14	0.26	**4.3**
20	0.82	4.80	4.75	0.05	**1.0**
30	1.18	4.05	3.88	0.17	**4.4**
40	1.53	3.60	3.28	0.33	**9.9**
50	1.89	3.40	2.83	0.57	**20.0**

Calibration results for a p_i of 10 MPa and 0.3 m thickness of the concrete:

Comparison of the achieved result of the value for p_v from the calibrated numerical model with Seeber for a 0.3 m thick concrete lining, a p_i of 10 MPa and the use of the calibrated equation including Ankerit

Equation including Ankerit: y = 0.0304x + 0.134			Seeber: Medium p_v	Analysis Numerical versus Seeber	
E_{rm} [GPa]	E_{gap} [MPa]	numerical p_v [MPa]	Seeber p_v [MPa]	Difference [-]	Difference [%]
5	0.27	9.60	7.07	2.53	**35.8**
10	0.42	7.05	6.34	0.71	**11.2**
20	0.72	5.25	5.25	0.00	**0.0**
30	1.03	4.40	4.48	0.07	**1.7**
40	1.33	3.85	3.91	0.05	**1.4**
50	1.63	3.45	3.46	0.01	**0.4**

Comparison of the achieved result of the value for p_v from the calibrated numerical model with Seeber for a 0.3 m thick concrete lining, a p_i of 10 MPa and the use of the calibrated equation excluding Ankerit

Equation excluding Ankerit: y = 0.0423x - 0.1265			Seeber: Medium p_v	Analysis Numerical versus Seeber	
E_{rm} [GPa]	E_{gap} [MPa]	numerical p_v [MPa]	Seeber p_v [MPa]	Difference [-]	Difference [%]
5	0.15	8.10	7.07	1.03	**14.6**
10	0.35	6.65	6.34	0.31	**4.9**
20	0.75	5.30	5.25	0.05	**1.0**
30	1.15	4.60	4.48	0.13	**2.7**
40	1.55	4.15	3.91	0.25	**5.9**
50	1.95	3.90	3.46	0.44	**11.2**

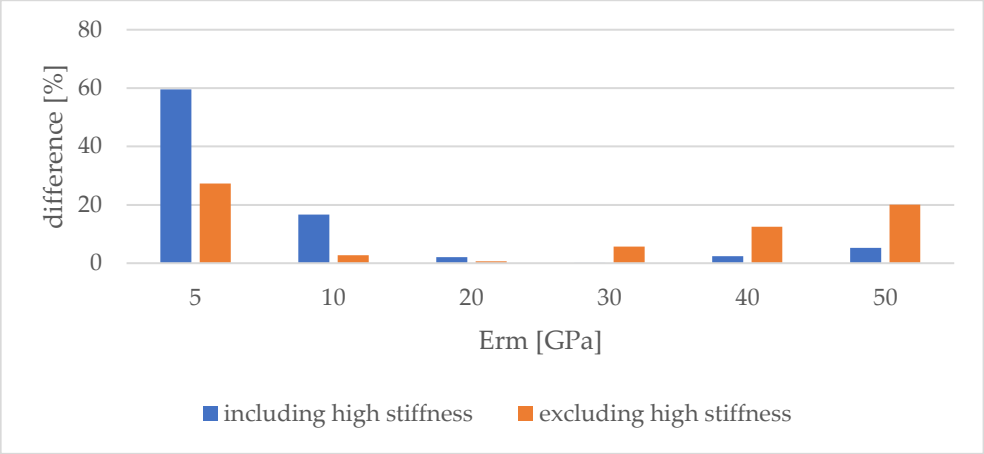

Analysis of the achieved accuracy for the calibration of the 0.1 m thick pre-stressed concrete lining and a p_i of 10 MPa

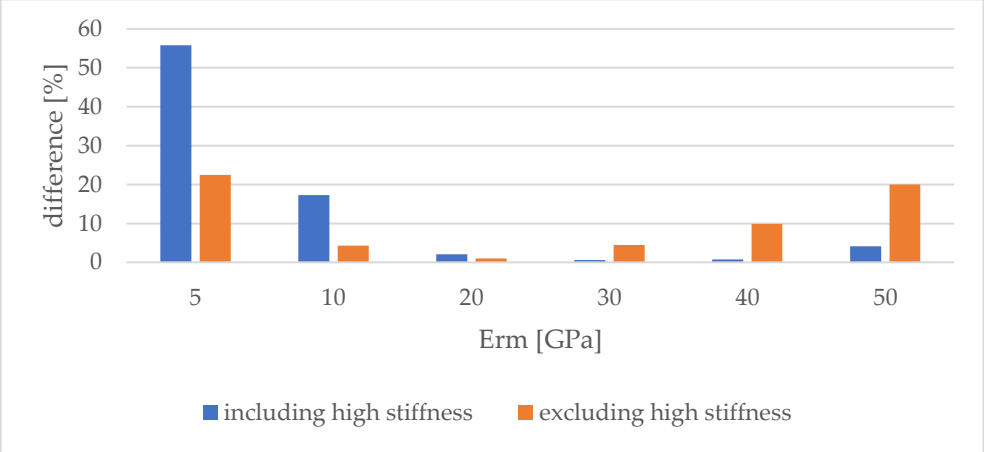

Analysis of the achieved accuracy for the calibration of the 0.2 m thick pre-stressed concrete lining and a p_i of 10 MPa

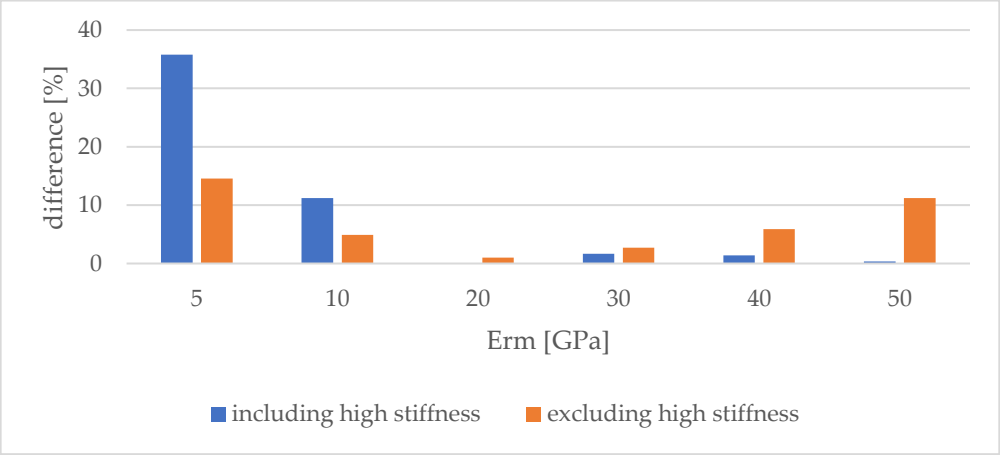

Analysis of the achieved accuracy for the calibration of the 0.3 m thick pre-stressed concrete lining and a p_i of 10 MPa

Appendix C.2 for Chapter 8.1 Calibration of the pre-stressed concrete

Calibration results for different diameters of the storage and a p_i of 10 MPa:

Calibrated E_{gap} for Ankerit, a storage diameter of 4, 5, 6 and 7 m, a p_i of 10 MPa, different concrete input parameters like concrete quality, E_{cm} and thickness as well as the Seeber input parameters $p_{v,0}$ and p_v

Ankerit – p_i of 10 MPa							
Storage diameter [m]	concrete			Seeber		gap injection material	
	Quality [-]	E_{cm} [GPa]	thickness [m]	$p_{v,0}$ [MPa]	p_v [MPa]	E_{gap} [MPa]	$E_{gap,hardened}$ [MPa]
4	C30/37	33	0.1	4.06	1.17	**0.75**	2000
		33	0.2	6.26	2.03	**1.30**	2000
		33	0.3	7.82	2.65	**1.60**	2000
	C35/45	34	0.1	3.84	1.20	**0.75**	2000
		34	0.2	6.00	2.08	**1.30**	2000
		34	0.3	7.55	2.71	**1.60**	2000
5	C30/37	33	0.1	3.33	0.97	**0.50**	2000
		33	0.2	5.24	1.72	**0.90**	2000
		33	0.3	6.66	2.31	**1.15**	2000
	C35/45	34	0.1	3.15	0.99	**0.50**	2000
		34	0.2	5.03	1.76	**0.90**	2000
		34	0.3	6.44	2.36	**1.15**	2000
6	C30/37	33	0.1	2.83	0.82	**0.35**	2000
		33	0.2	4.51	1.49	**0.65**	2000
		33	0.3	5.80	2.03	**0.90**	2000
	C35/45	34	0.1	2.67	0.84	**0.35**	2000
		34	0.2	4.32	1.53	**0.65**	2000
		34	0.3	5.61	2.08	**0.90**	2000
7	C30/37	33	0.1	2.45	0.71	**0.25**	2000
		33	0.2	3.95	1.31	**0.50**	2000
		33	0.3	5.13	1.82	**0.70**	2000
	C35/45	34	0.1	2.31	0.73	**0.25**	2000
		34	0.2	3.79	1.35	**0.50**	2000
		34	0.3	4.96	1.86	**0.70**	2000

Calibrated value of E_{gap} for Ankerit, a concrete lining thickness of 0.1 m, 0.2 m and 0.3 m, a diameter of the storage of 3, 4, 5, 6 and 7 m as well as a p_i of 10 MPa

Storage diameter	Thickness of the concrete lining		
	0.1 m	**0.2 m**	**0.3 m**
3 m	1.15 MPa	1.95 MPa	2.20 MPa
4 m	0.75 MPa	1.30 MPa	1.60 MPa
5 m	0.50 MPa	0.90 MPa	1.15 MPa
6 m	0.35 MPa	0.65 MPa	0.90 MPa
7 m	0.25 MPa	0.50 MPa	0.70 MPa

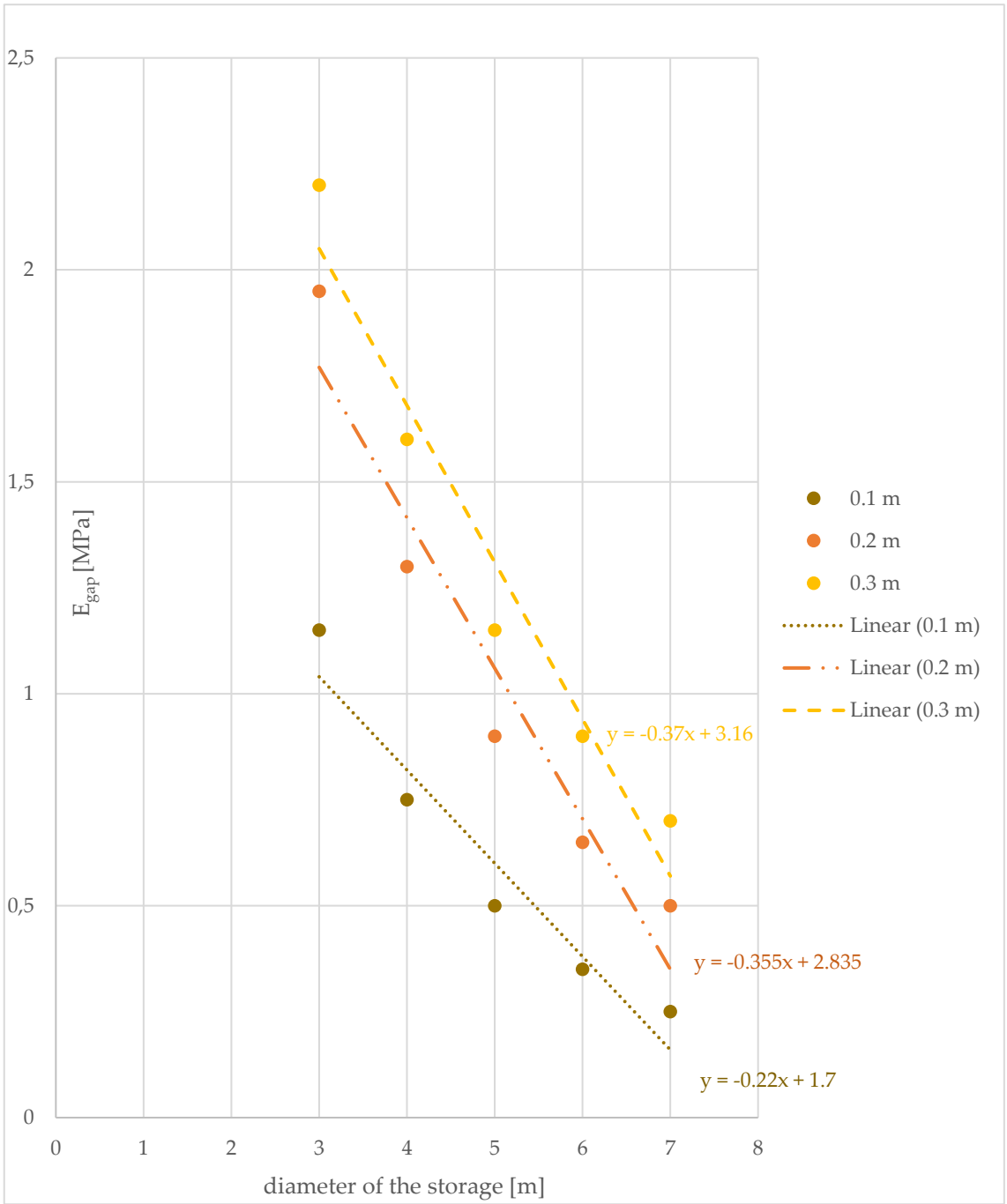

Graphical display of the resulting E_{gap} of the calibration depending on the storage diameter for Ankerit, a p_i of 10 MPa as well as a lining thickness of 0.1, 0.2 and 0.3 m

Calibrated E_{gap} for Rock mass 1, a storage diameter of 4, 5, 6 and 7 m, a p_i of 10 MPa, different concrete input parameters like concrete quality, E_{cm} and thickness as well as the Seeber input parameters $p_{v,0}$ and p_v

Rock mass 1 – p_i of 10 MPa							
Storage diameter [m]	concrete			Seeber		gap injection material	
	Quality [-]	E_{cm} [GPa]	thickness [m]	$p_{v,0}$ [MPa]	p_v [MPa]	E_{gap} [MPa]	$E_{gap,hardened}$ [MPa]
4	C30/37	33	0.1	5.6	1.9	**0.70**	2000
		33	0.2	7.97	3.06	**1.05**	2000
		33	0.3	9.33	3.78	**1.15**	2000
	C35/45	34	0.1	5.28	1.94	**0.70**	2000
		34	0.2	7.63	3.12	**1.05**	2000
		34	0.3	9.01	3.84	**1.15**	2000
5	C30/37	33	0.1	4.69	1.59	**0.45**	2000
		33	0.2	6.89	2.66	**0.75**	2000
		33	0.3	8.27	3.39	**0.95**	2000
	C35/45	34	0.1	4.42	1.63	**0.45**	2000
		34	0.2	6.59	2.72	**0.75**	2000
		34	0.3	7.98	3.46	**0.95**	2000
6	C30/37	33	0.1	4.03	1.36	**0.30**	2000
		33	0.2	6.05	2.35	**0.55**	2000
		33	0.3	7.41	3.06	**0.70**	2000
	C35/45	34	0.1	3.80	1.40	**0.30**	2000
		34	0.2	5.79	2.4	**0.55**	2000
		34	0.3	7.15	3.12	**0.70**	2000
7	C30/37	33	0.1	3.53	1.20	**0.25**	2000
		33	0.2	5.40	2.10	**0.45**	2000
		33	0.3	6.70	2.78	**0.55**	2000
	C35/45	34	0.1	3.33	1.23	**0.25**	2000
		34	0.2	5.17	2.15	**0.45**	2000
		34	0.3	6.46	2.84	**0.55**	2000

Calibrated value of E_{gap} for Rock mass 1, a concrete lining thickness of 0.1 m, 0.2 m and 0.3 m, a diameter of the storage of 3, 4, 5, 6 and 7 m as well as a p_i of 10 MPa

Storage diameter	Thickness of the concrete lining		
	0.1 m	**0.2 m**	**0.3 m**
3 m	1.00 MPa	1.45 MPa	1.50 MPa
4 m	0.70 MPa	1.05 MPa	1.15 MPa
5 m	0.45 MPa	0.75 MPa	0.95 MPa
6 m	0.30 MPa	0.55 MPa	0.70 MPa
7 m	0.25 MPa	0.45 MPa	0.55 MPa

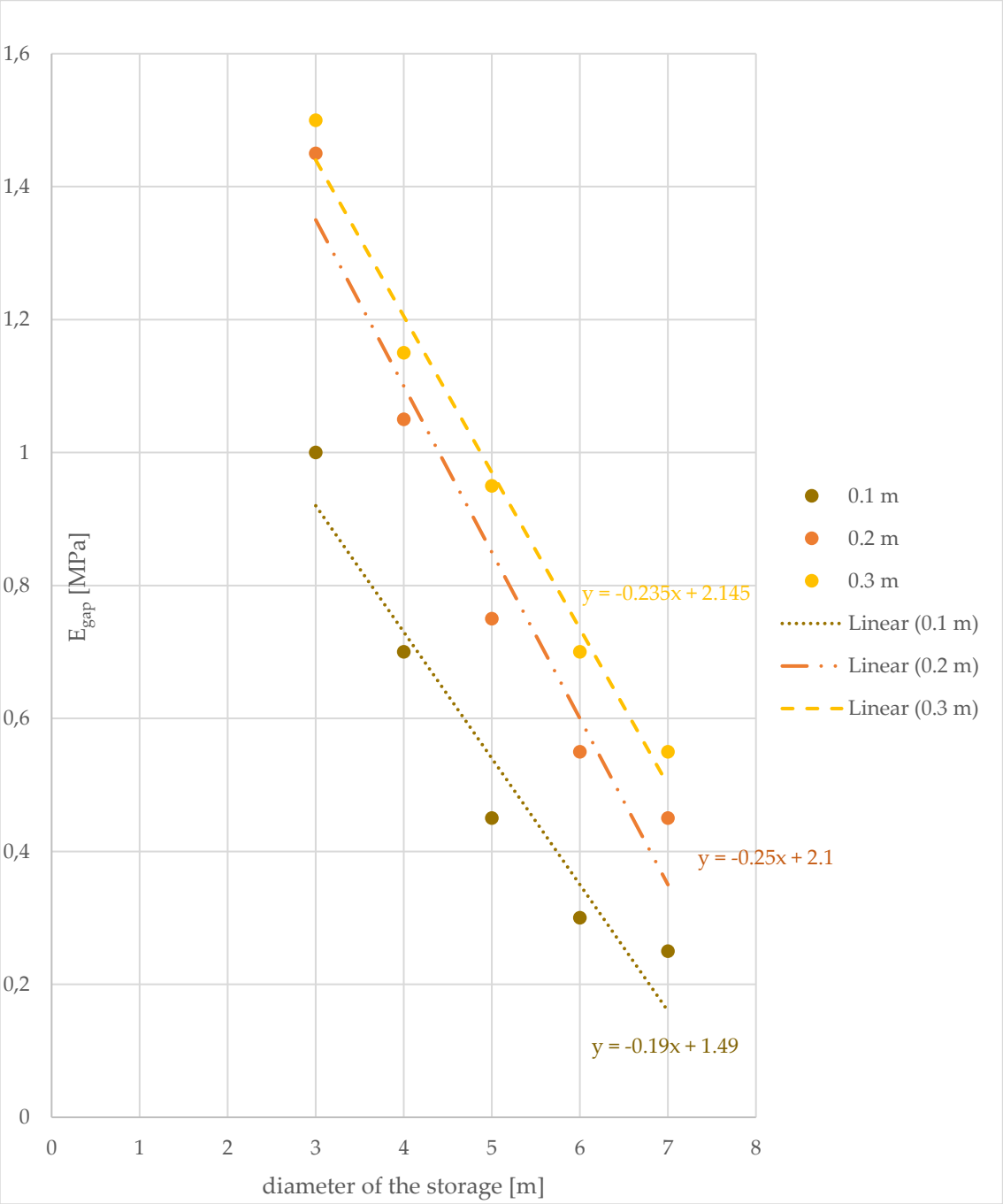

Graphical display of the resulting E_{gap} of the calibration depending on the storage diameter for Rock mass 1, a p_i of 10 MPa as well as a lining thickness of 0.1, 0.2 and 0.3 m

Calibrated E_{gap} for Tuff 1, a storage diameter of 4, 5, 6 and 7 m, a p_i of 10 MPa, different concrete input parameters like concrete quality, E_{cm} and thickness as well as the Seeber input parameters $p_{v,0}$ and p_v

Tuff 1 – p_i of 10 MPa							
Storage diameter [m]	concrete			Seeber		gap injection material	
	Quality [-]	E_{cm} [GPa]	thickness [m]	$p_{v,0}$ [MPa]	p_v [MPa]	E_{gap} [MPa]	$E_{gap,hardened}$ [MPa]
4	C30/37	33	0.1	7.90	3.12	**0.40**	2000
		33	0.2	9.82	4.52	**0.50**	2000
		33	0.3	10.46	5.19	**0.55**	2000
	C35/45	34	0.1	7.45	3.18	**0.40**	2000
		34	0.2	9.40	4.59	**0.50**	2000
		34	0.3	10.1	5.25	**0.55**	2000
5	C30/37	33	0.1	6.86	2.68	**0.30**	2000
		33	0.2	8.93	4.08	**0.40**	2000
		33	0.3	9.82	4.85	**0.45**	2000
	C35/45	34	0.1	6.47	2.74	**0.30**	2000
		34	0.2	8.54	4.15	**0.40**	2000
		34	0.3	9.47	4.92	**0.45**	2000
6	C30/37	33	0.1	6.06	2.35	**0.20**	2000
		33	0.2	8.16	3.71	**0.30**	2000
		33	0.3	9.19	4.52	**0.35**	2000
	C35/45	34	0.1	5.71	2.41	**0.20**	2000
		34	0.2	7.80	3.77	**0.30**	2000
		34	0.3	8.87	4.59	**0.35**	2000
7	C30/37	33	0.1	5.42	2.09	**0.15**	2000
		33	0.2	7.49	3.39	**0.25**	2000
		33	0.3	8.61	4.22	**0.30**	2000
	C35/45	34	0.1	5.10	2.14	**0.15**	2000
		34	0.2	7.17	3.45	**0.25**	2000
		34	0.3	8.30	4.29	**0.30**	2000

Calibrated value of E_{gap} for Tuff 1, a concrete lining thickness of 0.1 m, 0.2 m and 0.3 m, a diameter of the storage of 3, 4, 5, 6 and 7 m as well as a p_i of 10 MPa

E_{gap} for Tuff 1 and a p_i of 10 MPa			
Storage diameter	**Thickness of the concrete lining**		
	0.1 m	**0.2 m**	**0.3 m**
3 m	0.65 MPa	0.75 MPa	0.60 MPa
4 m	0.40 MPa	0.50 MPa	0.55 MPa
5 m	0.30 MPa	0.40 MPa	0.45 MPa
6 m	0.20 MPa	0.30 MPa	0.35 MPa
7 m	0.15 MPa	0.25 MPa	0.30 MPa

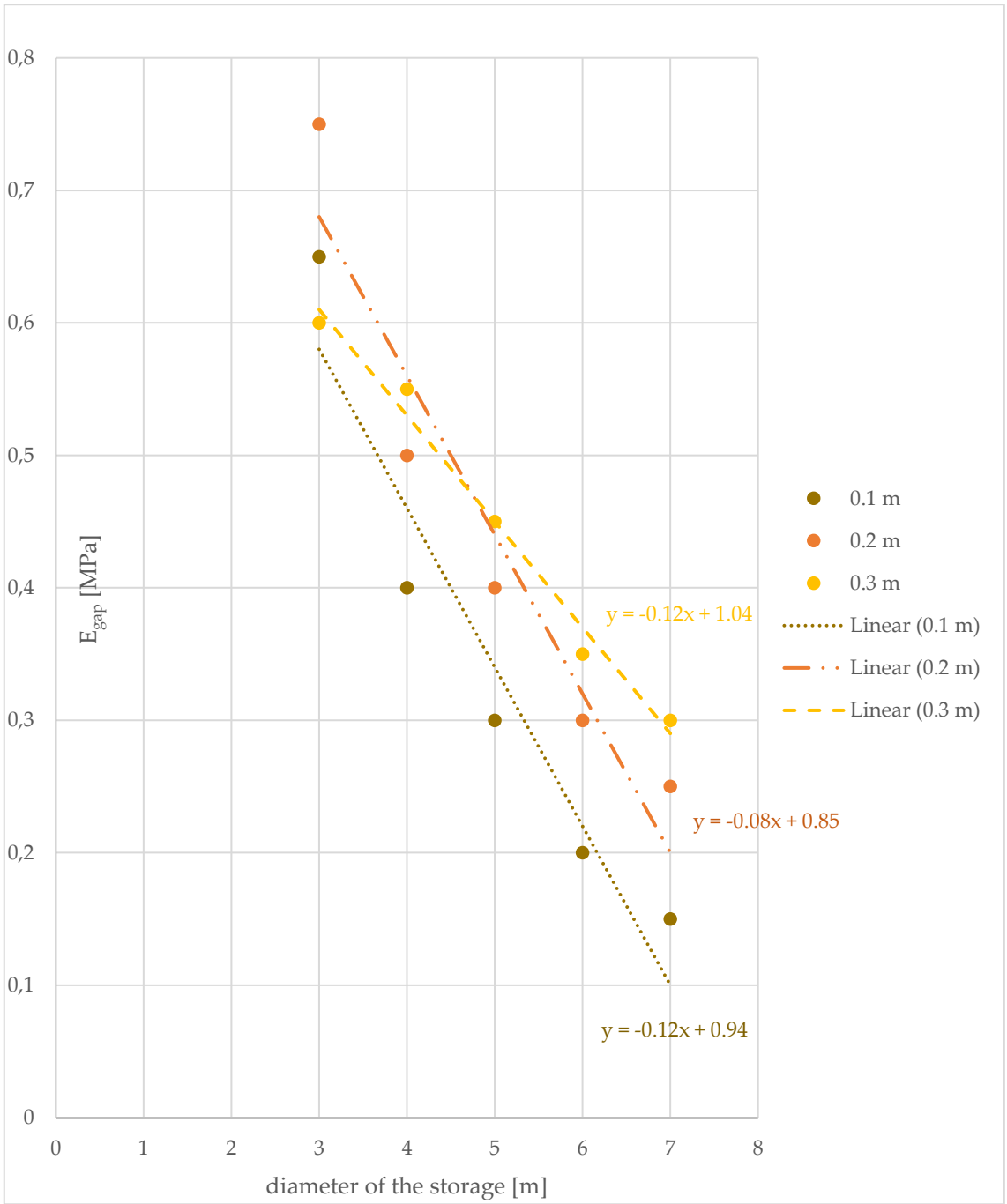

Graphical display of the resulting E_{gap} of the calibration depending on the storage diameter for Tuff 1, a p_i of 10 MPa as well as a lining thickness of 0.1, 0.2 and 0.3 m

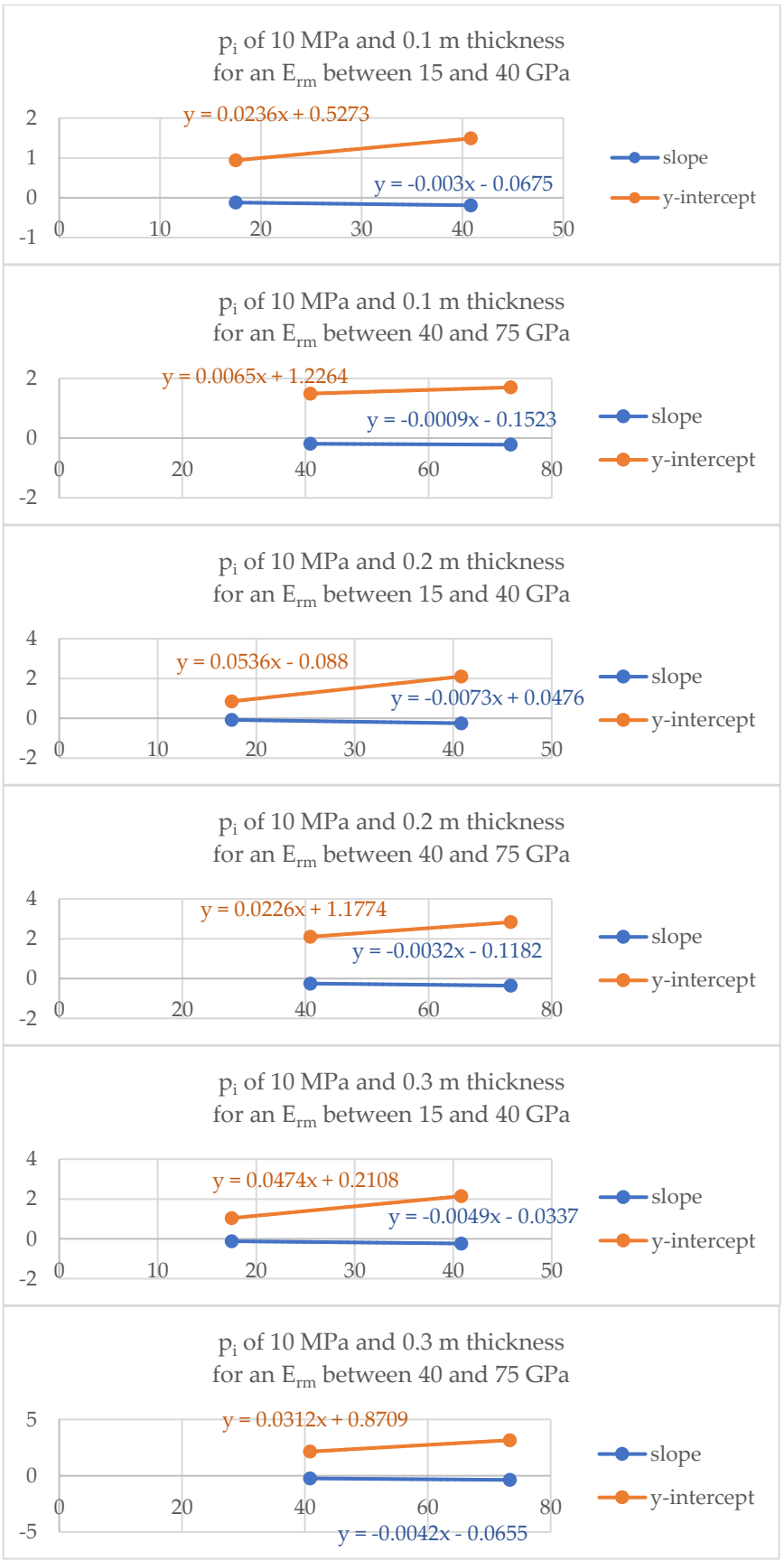

Determined equations to calculate the calibrated slope and y-intercept of the final equation for a p_i of 10 MPa

Appendix C.3 for Chapter 8.1 Calibration of the pre-stressed concrete

Numerical simulation with plastic material behaviour:

State of the pre-stressed concrete lining and surrounding rock mass of a storage built in Ankerit for a p_i of 4 MPa, different concrete qualities and thicknesses of 0.1, 0.2 and 0.3 m

Concrete quality	Lining thickness	State of concrete lining	State of rock mass
C25/30	0.1 m	Model does not reach equilibrium	
	0.2 m	Stable	Stable
	0.3 m	Stable	Stable
C30/37	0.1 m	Model does not reach equilibrium	
	0.2 m	Stable	Stable
	0.3 m	Stable	Stable
C35/45	0.1 m	Model does not reach equilibrium	
	0.2 m	Stable	Stable
	0.3 m	Stable	Stable
C40/50	0.1 m	Model does not reach equilibrium	
	0.2 m	Stable	Stable
	0.3 m	Stable	Stable

State of the pre-stressed concrete lining and surrounding rock mass of a storage built in Ankerit for a p_i of 7 MPa, different concrete qualities and thicknesses of 0.1, 0.2 and 0.3 m

Concrete quality	Lining thickness	State of concrete lining	State of rock mass
C25/30	0.1 m	Model does not reach equilibrium	
	0.2 m	Model does not reach equilibrium	
	0.3 m	Stable	Stable
C30/37	0.1 m	Model does not reach equilibrium	
	0.2 m	Model does not reach equilibrium	
	0.3 m	Stable	Stable
C35/45	0.1 m	Model does not reach equilibrium	
	0.2 m	Model does not reach equilibrium	
	0.3 m	Stable	Stable
C40/50	0.1 m	Model does not reach equilibrium	
	0.2 m	Model does not reach equilibrium	
	0.3 m	Stable	Stable

State of the pre-stressed concrete lining and surrounding rock mass of a storage built in Ankerit for a p_i of 10 MPa, different concrete qualities and thicknesses of 0.1, 0.2 and 0.3 m

Concrete quality	Lining thickness	State of concrete lining	State of rock mass
C25/30	0.1 m	Model does not reach equilibrium	
	0.2 m	Model does not reach equilibrium	
	0.3 m	Stable	Stable
C30/37	0.1 m	Model does not reach equilibrium	
	0.2 m	Model does not reach equilibrium	
	0.3 m	Stable	Stable
C35/45	0.1 m	Model does not reach equilibrium	
	0.2 m	Model does not reach equilibrium	
	0.3 m	Stable	Stable
C40/50	0.1 m	Model does not reach equilibrium	
	0.2 m	Model does not reach equilibrium	
	0.3 m	Stable	Stable

State of the pre-stressed concrete lining and rock mass of a storage built in Sauberger Kalk for a p_i of 4 MPa, different concrete qualities and thicknesses of 0.1, 0.2 and 0.3 m

Concrete quality	Lining thickness	State of concrete lining	State of rock mass
C25/30	0.1 m	Model does not reach equilibrium	
	0.2 m	Stable	Stable
	0.3 m	Stable	Stable
C30/37	0.1 m	Model does not reach equilibrium	
	0.2 m	Stable	Stable
	0.3 m	Stable	Stable
C35/45	0.1 m	Model does not reach equilibrium	
	0.2 m	Stable	Stable
	0.3 m	Stable	Stable
C40/50	0.1 m	Model does not reach equilibrium	
	0.2 m	Stable	Stable
	0.3 m	Stable	Stable

State of the pre-stressed concrete lining and rock mass of a storage built in Sauberger Kalk for a p_i of 7 MPa, different concrete qualities and thicknesses of 0.1, 0.2 and 0.3 m

Concrete quality	Lining thickness	State of concrete lining	State of rock mass
C25/30	0.1 m	Model does not reach equilibrium	
	0.2 m	Failed	Failed
	0.3 m	Stable	Stable
C30/37	0.1 m	Model does not reach equilibrium	
	0.2 m	Stable	Stable
	0.3 m	Stable	Stable
C35/45	0.1 m	Model does not reach equilibrium	
	0.2 m	Stable	Stable
	0.3 m	Stable	Stable
C40/50	0.1 m	Model does not reach equilibrium	
	0.2 m	Stable	Stable
	0.3 m	Stable	Stable

State of the pre-stressed concrete lining and rock mass of a storage built in Sauberger Kalk for a p_i of 10 MPa, different concrete qualities and thicknesses of 0.1, 0.2 and 0.3 m

Concrete quality	Lining thickness	State of concrete lining	State of rock mass
C25/30	0.1 m	Model does not reach equilibrium	
	0.2 m	Failed	Failed
	0.3 m	Failed	Failed
C30/37	0.1 m	Model does not reach equilibrium	
	0.2 m	Failed	Stable
	0.3 m	Stable	Stable
C35/45	0.1 m	Model does not reach equilibrium	
	0.2 m	Stable	Stable
	0.3 m	Stable	Stable
C40/50	0.1 m	Model does not reach equilibrium	
	0.2 m	Stable	Stable
	0.3 m	Stable	Stable

State of the pre-stressed concrete lining and surrounding rock mass of a storage built in Tuff 1 for a p_i of 4 MPa, different concrete qualities and thicknesses of 0.1, 0.2 and 0.3 m

Concrete quality	Lining thickness	State of concrete lining	State of rock mass
C25/30	0.1 m	Model does not reach equilibrium	
	0.2 m	Stable	Stable
	0.3 m	Stable	Stable
C30/37	0.1 m	Model does not reach equilibrium	
	0.2 m	Stable	Stable
	0.3 m	Stable	Stable
C35/45	0.1 m	Stable	Stable
	0.2 m	Stable	Stable
	0.3 m	Stable	Stable
C40/50	0.1 m	Model does not reach equilibrium	
	0.2 m	Model does not reach equilibrium	
	0.3 m	Stable	Stable

State of the pre-stressed concrete lining and surrounding rock mass of a storage built in Tuff 1 for a p_i of 7 MPa, different concrete qualities and thicknesses of 0.1, 0.2 and 0.3 m

Concrete quality	Lining thickness	State of concrete lining	State of rock mass
C25/30	0.1 m	Model does not reach equilibrium	
	0.2 m	Failed	Stable
	0.3 m	Stable	Stable
C30/37	0.1 m	Model does not reach equilibrium	
	0.2 m	Failed	Stable
	0.3 m	Stable	Stable
C35/45	0.1 m	Model does not reach equilibrium	
	0.2 m	Stable	Stable
	0.3 m	Stable	Stable
C40/50	0.1 m	Model does not reach equilibrium	
	0.2 m	Stable	Stable
	0.3 m	Stable	Stable

State of the pre-stressed concrete lining and surrounding rock mass of a storage built in Tuff 1 for a p_i of 10 MPa, different concrete qualities and thicknesses of 0.1, 0.2 and 0.3 m

Concrete quality	Lining thickness	State of concrete lining	State of rock mass
C25/30	0.1 m	Model does not reach equilibrium	
	0.2 m	Failed	Stable
	0.3 m	Failed	Stable
C30/37	0.1 m	Model does not reach equilibrium	
	0.2 m	Failed	Stable
	0.3 m	Model does not reach equilibrium	
C35/45	0.1 m	Model does not reach equilibrium	
	0.2 m	Failed	Stable
	0.3 m	Stable	Stable
C40/50	0.1 m	Model does not reach equilibrium	
	0.2 m	Failed	Stable
	0.3 m	Stable	Stable

State of the pre-stressed concrete lining and surrounding rock mass of a storage built in Tuff 2 for a p_i of 4 MPa, different concrete qualities and thicknesses of 0.1, 0.2 and 0.3 m

Concrete quality	Lining thickness	State of concrete lining	State of rock mass
C25/30	0.1 m	Model does not reach equilibrium	
	0.2 m	Model does not reach equilibrium	
	0.3 m	Model does not reach equilibrium	
C30/37	0.1 m	Stable	Stable
	0.2 m	Stable	Stable
	0.3 m	Stable	Stable
C35/45	0.1 m	Stable	Stable
	0.2 m	Stable	Stable
	0.3 m	Stable	Stable
C40/50	0.1 m	Stable	Stable
	0.2 m	Stable	Stable
	0.3 m	Stable	Stable

State of the pre-stressed concrete lining and surrounding rock mass of a storage built in Tuff 2 for a p_i of 7 MPa, different concrete qualities and thicknesses of 0.1, 0.2 and 0.3 m

Concrete quality	Lining thickness	State of concrete lining	State of rock mass
C25/30	0.1 m	Model does not reach equilibrium	
	0.2 m	Failed	Failed
	0.3 m	Failed	Failed
C30/37	0.1 m	Model does not reach equilibrium	
	0.2 m	Failed	Stable
	0.3 m	Failed	Stable
C35/45	0.1 m	Failed	Failed
	0.2 m	Failed	Failed
	0.3 m	Stable	Stable
C40/50	0.1 m	Failed	Stable
	0.2 m	Failed	Stable
	0.3 m	Stable	Stable

State of the pre-stressed concrete lining and surrounding rock mass of a storage built in Tuff 2 for a p_i of 10 MPa, different concrete qualities and thicknesses of 0.1, 0.2 and 0.3 m

Concrete quality	Lining thickness	State of concrete lining	State of rock mass
C25/30	0.1 m	Failed	Failed
	0.2 m	Failed	Failed
	0.3 m	Failed	Failed
C30/37	0.1 m	Failed	Failed
	0.2 m	Failed	Failed
	0.3 m	Failed	Failed
C35/45	0.1 m	Failed	Failed
	0.2 m	Failed	Failed
	0.3 m	Failed	Failed
C40/50	0.1 m	Failed	Failed
	0.2 m	Failed	Failed
	0.3 m	Failed	Failed

State of the pre-stressed concrete lining and surrounding rock mass of a storage built in Rock mass 1 for a p_i of 4 MPa, different concrete qualities and thicknesses of 0.1, 0.2 and 0.3 m

Concrete quality	Lining thickness	State of concrete lining	State of rock mass
C25/30	0.1 m	Model does not reach equilibrium	
	0.2 m	Model does not reach equilibrium	
	0.3 m	Model does not reach equilibrium	
C30/37	0.1 m	Model does not reach equilibrium	
	0.2 m	Model does not reach equilibrium	
	0.3 m	Stable	Stable
C35/45	0.1 m	Model does not reach equilibrium	
	0.2 m	Model does not reach equilibrium	
	0.3 m	Stable	Stable
C40/50	0.1 m	Model does not reach equilibrium	
	0.2 m	Model does not reach equilibrium	
	0.3 m	Model does not reach equilibrium	

State of the pre-stressed concrete lining and surrounding rock mass of a storage built in Rock mass 1 for a p_i of 7 MPa, different concrete qualities and thicknesses of 0.1, 0.2 and 0.3 m

Concrete quality	Lining thickness	State of concrete lining	State of rock mass
C25/30	0.1 m	Model does not reach equilibrium	
	0.2 m	Model does not reach equilibrium	
	0.3 m	Stable	Stable
C30/37	0.1 m	Model does not reach equilibrium	
	0.2 m	Model does not reach equilibrium	
	0.3 m	Stable	Stable
C35/45	0.1 m	Model does not reach equilibrium	
	0.2 m	Model does not reach equilibrium	
	0.3 m	Stable	Stable
C40/50	0.1 m	Model does not reach equilibrium	
	0.2 m	Model does not reach equilibrium	
	0.3 m	Stable	Stable

State of the pre-stressed concrete lining and surrounding rock mass of a storage built in Rock mass 1 for a p_i of 10 MPa, different concrete qualities and thicknesses of 0.1, 0.2 and 0.3 m

Concrete quality	Lining thickness	State of concrete lining	State of rock mass
C25/30	0.1 m	Model does not reach equilibrium	
	0.2 m	Stable	Stable
	0.3 m	Stable	Stable
C30/37	0.1 m	Model does not reach equilibrium	
	0.2 m	Stable	Stable
	0.3 m	Model does not reach equilibrium	
C35/45	0.1 m	Model does not reach equilibrium	
	0.2 m	Model does not reach equilibrium	
	0.3 m	Stable	Stable
C40/50	0.1 m	Model does not reach equilibrium	
	0.2 m	Model does not reach equilibrium	
	0.3 m	Stable	Stable

State of the pre-stressed concrete lining and surrounding rock mass of a storage built in Rock mass 2 for a p_i of 4 MPa, different concrete qualities and thicknesses of 0.1, 0.2 and 0.3 m

Concrete quality	Lining thickness	State of concrete lining	State of rock mass
C25/30	0.1 m	Model does not reach equilibrium	
	0.2 m	Stable	Stable
	0.3 m	Model does not reach equilibrium	
C30/37	0.1 m	Model does not reach equilibrium	
	0.2 m	Model does not reach equilibrium	
	0.3 m	Stable	Stable
C35/45	0.1 m	Model does not reach equilibrium	
	0.2 m	Stable	Stable
	0.3 m	Model does not reach equilibrium	
C40/50	0.1 m	Model does not reach equilibrium	
	0.2 m	Model does not reach equilibrium	
	0.3 m	Stable	Stable

State of the pre-stressed concrete lining and surrounding rock mass of a storage built in Rock mass 2 for a p_i of 7 MPa, different concrete qualities and thicknesses of 0.1, 0.2 and 0.3 m

Concrete quality	Lining thickness	State of concrete lining	State of rock mass
C25/30	0.1 m	Model does not reach equilibrium	
	0.2 m	Stable	Stable
	0.3 m	Stable	Stable
C30/37	0.1 m	Model does not reach equilibrium	
	0.2 m	Stable	Stable
	0.3 m	Stable	Stable
C35/45	0.1 m	Model does not reach equilibrium	
	0.2 m	Model does not reach equilibrium	
	0.3 m	Stable	Stable
C40/50	0.1 m	Model does not reach equilibrium	
	0.2 m	Model does not reach equilibrium	
	0.3 m	Stable	Stable

State of the pre-stressed concrete lining and surrounding rock mass of a storage built in Rock mass 2 for a p_i of 10 MPa, different concrete qualities and thicknesses of 0.1, 0.2 and 0.3 m

Concrete quality	Lining thickness	State of concrete lining	State of rock mass
C25/30	0.1 m	Model does not reach equilibrium	
	0.2 m	Model does not reach equilibrium	
	0.3 m	Stable	Stable
C30/37	0.1 m	Model does not reach equilibrium	
	0.2 m	Model does not reach equilibrium	
	0.3 m	Stable	Stable
C35/45	0.1 m	Model does not reach equilibrium	
	0.2 m	Model does not reach equilibrium	
	0.3 m	Stable	Stable
C40/50	0.1 m	Model does not reach equilibrium	
	0.2 m	Model does not reach equilibrium	
	0.3 m	Stable	Stable

Appendix D.1 for Chapter 8.2 Comparison of the results from the steel lining:

Minimum steel lining thickness according to Seeber:

Minimum thickness of the steel lining according to the analytical method from Seeber for the rock types Ankerit and Sauberger Kalk as well as for a p_i of 10, 15 and 20 MPa

Ankerit			Sauberger Kalk		
Steel grade	p_i [MPa]	Thickness [mm]	Steel grade	p_i [MPa]	Thickness [mm]
S460	10	Negative	S460	10	13.03
S460	15	Negative	S460	15	33.41
S460	20	2.72	S460	20	53.79
S550	10	Negative	S550	10	6.36
S550	15	Negative	S550	15	23.41
S550	20	Negative	S550	20	40.45
S690	10	Negative	S690	10	Negative
S690	15	Negative	S690	15	13.03
S690	20	Negative	S690	20	26.62

Minimum thickness of the steel lining according to the analytical method from Seeber for the rock types Rock mass 1 and Rock mass 2 as well as for a p_i of 10, 15 and 20 MPa

Rock mass 1			Rock mass 2		
Steel grade	p_i [MPa]	Thickness [mm]	Steel grade	p_i [MPa]	Thickness [mm]
S460	10	Negative	S460	10	3.05
S460	15	12.16	S460	15	23.43
S460	20	32.54	S460	20	43.81
S550	10	Negative	S550	10	Negative
S550	15	2.16	S550	15	13.42
S550	20	19.2	S550	20	30.47
S690	10	Negative	S690	10	Negative
S690	15	Negative	S690	15	3.05
S690	20	5.37	S690	20	16.63

Minimum thickness of the steel lining according to the analytical method from Seeber for the rock types Tuff 1 and Tuff 2 as well as for a p_i of 10, 15 and 20 MPa

Tuff 1			Tuff 2		
Steel grade	p_i [MPa]	Thickness [mm]	Steel grade	p_i [MPa]	Thickness [mm]
S460	10	15.76	S460	10	29.33
S460	15	36.14	S460	15	49.71
S460	20	56.52	S460	20	70.09
S550	10	9.09	S550	10	22.66
S550	15	26.14	S550	15	39.71
S550	20	43.18	S550	20	56.75
S690	10	2.17	S690	10	15.75
S690	15	15.76	S690	15	29.33
S690	20	29.35	S690	20	42.92

Determined strain of the steel lining with the numerical simulation:

Calculated strain of the steel lining from the numerical simulation for Ankerit, a p_i of 10, 15 and 20 MPa as well as steel grades S460, S550 and S690

Strain of the steel lining for Ankerit - elastic material behaviour									
Steel grade	S690			S550			S460		
p_i [MPa]	10	15	20	10	15	20	10	15	20
radial displacement [mm]	No steel lining needed			No steel lining needed			No steel lining needed		0.48
New circumference [m]									9.431
Old circumference [m]									9.425
ε_{steel} [‰]									0.64
ε_{zul} [‰]	**2.63**	**2.63**	**2.63**	**2.1**	**2.1**	**2.1**	**1.75**	**1.75**	**1.75**

Calculated strain of the steel lining from the numerical simulation for Sauberger Kalk, a p_i of 10, 15 and 20 MPa as well as steel grades S460, S550 and S690

Strain of the steel lining for Sauberger Kalk - elastic material behaviour									
Steel grade	S690			S550			S460		
p_i [MPa]	10	15	20	10	15	20	10	15	20
radial displacement [mm]	0.74	1.01	1.23	0.71	0.94	1.13	0.67	0.89	1.05
new circumference [m]	9.434	9.437	9.440	9.434	9.437	9.439	9.433	9.436	9.438
old circumference [m]	9.425	9.425	9.425	9.425	9.425	9.425	9.425	9.425	9.425
ε_{steel} [‰]	0.99	1.35	1.64	0.94	1.26	1.51	0.9	1.18	1.4
ε_{zul} [‰]	**2.63**	**2.63**	**2.63**	**2.1**	**2.1**	**2.1**	**1.75**	**1.75**	**1.75**

Calculated strain of the steel lining from the numerical simulation for Tuff 1, a p_i of 10, 15 and 20 MPa as well as steel grades S460, S550 and S690

Strain of the steel lining for Tuff 1 - elastic material behaviour									
Steel grade	S690			S550			S460		
p_i [MPa]	10	15	20	10	15	20	10	15	20
radial displacement [mm]	1.0	1.3	1.5	0.9	1.2	1.5	0.9	1.1	1.3
new circumference [m]	9.437	9.441	9.444	9.436	9.439	9.444	9.435	9.438	9.441
old circumference [m]	9.425	9.425	9.425	9.425	9.425	9.425	9.425	9.425	9.425
ε_{steel} [‰]	1.29	1.70	2.03	1.21	1.56	2.03	1.14	1.45	1.68
ε_{zul} [‰]	**2.63**	**2.63**	**2.63**	**2.1**	**2.1**	**2.1**	**1.75**	**1.75**	**1.75**

Calculated strain of the steel lining from the numerical simulation for Tuff 2, a p_i of 10, 15 and 20 MPa as well as steel grades S460, S550 and S690

Strain of the steel lining for Tuff 2 – elastic material behaviour									
Steel grade	S690			S550			S460		
p_i [MPa]	10	15	20	10	15	20	10	15	20
radial displacement [mm]	1.60	1.96	2.22	1.44	1.72	1.92	1.31	1.54	1.69
New circumference [m]	9.445	9.449	9.453	9.443	9.446	9.449	9.441	9.444	9.446
Old circumference [m]	9.425	9.425	9.425	9.425	9.425	9.425	9.425	9.425	9.425
ε_{steel} [‰]	2.13	2.62	2.96	1.92	2.30	2.55	1.75	2.06	2.26
ε_{zul} [‰]	**2.63**	**2.63**	**2.63**	**2.1**	**2.1**	**2.1**	**1.75**	**1.75**	**1.75**

Calculated strain of the steel lining from the numerical simulation for Rock mass 1, a p_i of 10, 15 and 20 MPa as well as steel grades S460, S550 and S690

Strain of the steel lining for Rock mass 1 – elastic material behaviour									
Steel grade	S690			S550			S460		
p_i [MPa]	10	15	20	10	15	20	10	15	20
radial displacement [mm]	No steel lining needed		0.83	no lining	0.63	1.04	no lining	0.60	0.74
new circumference [m]			9.435		9.433	9.435		9.432	9.434
Old circumference [m]			9.425		9.425	9.425		9.425	9.425
ε_{steel} [‰]			1.10		0.84	1.04		0.80	0.99
ε_{zul} [‰]	**2.63**	**2.63**	**2.63**	**2.1**	**2.1**	**2.1**	**1.75**	**1.75**	**1.75**

Calculated strain of the steel lining from the numerical simulation for Rock mass 2, a p_i of 10, 15 and 20 MPa as well as steel grades S460, S550 and S690

Strain of the steel lining for Rock mass 2 – elastic material behaviour									
Steel grade	S690			S550			S460		
p_i [MPa]	10	15	20	10	15	20	10	15	20
radial displacement [mm]	no lining	0.77	0.96	no lining	0.73	0.90	0.52	0.70	0.85
New circumference [m]		9.434	9.437		9.434	9.436	9.431	9.434	9.435
Old circumference [m]		9.425	9.425		9.425	9.425	9.425	9.425	9.425
ε_{steel} [‰]		1.03	1.28		0.98	1.20	0.69	0.93	1.13
ε_{zul} [‰]	**2.63**	**2.63**	**2.63**	**2.1**	**2.1**	**2.1**	**1.75**	**1.75**	**1.75**

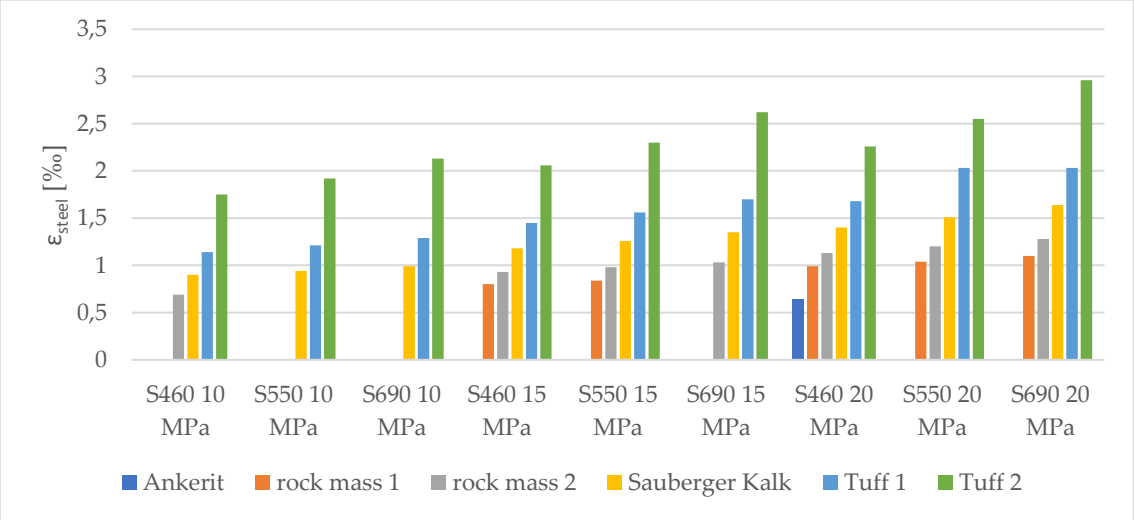

Strain of the steel lining for every rock type and steel grade with a p_i of 10, 15 and 20 MPa and elastic rock mass behaviour

Appendix D.2 for Chapter 8.2 Comparison of the results from the steel lining: Tangential strain of the unlined storage boundary

Calculated tangential strain of the unlined storage boundary from the numerical simulation for Ankerit as well as for a p_i of 10, 15 and 20 MPa

p_i [MPa]	10	15	20
Radial displacement [mm]	0.24	0.36	0.48
Increase of circumference [m]	0.003	0.005	0.006
Tangential strain [‰]	0.32	0.48	0.64

Calculated tangential strain of the unlined storage boundary from the numerical simulation for Sauberger Kalk as well as for a p_i of 10, 15 and 20 MPa

p_i [MPa]	10	15	20
Radial displacement [mm]	0.76	1.15	1.53
Increase of circumference [m]	0.01	0.014	0.019
Tangential strain [‰]	1.02	1.53	2.04

Calculated tangential strain of the unlined storage boundary from the numerical simulation for Tuff 1 as well as for a p_i of 10, 15 and 20 MPa

p_i [MPa]	10	15	20
Radial displacement [mm]	1.02	1.52	2.03
Increase of circumference [m]	0.013	0.019	0.026
Tangential strain [‰]	1.36	2.03	2.71

Calculated tangential strain of the unlined storage boundary from the numerical simulation for Tuff 2 as well as for a p_i of 10, 15 and 20 MPa

p_i [MPa]	10	15	20
Radial displacement [mm]	2.22	3.33	4.44
Increase of circumference [m]	0.028	0.042	0.056
Tangential strain [‰]	2.96	4.44	5.92

Calculated tangential strain of the unlined storage boundary from the numerical simulation for Rock mass 1 as well as for a p_i of 10, 15 and 20 MPa

p_i [MPa]	10	15	20
Radial displacement [mm]	0.43	0.65	0.86
Increase of circumference [m]	0.005	0.008	0.011
Tangential strain [‰]	0.58	0.86	1.15

Calculated tangential strain of the unlined storage boundary from the numerical simulation for Rock mass 2 as well as for a p_i of 10, 15 and 20 MPa

p_i [MPa]	10	15	20
Radial displacement [mm]	0.54	0.80	1.07
Increase of circumference [m]	0.007	0.010	0.013
Tangential strain [‰]	0.71	1.07	1.43

Appendix D.3 for Chapter 8.2 Comparison of the results from the steel lining:

Comparison of the tangential strain of the unlined with steel lined storage boundary:

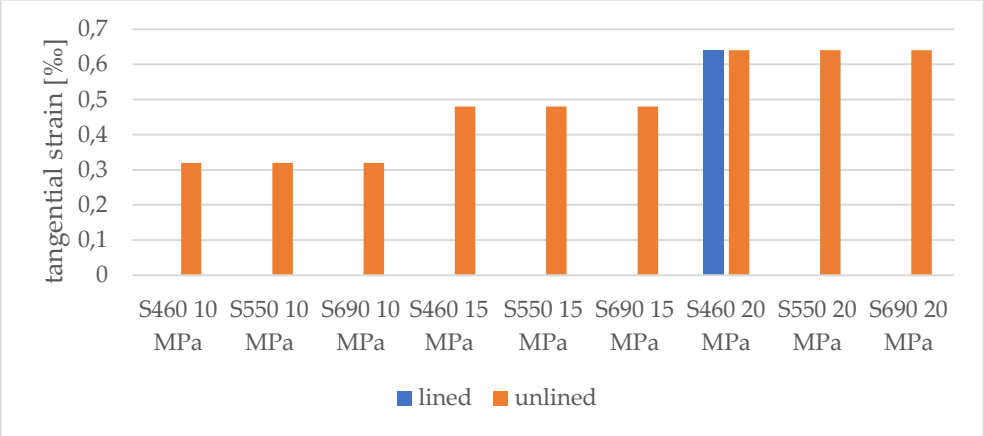

Comparison of the tangential strain from the unlined and lined storage boundary for Ankerit, a p_i of 10, 15 and 20 MPa and different high-strength steel grades

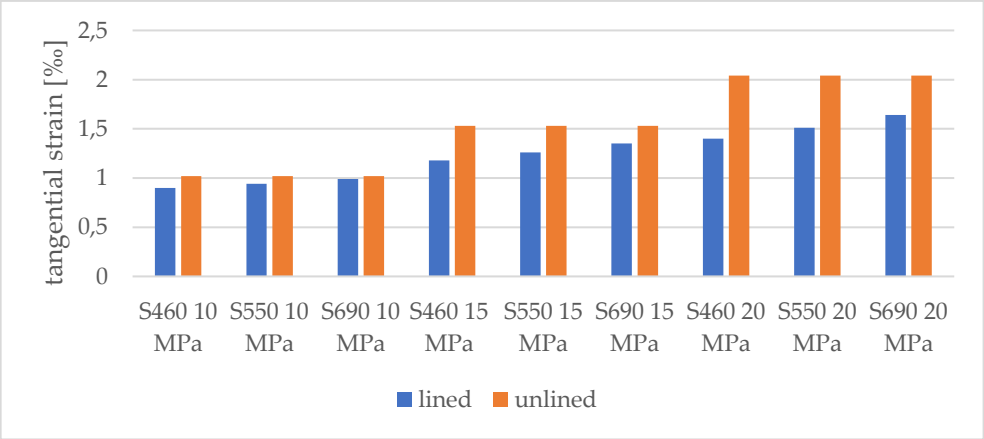

Comparison of the tangential strain from the unlined and lined storage boundary for Sauberger Kalk, a p_i of 10, 15 and 20 MPa and different high-strength steel grades

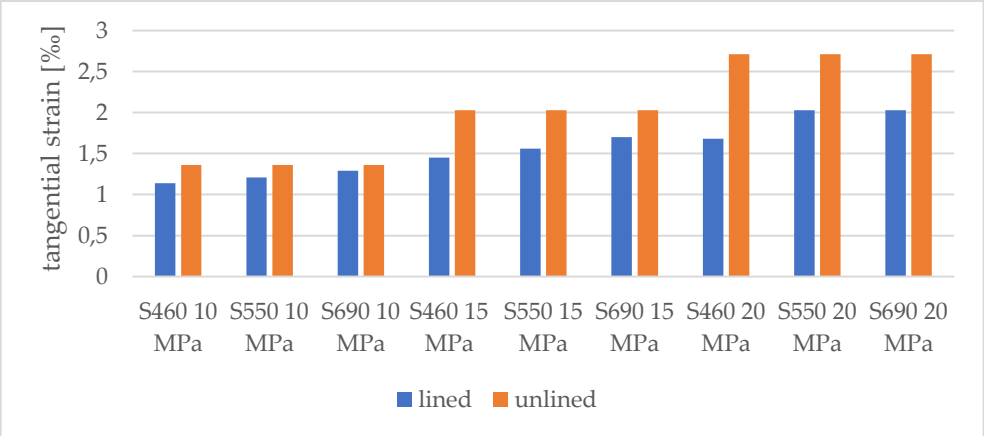

Comparison of the tangential strain from the unlined and lined storage boundary for Tuff 1, a p_i of 10, 15 and 20 MPa and different high-strength steel grades

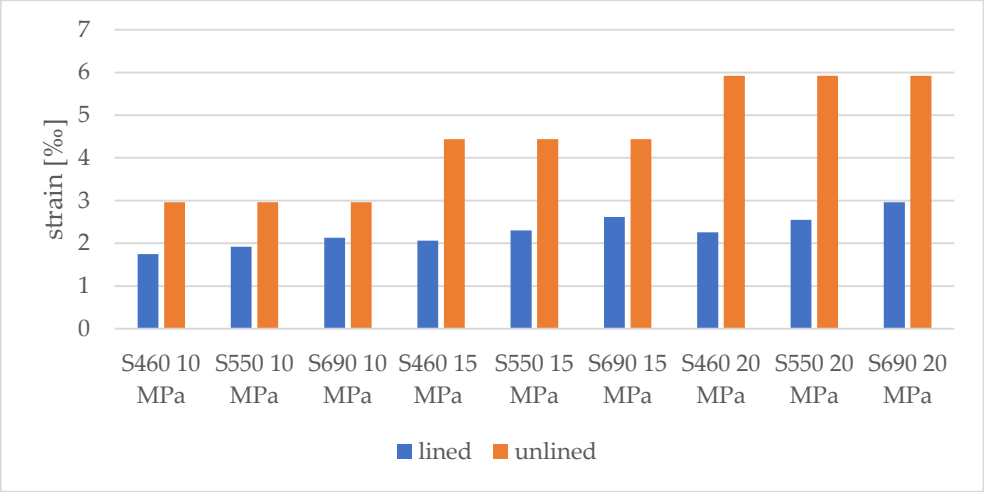

Comparison of the tangential strain from the unlined and lined storage boundary for Tuff 2, a p_i of 10, 15 and 20 MPa and different high-strength steel grades

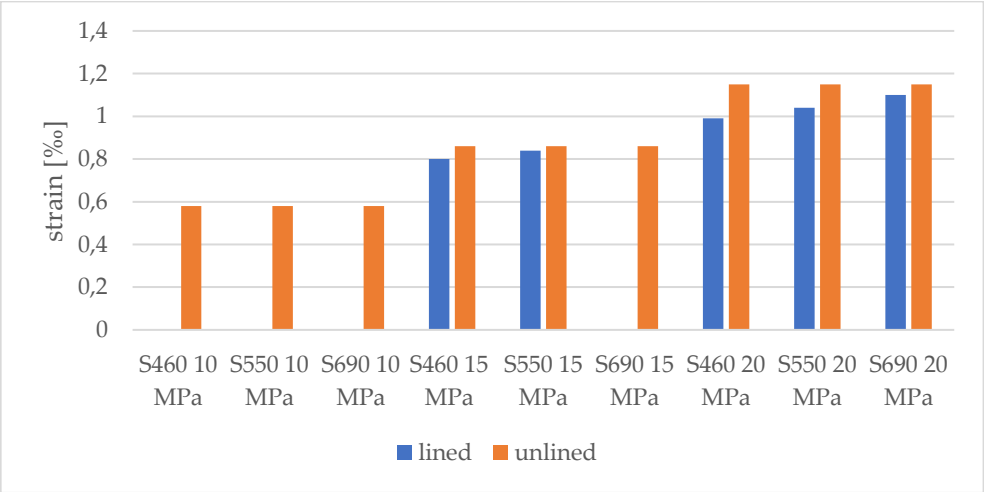

Comparison of the tangential strain from the unlined and lined storage boundary for Rock mass 1, a p_i of 10, 15 and 20 MPa and different high-strength steel grades

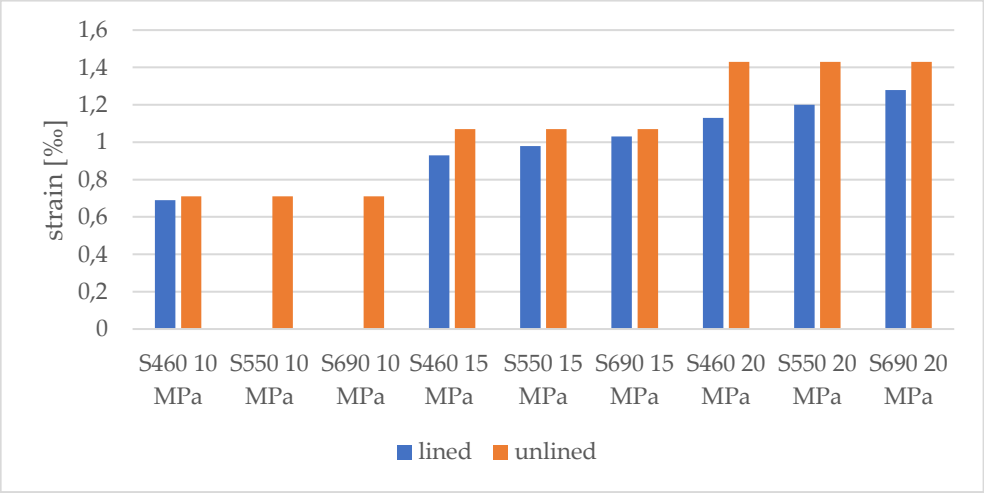

Comparison of the tangential strain from the unlined and lined storage boundary for Rock mass 2, a p_i of 10, 15 and 20 MPa and different high-strength steel grades

Appendix D.4 for Chapter 8.2 Comparison of the results from the steel lining: Comparison of ε_{steel} between an elastic and plastic material behaviour

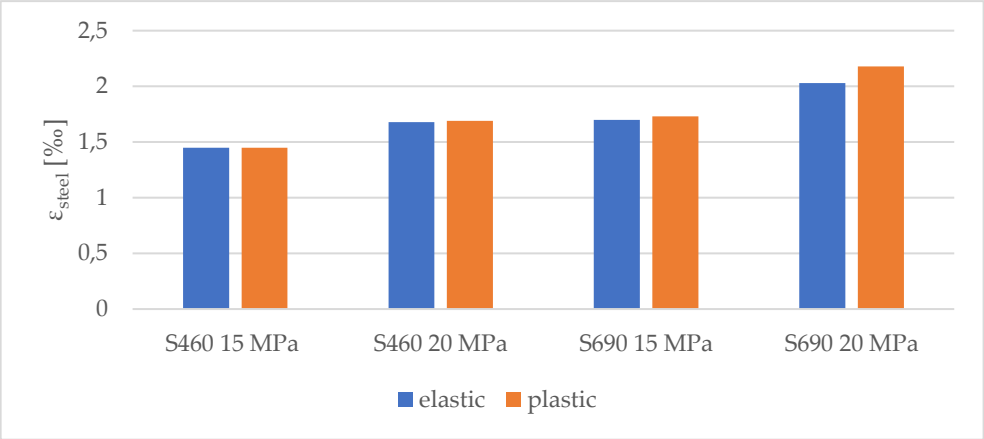

Comparison of the strain of the steel lining for elastic and plastic rock mass behaviour for Tuff 1, a p_i of 15 and 20 MPa and different high-strength steel grades

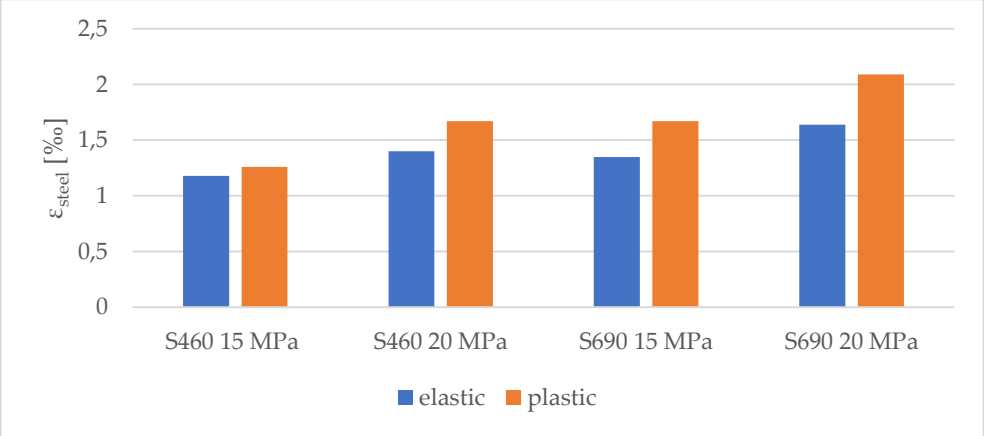

Comparison of the strain of the steel lining for elastic and plastic rock mass behaviour for Sauberger Kalk, a p_i of 15 and 20 MPa and different high-strength steel grades

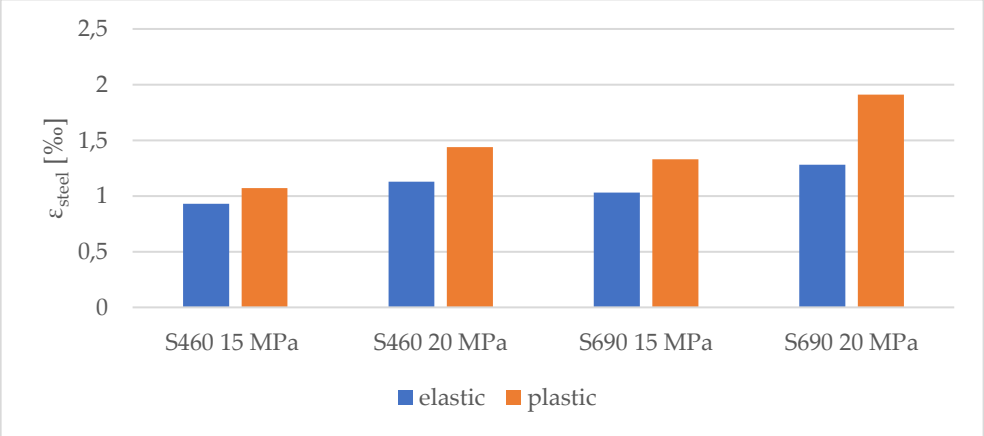

Comparison of the strain of the steel lining for elastic and plastic rock mass behaviour for Rock mass 2, a p_i of 15 and 20 MPa and different high-strength steel grades

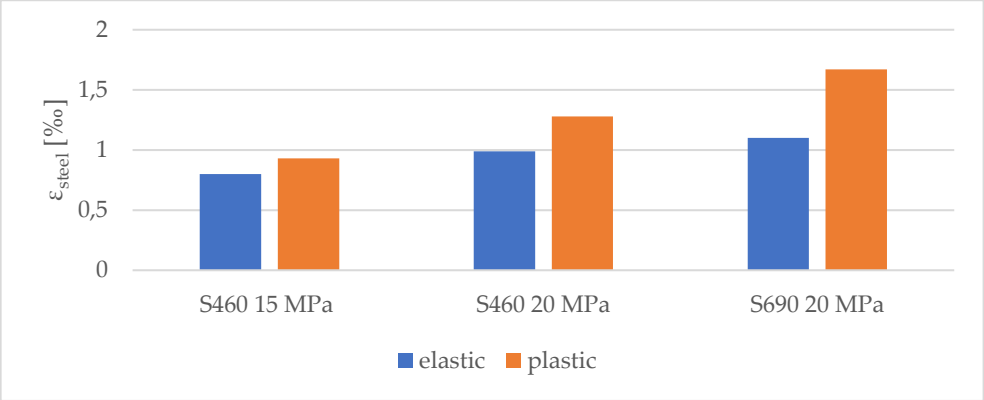

Comparison of the strain of the steel lining for elastic and plastic rock mass behaviour for Rock mass 1, a p_i of 15 and 20 MPa and different high-strength steel grades

Appendix E for Chapter 8.3 Gap injection influence on the surrounding rock mass:

Comparison of the maximum radial displacement for different in-situ stresses:

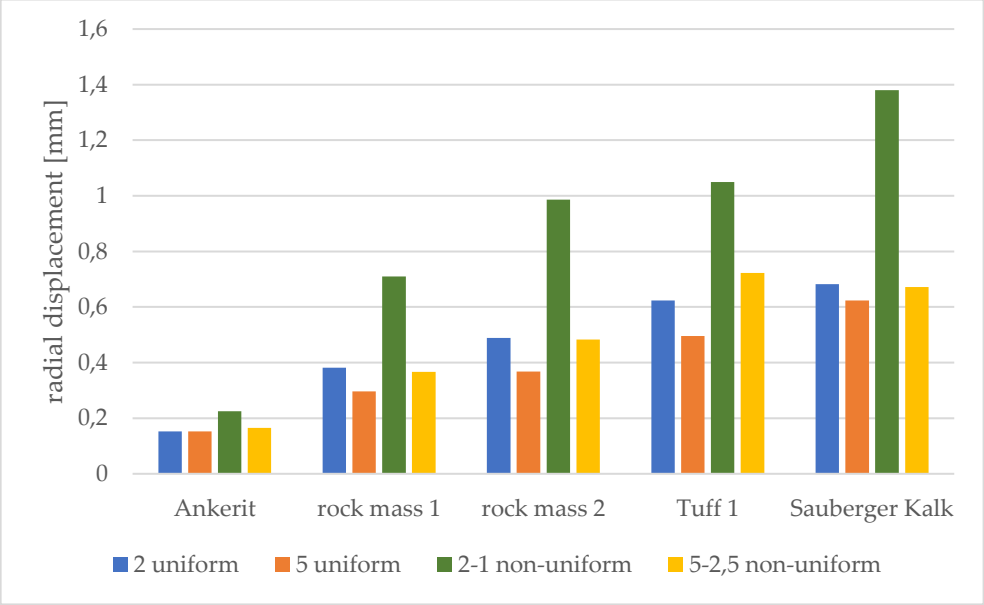

Comparison of the maximum radial displacement of the storage boundary for different uniform and non-uniform in-situ stress conditions caused by the maximum $p_{v,0}$ according to Seeber for a pre-stressed concrete lining and a p_i of 4 Mpa

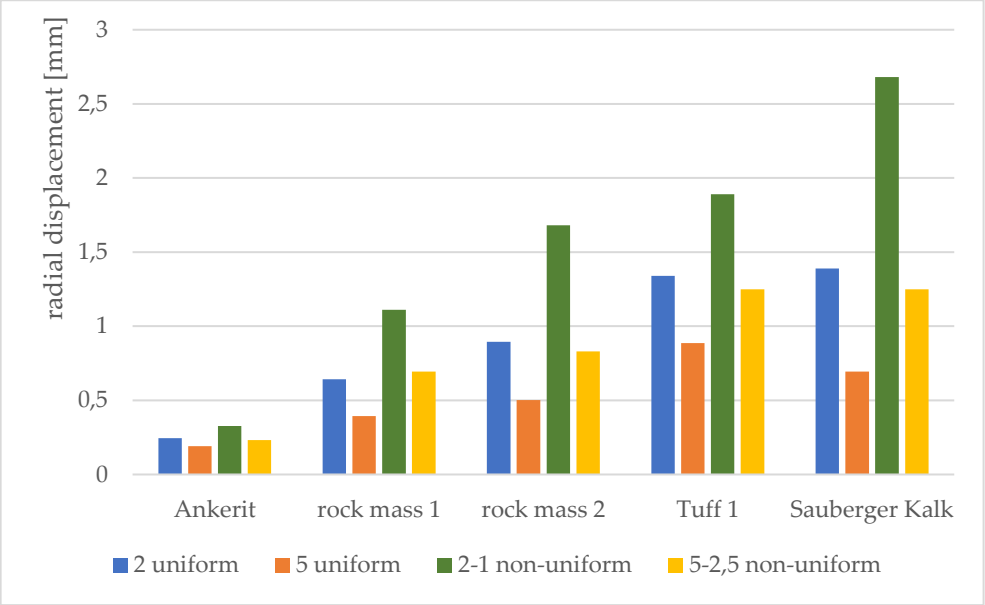

Comparison of the maximum radial displacement of the storage boundary for different uniform and non-uniform in-situ stress conditions caused by the maximum $p_{v,0}$ according to Seeber for a pre-stressed concrete lining and a p_i of 7 MPa

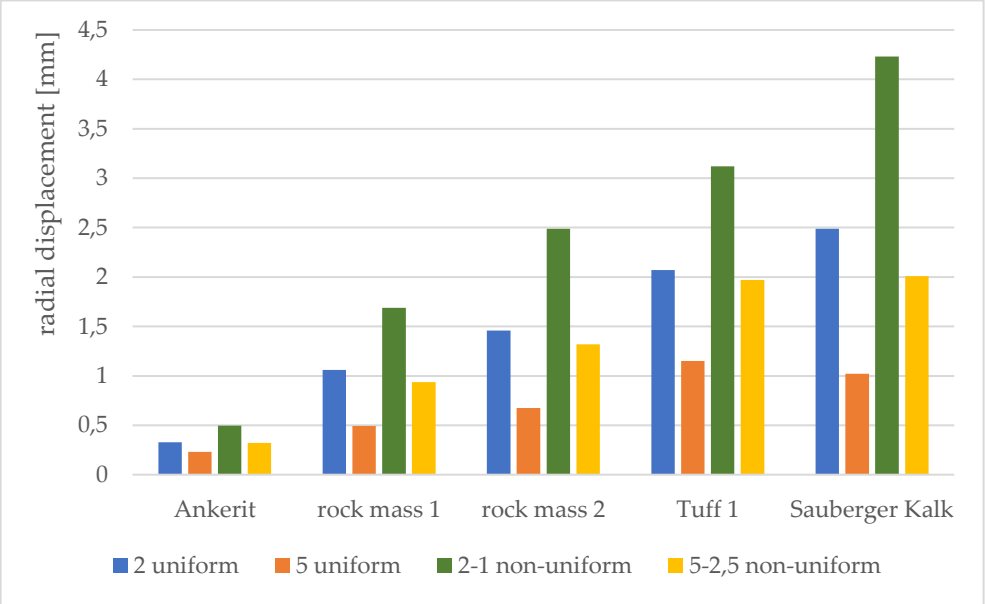

Comparison of the maximum radial displacement of the storage boundary for different uniform and non-uniform in-situ stress conditions caused by the maximum $p_{v,0}$ according to Seeber for a pre-stressed concrete lining and a p_i of 10 MPa

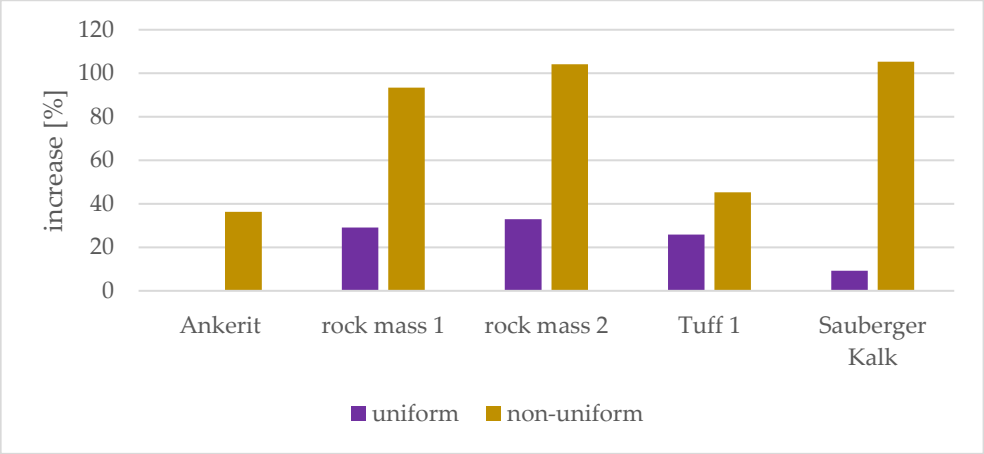

Comparison of the increase of the radial displacement of the storage boundary between uniform and non-uniform in-situ stress conditions for each rock type caused by the maximum $p_{v,0}$ according to Seeber for a pre-stressed concrete lining and a p_i of 4 Mpa

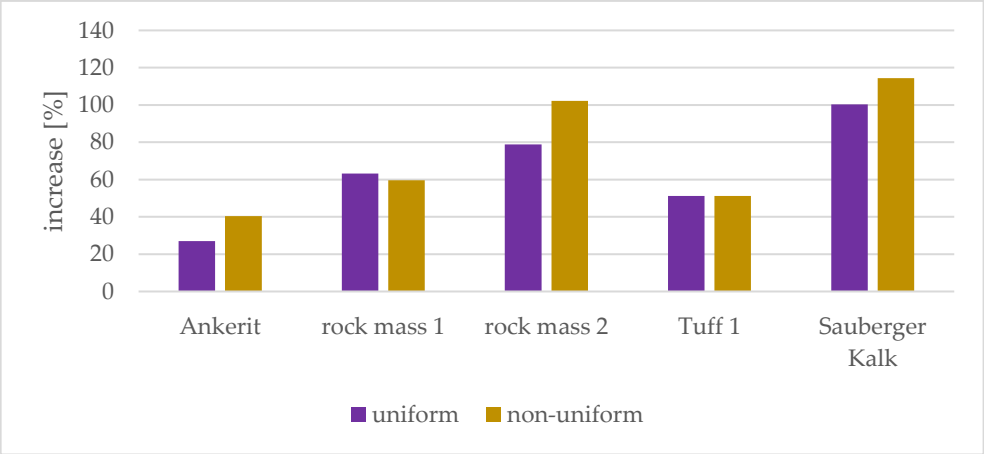

Comparison of the increase of the radial displacement of the storage boundary between uniform and non-uniform in-situ stress conditions for each rock type caused by the maximum $p_{v,0}$ according to Seeber for a pre-stressed concrete lining and a p_i of 7 Mpa

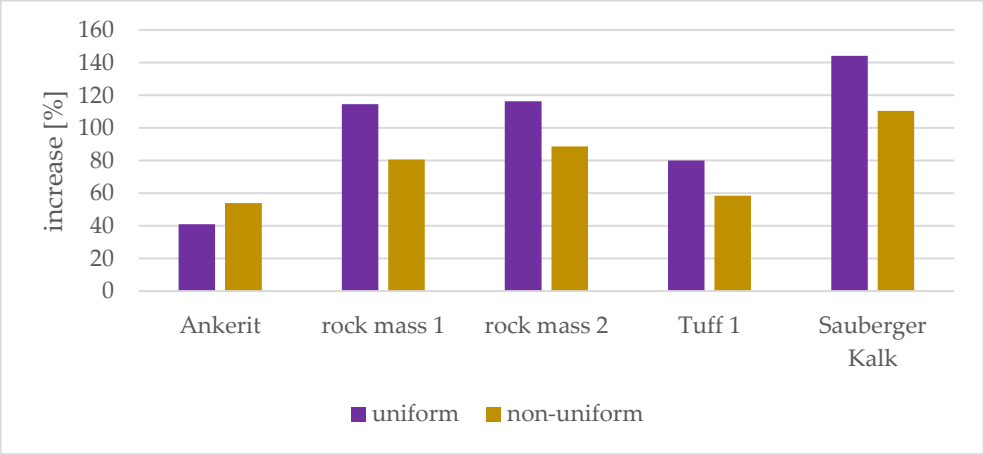

Comparison of the increase of the radial displacement of the storage boundary between uniform and non-uniform in-situ stress conditions for each rock type caused by the maximum $p_{v,0}$ according to Seeber for a pre-stressed concrete lining and a p_i of 10 MPa

Appendix F for Chapter 8.4.1 In-situ stress influence on the pre-stressed concrete lining:

Resulting maximum radial displacement and lowest value of induced σ_3 in the surrounding rock mass for Ankerit, a p_i of 4 MPa and different magnitudes of in-situ stress

Ankerit – p_i of 4 MPa							
In-situ stress [MPa]	5 uniform	10-5	8-4	6-3	5-2.5	4-2	2-1
σ_3 [MPa]	1.43	0.53	0.35	-0.75	-1.28	-1.81	-2.37
max. displacement [mm]	0.0968	0.0983	0.0977	0.0971	0.0969	0.0967	0.104

Resulting maximum radial displacement and lowest value of induced σ_3 in the surrounding rock mass for Sauberger Kalk, a p_i of 4 MPa and different magnitudes of in-situ stress

Sauberger Kalk – p_i of 4 MPa							
In-situ stress [MPa]	5 uniform	10-5	8-4	6-3	5-2.5	4-2	2-1
σ_3 [MPa]	1.43	0.09	0.26	-0.36	-0.34	-0.35	-0.9
max. displacement [mm]	0.297	0.324	0.32	0.3	0.302	0.311	0.513

Resulting maximum radial displacement and lowest value of induced σ_3 in the surrounding rock mass for Rock mass 1, a p_i of 4 MPa and different magnitudes of in-situ stress

Rock mass 1 – p_i of 4 MPa							
In-situ stress [MPa]	5 uniform	10-5	8-4	6-3	5-2.5	4-2	2-1
σ_3 [MPa]	1.42	0.54	0.33	-0.77	-1.14	-1.07	-4.78
max. displacement [mm]	0.178	0.181	0.18	0.179	0.179	0.182	0.225

Resulting maximum radial displacement and lowest value of induced σ_3 in the surrounding rock mass for Rock mass 2, a p_i of 4 MPa and different magnitudes of in-situ stress

Rock mass 2 – p_i of 4 MPa							
In-situ stress [MPa]	5 uniform	10-5	8-4	6-3	5-2.5	4-2	2-1
σ_3 [MPa]	1.42	0.54	0.19	-0.58	-0.61	-0.62	-2.95
max. displacement [mm]	0.22	0.241	0.233	0.221	0.223	0.228	0.338

Resulting maximum radial displacement and lowest value of induced σ_3 in the surrounding rock mass for Tuff 1, a p_i of 4 MPa and different magnitudes of in-situ stress

Tuff 1 – p_i of 4 MPa							
In-situ stress [MPa]	5 uniform	10-5	8-4	6-3	5-2.5	4-2	2-1
σ_3 [MPa]	1.43	1.58	0.38	-0.75	-1.3	-0.27	-2.26
max. displacement [mm]	0.386	0.392	0.391	0.392	0.393	0.833	0.415

Resulting maximum radial displacement and lowest value of induced σ_3 in the surrounding rock mass for Tuff 2, a p_i of 4 MPa and different magnitudes of in-situ stress

Tuff 2– p_i of 4 MPa							
In-situ stress [MPa]	5 uniform	10-5	8-4	6-3	5-2.5	4-2	2-1
σ_3 [MPa]	1.43	0.53	0.3	-0.27	-0.3	-0.29	-0.27
max. displacement [mm]	0.829	0.817	0.822	0.833	0.844	0.869	1.48

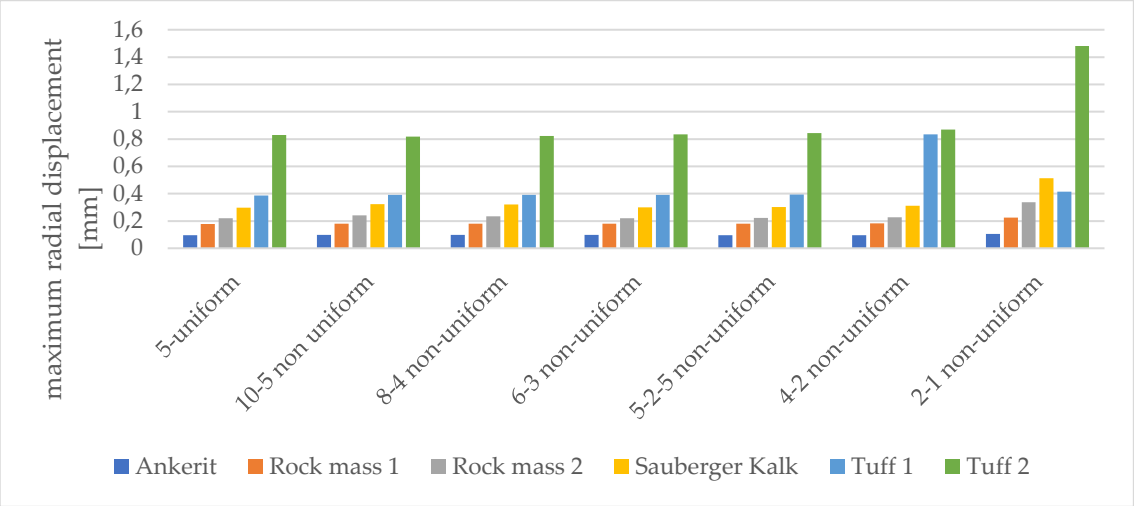

Maximum radial displacements of the storage boundary constructed with a pre-stressed concrete lining for every rock type, a p_i of 4 MPa and different in-situ stress magnitudes

Resulting maximum radial displacement and lowest value of induced σ_3 in the surrounding rock mass for Ankerit, a p_i of 7 MPa and different magnitudes of in-situ stress

Ankerit – p_i of 7 MPa							
In-situ stress [MPa]	5 uniform	10-5	8-4	6-3	5-2.5	4-2	2-1
σ_3 [MPa]	1.43	-1.56	-2.64	-2.19	-2.8	-2.78	-3.62
max. displacement [mm]	0.169	0.17	0.17	0.18	0.191	0.196	0.24

Resulting maximum radial displacement and lowest value of induced σ_3 in the surrounding rock mass for Sauberger Kalk, a p_i of 7 MPa and different magnitudes of in-situ stress

Sauberger Kalk – p_i of 7 MPa							
In-situ stress [MPa]	5 uniform	10-5	8-4	6-3	5-2.5	4-2	2-1
σ_3 [MPa]	1.43	-0.29	-0.3	-0.29	-0.27	-2.71	-9.62
max. displacement [mm]	0.523	0.571	0.565	0.623	0.726	0.959	1.87

Resulting maximum radial displacement and lowest value of induced σ_3 in the surrounding rock mass for Rock mass 1, a p_i of 7 MPa and different magnitudes of in-situ stress

Rock mass 1 – p_i of 7 MPa							
In-situ stress [MPa]	5 uniform	10-5	8-4	6-3	5-2.5	4-2	2-1
σ_3 [MPa]	1.43	-1.04	-1.01	-0.94	-1.08	-1.31	-3.1
max. displacement [mm]	0.314	0.315	0.321	0.347	0.395	0.471	0.684

Resulting maximum radial displacement and lowest value of induced σ_3 in the surrounding rock mass for Rock mass 2, a p_i of 7 MPa and different magnitudes of in-situ stress

Rock mass 2 – p_i of 7 MPa							
In-situ stress [MPa]	5 uniform	10-5	8-4	6-3	5-2.5	4-2	2-1
σ_3 [MPa]	1.43	-0.47	-0.51	-0.54	-0.67	-1.41	-4.39
max. displacement [mm]	0.388	0.424	0.421	0.443	0.496	0.635	1.09

Resulting maximum radial displacement and lowest value of induced σ_3 in the surrounding rock mass for Tuff 1, a p_i of 7 MPa and different magnitudes of in-situ stress

Tuff 1 – p_i of 7 MPa							
In-situ stress [MPa]	5 uniform	10-5	8-4	6-3	5-2.5	4-2	2-1
σ_3 [MPa]	1.43	-1.54	-2.17	-2.02	-2.88	-4.72	-7.99
max. displacement [mm]	0.684	0.685	0.688	0.705	0.761	0.818	1.16

Resulting maximum radial displacement and lowest value of induced σ_3 in the surrounding rock mass for Tuff 2, a p_i of 7 MPa and different magnitudes of in-situ stress

Tuff 2– p_i of 7 MPa							
In-situ stress [MPa]	5 uniform	10-5	8-4	6-3	5-2.5	4-2	2-1
σ_3 [MPa]	1.43	-0.22	-0.16	-0.35	-0.28	-4.32	-12.8
max. displacement [mm]	1.5	1.5	1.55	1.78	2.02	2.68	5.41

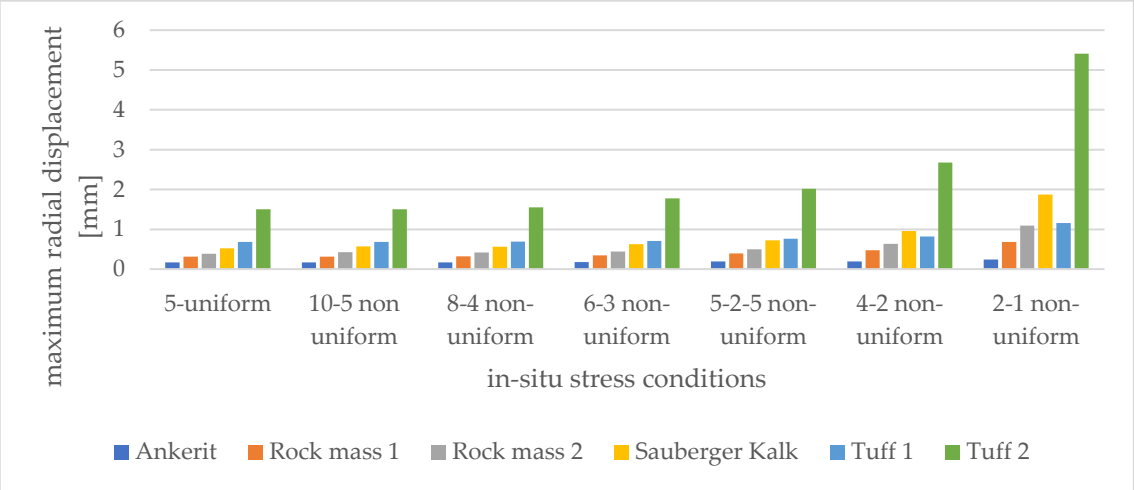

Maximum radial displacements of the storage boundary constructed with a pre-stressed concrete lining for every rock type, a p_i of 7 MPa and different in-situ stress magnitudes

Resulting maximum radial displacement and lowest value of induced σ_3 in the surrounding rock mass for Ankerit, a p_i of 10 MPa and different magnitudes of in-situ stress

Ankerit – p_i of 10 MPa							
In-situ stress [MPa]	5 uniform	10-5	8-4	6-3	5-2.5	4-2	2-1
σ_3 [MPa]	-0,01	-2,55	-2,98	-2,94	-5,27	-3,91	-10,46
max. displacement [mm]	0,243	0,254	0,274	0,32	0,377	0,384	0,536

Resulting maximum radial displacement and lowest value of induced σ_3 in the surrounding rock mass for Sauberger Kalk, a p_i of 10 MPa and different magnitudes of in-situ stress

Sauberger Kalk – p_i of 10 MPa							
In-situ stress [MPa]	5 uniform	10-5	8-4	6-3	5-2.5	4-2	2-1
σ_3 [MPa]	-0.1	-0.15	-0.14	-4.34	-5.28	-7.22	-9.61
max. displacement [mm]	0.757	0.861	0.994	1.31	1.54	2.05	3.28

Resulting maximum radial displacement and lowest value of induced σ_3 in the surrounding rock mass for Rock mass 1, a p_i of 10 MPa and different magnitudes of in-situ stress

Rock mass 1 – p_i of 10 MPa							
In-situ stress [MPa]	5 uniform	10-5	8-4	6-3	5-2.5	4-2	2-1
σ_3 [MPa]	-0.01	-0.73	-0.83	-0.96	-3.19	-3.31	-4.17
max. displacement [mm]	0.45	0.483	0.565	0.67	0.791	0.944	1.46

Resulting maximum radial displacement and lowest value of induced σ_3 in the surrounding rock mass for Rock mass 2, a p_i of 10 MPa and different magnitudes of in-situ stress

Rock mass 2 – p_i of 10 MPa							
In-situ stress [MPa]	5 uniform	10-5	8-4	6-3	5-2.5	4-2	2-1
σ_3 [MPa]	0.01	-0.32	-0.29	-1.78	-3.28	-4.03	not
max. displacement [mm]	0.553	0.626	0.705	0.93	1.09	1.37	stable

Resulting maximum radial displacement and lowest value of induced σ_3 in the surrounding rock mass for Tuff 1, a p_i of 10 MPa and different magnitudes of in-situ stress

Tuff 1 – p_i of 10 MPa							
In-situ stress [MPa]	5 uniform	10-5	8-4	6-3	5-2.5	4-2	2-1
σ_3 [MPa]	0.09	-1.75	-2	not	not	not	not
max. displacement [mm]	1.7	1.74	1.72	stable	stable	stable	stable

Resulting maximum radial displacement and lowest value of induced σ_3 in the surrounding rock mass for Tuff 2, a p_i of 10 MPa and different magnitudes of in-situ stress

Tuff 2– p_i of 10 MPa							
In-situ stress [MPa]	5 uniform	10-5	8-4	6-3	5-2.5	4-2	2-1
σ_3 [MPa]	-0.48	-1.51	-5.26	not	not	not	not
max. displacement [mm]	7.44	7.59	7.45	stable	stable	stable	stable

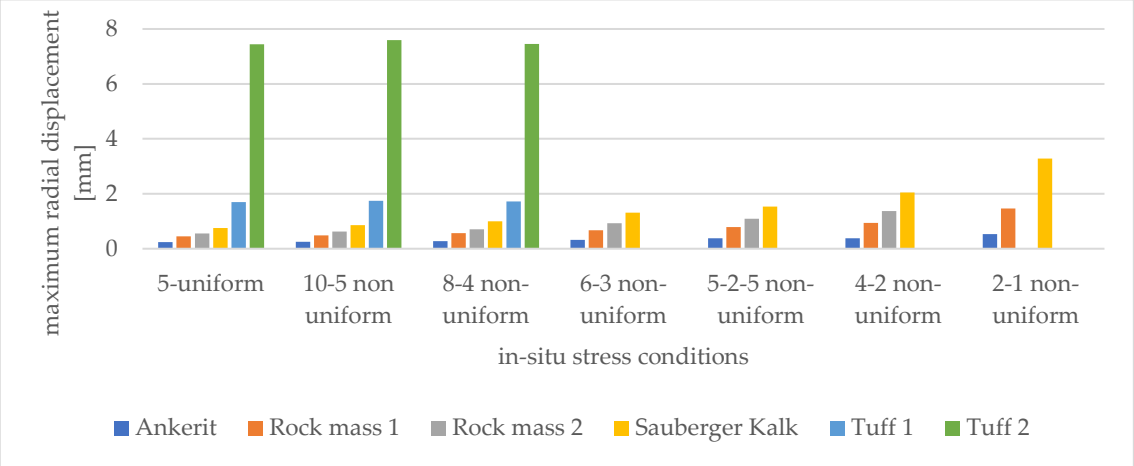

Maximum radial displacements of the storage boundary constructed with a pre-stressed concrete lining for every rock type, a p_i of 10 MPa and different in-situ stress magnitudes

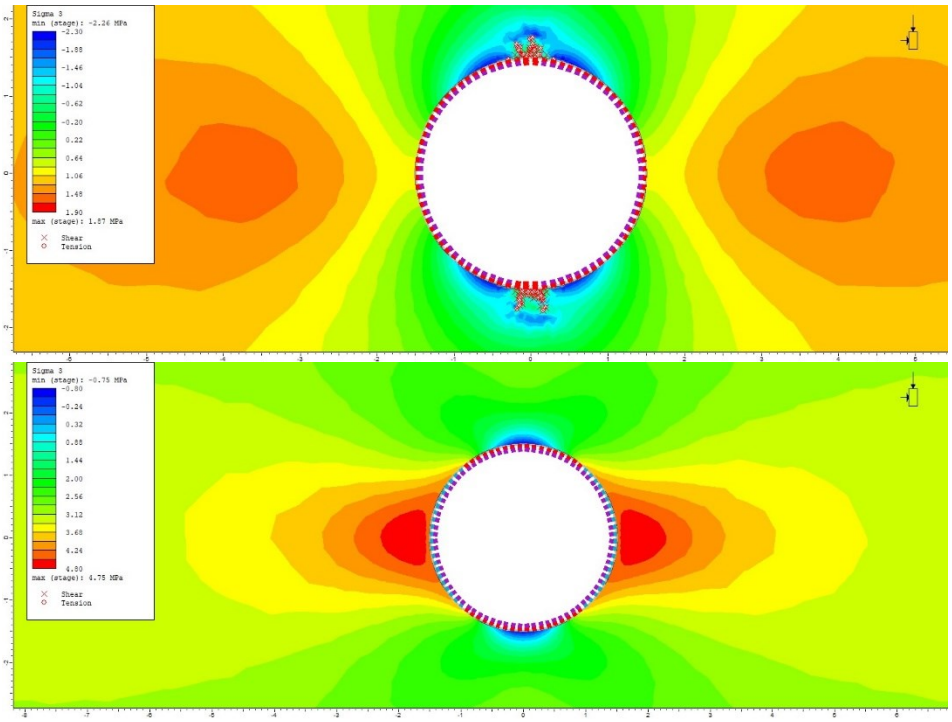

Comparison of the maximum σ_3 and the potential failure of the concrete lining and rock mass for Tuff 1, a p_i of 4 MPa and different non-uniform in-situ stresses with a magnitude of 2-1 (top image) and 6-3 (bottom image)

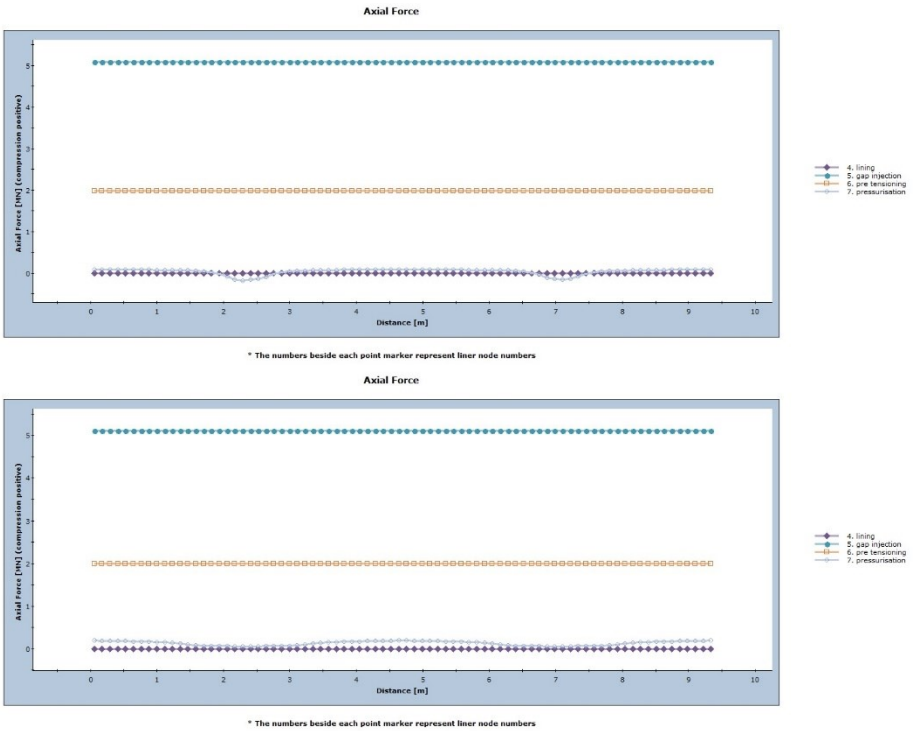

Comparison of the axial force of the pre-stressed concrete for Tuff 1, a p_i of 4 MPa and different non-uniform in-situ stresses with a magnitude of 2-1 (top image) and 6-3 (bottom image)

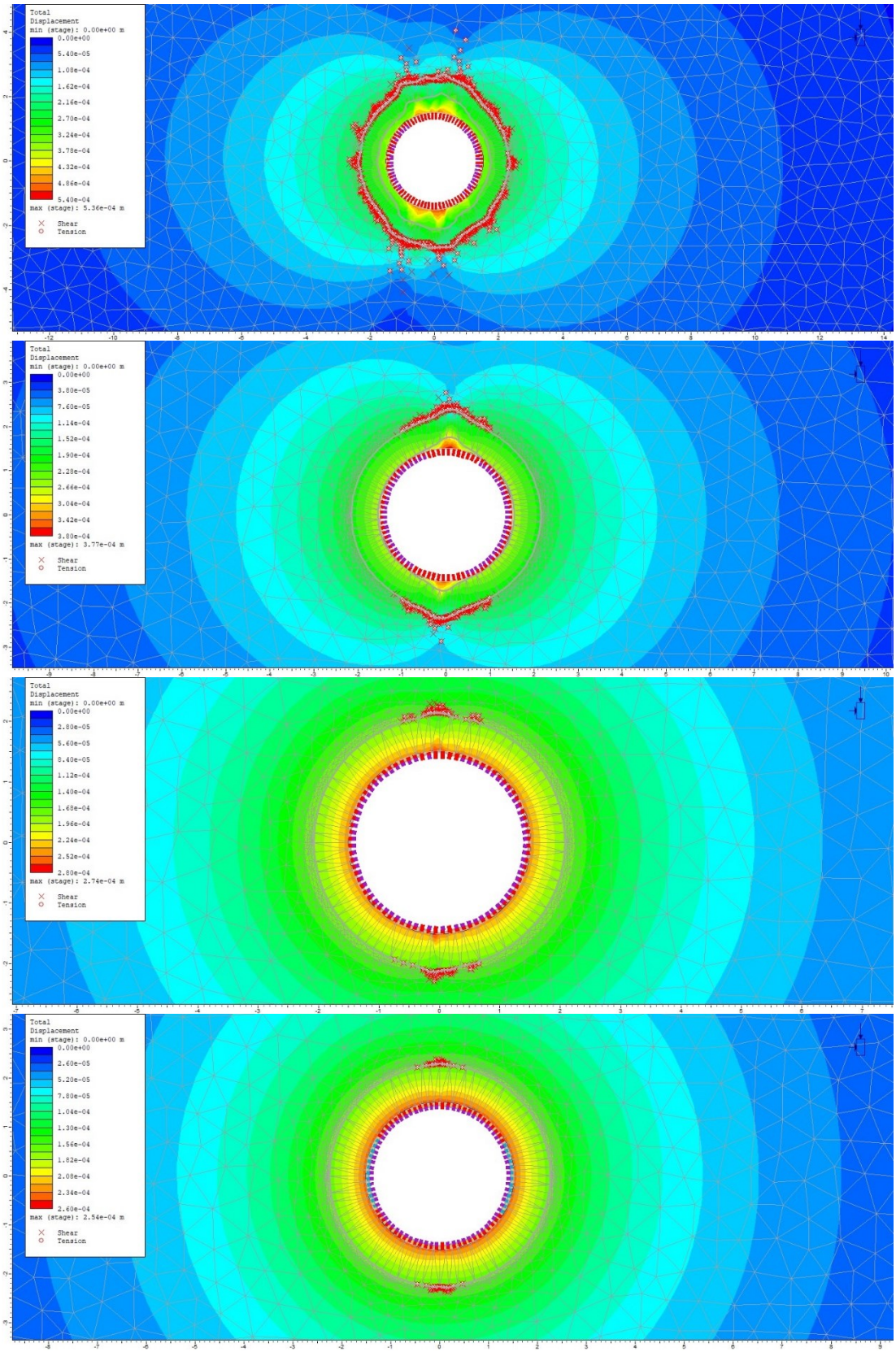

Comparison of the maximum radial displacement and the potential failure of the concrete lining and rock mass for Ankerit, a p_i of 10 MPa and different non-uniform in-situ stresses with a magnitude of 2-1 (first image), 5-2.5 (second image) 8-4 (third image) and 10-5 (fourth)

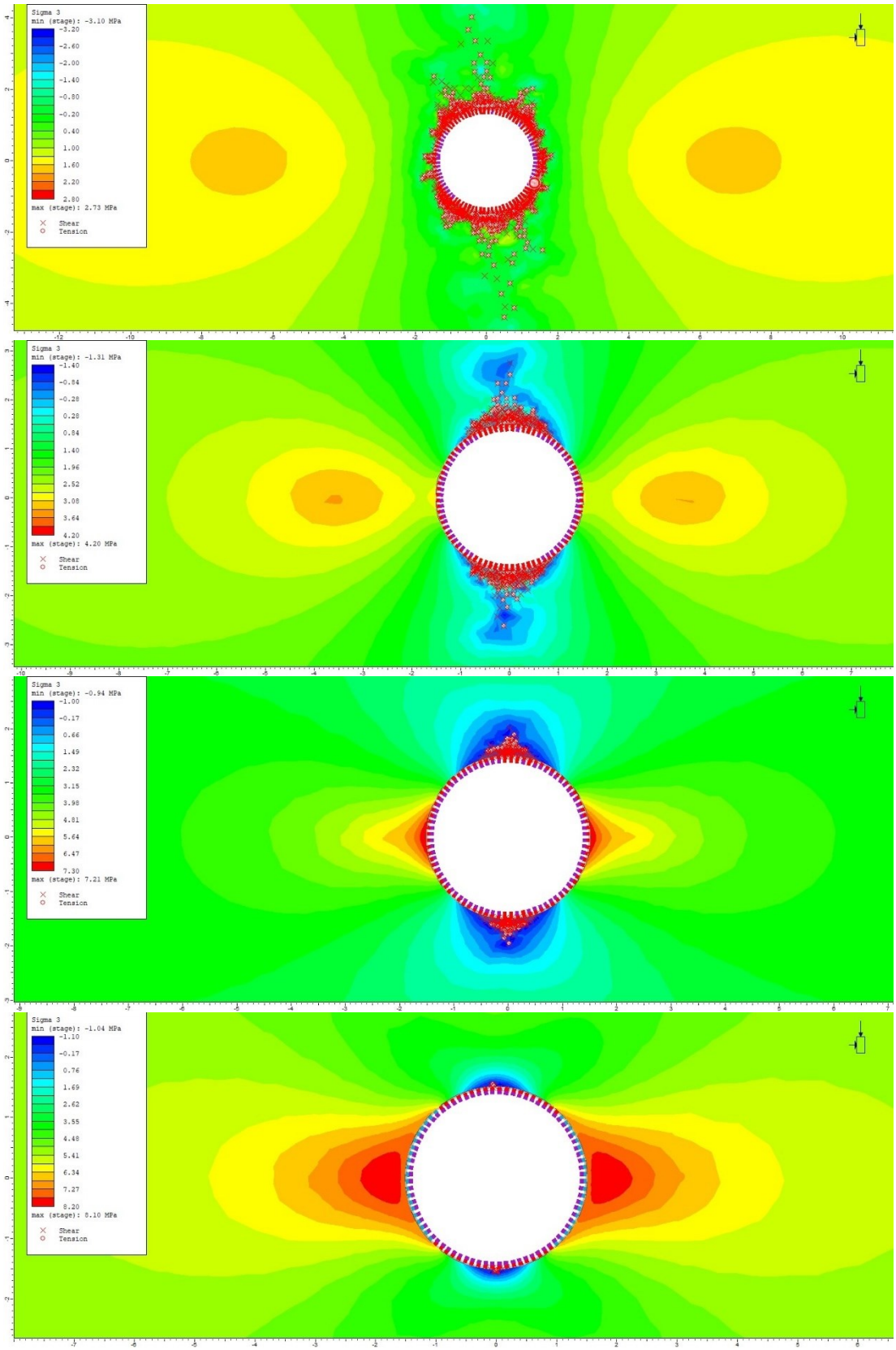

Comparison of the maximum σ_3 and the potential failure of the concrete lining and rock mass for rock mass 1, a p_i of 7 MPa and different non-uniform in-situ stresses with a magnitude of 2-1 (first image), 4-2 (second image) 6-3 (third image) and 10-5 (fourth image)

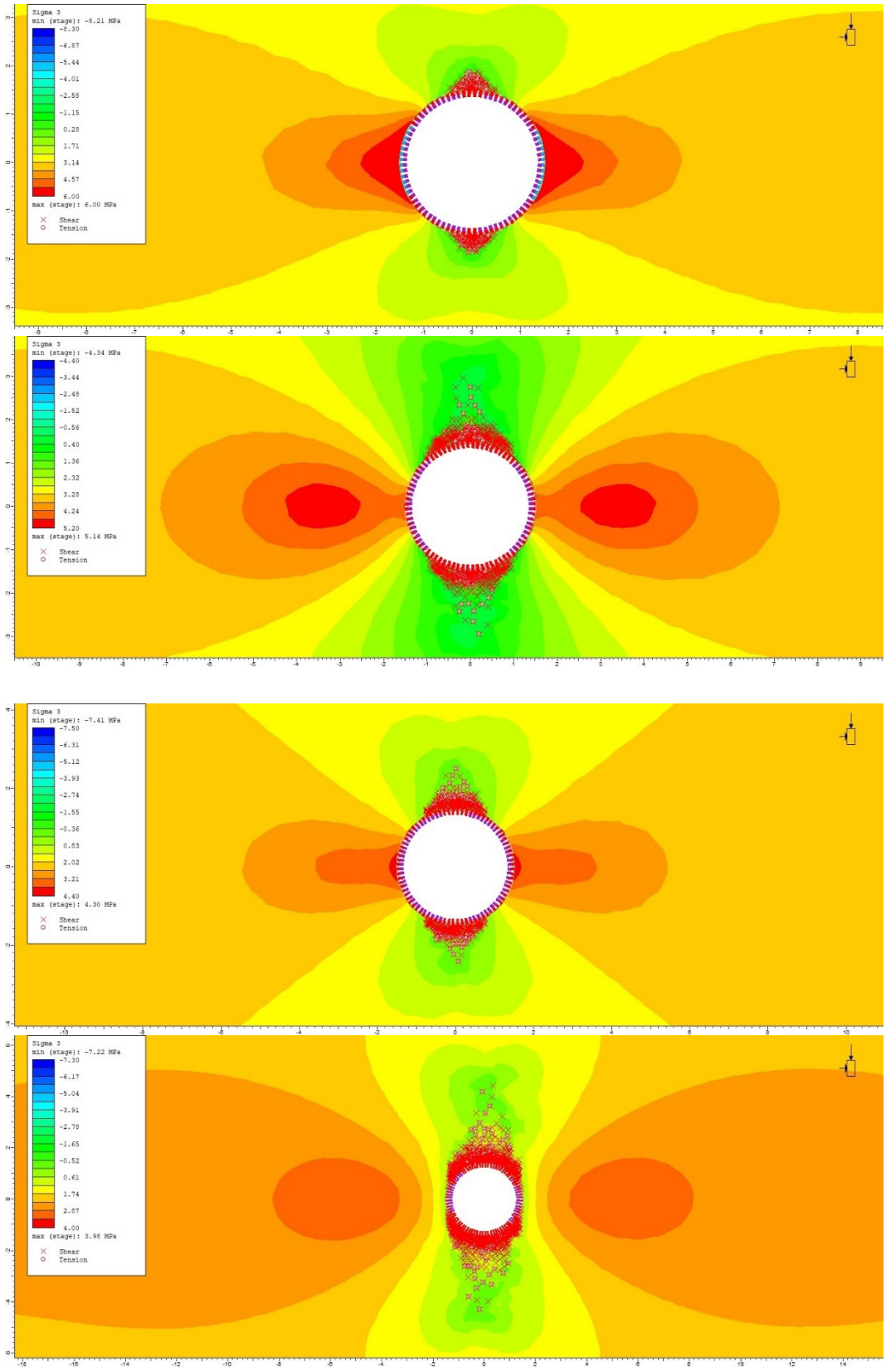

Comparison between the gap injection and pressurisation stage of the σ_3 and the potential failure of the concrete lining and rock mass for Sauberger Kalk considering a p_i of 10 MPa and different non-uniform in-situ stresses with a magnitude of 6-3 (first two images) and 4-2 (second two images)

Appendix G for Chapter 8.4.2 In-situ stress influence on the steel lining:

Comparison of the maximum radial displacement of the storage boundary for different in-situ stress conditions:

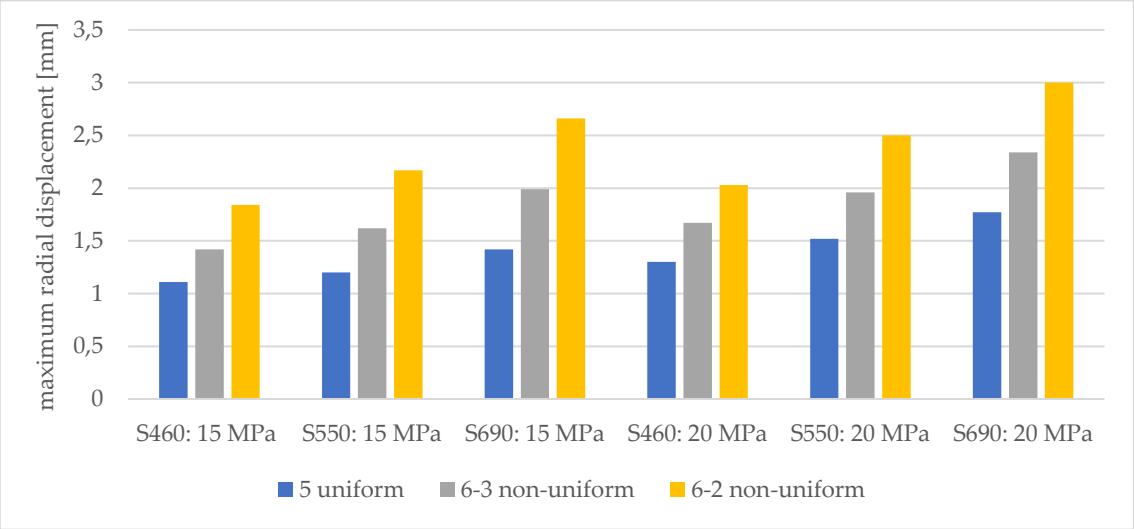

Comparison of the maximum radial displacement of the steel lined storage boundary for Tuff 1, steel grades S460, S550 and S690 as well as a p_i of 15 and 20 MPa

Comparison of the maximum radial displacement of the steel lined storage boundary for Sauberger Kalk, steel grades S460, S550 and S690 as well as a p_i of 15 and 20 MPa

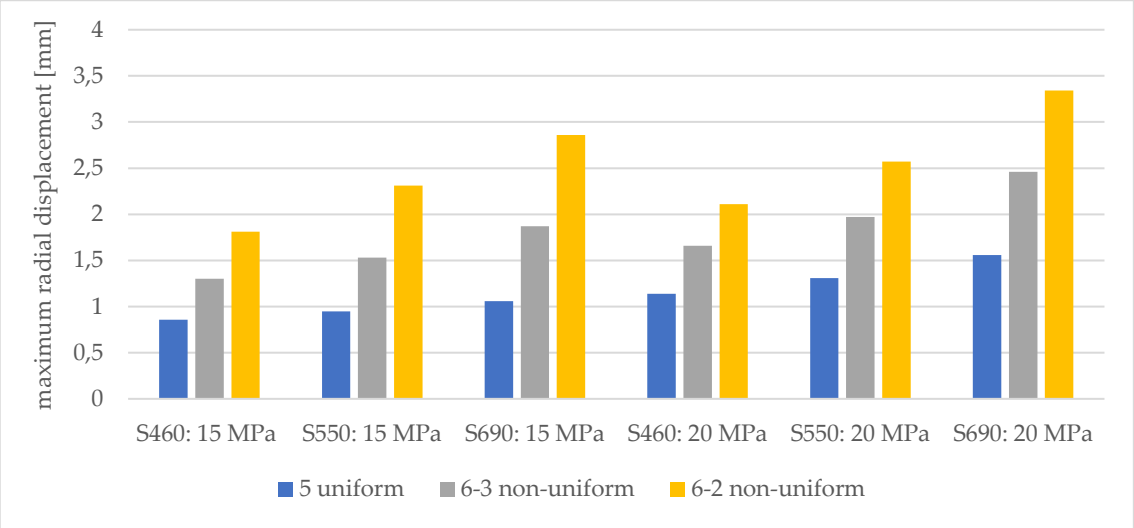

Comparison of the maximum radial displacement of the steel lined storage boundary for Rock mass 2, steel grades S460, S550 and S690 as well as a p_i of 15 and 20 MPa

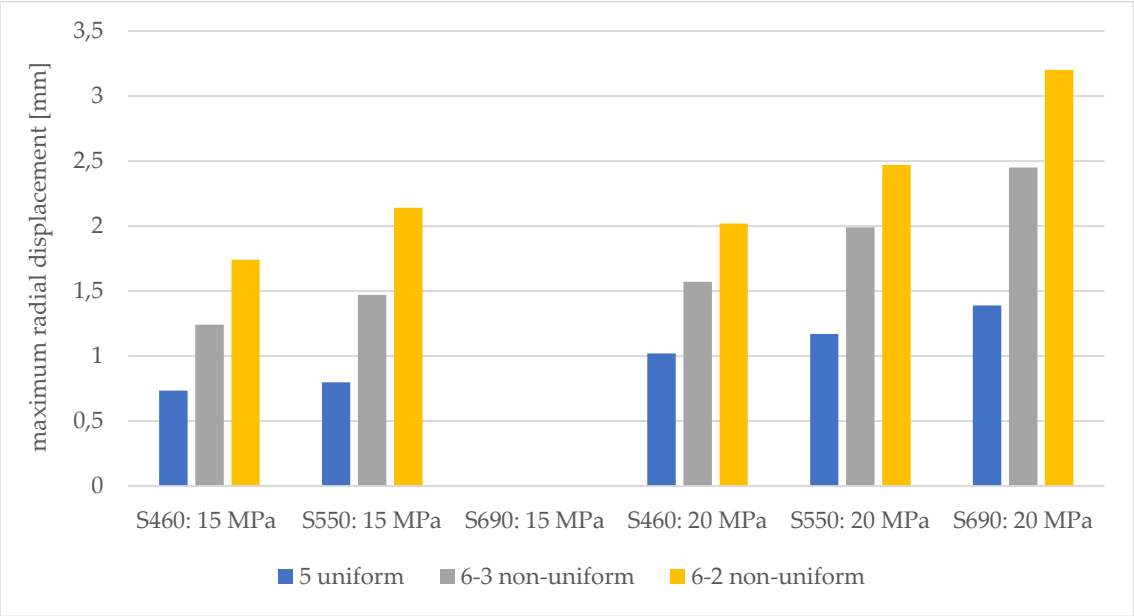

Comparison of the maximum radial displacement of the steel lined storage boundary for Rock mass 1, steel grades S460, S550 and S690 as well as a p_i of 15 and 20 MPa

Calculated σ_n and μ of the storage steel lining in Sauberger Kalk for a p_i of 15 and 20 MPa, 5 MPa uniform in-situ stress as well as steel grades S460, S550 and S690

Sauberger Kalk					
in-situ stress: 5 MPa uniform					
steel grade	p_i [MPa]	lining thickness [m]	axial force [MN]	σ_n [MPa]	μ [%]
S460	15	0.03341	5.1	153	41
S550	15	0.02341	4.1	175	40
S690	15	0.01303	2.7	207	38
S460	20	0.05379	10.6	197	54
S550	20	0.04045	9.2	227	52
S690	20	0.02662	7.3	274	50

Calculated σ_n and μ of the storage steel lining in Sauberger Kalk for a p_i of 15 and 20 MPa, non- uniform in-situ stress with a σ_1 of 6 MPa and a σ_3 of 3 MPa as well as steel grades S460, S550 and S690

Sauberger Kalk					
in-situ stress: 6-3 MPa non-uniform					
steel grade	p_i [MPa]	lining thickness [m]	axial force [MN]	σ_n [MPa]	μ [%]
S460	15	0.03341	6.5	195	53
S550	15	0.02341	5.3	226	51
S690	15	0.01303	3.7	284	51
S460	20	0.05379	12.4	231	63
S550	20	0.04045	11.0	272	62
S690	20	0.02662	8.9	334	61

Calculated σ_n and μ of the storage steel lining in Sauberger Kalk for a p_i of 15 and 20 MPa, non- uniform in-situ stress with a σ_1 of 6 MPa and a σ_3 of 2 MPa as well as steel grades S460, S550 and S690 and

Sauberger Kalk					
in-situ stress: 6-2 MPa non-uniform					
steel grade	p_i [MPa]	lining thickness [m]	axial force [MN]	σ_n [MPa]	μ [%]
S460	15	0.03341	7.8	233	63
S550	15	0.02341	6.5	278	63
S690	15	0.01303	4.6	353	64
S460	20	0.05379	14.0	260	71
S550	20	0.04045	12.6	311	71
S690	20	0.02662	11.0	413	75

Comparison of σ_n of the steel lining for Sauberger Kalk, using steel grades S460, S550 and S690 as well as a p_i of 15 and 20 MPa

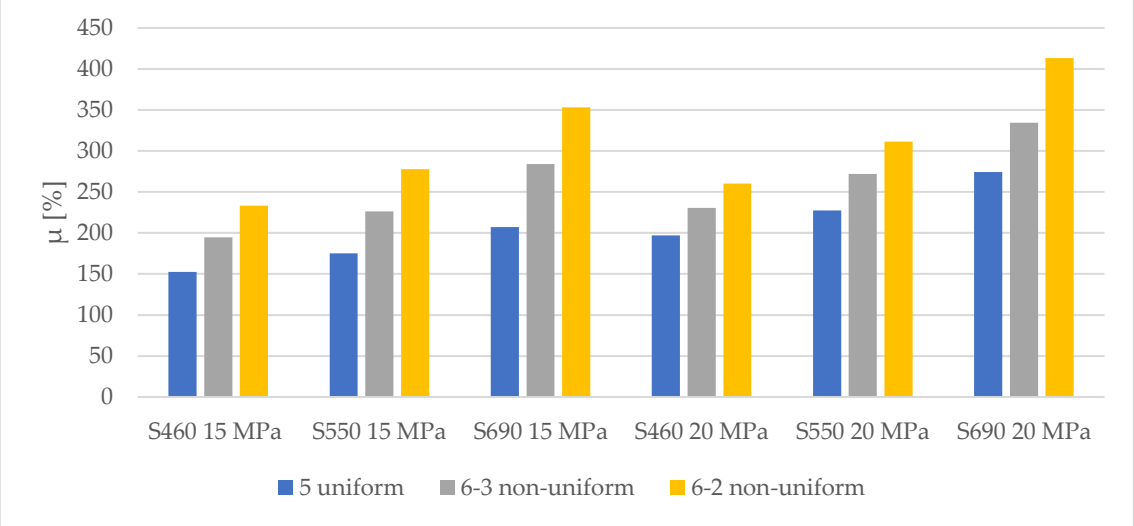

Comparison of the utilization (μ) of the steel strength capacity for Sauberger Kalk, using steel grades S460, S550 and S690 as well as a p_i of 15 and 20 MPa

Calculated σ_n and μ of the storage steel lining in Rock mass 2 for a p_i of 15 and 20 MPa, 5 MPa uniform in-situ stress as well as steel grades S460, S550 and S690

Rock mass 2					
in-situ stress: 5 MPa uniform					
steel grade	p_i [MPa]	lining thickness [m]	axial force [MN]	σ_n [MPa]	μ [%]
S460	15	0.02343	3.10	132	36
S550	15	0.01342	2.00	149	34
S690	15	0.00305	0.55	180	33
S460	20	0.04381	7.50	171	47
S550	20	0.03047	6.00	197	45
S690	20	0.01663	3.90	235	42

Calculated σ_n and μ of the storage steel lining in Rock mass 2 for a p_i of 15 and 20 MPa, non- uniform in-situ stress with a σ_1 of 6 MPa and a σ_3 of 3 MPa as well as steel grades S460, S550 and S690

Rock mass 2					
in-situ stress: 6-3 MPa non-uniform					
steel grade	p_i [MPa]	lining thickness [m]	axial force [MN]	σ_n [MPa]	μ [%]
S460	15	0.02343	4.40	188	51
S550	15	0.01342	3.00	224	51
S690	15	0.00305	1.00	328	59
S460	20	0.04381	9.40	215	58
S550	20	0.03047	7.80	256	58
S690	20	0.01663	5.40	325	59

Calculated σ_n and μ of the storage steel lining in Rock mass 2 for a p_i of 15 and 20 MPa, non- uniform in-situ stress with a σ_1 of 6 MPa and a σ_3 of 2 MPa as well as steel grades S460, S550 and S690

Rock mass 2					
in-situ stress: 6-2 MPa non-uniform					
steel grade	p_i [MPa]	lining thickness [m]	axial force [MN]	σ_n [MPa]	μ [%]
S460	15	0.02343	5.50	235	64
S550	15	0.01342	4.10	306	69
S690	15	0.00305	1.50	492	89
S460	20	0.04381	11.30	258	70
S550	20	0.03047	9.60	315	72
S690	20	0.01663	6.80	409	74

Comparison of σ_n of the steel lining for Rock mass 2, using steel grades S460, S550 and S690 as well as a p_i of 15 and 20 MPa

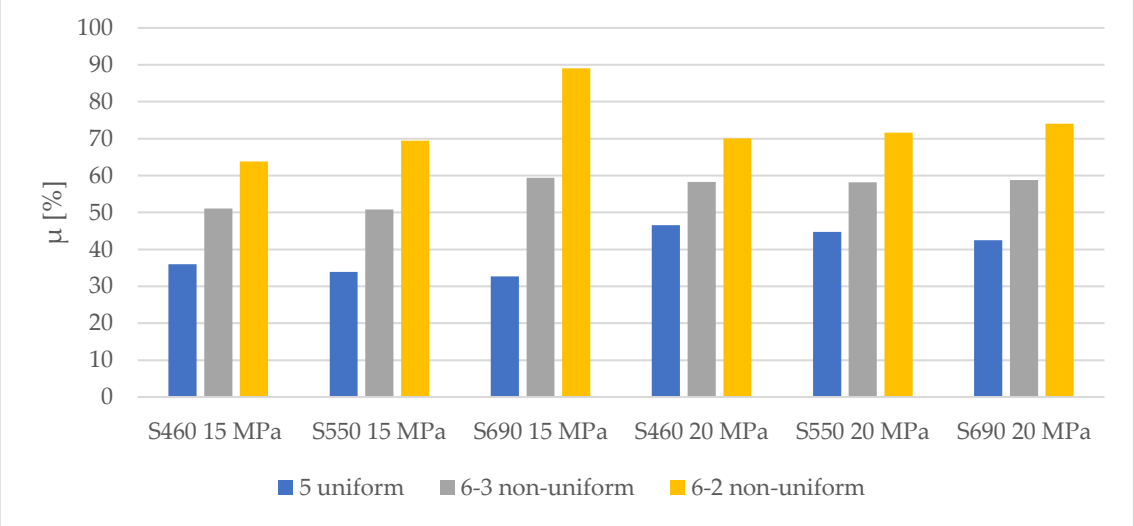

Comparison of the utilization (μ) of the steel strength capacity for Rock mass 2, using steel grades S460, S550 and S690 as well as a p_i of 15 and 20 MPa

Calculated σ_n and μ of the storage steel lining in Rock mass 1 for a p_i of 15 and 20 MPa, 5 MPa uniform in-situ stress as well as steel grades S460, S550 and S690

Rock mass 1					
in-situ stress: 5 MPa uniform					
steel grade	p_i [MPa]	lining thickness [m]	axial force [MN]	σ_n [MPa]	μ [%]
S460	15	0.01216	1.40	115	31
S550	15	0.00216	0.30	139	32
S690	15	no lining needed			
S460	20	0.03254	5.00	154	42
S550	20	0.0192	3.40	177	40
S690	20	0.00537	1.25	233	42

Calculated σ_n and μ of the storage steel lining in Rock mass 1 for a p_i of 15 and 20 MPa, non- uniform in-situ stress with a σ_1 of 6 MPa and a σ_3 of 3 MPa as well as steel grades S460, S550 and S690

Rock mass 1					
in-situ stress: 6-3 MPa non-uniform					
steel grade	p_i	lining thickness	axial force	σ_n	μ
-	[MPa]	[m]	[MN]	[MPa]	[%]
S460	15	0.01216	2.40	197	54
S550	15	0.00216	0.75	347	79
S690	15	no lining needed			
S460	20	0.03254	6.80	209	57
S550	20	0.0192	5.20	271	62
S690	20	0.00537	2.20	410	74

Calculated σ_n and μ of the storage steel lining in Rock mass 1 for a p_i of 15 and 20 MPa, non- uniform in-situ stress with a σ_1 of 6 MPa and a σ_3 of 2 MPa as well as steel grades S460, S550 and S690

Rock mass 1					
in-situ stress: 6-2 MPa non-uniform					
steel grade	p_i [MPa]	lining thickness [m]	axial force [MN]	σ_n [MPa]	μ [%]
S460	15	0.01216	3.20	263	72
S550	15	0.00216	0.80	370	84
S690	15	no lining needed			
S460	20	0.03254	8.50	261	71
S550	20	0.0192	6.30	328	75
S690	20	0.00537	2.70	503	91

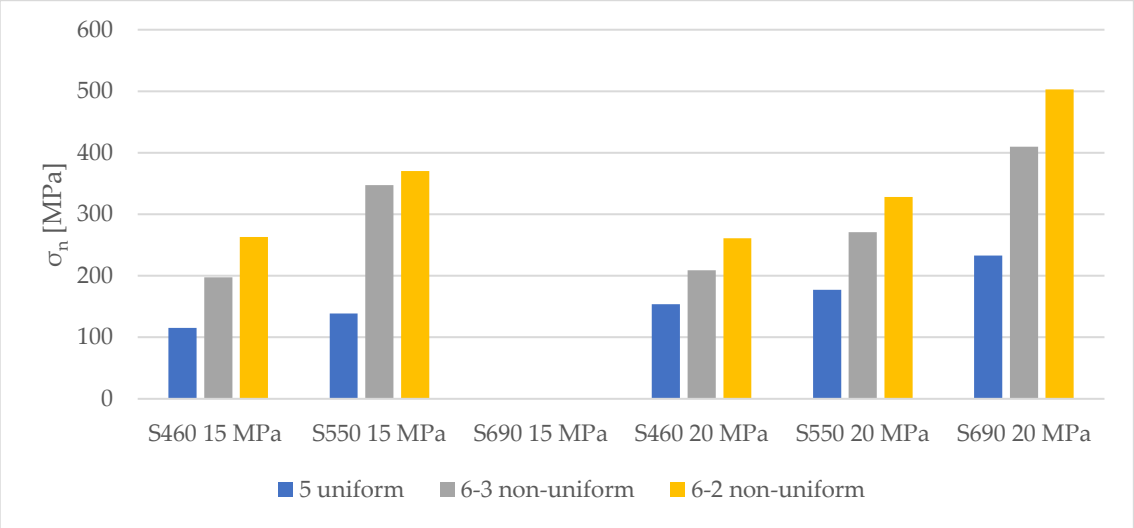

Comparison of σ_n of the steel lining for Rock mass 1, using steel grades S460, S550 and S690 as well as a p_i of 15 and 20 MPa

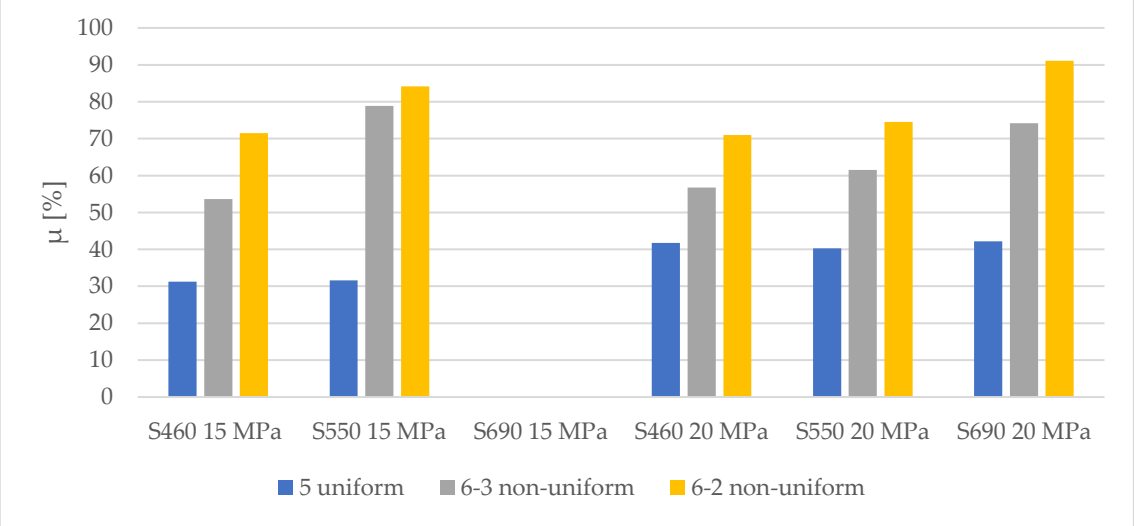

Comparison of the utilization (μ) of the steel strength capacity for Rock mass 1, using steel grades S460, S550 and S690 as well as a p_i of 15 and 20 MPa